OVERVOLTAGES AND COUPLING EFFECTS ON AN AC–DC HYBRID TRANSMISSION SYSTEM

By

Rogério T. Verdolin

A THESIS

Submitted to the Faculty of Graduate Studies in partial fulfillment of the requirements for the degree of

DOCTOR OF PHILOSOPHY

Department of Electrical and Computer Engineering
The University of Manitoba
Winnipeg, Manitoba, Canada

January 1995

ISBN 0-612-16353-9

Canada

OVERVOLTAGES AND COUPLING EFFECTS ON AN AC-DC HYBRID TRANSMISSION SYSTEM

BY

ROGERIO T. VERDOLIN

A Thesis submitted to the Faculty of Graduate Studies of the University of Manitoba in partial fulfillment of the requirements of the degree of

DOCTOR OF PHILOSOPHY

To all my teachers

and to two great teachers

my parents João and Tereza

and to those who provided inspiration,

my wife Regina and my son Rogério

Abstract

Adding a dc circuit to an existing transmission line is one method of significantly increasing the power transfer capability of a transmission corridor. The resulting hybrid system has significant coupling between the ac and dc circuits, not only because of the proximity of the circuits, but also from the fact that they may share the same sending end or receiving end ac systems. The resultant interaction produces overvoltages on the dc system which can be somewhat higher than for a conventional dc scheme.

This thesis investigates the overvoltages on a hybrid ac–dc transmission system and suggests some design considerations which could be taken into account to reduce stresses on certain critical components which result from such an arrangement.

Blocking filters consisting of a parallel L–C combination in series with the dc converter were included to limit the flow of fundamental frequency current in the dc line. This thesis also investigates the proper blocking filter configuration to be used as an incorrectly chosen blocking filter can cause resonance overvoltages on the dc line at fundamental frequency.

A method of eliminating dc components of the currents in the transformer windings of a dc converter is presented. The method uses the technique of firing angle modulation. It is shown that merely eliminating the fundamental frequency component on the dc side may not remove this dc component. The impact of such control action at one converter on the other converters in the dc transmission system is also presented. It is also shown that the undesirable side effects of such a scheme include increased generation of non–characteristic harmonics on both the ac and dc sides. The study is performed using an electromagnetic transients simulation program and theoretical calculations.

Acknowledgement

The author wishes to express his sincere appreciation to his advisors Prof. A.M. Gole and Dr. E. Kuffel for their guidance and valuable discussion during the course of this work.

The author expresses his thanks to Mr. B. Bisewski and Dr. N. Diseko for their significant advising during the project.

The author also thanks Prof. R.W. Menzies and Mr. D. Woodford from the Manitoba HVDC Research Centre for their valuable input as members of the advisory committee.

The author also acknowledge the assistance of Mr. Rohitha Jayasinghe and Ms. Ioni Fernando.

The sponsorship of the Brazilian Federal Agency for Post–Graduate Education (CAPES), the Electrical Energy Research Centre (CEPEL) and the Manitoba HVDC Research Centre is gratefully acknowledged.

Finally, the author expresses his sincere appreciation to his wife, Regina and his son Rogério for their understanding, support and encouragement.

Table of Contents

Abstract i

Acknowledgement ii

Table of Contents iii

List of Figures vii

List of Tables xv

List of Principal Symbols and Abbreviations xvi

Chapter 1 1

Introduction 1

1 .1 Contribution from the thesis 4

1 .2 Overview of the thesis 4

1 .2 .1 chapter 2: Description of the study system 4

1 .2 .2 chapter 3 : Overvoltages studies 5

1 .2 .3 chapter 4 : Firing angle modulation for eliminating DC Line 60 hz currents 6

1 .2 .4 chapter 5 : Firing angle modulation for eliminating Transformer dc currents 6

1 .2 .5 chapter 6 : Conclusion 7

Chapter 2 8

Description of the Study system 8

2 .1 Introduction 8

2 .2 Selection of the hybrid line [3] 9

2 .3 Main system data 11

2 .4 Ac system equivalent 13

2 .5 Ac filters 13

2 .6 Converter transformers 15
2 .7 Hybrid ac–dc line 17
2 .7 .1 Additional power provided by the dc bipole [8] 18
2 .7 .2 Electrical effects from the hybrid line [8] 19
2 .7 .3 Insulation [8] 20
2 .7 .4 Hot line construction and maintenance [8] 20
2 .7 .5 Lightning performance of hybrid line [8] 21
2 .8 Electrode line parameters 21
2 .9 Dc filters 22
2 .10 Thyristor valves 22
2 .11 Blocking filters (BF) 23
2 .12 Other converter equipment 25
2 .13 DC controls 25
2 .14 Single line diagram of the hybrid ac–dc system 26
2 .15 Initialization of the simulation (waveforms) 26

Chapter 3 30

Overvoltages Studies 30

3 .1 Second harmonic overvoltage 30
3 .1 .1 Resonances 30
3 .1 .2 Second harmonic overvoltage versus coupling effect 34
3 .1 .3 Effect of negative–sequence voltage on dc line overvoltages 40
3 .1 .4 Second harmonic filter 41
3 .2 Line overvoltage studies 45
3 .2 .1 Ac and dc overvoltages waveform 56
3 .2 .1 .1 Fault applied at the rectifier side 56
3 .2 .1 .2 Fault applied in the middle of the line 60
3 .3 Overvoltages on the Blocking Filters 69

3 .4 Transmission line model comparison 72
3 .5 Effect of blocking filter on an ac untransposed line 73
3 .6 Effect of ground resistivity on overvoltage 74
3 .7 Ac line transposed versus dc line transposed 75
3 .8 Fault philosophy 76
3 .8 .1 DC line fault 76
3 .8 .2 Ac–dc conductor contact fault 78
3 .9 Ac–dc conductor contact fault to ground 78
3 .10 Summary 80

Chapter 4 83

Firing Angle Modulation for Eliminating DC Line 60 Hz Currents 83

4 .1 Introduction 83
4 .2 Measurement of the coupling between the ac and dc line 84
4 .3 Relation between the 60 Hz component in the dc line and the dc component in the secondary of the transformer 87
4 .3 .1 Analytical approach 89
4 .3 .2 Simulation approach 96
4 .4 Firing Angle Modulation to Eliminate the 60 Hz Current 99
4 .4 .1 Analytical approach 99
4 .4 .1 .1 Without overlap angle 99
4 .4 .1 .2 With overlap angle 103
4 .4 .2 Alternative analytical modulation approach 109
4 .4 .2 .1 Without overlap angle 111
4 .4 .2 .2 With overlap angle 112
4 .4 .3 Simulation approach 114
4 .5 Summary 120

Chapter 5 121

Firing Angle Modulation for Eliminating Converter Transformer DC Currents 121

5 .1 Theoretical considerations 121

5 .1 .1 Newton–Raphson method [26] 126
5 .2 Elimination of Converter Transformer dc currents 129
5 .2 .1 Numerical calculation approach 129
5 .2 .2 Simulation approach on a simple system 130
5 .3 Designing of a control system 134
5 .4 Test on a simple system 135
5 .5 Test on a large hybrid ac–dc system 138
5 .5 .1 Ac line untransposed and without blocking filter
SCR = 11.33 , Q = 33% (200 MVar) 138
5 .5 .2 Ac line transposed and without blocking filter
SCR = 11.33 and Q = 33% (200 Mvar) 144
5 .5 .3 Ac line untransposed and without blocking filter
SCR = 2.42 and q=60% (360 Mvar) 144
5 .5 .3 .1 Frequency scanning of the hybrid system 146
5 .6 Drawbacks 151
5 .7 Simulation aspects 152
5 .8 Summary 152

Chapter 6 153

Conclusions 153

6 .1 Overvoltage study 153
6 .2 Firing angle modulation 154
6 .3 Suggestions for future studies 155

References 157

Appendix A 160

Appendix B 173

B.1 Relation between the 60 Hz component in the dc line and the dc component in the secondary of the transformer. 173

B.2 Firing Angle Modulation to Eliminate the 60 Hz Current 176

B.2.1 Without overlap angle 176

B.2.2 With overlap angle 180

Appendix C 183

List of Figures

Figure 2 .1 : Gulfport structure [2] 9

Figure 2 .2 : Modified tower top of a gulfport structure to accommodate the dc line [2] 10

Figure 2 .3 : Simplified single line diagram of the ac–dc hybrid transmission line 12

Figure 2 .4 : Ac system equivalent representation. 14

Figure 2 .5 : Ac system equivalent impedance and impedance angle (rectifier and inverter). 14

Figure 2 .6 : Single line diagram of ac filters. 15

Figure 2 .7 : Impedance plots for the ac system (including filters and shunt capacitors). 16

Figure 2 .8 : Transmission line conductor configuration. 17

Figure 2 .9 : Electrode line and ground electrode. 21

Figure 2 .10 : Single line diagram of dc filters. 22

Figure 2 .11 : Thyristor valve components. 23

Figure 2 .12 : Blocking filter design. 24

Figure 2 .13 : Impedance plots for the blocking filter. 24

Figure 2 .14 : Simplified dc control diagram. 25

Figure 2 .15 : Single line diagram of the system studied (Rectifier and Inverter). 27

Figure 2 .16 : Waveforms of the hybrid ac–dc system during the initialization of the simulation. 28

Figure 2 .17 : Waveforms of the hybrid ac–dc system in steady state. 29

Figure 3 .1 : 2nd harmonic overvoltage on the dc line for an ac single line to ground fault, L=0.5 H. 31

Figure 3 .2 : Frequency scan of the ac–dc hybrid system. 32

Figure 3 .3 : Resonant frequency as function of the smoothing reactor inductance. 33

Figure 3 .4 : Dc line overvoltages for single line to ground fault, for different values of inductance. 33

Figure 3 .5 : 2nd harmonic overvoltage on the dc line for an ac single line to ground fault, L= 0.25 H. 34

Figure 3 .6 : System configurations for ac single line to ground fault. 36

Figure 3 .7 : Maximum dc line overvoltage recorded any where along the line for an ac single line to ground fault for different system configurations,
a) Location where the fault was applied along the line (15 points of fault inception/location),
b) Enlargement of Figure a) above (only for the REC location). 37

Figure 3 .8 : Maximum dc line overvoltage profile for ac single line to ground fault. . . 38

Figure 3 .9 : Illustration of the converter for sequence component applied in the ac side. 39

Figure 3 .10 : Generation of 2nd harmonic overvoltage on the dc line with generation of 30% negative–sequence voltage in the ac rectifier source. 40

Figure 3 .11 : Negative–sequence voltage versus maximum dc overvoltage. 41

Figure 3 .12 : Single line diagram of 2nd harmonic filter. 42

Figure 3 .13 : Impedance x frequency characteristic of the 2nd harmonic filters. 42

Figure 3 .14 : Maximum dc line overvoltage recorded any where along the line for an ac single line to ground fault for different 2nd harmonic filters,
a) Location where the fault was applied along the line (15 points of fault inception/location),
b) Enlargement of Figure a) above (only for the REC location). 44

Figure 3 .15 : Maximum dc line overvoltage recorded any where along the line for different 2nd harmonic filters,
a) Ac–dc conductor contact fault to ground,
b) Ac line to line fault. 45

Figure 3 .16 : Maximum dc and ac line overvoltage for different types of faults. 48

Figure 3 .17 : Maximum dc and ac line overvoltage for different types of faults. 48

Figure 3 .18 : Maximum dc and ac line overvoltage for different types of faults. 48

Figure 3 .19 : Maximum dc and ac line overvoltage for different types of faults and system configuration. 49

Figure 3 .20 : Maximum dc and ac line overvoltage for different types of faults and system configurations. 49

Figure 3 .21 : Maximum ac line overvoltage at points along the line as a function of location where the fault was applied (SCR=11.33). 50

Figure 3 .22 : Maximum dc line overvoltage at points along the line as a function of location where the fault was applied (SCR=11.33). 51

Figure 3 .23 : Maximum ac line overvoltage at points along the line as a function of location where the fault was applied (SCR=2.84). 54

Figure 3 .24 : Maximum dc line overvoltage at points along the line as a function of location where the fault was applied (SCR=2.84). 55

Figure 3 .25 : Voltage and current waveforms for ac–dc contact fault (CF). (fault applied at REC) 57

Figure 3 .26 : Voltage and current waveforms for ac–dc contact fault to ground (CFG). (fault applied at REC) 58

Figure 3 .27 : Voltage and current waveforms for ac single line to ground fault (LGac). (fault applied at REC) 59

Figure 3 .28 : Voltage and current waveforms for ac–dc conductor contact fault (CF). (fault applied at TL3) 62

Figure 3 .29 : Voltage and current waveforms for ac–dc conductor contact fault to ground (CFG). (fault applied at TL3) 63

Figure 3 .30 : Voltage and current waveforms for ac single line to ground fault (LGac). (fault applied at TL3) 64

Figure 3 .31 : Voltage waveforms for ac single line to ground fault. (fault applied at TL3 at crest of positive voltage phase "b") 65

Figure 3 .32 : Voltage waveforms for ac single line to ground fault. (fault applied at TL3 at zero crossing voltage phase "b") 65

Figure 3 .33 : Voltage waveforms for ac single line to ground fault. (fault applied at TL3 at crest of negative voltage phase "b") 65

Figure 3 .34 : Voltage waveforms for ac–dc contact fault to ground. (fault applied at TL3 at crest of positive voltage phase "b") 66

Figure 3 .35 : Voltage waveforms for ac–dc contact fault to ground. (fault applied at TL3 at zero crossing voltage phase "b") 66

Figure 3 .36 : Voltage waveforms for ac–dc contact fault to ground. (fault applied at TL3 at crest of negative voltage phase "b") 66

Figure 3 .37 : Voltage waveforms for ac–dc contact fault. (fault applied at TL3 at crest of positive voltage phase "b") 67

Figure 3 .38 : Voltage waveforms for ac–dc contact fault.
(fault applied at TL3 at zero crossing voltage phase "b") 67

Figure 3 .39 : Voltage waveforms for ac–dc contact fault.
(fault applied at TL3 at crest of negative voltage phase "b") 67

Figure 3 .40 : Voltage waveforms for dc line to ground fault.
(fault applied at TL3 at instant of the crest of positive voltage phase "b") 68

Figure 3 .41 : Voltage waveforms for dc line to ground fault.
(fault applied at TL3 at instant of the zero crossing voltage phase "b") . . 68

Figure 3 .42 : Voltage waveforms for dc line to ground fault.
(fault applied at TL3 at instant of the crest of negative voltage phase "b") 68

Figure 3 .43 : Voltage and current waveforms for ac–dc contact fault
(without blocking filter arrester). 70

Figure 3 .44 : Voltage and current waveforms for ac–dc contact fault
(with blocking filter arrester). 70

Figure 3 .45 : Waveforms for ac–dc contact fault for different blocking
filter configurations. 71

Figure 3 .46 : Blocking filter design 71

Figure 3 .47 : Maximum dc and ac and dc line overvoltage for different types of faults.
(ac line transposed). 73

Figure 3 .48 : Maximum dc and ac line overvoltage for different types of faults.
(no coupling between ac and dc lines). 73

Figure 3 .49 : Maximum dc and ac line overvoltage for different types of faults. 74

Figure 3 .50 : Maximum dc and ac line overvoltage for different types of faults. 75

Figure 3 .51 : Maximum dc and ac and dc line overvoltage for different types of faults.
(ac line transposed) 76

Figure 3 .52 : Forced retard strategy applied in the rectifier. 77

Figure 3 .53 : Voltage and current waveforms for ac–dc contact fault to ground. 79

Figure 3 .54 : Maximum ac line overvoltage x tripping time of the circuit breakers. 80

Figure 3 .55 : Voltage and current waveforms for ac–dc contact fault to ground. 81

Figure 4 .1 : Conceptual circuit illustrating the coupling between the ac line and dc line
and the effect in the secondary of the HVDC converter transformer. 85

Figure 4 .2 : Conceptual circuit for driving current in coupled line. 86

Figure 4 .3 : Percentage of current, a) dc component in the secondary o the transformer, b) 2nd harmonic component in the secondary of the transformer, c) Fundamental frequency component in the dc line induced from the ac line. 86

Figure 4 .4 : Percentage of dc, 2nd harmonic and 60 Hz current. 88

Figure 4 .5 : Dc offset current in the converter transformer winding. 89

Figure 4 .6 : Configuration of a six–pulse bridge converter. The valves are numbered in their firing order. 89

Figure 4 .7 : Representation of the rotating vectors from the six–pulse bridge voltage source. 91

Figure 4 .8 : Instantaneous currents and voltages of six–pulse bridge converter with modulation of the firing angles. (with overlap) 92

Figure 4 .9 : Simplified diagram of the hybrid system and the measurement of the relation of the dc component and the 60 Hz component. 97

Figure 4 .10 : Relation between the ac components and dc component, according to Equation 4 .10 98

Figure 4 .11 : Waves of instantaneous voltage of ac source and direct voltage and modulation of the firing angle, without overlap. 100

Figure 4 .12 : Fundamental frequency voltage component as function of α_m and α_0 (Em=1.0 pu). 102

Figure 4 .13 : Phase angle of the fundamental component voltage as function of $\phi\alpha$ and α_0 (Em=1.0 pu). 103

Figure 4 .14 : Dc voltage for firing angle α_0=60 and 120 deg. (μ=0 and α_m=0 and 10 deg.). 104

Figure 4 .15 : Fundamental frequency voltage component as function of α_m and α_0 (Em=1.0 pu). 104

Figure 4 .16 : Waves of instantaneous voltage of ac source and direct voltage and modulation of the firing angle, with overlap. 105

Figure 4 .17 : Fundamental frequency voltage component as function of α_m and α_0 (Em=1.0 pu). 108

Figure 4 .18 : Phase angle of the fundamental component voltage as function of ϕ_a and α_0 (Em=1.0 pu). 109

Figure 4 .19 : Dc voltage for firing angle α_0=60 and 120 deg. (μ=10 deg. and α_m=0 and 10 deg.). 110

Figure 4 .20 : Fundamental frequency voltage component as function of α_m and α_0 (Em=1.0 pu). 110

Figure 4 .21 : Fundamental frequency voltage component as function of α_m and α_0 (μ=0 and Em=1.0 pu). 112

Figure 4 .22 : Fundamental frequency voltage component as function of α_m and α_0 (μ=10 deg. and Em=1.0 pu). 115

Figure 4 .23 : Simplified dc system. 115

Figure 4 .24 : Configuration of a six–pulse bridge converter. 116

Figure 4 .25 : Simulation of the coupling effect in a six–pulse bridge converter,
a) Induced 60 Hz current in the dc line,
b) Magnitude of the dc current in the three phases of the secondary of the converter transformer,
c) αm modulation and crest value of the 60 Hz voltage source;
d) α measured and α_i modulated
e) Current in the secondary of the converter transformer. 118

Figure 4 .26 : Dc current. 119

Figure 4 .27 : Harmonic Spectrum of the secondary current transformer Ia. 119

Figure 5 .1 : Instantaneous currents of six–pulse bridge converter with modulation of the firing angles.(without overlap angle) 122

Figure 5 .2 : Modulation of the firing angle. 125

Figure 5 .3 : Simplified dc system. 131

Figure 5 .4 : Dc current elimination in phase currents of a simplified six–pulse bridge converter system
a) 60 Hz current source and 60 Hz current measurement in the dc line (crest)
b) Magnitude of the dc current in the three phases of the secondary of the converter transformer,
c) Firing angle α_m modulation from Newton–Raphson. 132

Figure 5 .5 : Dc current (Idc) and phase current (Ia). 132

Figure 5 .6 : Harmonic Spectrum of the current Ia in the secondary of the transformer. 133

Figure 5 .7 : Theoretically calculated α_i values fitted with a sine wave. 134

Figure 5 .8 : Proposed control system. 136

Figure 5 .9 : Dc current elimination in phase currents of a simplified six–pulse bridge converter system
a) 60 Hz current source and 60 Hz current measurement in the dc line (crest)
b) Magnitude of the dc current in the three phases of the secondary of the converter transformer,
c) Firing angle α_i modulation from control action. 137

Figure 5 .10 : Harmonic spectrum of the secondary current transformer Ia. 138

Figure 5 .11 : Dc current elimination in phase currents in a large hybrid ac–dc system. Control action only in the rectifier side and positive pole. Ac line untransposed and without blocking filter
a) 60 Hz current measurement in the dc line (crest),
b)Magnitude of the dc component in the converter transformer (3 phases),
c) Firing angle α_i modulation. 140

Figure 5 .12 : Harmonic spectrum of the secondary current transformer Ia. 141

Figure 5 .13 : Harmonic spectrum of the secondary current transformer Ia 141

Figure 5 .14 : Dc current elimination in phase currents in a large hybrid ac–dc system. Control action on both sides and only positive pole. Ac line untransposed and without blocking filter, SCR=11.33, Q=33%
a) 60 Hz current measurement in the dc line (crest),
b)Magnitude of the dc component in the converter transformer (3 phases),
c) Firing angle α_i modulation. 142

Figure 5 .15 : Harmonic spectrum of the secondary current transformer Ia (Rec. and Inv. / Pos. Pole) 142

Figure 5 .16 : Dc current elimination in phase currents in a large hybrid ac–dc system. Control action on both sides and poles. Ac line untransposed and without blocking filter, SCR=11.33, Q=33%
a) 60 Hz current measurement in the dc line (crest),
b) Magnitude of the dc component in the converter transformer (3 phases),
c) Firing angle α_i modulation. 143

Figure 5 .17 : Dc current elimination in phase currents in a large hybrid ac–dc system. Control action on both sides and poles. Ac line transposed and without blocking filter, SCR=11.33 and Q=33%.
a) 60 Hz current measurement in the dc line (crest),
b) Magnitude of the dc component in the converter transformer (3 phases),
c) Firing angle α_i modulation. 145

Figure 5 .18 : Harmonic spectrum of the secondary current transformer Ia (Rec. and Inv., pos. pole). SCR=11.33, Q=33% 146

Figure 5 .19 : Rectifier and Inverter ac system configuration. 147

Figure 5 .20 : Total ac system impedance versus frequency (Rec. and Inv. SCR=2.42, Q=60%). 147

Figure 5 .21 : Frequency scanning method for system impedance of the hybrid ac–dc system. 148

Figure 5 .22 : The total ac system impedance x frequency (Rec. and Inv. SCR=2.42, Q=60%). 149

Figure 5 .23 : Dc current elimination in phase currents in a large hybrid ac–dc system. Control action on both sides and poles. Ac line untransposed and without blocking filter, SCR=2.42 and Q=60%
a) 60 Hz current measurement in the dc line (crest),
b)Magnitude of the dc component in the converter transformer (3 phases),
c) Firing angle αi modulation. 150

Figure 5 .24 : Harmonic spectrum of the secondary current transformer Ia (Rec. and Inv, both poles). 151

List of Tables

Table 2 .1 : Ac filters data for the rectifier and inverter. 15

Table 2 .2 : Converter Transformer data. 16

Table 2 .3 : Transmission line conductor data. 17

Table 2 .4 : Power provided by the dc bipole. 18

Table 2 .5 : Calculated electrical effects 19

Table 2 .6 : Thyristor valve components. 23

Table 3 .1 : 2nd harmonic filter 41

Table 3 .2 : 2nd harmonic overvoltage for ac single line to ground fault 43

Table 3 .3 : Comparison between ac and dc line results, SCR=11.33 52

Table 3 .4 : Comparison between ac and dc line results, SCR=2.84 53

Table 3 .5 : Negative–sequence voltage in the rectifier for different fault types 56

Table 3 .6 : Maximum negative–sequence voltage in the rectifier for different fault types 61

Table 5 .1 : Comparison of the dc component Ia_0, Ib_0, Ic_0 with modulation and without modulation 130

List of Principal Symbols and Abbreviations

HVDC	high voltage direct current
HVAC	high voltage alternating current
ESCR	effective short circuit ratio
SCR	short circuit ratio
α	converter bridge firing angle
γ	converter bridge extinction angle
β	$180^0 - \alpha$
LGac	ac single line to ground fault
LLG	ac line to line to ground fault
LL	ac line line to line fault
LLLG	ac three phase fault
CF	ac–dc conductor contact fault
CFG	ac–dc to ground contact fault
LGdc	dc conductor to ground
REC	rectifier
INV	inverter
TLn	location n along the line (1 is closer to REC and 5 is closer to INV)
L	inductance of the smoothing reactor

BF	blocking filter
e_a, e_b, e_c	line–to–neutral alternating voltage on phases *a, b* and *c*
e_{ac}	line–to–line alternating voltage between phases *a* and *c*
i_a, i_b, i_c	line current at phase *a, b* and *c*
λ	angle of the induced 60 Hz current in the dc line measured from the reference axis
I_{60}	60 Hz current component induced into the dc line
A	crest value of the 60 Hz current component induced into the dc line
I_{120}	120 Hz current component flowing into the secondary of the converter transformer
I_{dc}	dc current component flowing into the secondary of the converter transformer
I_{dc}	dc current in the dc line
ω	angular frequency ($d\theta/dt$)
I_d	constant ripple–free direct current flowing in the dc line
E_m	crest value of line–to–neutral alternating voltage
L_c	leakage inductance of the transformer
I_{a0}, I_{b0}, I_{c0}	average value of the dc current in phases *a, b* and *c*
μ	overlap angle
σ	$\alpha + \mu + \lambda$
α_i	firing pulse in the valve i
α_0	constant firing pulse in the valve

α_m	amplitude of the 60 Hz firing pulse modulation
ϕ_α	phase angle of firing pulse modulation
V_d	average value of the dc line voltage
a_n	cosine coefficient of the Fourier series
b_n	sine coefficient of the Fourier series
C_n	$\sqrt{(a_n^2 + b_n^2)}$
$c_{1_{v_d}}$	magnitude of the 60 Hz voltage component in the dc side which was generated by the modulation of the firing pulse of the six–pulse bridge converter .
$c_{1_{v_d}}$	fundamental component of the average dc line voltage
$\phi_{1_{v_d}}$	phase angle of fundamental component of the average dc line voltage
V_{d0}	ideal no–load direct current
rms	root–mean–square
$E_{LL_{rms}}$	line–to–line rms voltage
s	second (time)
V_{d60}	60 Hz component of the dc line voltage
cr	crest value
Q	reactive power

Chapter 1

Introduction

There are presently two different methods for the transmission of electric energy. These methods are high voltage alternating current (HVAC) and high voltage direct current (HVDC) transmission. Because of the easy stepping up and down transmission voltages by power transformers, and also because of the convenience in system interconnection, most transmission lines use three–phase alternating current operation. In recent years, however, increasing attention has been given to high–voltage dc transmission as an effective means of solving such problems as stability, short–circuit capacity and wide–area system operation, inherent to ac transmission. High voltage dc power transmission has been used all over the world for long–distance transmission of a vast amount of electric energy and submarine cable power transmission. This energy transmission method has become more advantageous economically. Each of the alternating current (ac) and direct current (dc) power transmission schemes has its own technical and economical advantages over the other [1].

The demand for electric power is steadily increasing, and despite efforts in conservation of energy and load management, the reserve capacity of existing transmission systems is gradually being reduced. Today rigid regulations are being imposed on the the expansion of power stations, switchyards or transmission lines. The restrictions on the construction of a new transmission line is more severe since it routes through different areas of land and is subjected to variety of regulations depending on the local conditions, some of which may be forest clearances, high cost of land in congested urban areas and environmental constraints.

Power system utilities are finding it difficult and sometimes impossible to obtain a licence for a new transmission lines. For such situations, the alternative to new lines is to enhance power transmission capacity of the existing lines. The utility transmission engineer must seek innovative ways to get power to the load centers under circumstances where no new right–of–way for the transmission can be readily acquired. These include:

a) Upgrading to a higher ac voltage;

b) Conversion to six phases;

c) Conversion to dc transmission;

d) Application of series capacitors and shunt var compensation;

e) Adding a dc line to an existing ac transmission circuit;

f) Replacing one circuit of a double circuit ac transmission by a dc line.

With the increasing use of the dc transmission in existing ac networks, the possibility of ac and dc circuits running parallel to each other and sharing the same right–of–way or even the same tower is increasing. It is recognized that there are potential applications for adding a high voltage dc transmission circuit to an existing or planned ac circuit. Adding a dc line to an existing ac transmission circuit or replacing one circuit of a double circuit ac transmission system by a dc circuit has been proposed as an effective method of significantly increasing the transmission capacity of the power corridor [2], [3], [4], [5], [6].

When a dc transmission circuit is added to an ac circuit the term "Hybrid" transmission is used. Although expected to be more costly than series/shunt compensation of ac lines, the ac–dc hybrid alternative of e) and f) above are going to be retained in this study due to the higher power transfer capability with these options. The application of series/shunt compensation is well known and well documented and thus this project concentrates on the investigation of the hybrid ac–dc alternative.

A number of papers have addressed in the literature the problems arising when ac and dc circuits are closely coupled. These include induction of 60 Hz currents on the dc line from the ac line which can lead to converter transformer saturation [3], and prolonged clearing times for dc line faults because of secondary induction effects from the ac line [5]. Some problems not addressed in the literature are the one related to induced overvoltage and when different types of faults at different locations are applied on the hybrid system and the effects of ac coupled voltages and currents on the dc circuit.

The dc converters generate harmonic voltages and currents on both ac and dc sides. The cyclical switching action of the dc converter generates harmonic voltage and currents on both ac and dc sides.

It is a well known property of the dc conversion process that a current component of frequency "f" on the dc side appears on the ac side as a component of frequency "$f_0 \pm f$"; "f_0" being the fundamental ac frequency, taken here to be 60 Hz [4]. If the dc transmission line lies adjacent to an ac transmission line, there is a possibility for a fundamental frequency (60 Hz) current component to be induced into the dc line, referred to as (I_{60}). This current would then appear in the secondary winding of the converter transformer as a dc component (I_{dc}) and also a 120 Hz component (I_{120}) superimposed on the fundamental 60 Hz component. This dc current component eventually flows as transformer magnetizing current and offsets the knee of the flux–current characteristic and if excessive, causes unsymmetrical saturation of the converter transformer. This can lead to an increase in audible noise and result in possible loss of life expectancy of the transformer. Other reported problems are inaccurate control and protection measurements because of saturation of current transformers on the ac side. Because of the very low magnetizing current requirement of HVDC transformers, even a few tens of amperes of dc current is considered by some as excessive [4].

There are several instances where a dc and ac line follow adjacent corridors and such induction effects could be detrimental. With the added difficulty of obtaining transmission line rights of way there is considerable interest in having hybrid ac–dc transmission systems in which ac and dc conductors are placed on the same tower structure. The coupling of the 60 Hz component would be even more severe in such cases.

Several alternatives have been proposed for mitigating the dc currents in the transformer windings. One proposed alternative is to use dc side blocking filters for the fundamental frequency (60 Hz) induced currents.

Blocking filters consisting of a parallel L–C combination in series with the dc converter were included to limit the flow of fundamental frequency current in the dc line. This thesis investigates the proper blocking filter configuration to be used as an incorrectly chosen blocking filters can cause resonance overvoltages on the dc line at fundamental frequency.

Another alternative is to transpose the ac lines. This option does not completely eliminate the induced harmonics especially when ac and dc conductors are on the same tower as in hybrid ac–dc lines.

Another possible alternative is to use modulation of the converter's firing angle. This method appears to have the advantage of not requiring extensive modifications to the power equipment as in the other choices. We explore this alternative in chapters 4 and 5 . Some theoretical results are presented on an idealized system to understand the essential phenomena. Subsequent investigations are carried out on a realistic system using an electromagnetic transients simulation program (PSCAD/EMTDC) [7]. The results indicate that it is possible to eliminate the dc currents in the transformer using such a scheme. However, there are some undesirable side–effects such as the generation of non–characteristic harmonics.

1 .1 CONTRIBUTIONS FROM THE THESIS

The thesis extended the earlier knowledge about ac–dc hybrid systems as follows:

– it evaluates the induced overvoltage and current on an ac–dc hybrid system for different types of faults and at a number of different locations along the ac–dc line for different system configurations.

– evaluates the coupling effect between the ac and dc line on an ac–dc hybrid system for different system configuration.

– formulates a method for eliminating the fundamental frequency current component induced from the ac line into the dc line.

– formulates a method for eliminating the dc component current in the converter transformer secondary winding on a simple six–pulse bridge and on an ac–dc hybrid systems.

1 .2 OVERVIEW OF THE THESIS

The study was organized into the following sections:

1 .2 .1 CHAPTER 2

DESCRIPTION OF THE STUDY SYSTEM

In this chapter is described the hybrid ac–dc system comprising a configuration of the tower, the ac source in the rectifier and inverter sides, electrical aspects of the ac–dc hybrid transmission lines,

converter transformers, ac and dc filters, thyristor valves, blocking filters and electrode line parameters and dc control configurations. At the end of this chapter it is shown the waveforms of a start up and the steady state condition of one simulation example.

1.2.2 CHAPTER 3

OVERVOLTAGES STUDIES

In this chapter the overvoltages on such a hybrid ac–dc transmission system are investigated and some design changes are suggested which could be implemented to reduce stresses on certain critical components.

The preliminary simulation study identified two problems with the hybrid system. In the first case, the smoothing inductor originally selected caused a second harmonic resonance on the dc system which resulted in excessive second harmonic overvoltages being generated during a line to ground fault on the ac system at either end. Lowering the value of the smoothing inductor significantly reduced this overvoltage. In the second problem, the dc blocking filters were determined to be subject to excessive overvoltages from ac–dc contact faults. This is due to the parallel resonance of the L–C components of the blocking filters at the fundamental frequency. This overvoltage can be limited by placing an arrester in parallel with the capacitor. In addition, a resistor can be placed across the filter to reduce the quality factor and hence increase damping of the oscillation following fault clearing.

The base configuration which was simulated for the majority of the cases reported in this chapter was as described in chapter 2 . Sensitivity studies were also carried out as follows:

a) different system strength

b) no transpositions of the ac conductors

c) no electromagnetic coupling between the ac and dc lines

d) ground resistivity of 10 ohms–m and 1000 ohms–m

e) ac line transposition versus blocking filter

f) frequency dependent versus Bergeron transmission line model

g) only dc line transposed

Investigating the overvoltages in such a hybrid system requires special tools. An electromagnetic transient simulation program (such as PSCAD/EMTDC) is ideally suited for such studies because it has the capability of detailed modeling of transmission lines for coupling effects as well as the capability to represent HVDC converters in full detail and to represent transformer saturation nonlinearities.

1 .2 .3 CHAPTER 4

FIRING ANGLE MODULATION FOR ELIMINATING DC LINE 60 HZ CURRENTS

An analytical and simulation methods of using control modulation to eliminate 60 Hz component of the current in the dc line are presented. We initially believed that eliminating the 60 Hz component of the current would result in the elimination of transformer dc currents. However it is shown that merely eliminating the fundamental component on the dc side may not remove the dc component in the secondary of the converter transformer.

1 .2 .4 CHAPTER 5

FIRING ANGLE MODULATION FOR ELIMINATING TRANSFORMER DC CURRENTS

The possibility of eliminating the dc components in the converter transformer windings was explored. First the feasibility of such a solution using a theoretical approach on a simplified system was investigated, and the analysis to more detailed system later was extended by means of simulation. Some theoretical results are presented on an idealized system to understand the essential phenomena. Subsequent investigation are carried out on a realistic system using the electromagnetic transients simulation program (PSCAD/EMTDC). The results indicate that is possible to eliminate the dc currents in the transformer using such a scheme.

1.2.5 CHAPTER 6

CONCLUSION

Chapter 2

Description of the Study system

2.1 INTRODUCTION

The main incentive for constructing a hybrid line is to significantly increase the power transfer capability of an existing right–of–way while retaining the power distributing feature of the original ac system. A review of commonly used transmission tower types identified a wood pole 230 kV ac Gulfport structure as representative of the type most likely to be candidate for upgrading, due to the fairly extensive use of this structure throughout North America. Manitoba Hydro, for example, has seven interconnection to Saskatchewan, North Dakota, Minnesota and Ontario with 230 kV Gulfport transmission lines [2], [3]. The Gulfport woodpole structure is shown in Figure 2.1 . The tower is essentially a wood pole "H" frame carrying the conductors in flat formation with the centre phase raised slightly above the outer phases and with lightning protection provided by two overhead shield wires.

Figure 2.2 shows an example of how the existing tower of a gulfport structure can be modified to include two dc conductors and two shield wires in addition to the three conductors of the 230 kV ac transmission circuit. This design was proposed by the Manitoba HVDC Research Centre[3], and takes into account factors such as structural integrity of the tower, electric field effects, insulation clearance and hot line maintenance. The dc circuit can be rated to carry up to 600 MW of power (bipolar operation). This would give a 200% increase in total power carrying capacity of the corridor, based on a maximum capacity of 300 MW for the ac line alone.

Several problems have been addressed in the literature concerning such hybrid lines. These include induction of 60 Hz currents on the dc line from the ac line which can lead to converter transformer

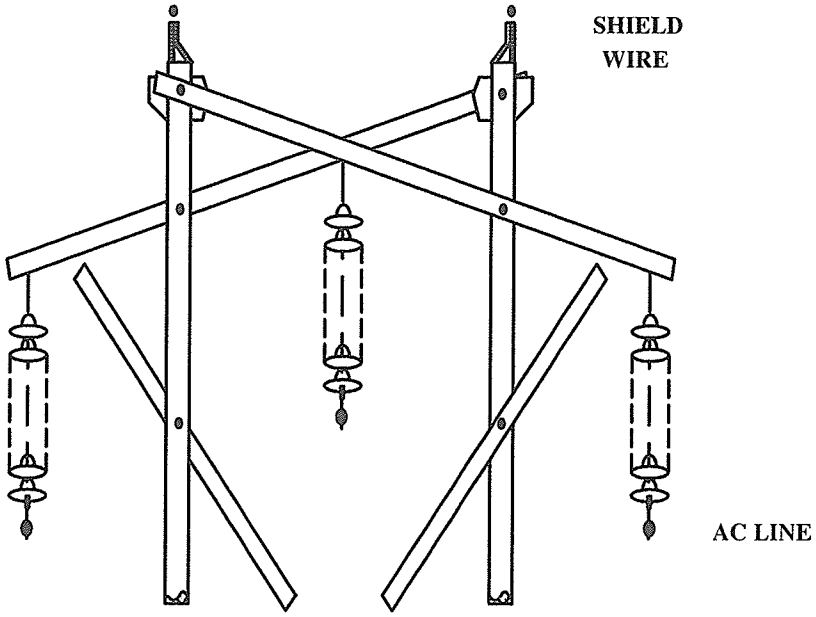

Figure 2 .1 : Gulfport structure [2]

saturation [2], and prolonged clearing times for dc line faults because of secondary induction effects from the ac line [4].

An electromagnetic transient simulation program (PSCAD/EMTDC) was used in the study [7]. The program has the capability of detailed modeling of transmission lines for coupling effects as well as the capability to represent HVDC converters in full detail and to represent transformer saturation nonlinearities. It is important to properly model the dc controls because the overvoltages can be affected by the control response.

2 .2 SELECTION OF THE HYBRID LINE [3]

The limited resources available for this study prohibit extensive examination of many different hybrid line configurations and voltages. Instead, one representative configuration of conductors and voltages is proposed based on responses from a survey of major North American utilities who may be

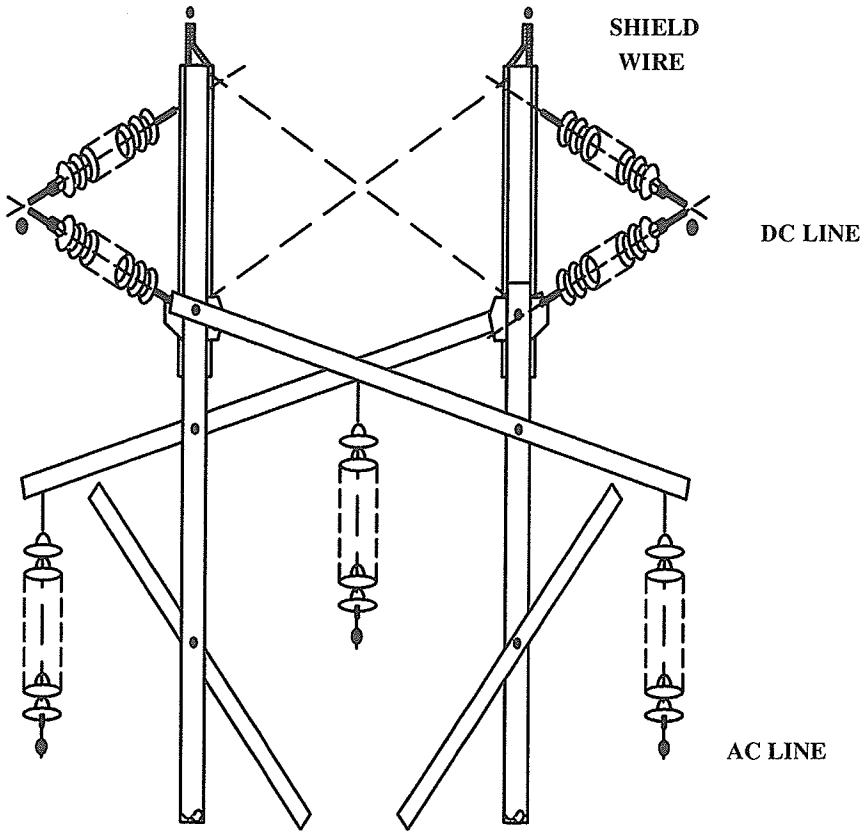

Figure 2 .2 : Modified tower top of a gulfport structure to accommodate the dc line [2]

considering the use of an ac–dc hybrid transmission line. The Manitoba HVDC Research Centre in 1987 undertook such a survey and the results are summarized as follow:

None of the utilities contacted at that time, with the exception of Southern California Edison, were considering adding a dc circuit to an ac circuit or converging an ac circuit to dc. A number of utilities expressed interest in a possible future conversion. Southern California Edison were planing to convert an existing 400 km, 220 kV ac line to dc by having the two outer conductors as the negative pole and adding an extra conductor to the inner phase for the positive pole. Their reasons were partially economic and particularly because of right–of–way considerations.

The New York Power Authority have been studying conversion of existing 230 kV single circuit lines of the wood pole "H" frame type to dc. They did not have a specific project planned but foresaw

pressures based on economics, environmental issues, acquisition of right–of–way and ac system interconnections, all forcing them into looking at dc conversion in the future.

Manitoba Hydro have indicated that the line in their system most likely to be studied with a view to providing increased transmission capacity by converting from ac to dc would be the "H" frame tower gulfport design.

Most of the other utilities contacted agreed that it was feasible to replace or convert ac conductors for dc usage. Alternatively, the addition of dc conductors at the overhead ground wire position was also feasible. However, most of the existing structures are of the single circuit type and not suitable for conversion unless the whole line is taken out of service for extended periods since the conversion cannot be done with the line "hot".

Both Manitoba Hydro and New York Power Authority have indicated that a single circuit 230 kV wood pole line is a good candidate for further study. The New York Power Authority studies have been with "H" frames whereas the Manitoba Hydro line is the similar wood pole "gulfport" structure. Since the latter type of structure is common use throughout North America, it is proposed that the Manitoba Hydro 230 kV gulfport structure be selected as a representative structure for conversion to a hybrid transmission line.

2 .3 MAIN SYSTEM DATA

The study system was adapted from an earlier investigation [3] , and is based on a potential upgrade of an existing tie line between Manitoba Hydro and the Northern United States. The strong sending and receiving end systems (6800 MVA) are typical of this situation.The dc filters include a 12th harmonic filter and a high pass filter.

Figure 2 .3 shows the hybrid ac–dc system modelled in the study. The total transmission distance is 390 km. The ac transmission line is rated at 230 kV, 300 MW and the dc scheme is a bipolar +/– 250 kV, 600 MW transmission system. The tower geometry is as shown in Figure 2 .2 , and an earth resistivities of 100 ohm–m is assumed. Sensitivity studies were also carried out at resistivity of 10 and 1000 ohm–m. The ac filters include a tuned 11th, 13th filter, a high pass filter and, together with a

fixed shunt capacitor, provide 200 Mvar of reactive power. The ac system equivalent has damping angle of 80° and a short circuit capacity of 6800 MVA. The transmission line was divided in five equally spaced locations called TL1, TL2, TL3, TL4, TL5 in between the rectifier and inverter. Each segment represents 65 km. Different types of faults were applied at either the sending or receiving ends or any one of the five equally spaced locations and the overvoltages were measured.

A blocking filter (BF) consisting of a parallel L–C combination was included to limit the flow of 60 Hz current in the dc line. The electrodes and electrode lines were modelled as lumped R–L elements.

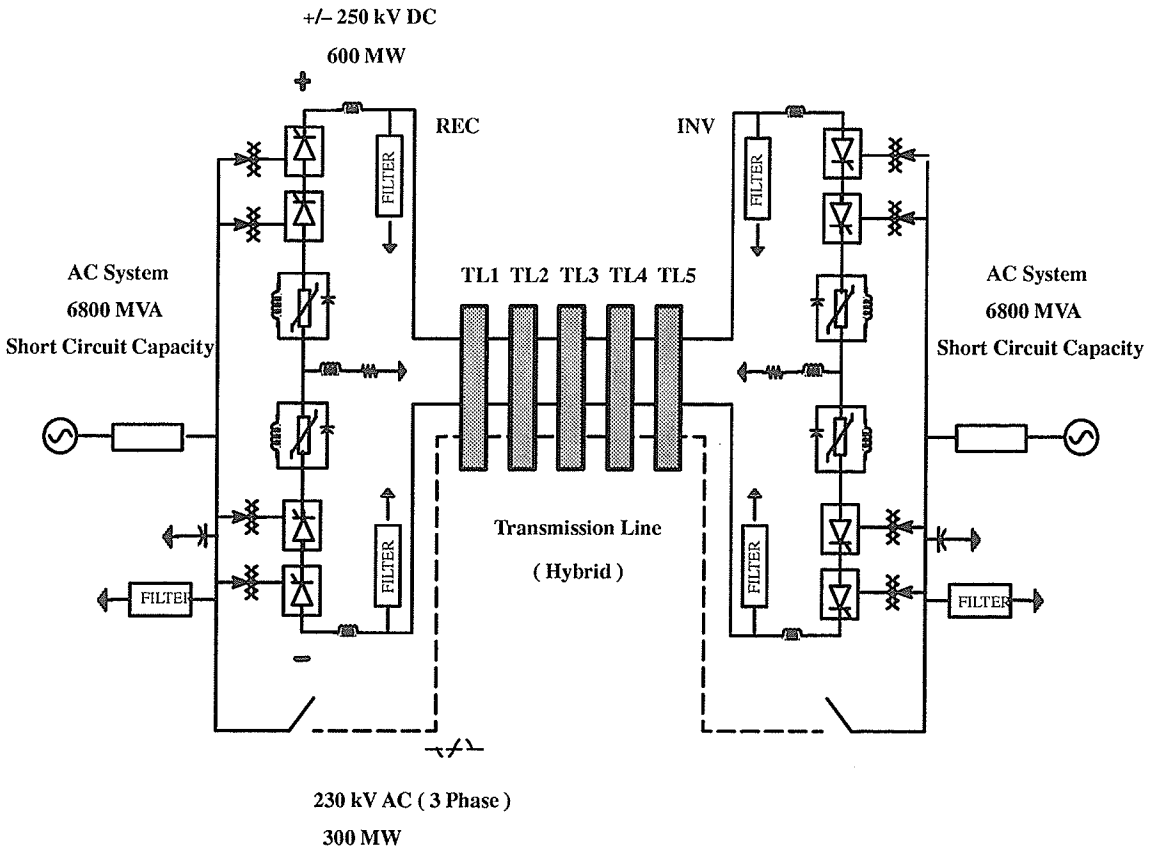

Figure 2 .3 : Simplified single line diagram of the ac–dc hybrid transmission line

2 .4 AC SYSTEM EQUIVALENT

The rated ac voltages at the commutation bus at both the rectifier and inverter were chosen to be 230 kV, line–line, rms at 60 Hz. The relative strength of each ac system compared with dc system capacity may be best quantified by the effective short circuit ratio (ESCR) or the short circuit ratio (SCR) as follows:

$$ESCR = \frac{MVA\ sys - Mvar\ additional}{MW\ dc\ link} \qquad (2.1)$$

$$SCR = \frac{MVA\ sys}{MW\ dc\ link} \qquad (2.2)$$

where at the rectifier and inverter:

MVA sys = Ac system equivalent fault level MVA = 6800 MVA

Mvar additional = Additional Mvar (filters, shunt capacitors) = 200 Mvar

MW dc link = Total dc link MW rating = 600 MW

$$ESCR = \frac{6800.0 - 200.0}{600.0} = 11.0 \qquad (2.3)$$

$$SCR = \frac{6800.0}{600.0} = 11.33 \qquad (2.4)$$

The ac system equivalent circuit shown in Figure 2 .4 was used for both the rectifier and the inverter ac system representation:

The parameters in the equivalent circuit are chosen such that the damping angle of the system equivalent at the fundamental frequency (60 Hz) is equal to 80^0.

The plots of impedance and impedance angle versus frequency for the ac system equivalents (excluding the ac filters) are shown in Figure 2 .5 .

2 .5 AC FILTERS

The rectifier and the inverter each has a total of 150.0 Mvar of filters connected to the ac bus. The 11th and 13th harmonic and high pass filters are each rated at 50.0 Mvar at both ends. At both ends a Cshunt

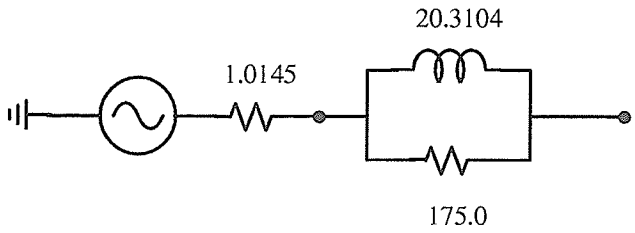

All resistances in Ω and *inductance in mH*

Figure 2 .4 : Ac system equivalent representation.

type filter is provided to make up the remaining 50.0 Mvar. The ac filters parameters are summarized in Figure 2 .6 and Table 2 .1

The impedance and impedance angle versus frequency plots for the entire ac system equivalent (with filters and shunt capacitors included) are shown in Figure 2 .7 .

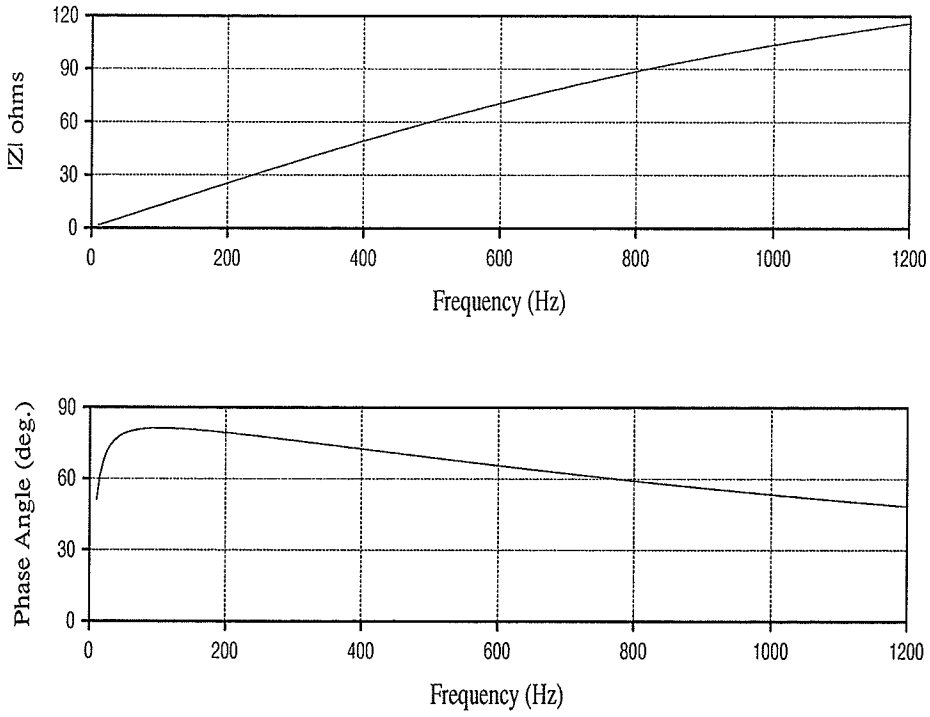

Figure 2 .5 : Ac system equivalent impedance and impedance angle (rectifier and inverter).

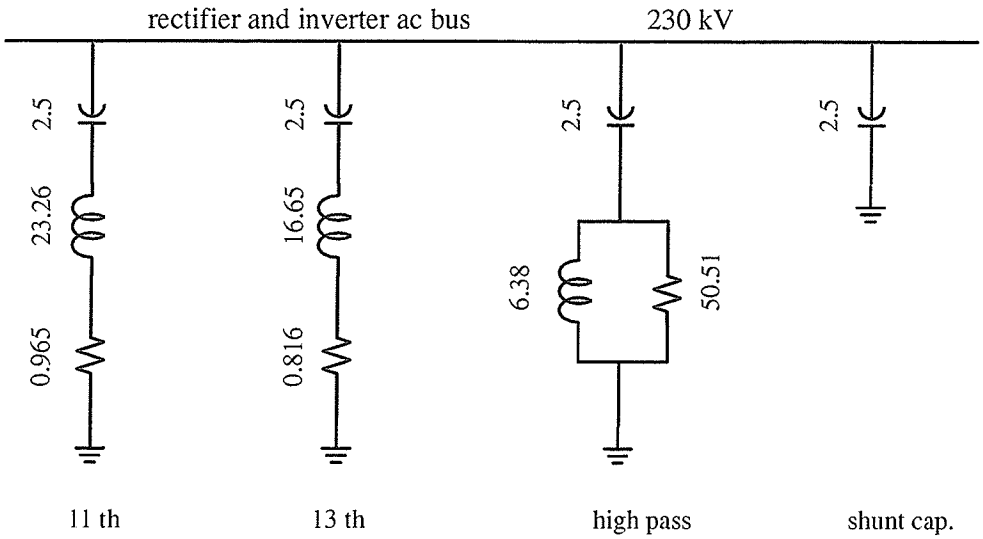

All resistances in Ω, *inductances in mH* and *capacitances in* μF

Figure 2 .6 : Single line diagram of ac filters.

Table 2 .1 : Ac filters data for the rectifier and inverter.

filter	11 th	13 th	hp	Cshunt
Q (Mvar)	50.0	50.0	50.0	50.0
fn (Hz)	660.0	780.0	1260.0	–
Quality factor (fn)	100.0	100.0	1.0	–
C (uF)	2.5	2.5	2.5	2.5
L (mH)	23.26	16.65	6.38	–
R (ohms)	0.965	0.816	50.51	–

2 .6 CONVERTER TRANSFORMERS

The converter transformers consist of three phase two winding units arranged to produce the desired star–star or star–delta configurations required for 12 pulse operation. The converter transformer data is summarized in Table 2 .2 .

Table 2 .2 : Converter Transformer data.

	Rectifier	Inverter
Base MVA rating per three phase unit (MVA)	146.0	143.0
Rated line side line–line voltage (kV rms)	230.0	230.0
Rated valve side line–line voltage (kV rms)	108	97.4
Leakage reactance at nominal tap (%)	13.0	12.6
Air core reactance (p.u.)	0.2	0.2
Knee point voltage at nominal tap (p.u.)	1.25	1.25
In rush decay time constant (s)	1.0	1.0

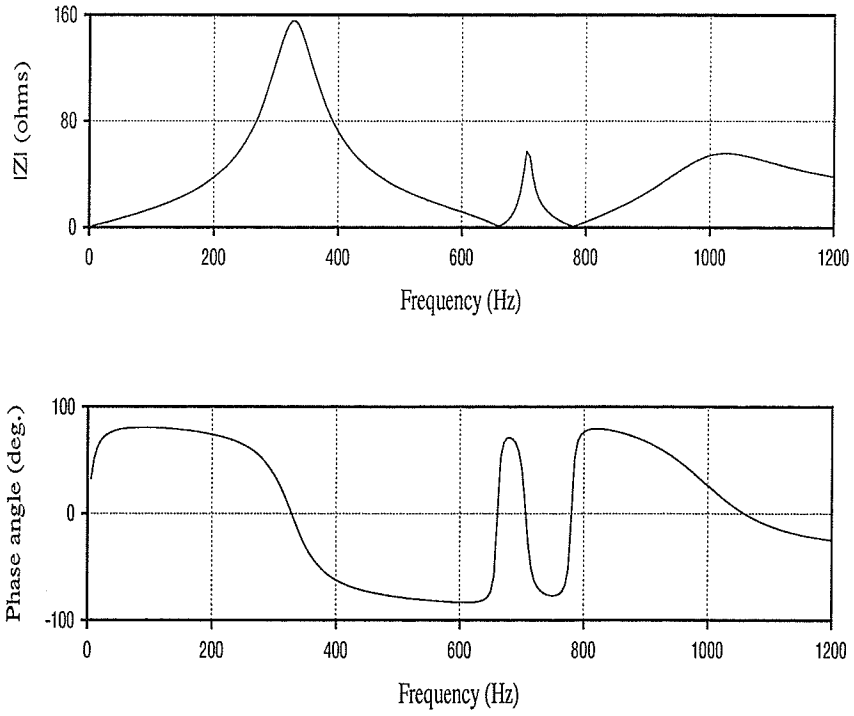

Figure 2 .7 : Impedance plots for the ac system (including filters and shunt capacitors).

2.7 HYBRID AC–DC LINE

The hybrid line is assumed to be 390 km long. The conductor data is summarized in Table 2.3. A ground resistivity of 100 ohm–m was assumed. Details of the transmission line conductor and tower configuration are summarized in Figure 2.8.

Table 2.3 : Transmission line conductor data.

	conductor data						
	ac conductor			dc conductor		ground wire	
	AC	AC	AC	DC	DC	GW	GW
Conductor number	C1	C2	C3	C4	C5	GW1	GW2
Conductor type	chukar	chukar	chukar	chukar	chukar	7/16 steel	7/16 steel
Conductor radius (cm)	1.481	1.481	1.481	1.908	1.908	0.554	0.554
Dc resistance (ohms/km)	0.05906	0.05906	0.05906	0.03576	0.03576	2.79617	2.79617
Height at tower y(m)	8.825	9.925	8.825	11.79	11.79	14.224	14.224
Mid–span height (m)	6.1	7.2	6.1	8.54	8.54	x	x
Horiz. dist. x(m)	0.0	5.486	10.973	–0.264	11.236	2.743	8.23

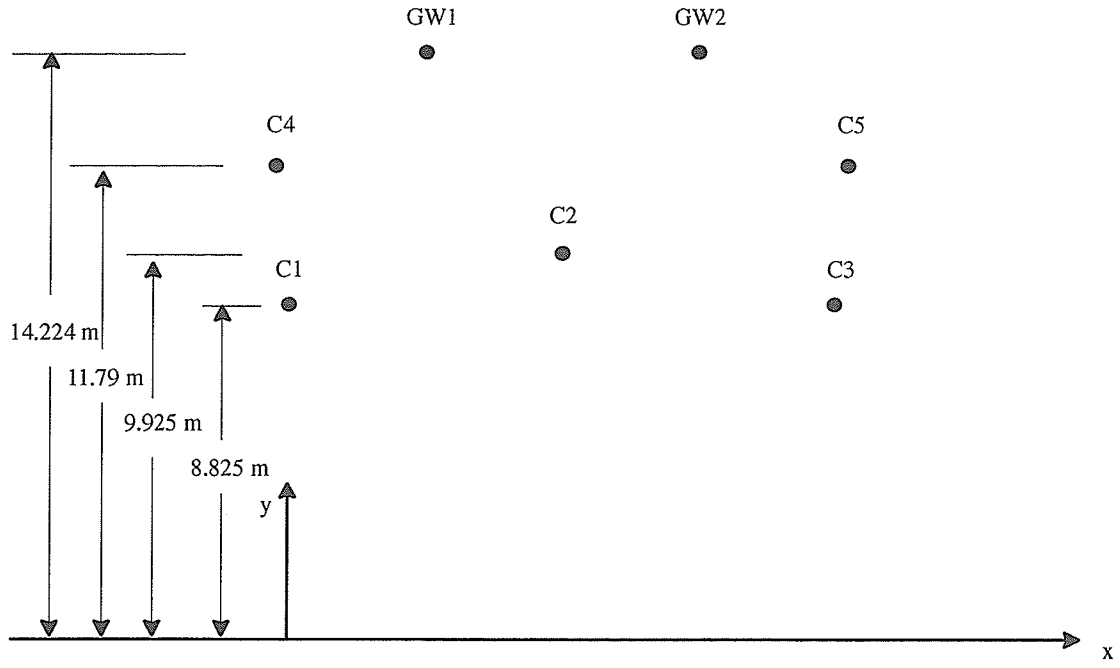

Figure 2.8 : Transmission line conductor configuration.

Earlier work performed by the Manitoba HVDC Research Centre developed conceptual outline for the ac–dc hybrid structure. The main results, related to the Gulfport structure used in this study is described in sections 2 .7 .1 to 2 .7 .5 [8].

2 .7 .1 ADDITIONAL POWER PROVIDED BY THE DC BIPOLE [8]

The 230 kV Gulport line would normally be expected to carry approximately 300 MW. Table 2 .4 shows that by adding the dc bipole to the Gulport structure, the power that is presently carried would be more than doubled. If it is assumed that there is always some wind present, the normal ampacity at 40^{0}C with sun present, is 1216 A which at ± 250 kV gives a power level of 608 MW, an increase of 200% over the present level of the 230 kV line.

Table 2 .4 : Power provided by the dc bipole.

voltage +/– 250 kV, conductor 1 x 1.908 radius per pole						
N = Normal E = Emergency Y = Yes N = not						
sun	amb. t.	wind speed	ampacity		power level	
	(^{0}C)	(m/s)	N	E	N	E
			80^{0}C	95^{0}C	80^{0}C	95^{0}C
Y	40	0.0	881	1141	440	570
N	40	0.0	1105	1314	553	657
Y	**40**	**0.61**	**1216**	**1463**	**608**	**732**
N	40	0.61	1386	1601	693	800
Y	50	0.0	669	985	335	492
N	50	0.0	944	1180	472	590
Y	50	0.61	1006	1302	503	651
N	50	0.61	1207	1455	603	728

2.7.2 ELECTRICAL EFFECTS FROM THE HYBRID LINE [8]

The electrical effects from the hybrid line on the Gulport structure have been assessed based on separate calculations for the ac and dc circuits respectively, i.e. the effects from the ac circuit were calculated ignoring the dc circuit and vice verse. The calculated values of conductor surface gradient, electric field, radio interference (RI) and audible noise (AN) for the separate ac and dc circuits are shown in Table 2.5.

Table 2.5 : Calculated electrical effects

230 kV AC Circuit Only			
Phase spacing 5.5 m, conductor 1 x 1.481 radius, mid–span height 6.1 m			
Maximum Conductor Gradient	Maximum Electric Field	RI at 1 MHz (15m from outer phase) Fair–Maximum	AN (at edge of ROW, 15m from centre line) Rain–L50 dB (A)
(kV/cm)	(kV/m)	dB(μV/m)	dB(A)
16.60	5.3	42.3	46.5
Generally Accepted Limits: (Based on current practice) [12]		48.0	52.0

+/– 250 kV DC Circuit Only				
conductor 1 x 1.908 radius, mid–span height 8.54 m				
Maximum Conductor Gradient	Maximum Nominal Electric Field	Maximum Total Electric Field	RI at 1 MHz (15m from outer phase) Fair–Maximum	AN (at edge of ROW, 15m from centre line) Rain–L50
(kV/cm)	(kV/m)	(kV/m)	dB(μV/m)	dB(A)
21.14	6.18	16.2	49.2	31.9
Generally Accepted (Recommended Limits:) [12]		30.0	52.0	52.0

Based on references [9] [10] it can be predicted that the principle effect of the hybrid arrangement, with the dc circuit above the ac circuit, will be to increase the maximum conductor surface gradient on

the ac conductors with resultant increase in RI and AN. The ac circuit will provide a significant screening effect on the dc electric field, ion current and charge densities at ground level and no problem is expected from the dc line electrical effects.

Examination of Table 2 .5 shows that for the ac circuit there is a margin of nearly 6 dB(μV/m) between the calculated fair weather maximum RI, 42.3 dB(μV/m), and the recommended limit of 48.0 dB (μV/m) for this weather condition and 230 kV voltage class [11] [12]. The calculated AN also has a nearly 6 dB(A) margin between the calculated rainy weather L50 value (46.5 dB(A)) and the recommended limit of 52 dB(A) [13] [14] [15].

Table 2 .5 indicates that ± 250 kV is marginally acceptable with the proposed arrangement but further studies should be carried out, particularly on the RI and AN from the ac circuit.

2 .7 .3 INSULATION [8]

Insulation for the dc line to be added to the Gulfport structure has been based on an insulator arrangement proposed for special applications on another HVDC project. The arrangement is, in essence, an insulated crossarm with the strut portion composed of a solid post type insulator and tie portion composed of normal cap and pin type insulators. The dimensions presented in Table 2 .3 are based upon light contamination levels requiring a specific creep factor of only 23 mm/kV.

2 .7 .4 HOT LINE CONSTRUCTION AND MAINTENANCE [8]

With the Gulfport structure, the fact that the dc conductors are located almost directly above the outer conductors of the ac circuit makes it extremely difficult to install the dc conductors while the ac circuit is live. The new pole top arrangement could be lifted into place either with a tall crane or by helicopter, however, the dc conductors would need to be lifted into place under tension in order for the dc conductor sags to match the sags of the ac conductors and this could prove extremely difficult. It is considered unlikely that it would be possible to install the dc conductors while the ac circuit is live.

Hot line maintenance aspects of the Gulport hybrid arrangement were discussed with Manitoba Hydro. No major difficulties are foreseen in being able to carry out maintenance on either the ac or dc circuits while the lines are live.

2 .7 .5 LIGHTNING PERFORMANCE OF HYBRID LINE [8]

The conceptual arrangements for the hybrid ac–dc towers that are considered in this report retain the use of overhead shield wires on the structures. The dc circuit is located above the existing 230 kV ac circuit and the overhead shield wires are raised about 2.4m.

With this arrangement, the ac circuit is shielded by both the dc circuit and the overhead shield wires and hence the probability of direct lightning strokes to the ac conductors will be reduced. The probability of back–flashovers from the ac circuit to the ground lead on the structure may increase slightly due to the greater height of the overhead shield wires, but the increase is expected to be small or negligible. On an overall basis, the lightning performance of the ac circuit should be improved.

The dc circuit will be shielded by the overhead shield wires. The shielded angle will be about 51 degrees. With this relatively large shielding angle, there would likely be a significant number of direct lightning strokes to the dc circuit. However, this should be acceptable because of the relatively small disturbance to the ac system caused by the dc line monopolar faults and the rapid restart capability of a dc system.

2 .8 ELECTRODE LINE PARAMETERS

The electrode lines at each end were modelled as lumped R–L elements, terminating in ground electrodes with 0.1 ohms grounding resistance as shown in Figure 2 .9 .

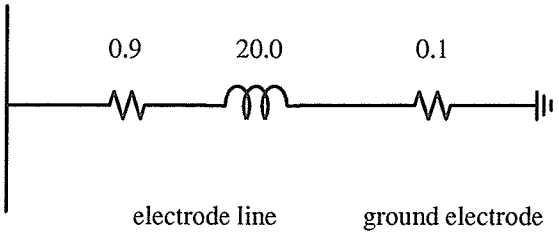

resistance in Ω and *inductance in mH*

Figure 2 .9 : Electrode line and ground electrode.

2 .9 DC FILTERS

The filters at each end of the dc line consists of a 12th harmonic filter and a high pass filter tuned to the 24th harmonic frequency. The components and parameters of the filters at each end are summarized in Figure 2 .10 .

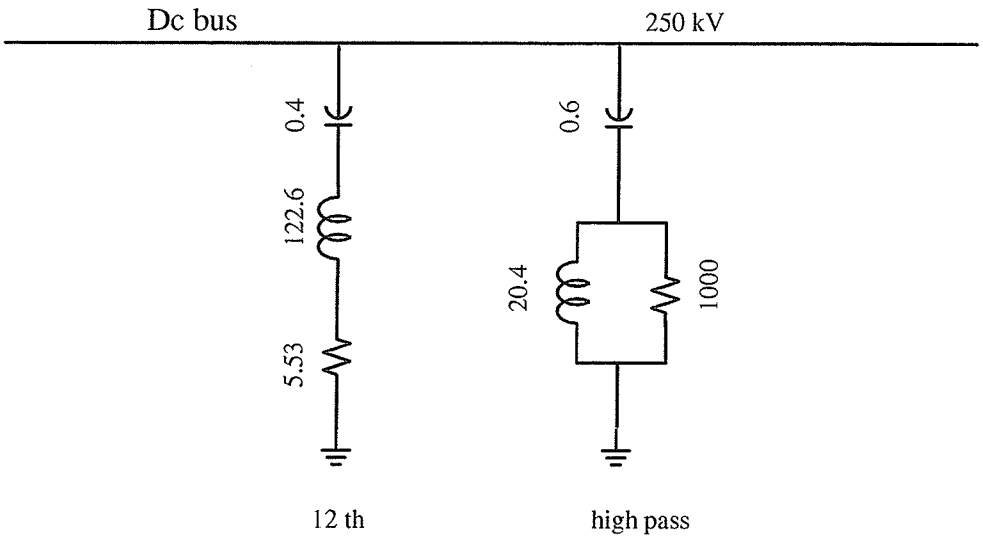

All resistances in Ω, *inductances in mH* and *capacitances in* μF

Figure 2 .10 : Single line diagram of dc filters.

2 .10 THYRISTOR VALVES

The thyristor valves for the bipole are arranged in two 12 pulse poles. The basic components and parameters of the valve are summarized in Figure 2 .11 .

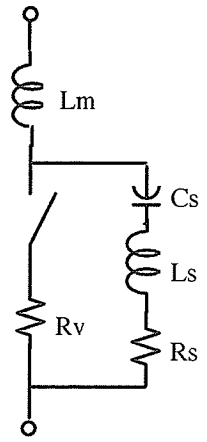

Figure 2 .11 : Thyristor valve components.

Table 2 .6 : Thyristor valve components.

Snubber resistance Rs (ohms)	5000.0
Snubber capacitance Cs (μF)	0.05
Snubber inductance Ls (mH)	1.0
Valve reactor inductance (at rated current) Lm (mH)	1.0
Valve ON resistance Rv (ohms)	0.01
Valve OFF resistance (ohms)	1.0E6
Forward voltage drop (kV)	0.001
Forward breakover voltage (kV)	1.0E5

2 .11 BLOCKING FILTERS (BF)

A blocking filter (BF) consisting of a parallel L–C combination was included to limit the flow of 60 Hz current in the dc line. The blocking filters were simulated with quality factors for the inductance equal to 200. Blocking filter as shown in Figure 2 .12 was used in the converter station, at both ends. A 39 kV rated metal oxide arrester was installed in order to protect the blocking filter against overvoltage. Figure 2 .13 shows a curve of the blocking filter impedance |Z| and phase angle versus frequency without the arrester.

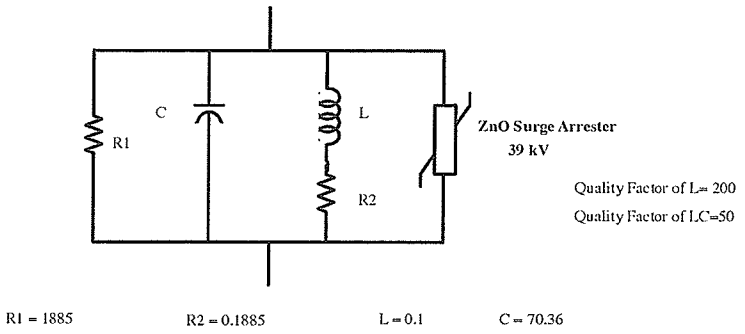

All resistances in Ω, *inductances in H* and *capacitances in* μF

Figure 2 .12 : Blocking filter design.

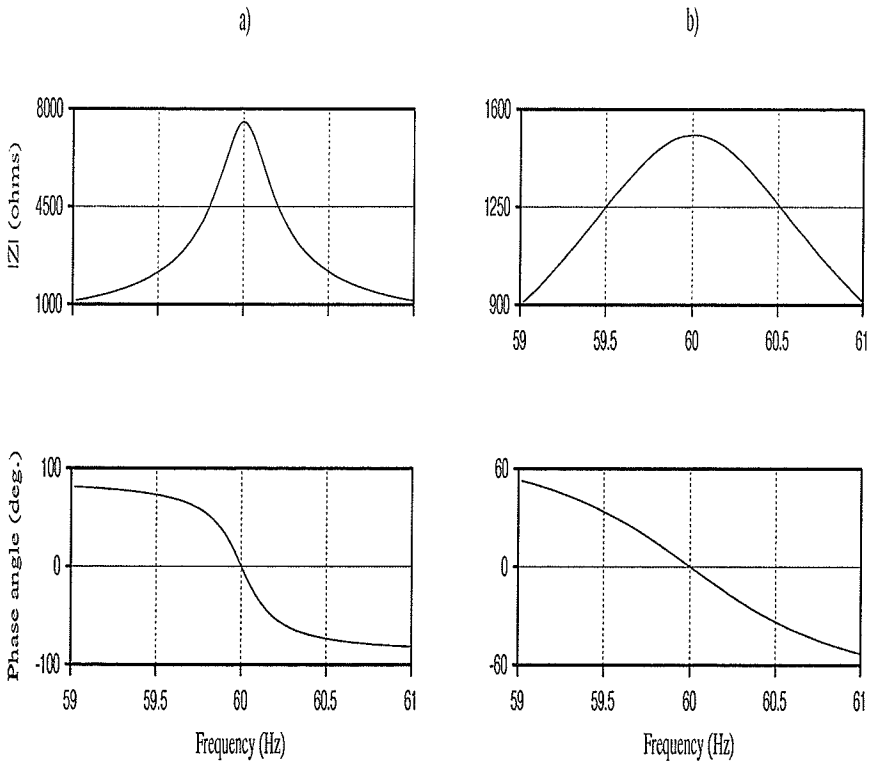

Figure 2 .13 : Impedance plots for the blocking filter.

a) without the resistor R1

b) with the resistor R1

2 .12 OTHER CONVERTER EQUIPMENT

The smoothing reactor at each end of the dc line consist of air core reactors, each of 0.5 H.

2 .13 DC CONTROLS

The control system for the HVDC converter is shown in Figure 2 .14 and was modified from that proposed in the first CIGRE benchmark model [16]. The basic control system has a current control path which generates a firing angle order that attempts to keep the measured current equal to the ordered current. This mode of control is normally active at the rectifier. The ordered current is effectively reduced during dc undervoltage conditions via a signal from the voltage dependent current limit (Vdc). The firing angle order is generated as the output of a proportional–integral (PI) type controller which ensures zero steady–state error. The inverse cosine nonlinear block linearizes the relationship between current error and the converter dc voltage.

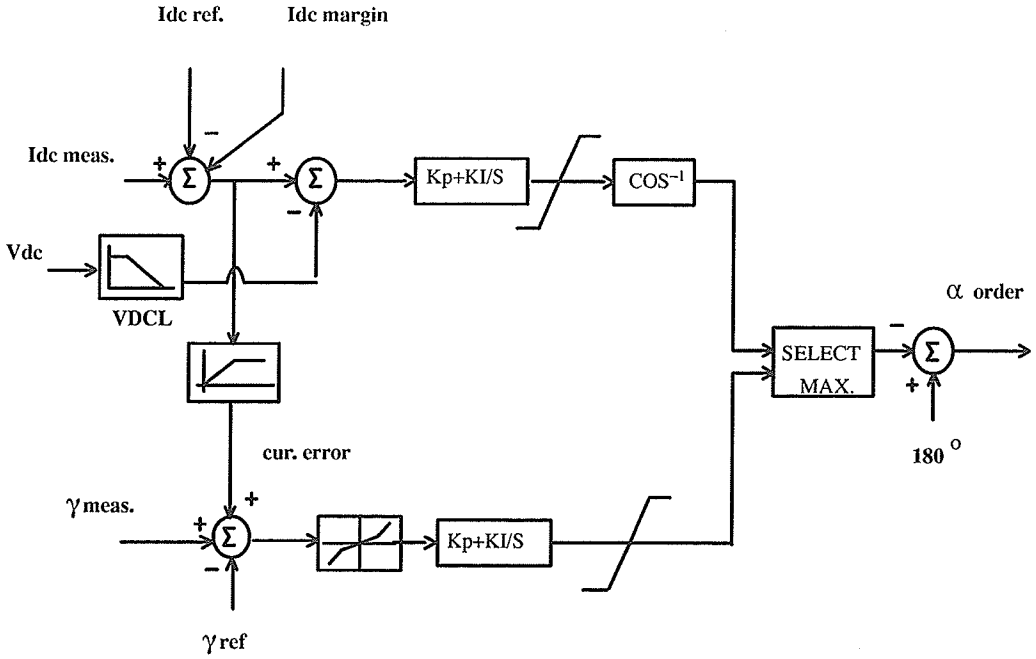

Figure 2 .14 : Simplified dc control diagram.

A second path regulates the extinction angle (γ) of the the inverter to a set reference value (γ ref) by generating a firing angle order using PI control. This mode is normally active at the inverter. The γ ref

value can be effectively increased for a current less than the ordered current by means of the current error signal . The actual selection between the current control and the extinction angle control paths is achieved by selecting the smaller of the two firing angle orders. (Note: The inputs to the "Select Max" block in Figure 2 .14 are actually $\beta=180^{o}-\alpha$, so the minimum α is selected by choosing the maximum β).

2 .14 SINGLE LINE DIAGRAM OF THE HYBRID AC–DC SYSTEM

A single line diagram of this study system with the main components is shown in Figure 2 .15 .

2 .15 INITIALIZATION OF THE SIMULATION (WAVEFORMS)

Figure 2 .16 and 2 .17 show the waveforms of the hybrid ac–dc system during the initialization of the simulation and during the steady state, respectively. The load flow was calculated using a MATHCAD program. The voltage and phase at both ac source ends and the adjust of the tap of the transformers are described below.

$VREC = 245kV \measuredangle 45^{0}$

$VINV = 238kV \measuredangle -10^{0}$

$Tap\ REC = 1.05$

$Tap\ INV = 1.0$

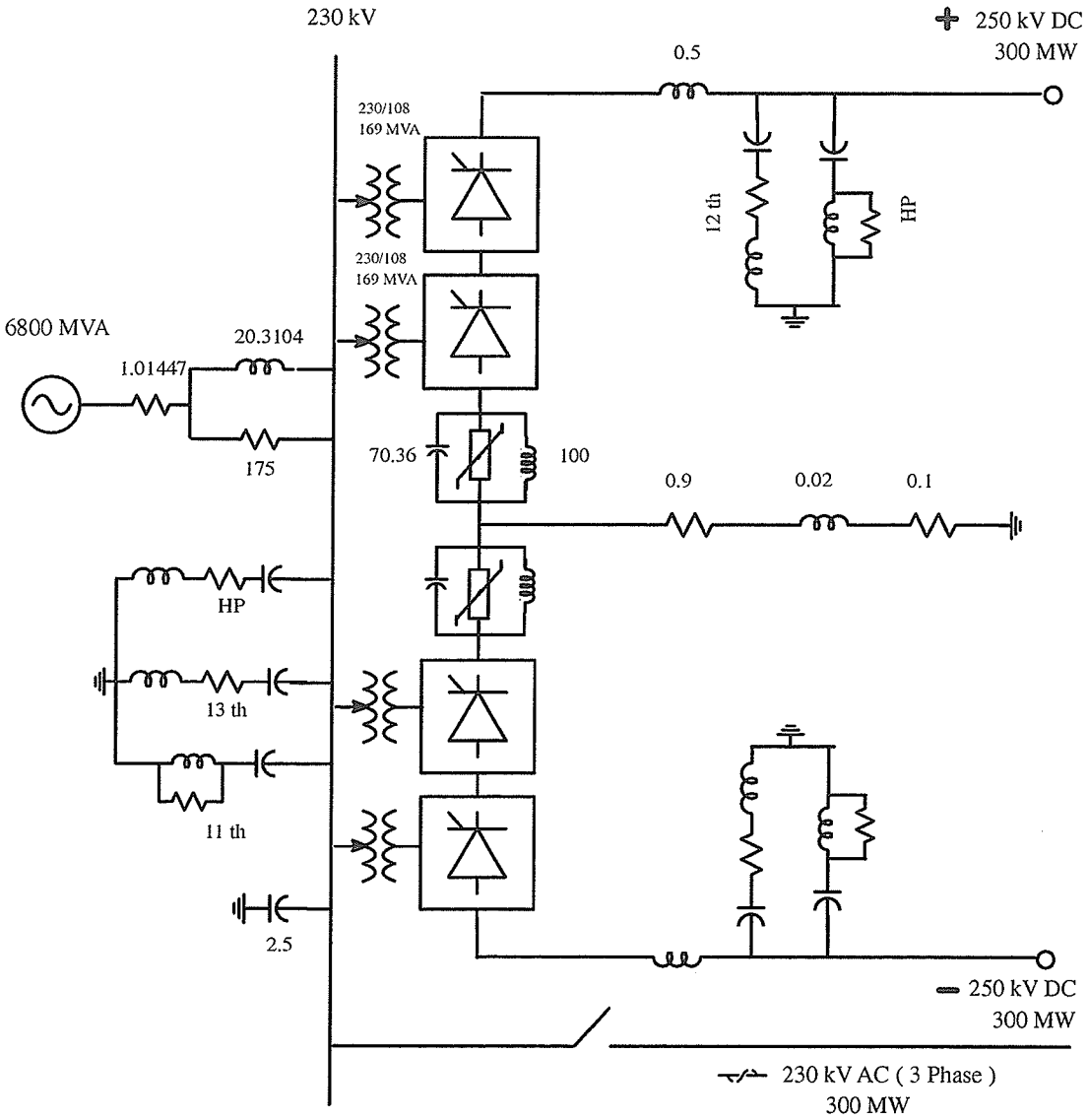

All resistances in Ω, *inductances in mH* and *capacitances in μF*

Figure 2 .15 : Single line diagram of the system studied (Rectifier and Inverter).

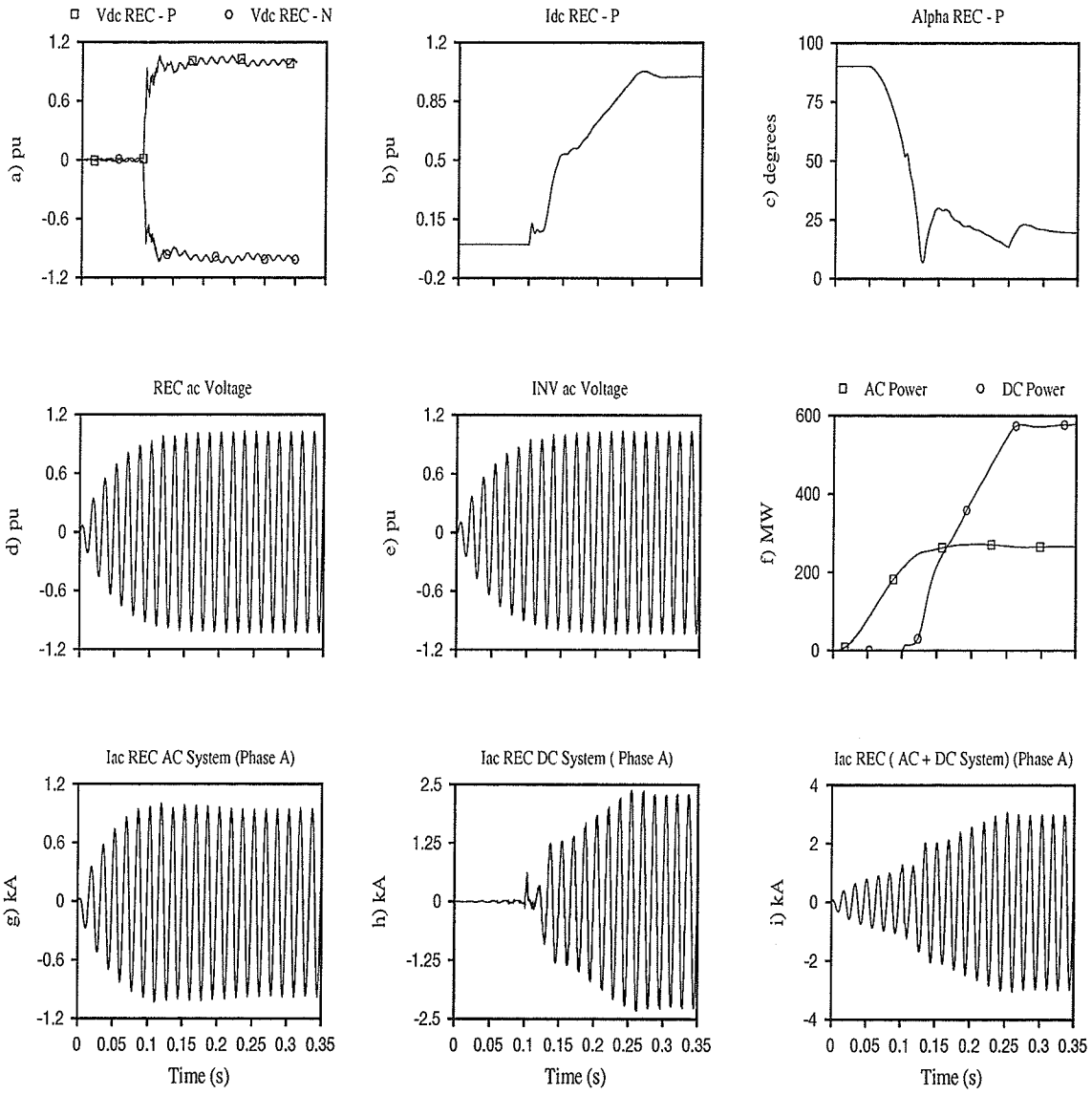

Figure 2 .16 : Waveforms of the hybrid ac–dc system during the initialization of the simulation.

a) Dc voltage at rectifier positive and negative pole

b) Dc current at rectifier positive pole

c) Alpha order rectifier positive pole

d) Rectifier ac voltage phase a

e) Inverter ac voltage phase a

f) Ac and dc power at rectifier

g) Rectifier ac current phase a (ac system)

h) Rectifier ac current phase a (dc system)

i) Rectifier ac current phase a (ac + dc system)

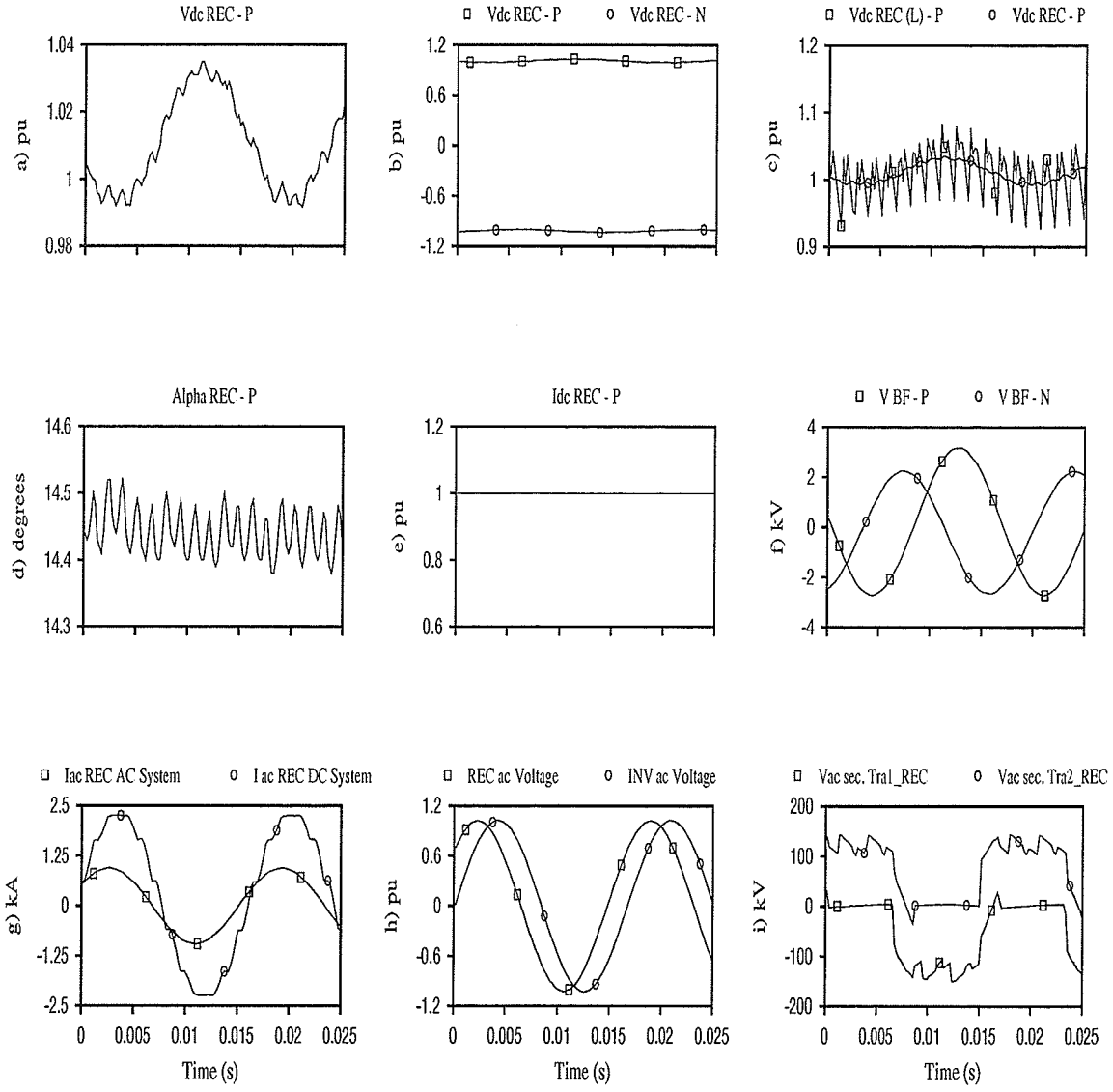

Figure 2 .17 : Waveforms of the hybrid ac–dc system in steady state.

a , b) Dc voltage at rectifier

c) Dc voltage at rectifier positive pole, before and after the smoothing reactor

d) Alpha order rectifier positive pole

e) Dc current at rectifier positive pole

f) Voltage across the blocking filter

g) Rectifier ac current phase a (ac and dc system)

h) Rectifier and inverter ac voltage phase a

i) Voltage on the secondary of the converter transformer

Chapter 3

Overvoltages Studies

The study was conducted primarily to evaluate voltage profiles along the ac–dc hybrid line for ac and dc line faults of different types and at a number of different locations. During the course of the study it was discovered that in some of the original study data was inappropriate as it resulted in a sharply tuned resonance on the dc line which lead to high overvoltages on the dc line during single line to ground ac faults. It was also observed that during ac–dc contact faults there were high fundamental frequency overvoltages on the blocking filters. Even after fault clearing these overvoltages were very poorly damped. Remedial measures were investigated and verified using digital simulation [17], [18].

3 .1 SECOND HARMONIC OVERVOLTAGE

3 .1 .1 RESONANCES

The originally selected value for the smoothing reactor (L) resulted in excessive 2^{nd} harmonic overvoltage on the dc side when the ac system was subjected to a single line to ground fault. Figure 3 .1 shows a plot of the dc line voltage during this condition. Such a fault introduces a 2^{nd} harmonic component in the dc current and can cause excessive harmonic overvoltages if a resonance condition exists at the corresponding harmonic frequency.

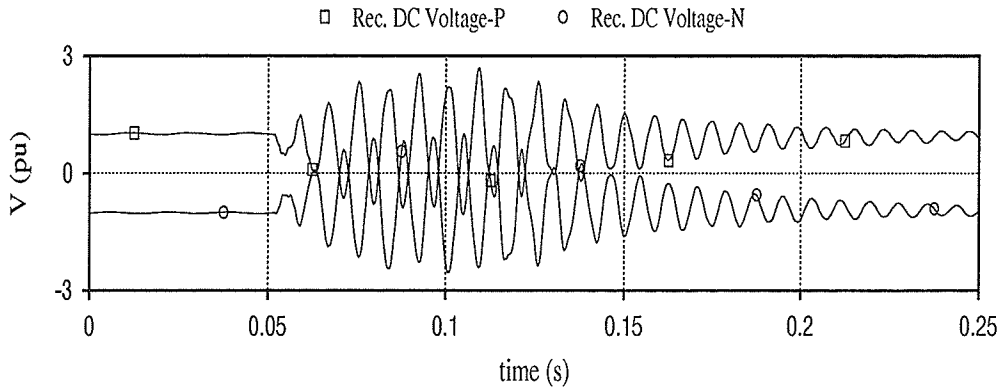

Figure 3 .1 : 2nd harmonic overvoltage on the dc line for an ac single line to ground fault, L=0.5 H.

This indicated that the original selection of component values was not appropriate. A frequency scan of the dc network was performed by isolating the dc transmission line at the rectifier end and exciting it with a train of impulses. It was found that the combination of the smoothing reactance, the line and the dc filters resonanted at a frequency very close to 120 Hz.

The smoothing reactor, at both ends of the converter was changed in order to find an appropriate value which gives lower 2nd harmonic overvoltage in the dc system when the ac system was subjected to a single line to ground fault.

Figure 3 .2 shows a simplified diagram of the hybrid ac–dc system used in performing the frequency scan. A train of impulse, represented by a voltage source, was applied at the rectifier side. The current flowing into the dc transmission line was measured by an ammeter. The smoothing reactors (L) and the dc filters at both ends and the hybrid ac–dc transmission line were represented in the circuit. The dc line at the inverter end and the ac line were short circuited by a resistance of very small value, R=0.01 ohm.

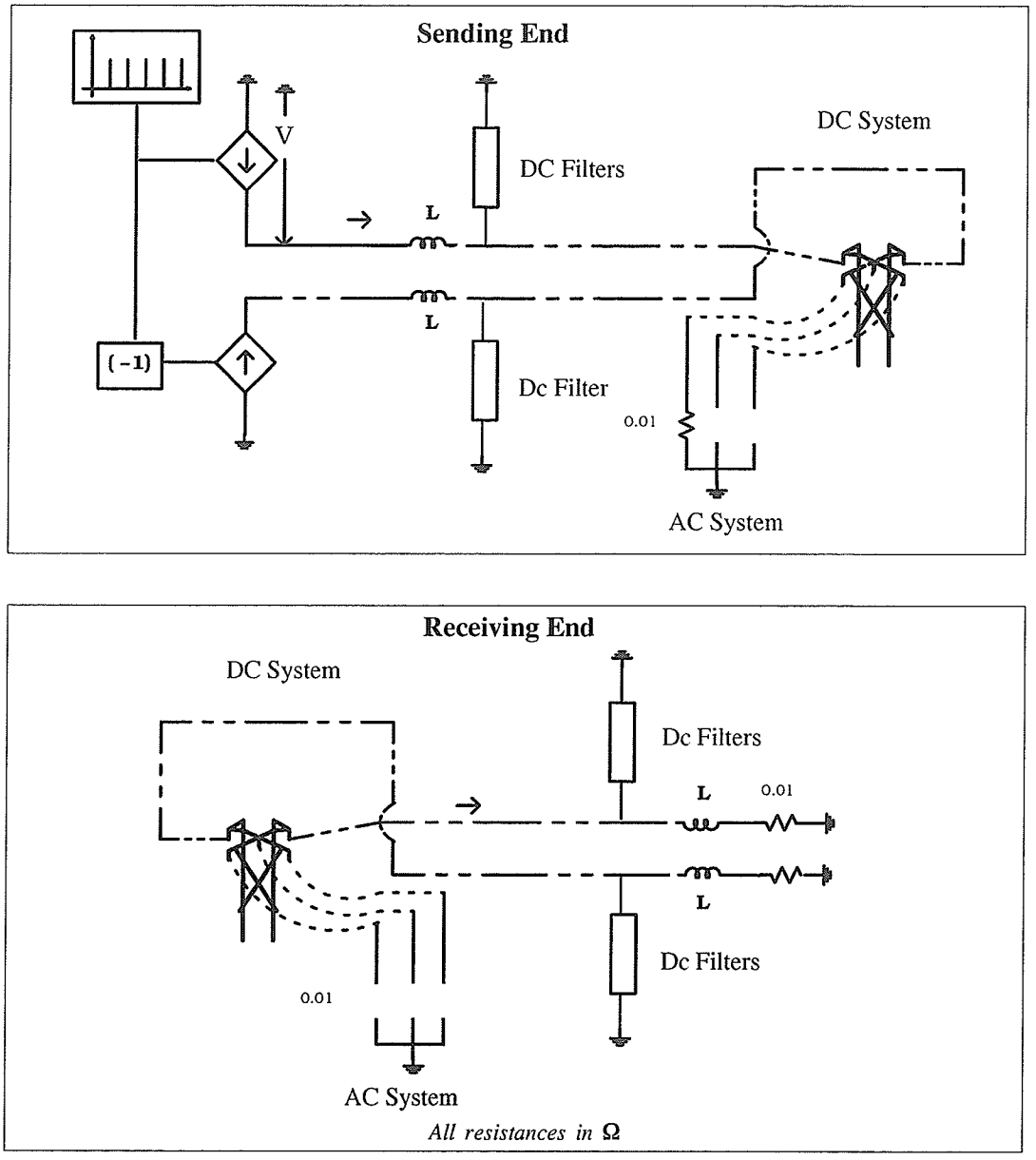

Figure 3 .2 : Frequency scan of the ac–dc hybrid system.

A fourier analyses of the relation V/I was performed for different values of inductance (L) of the smoothing reactor. Figure 3 .3 shows the result of the resonance frequency of the dc system as a function of the inductance (L). In order to reduce the overvoltage on the dc line the inductance of smoothing reactor was chosen to shift the resonance point towards the 3rd harmonic frequency. Therefor the inductance of 0.25 H was selected. Figure 3 .4 shows the results of overvoltages on the

dc line when a single line to ground fault was applied at the rectifier for different values of inductance of the smoothing reactor.

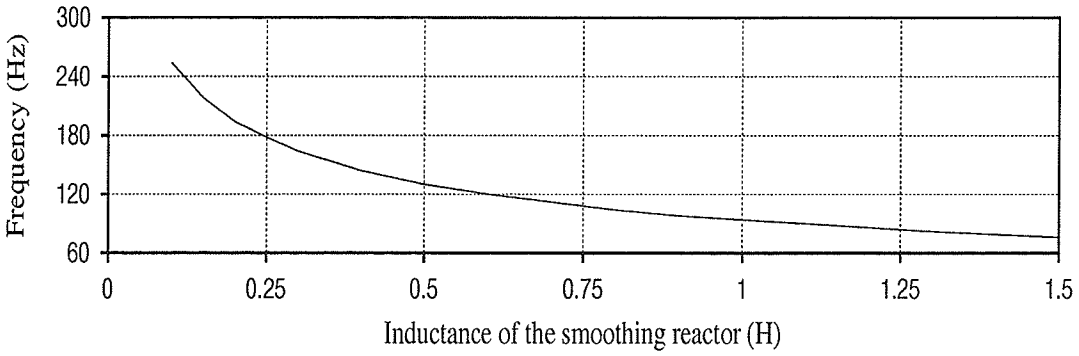

Figure 3 .3 : Resonant frequency as function of the smoothing reactor inductance.

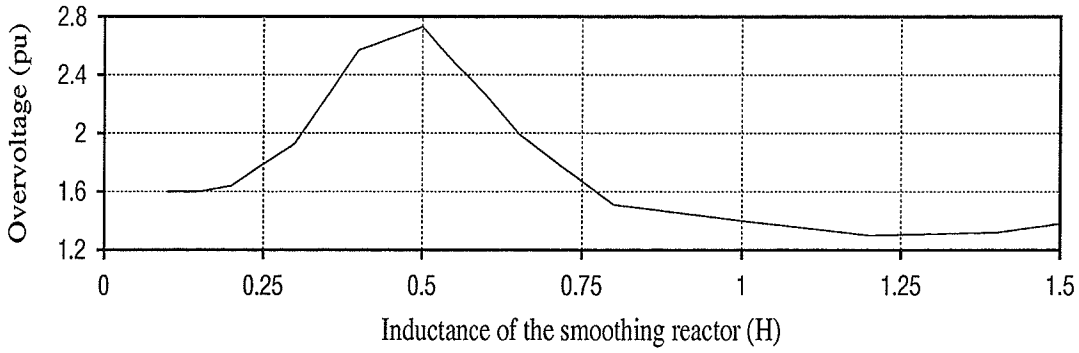

Figure 3 .4 : Dc line overvoltages for single line to ground fault, for different values of inductance.

Subsequent simulations showed that the 2nd harmonic overvoltage was greatly reduced, as shown in Figure 3 .5 .

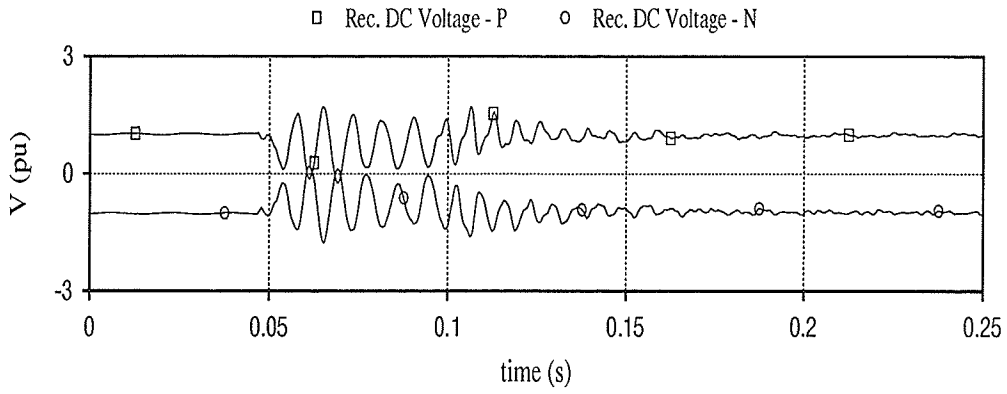

Figure 3 .5 : 2nd harmonic overvoltage on the dc line for an ac single line to ground fault, L= 0.25 H.

The inductance of such a reactor is usually determined from two main considerations [20]:

a) to prevent consequent commutation failures in the inverter by limiting the rate of increase of direct current during commutation in one bridge when the direct voltage of another bridge collapses.

b) to smooth the ripple in the direct current sufficiently to prevent the current from becoming discontinuous or almost so at light loads.

Practically speaking, then, a smoothing reactor is always required, and its inductance is the principal factor limiting the rate of rise of direct current.

When the inductance was reduced from 0.25 H there was a problem of commutation failure. This problem was solved by making a modification in the control system. A delay filter was added to the input of control system, for the following parameters: the measured current in the rectifier and inverter; gamma measurement in the inverter and middle voltage of the dc line.

3 .1 .2 SECOND HARMONIC OVERVOLTAGE VERSUS COUPLING EFFECT

A single line to ground fault applied on the ac system generates 2nd harmonic overvoltages on the dc system as we have seen in the previous section. In this section we are going to evaluate the influence of the coupling effect between the ac line on the dc line in this 2nd harmonic overvoltage.

In order to investigate this overvoltage on the dc line a study was conducted on four system configurations as shown in Figure 3 .6 and described below.

a) hybrid ac–dc configuration and same ac source;

b) ac and dc line share the same sending and receiving end systems with the ac and dc lines not electromagnetically coupled;

c) ac and dc lines ending in different ac systems but sharing the same right of way with the ac and dc lines electromagnetically coupled;

d) dc line without any parallel ac line.

Figure 3 .7 and 3 .8 show the results of the maximum dc overvoltages recorded any where along the line for an ac single line to ground fault applied at each locations REC, TL1, TL3, TL4, TL5 and INV. Faults were simulated at time intervals of 24^0 of inception point of the fault in one period ($360^0/24^0$=15 fault inception points) and the maximum overvoltage at any of the measuring locations was recorded. Figure 3 .7 a) shows the maximum overvoltage for each fault applied, 15 faults were applied per location, and consequently 105 faults were applied along the line (REC, TL1, TL2,... INV). Figure 3 .7 b) shows the enlargement of Figure 3 .7 a) (only for the fault applied at the rectifier location). The numbers 1,2,3,...15 on x axis in Figure 3 .7 b) represent the points of fault inception along of one period of sinewave (1/60 s).

In case D the fault is only applied at the rectifier or inverter ends as there is no ac line along which to move the fault position. Hence only the REC and INV locations have bars for case D in Figure 3 .8 .

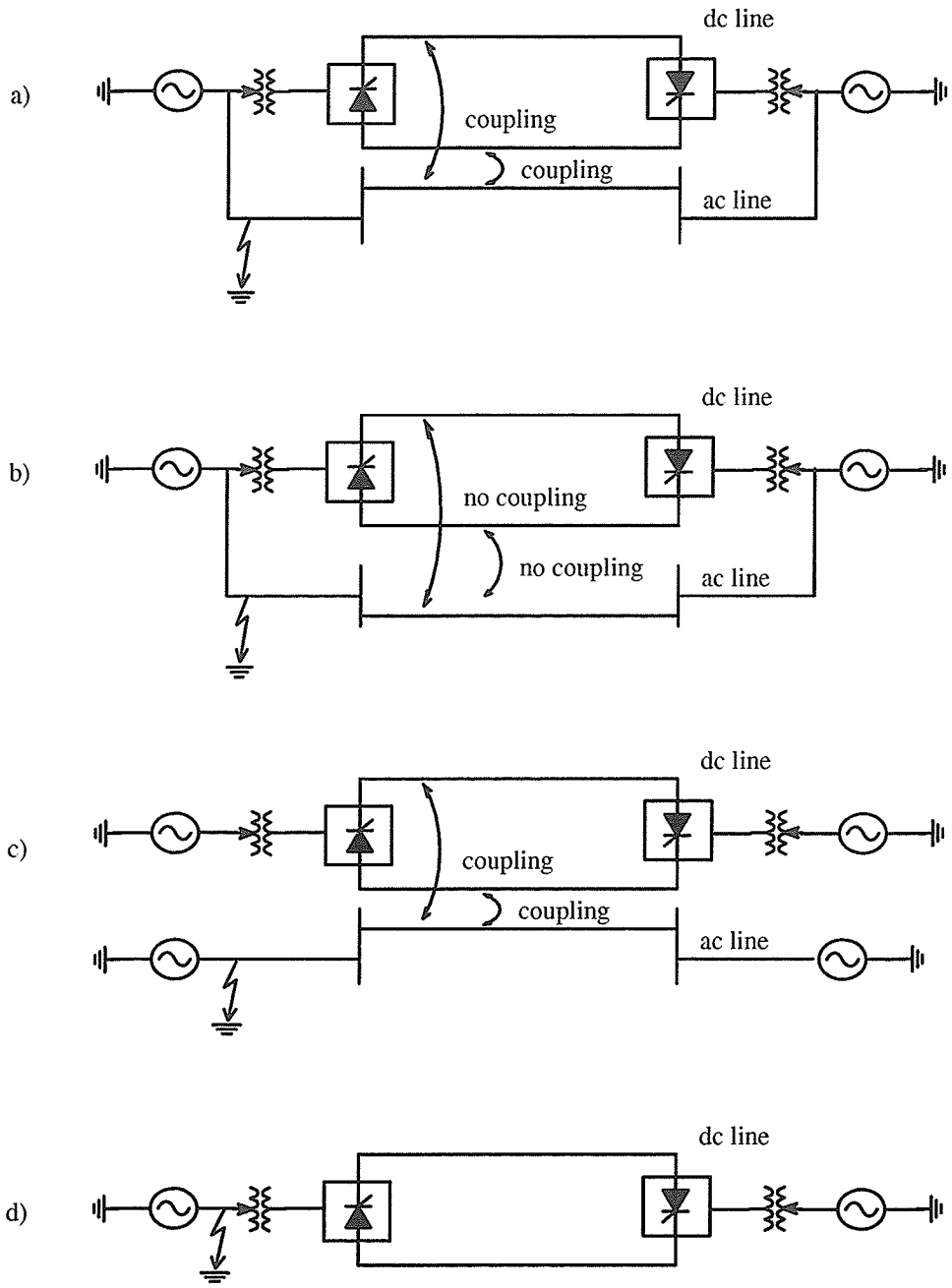

Figure 3 .6 : System configurations for ac single line to ground fault.

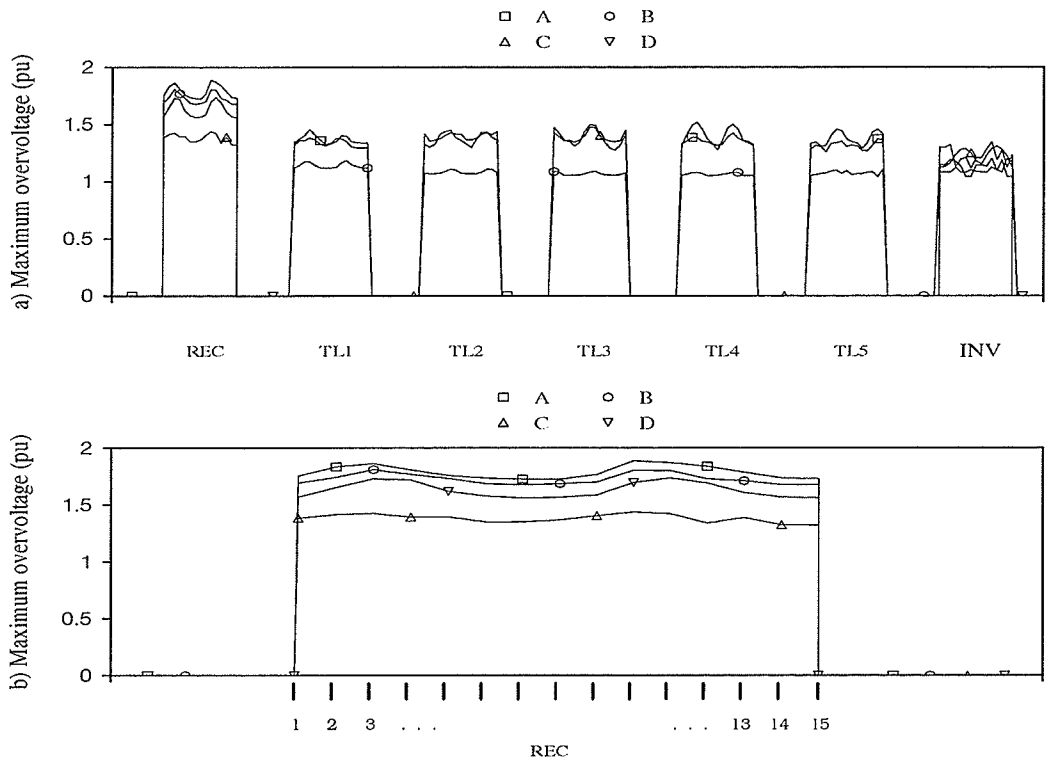

Figure 3 .7 : Maximum dc line overvoltage recorded any where along the line for an ac single line to ground fault for different system configurations, a)Location where the fault was applied along the line (15 points of fault inception/location), b)Enlargement of Figure a) above (only for the REC location).

A – Ac line transposed and with coupling

B – Ac and dc lines are not electromagnetically coupled

C – Ac and dc sources are independent (ac–dc line coupled)

D – Only dc line

After an investigation of the overvoltage on the dc line for ac single line to ground fault the following conclusions can be made:

a) For the case A , B and D where the ac source supplies both the current fault and dc converter there is always a 2nd harmonic overvoltage on the dc line when the ac single line to ground fault is applied at the rectifier side. The reason for the 2nd harmonic overvoltage is due to the negative–sequence voltage component generated at the rectifier side during the fault. The overvoltages for faults at other line locations (TL1, TL2, ... etc.) are mainly fundamental frequency overvoltages and because of the

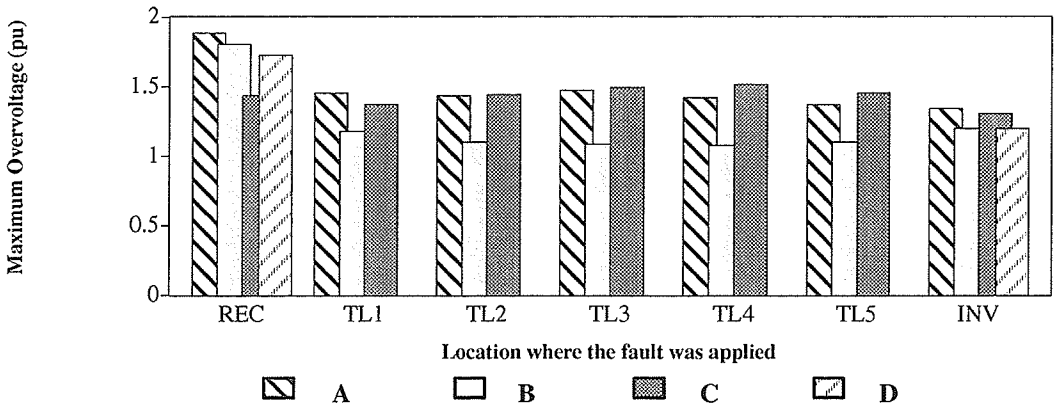

Figure 3 .8 : Maximum dc line overvoltage profile for ac single line to ground fault.

line coupling, this fundamental frequency overvoltage does exist (and in fact is largest at locations TL2 through TL5) for case C. However the maximum overvoltages are relatively low.

b) For case B the overvoltage along the dc line is much smaller compared to the other cases because there is no coupling effect between the ac and dc lines. Only for the fault applied at the rectifier, the overvoltages are almost the same as in the other cases because in this situation the overvoltage is principally 2nd harmonic overvoltage.

c) In the case C there is no significant negative–sequence voltage component on the converter bus due to the lack of a direct connection between the systems. Hence no significant second harmonic exists on the dc line, and consequently case C shows the lowest overvoltage for a fault at the rectifier location. In this case the overvoltage are due only the coupling effect between the lines.

Figure 3 .8 only shows the overvoltage crest magnitude, but says nothing about the frequency. For rectifier faults, ac bus waveforms show that cases A, B and D produce second harmonic overvoltages, whereas the overvoltage for C is of fundamental frequency.

It can also be seen that the overvoltage for rectifier fault is higher for case A than for B and D. This shows that the coupling effect of the ac line (as in case A) does present a higher impedance to the 2nd harmonic and hence results in higher overvoltages. It should also be noted that we have carried out inductive coordination in the original study to the extent possible without the addition of 2nd

harmonic filters (as described in section 3 .1 .1) and that we have moved the resonance from 2nd harmonic to 3rd harmonic to reduce this overvoltage as much as possible.

The explanation of the 2nd harmonic overvoltage on the dc line is due to the negative–sequence component which is generated during the single line to ground fault. In the single line to ground fault, three sequences components are present during the fault (positive, negative and zero sequence). These components generate the dc voltage, 2nd harmonic and zero voltage in the dc side of the converter, respectively. Figure 3 .9 illustrates how the converter behaves when the three sequence components are applied individually in the ac side during an ac single line to ground fault.

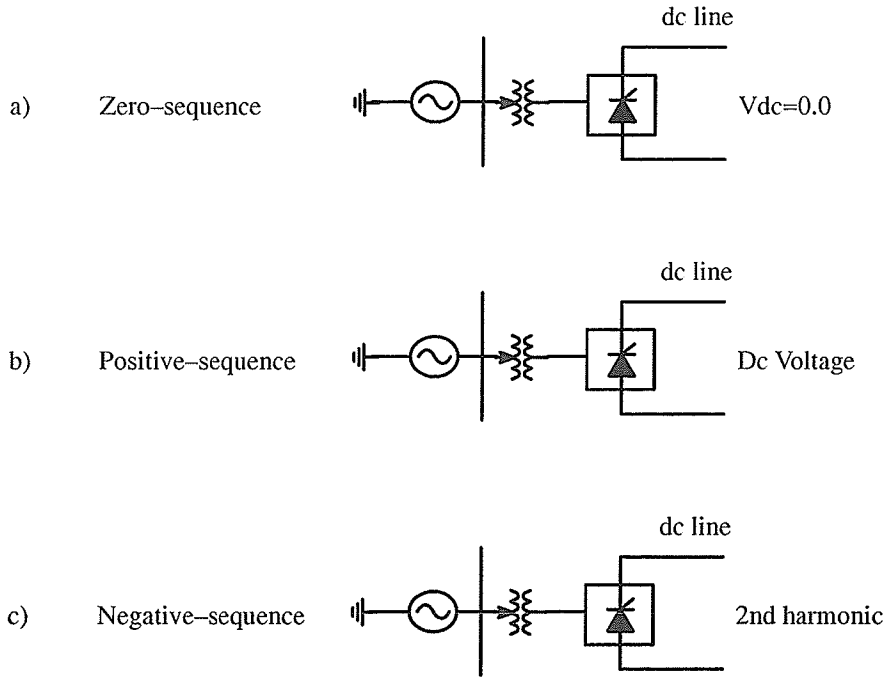

Figure 3 .9 : Illustration of the converter for sequence component applied in the ac side.

3 .1 .3 EFFECT OF NEGATIVE–SEQUENCE VOLTAGE ON DC LINE OVERVOLTAGES

Figure 3 .10 shows how the negative–sequence voltage component effects the dc line overvoltage. In this case the negative–sequence voltage was increased from 0% to 30% (related to the positive–sequence voltage in the ac source of the rectifier side). Immediately after the negative–sequence was applied (at time=0.01 seconds), the maximum dc line voltage increased from 1.04 pu to 1.50 pu with the 2nd harmonic component.

Figure 3 .11 shows the negative–sequence voltage versus maximum dc line overvoltage characteristic on the hybrid ac–dc system. We can see that the dc line overvoltage increases proportionally to the magnitude of the negative–sequence voltage applied at the ac source at the rectifier.

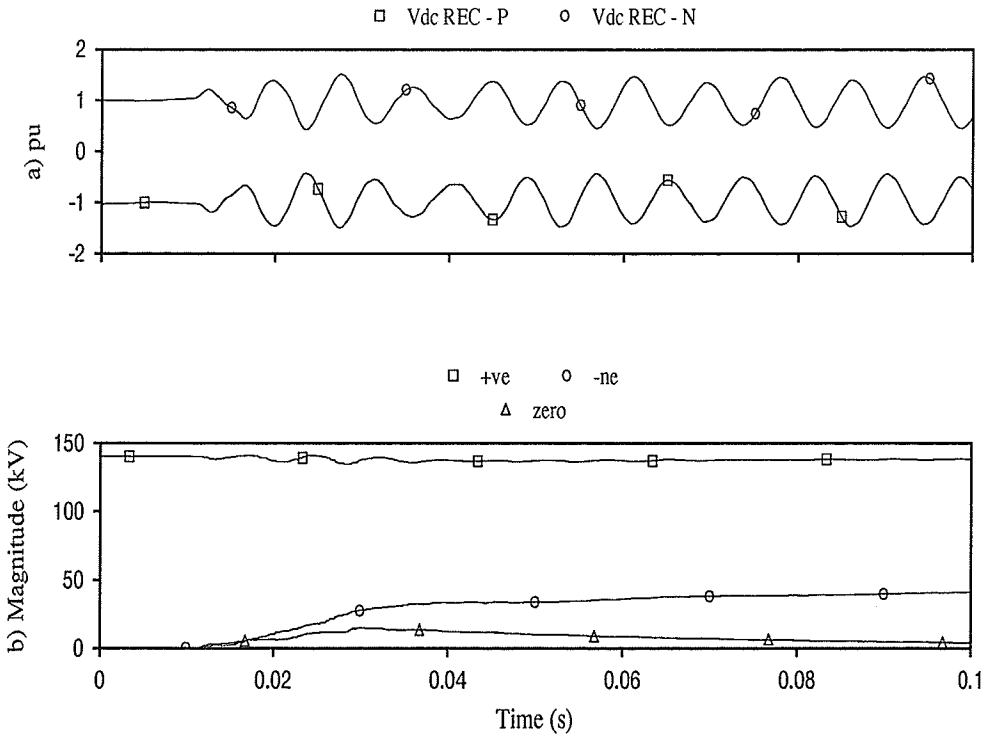

Figure 3 .10 : Generation of 2nd harmonic overvoltage on the dc line with generation of 30% negative–sequence voltage in the ac rectifier source.

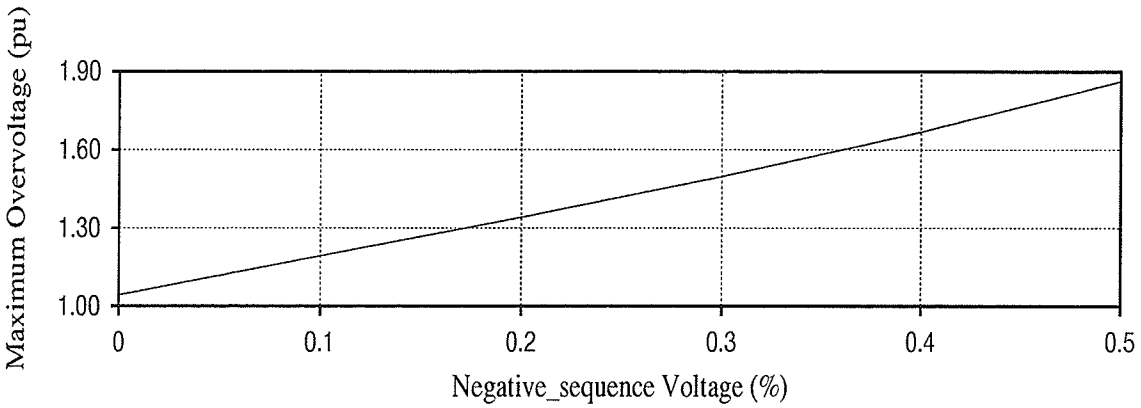

Figure 3 .11 : Negative–sequence voltage versus maximum dc overvoltage.

3 .1 .4 SECOND HARMONIC FILTER

In order to reduce the 2nd harmonic overvoltage on the dc line a 2nd harmonic filter was installed at both rectifier and inverter ends. Three different parameters of the 2nd harmonic filter were selected as shown in Figure 3 .12 and table 3 .1 .

Table 3 .1 : 2nd harmonic filter

	2nd harmonic filter		
Quality factor	40	40	40
Capacitance C2 (μF)	0.1	0.5	1.0
Inductance L2 (H)	17.59	1.759	3.518
Resistance R2 (ohms)	331.57	33.157	66.315

Figure 3 .13 shows the impedance x frequency characteristics of these three 2nd harmonic filters. With inclusion of the 2nd harmonic filter the overvoltage on the dc line at the rectifier side was substantially reduced as shown in table 3 .2 .

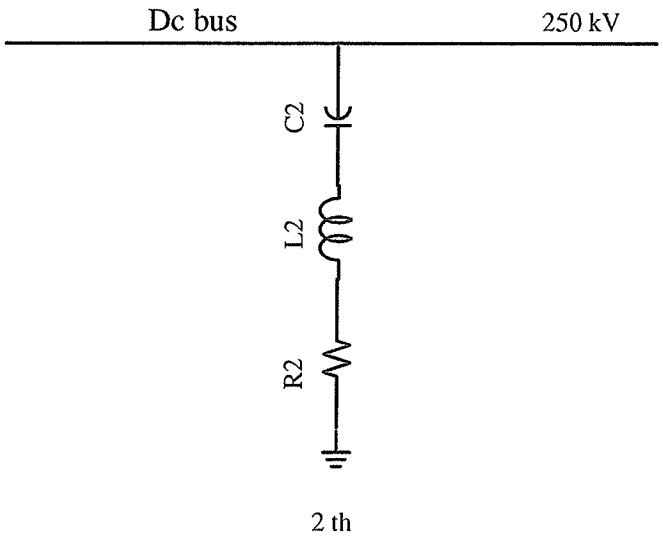

Figure 3 .12 : Single line diagram of 2nd harmonic filter.

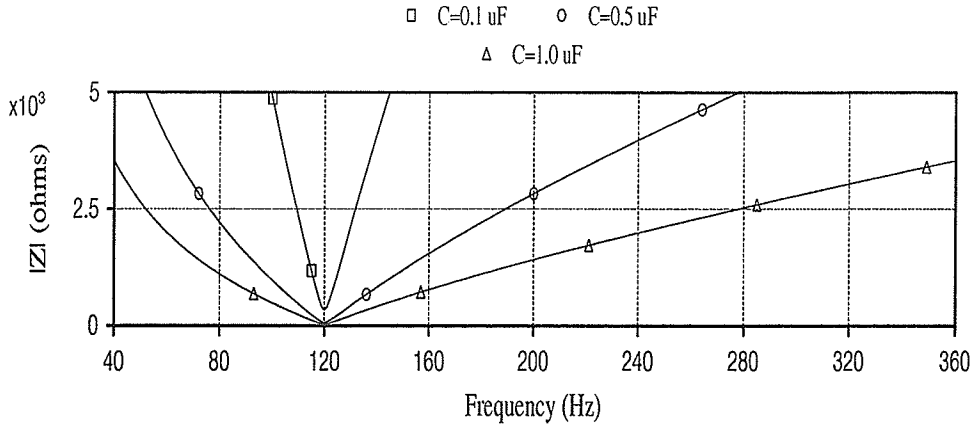

Figure 3 .13 : Impedance x frequency characteristic of the 2nd harmonic filters.

Table 3 .2 : 2nd harmonic overvoltage for ac single line to ground fault

Filter capacitance (μF)	Maximum dc overvoltage (pu)	
	faults applied at REC	faults applied at TL1
Without 2nd harm. filter	1.89	1.46
C=0.1	1.76	1.45
C=0.5	1.56	1.42
C=1.0	1.45	1.39

On the other hand the 2nd harmonic filter shows no effect in the dc overvoltage along the dc line when the ac single line to ground fault is applied at a location along the line other than rectifier side. Figure 3 .14 a) shows the overvoltage profile on the dc line for the ac single line to ground fault for three different 2nd harmonic filters (C=0.1, 0.5 and 1.0 μF). As we can see in table 3 .2 and Figure 3 .14 , there was not a significant reduction of overvoltage along the dc line at locations TL1, TL2, TL3, TL4, TL5 and INV. At these locations on the hybrid system the overvoltages are mainly due to the coupling effect between the ac and dc lines.

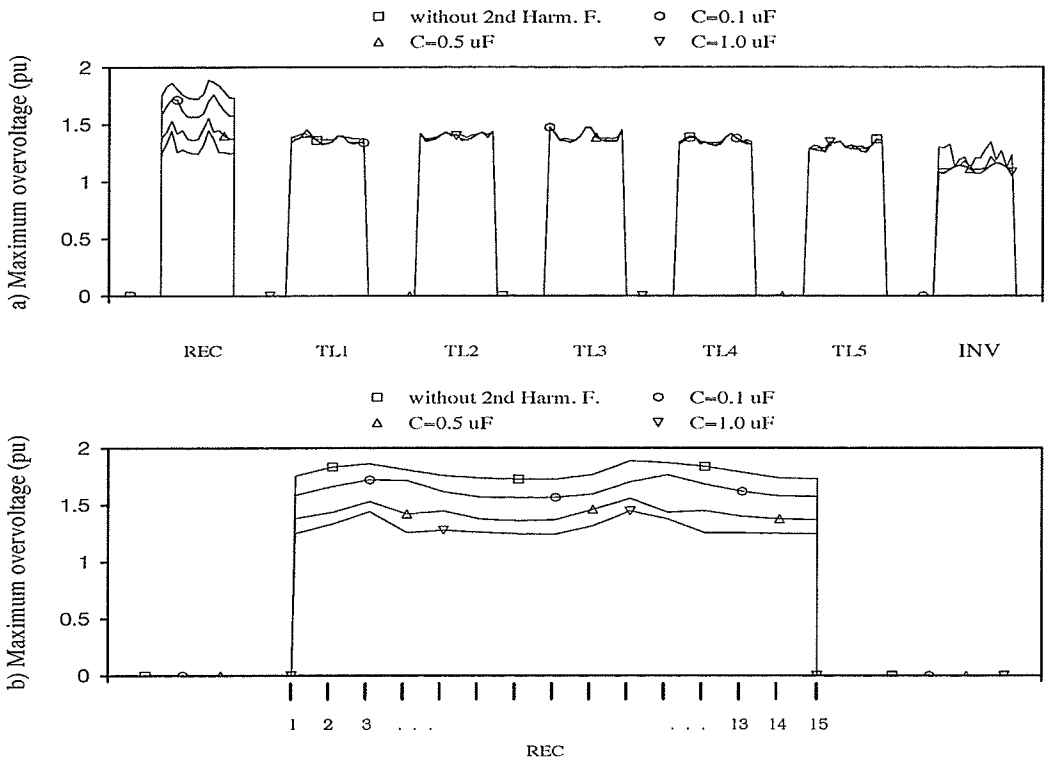

Figure 3 .14 : Maximum dc line overvoltage recorded any where along the line for an ac single line to ground fault for different 2nd harmonic filters, a)Location where the fault was applied along the line (15 points of fault inception/location), b)Enlargement of Figure a) above (only for the REC location).

Figure 3 .15 shows the dc line overvoltages for two others types of faults, ac–dc contact fault to ground (CFG) and ac line to line fault, that generates negative–sequence voltage components. In these cases the overvoltages present approximately the same profile as we have for the ac single line to ground fault.

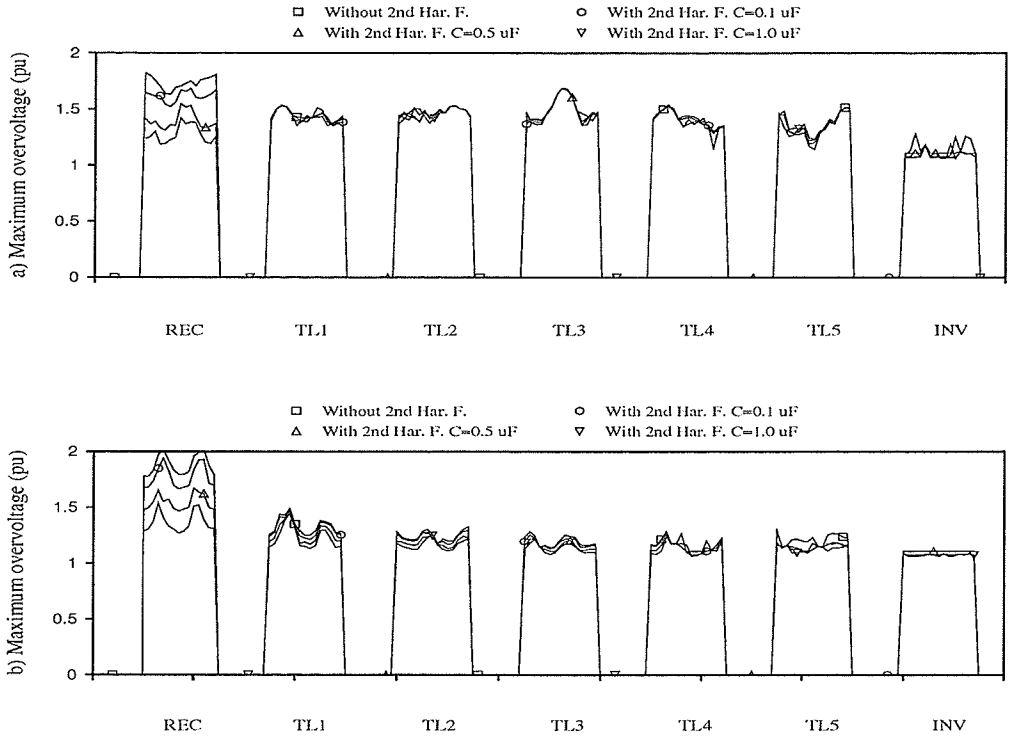

Figure 3 .15 : Maximum dc line overvoltage recorded any where along the line for different 2nd harmonic filters, a) Ac–dc conductor contact fault to ground, b) Ac line to line fault.

This study shows that addition of a second harmonic filter branch would reduce the dc line overvoltages for the ac line to ground, ac–dc conductor contact and line to line faults. The cost of such filters would need to be weighed against the cost of providing increased insulation on the dc line.

3 .2 LINE OVERVOLTAGE STUDIES

Ac and dc line overvoltages were calculated for the following types of fault:

a) ac single line to ground (LGac);

b) ac line to line to ground (LLG);

c) ac line to line (LL);

d) ac three phase to ground (LLLG);

e) ac–dc conductor contact fault (CF);

f) ac–dc to ground contact fault (CFG);

g) dc conductor to ground fault (LGdc).

These faults were applied at either the sending or receiving ends or at any one of the five equally spaced locations in between. Each segment represents 65 km of line. The overvoltages were recorded at these locations for all faults at all locations.

The base configuration which was simulated for the majority of the cases reported in this paper was as described in chapter 2 and shown in Figure 2 .3 . An electromagnetic transient simulation program PSCAD/EMTDC was used in this study. Appendix A shows the PSCAD/EMTDC draft diagram. Sensitivity studies were also carried out for the following conditions:

a) soil resistivity of 10 ohms–m and 1000 ohms–m;

b) ac system short circuit capacity reduced to 1700 MVA (SCR=2.84) at both ends.

c) no transpositions of the ac conductors.

d) only dc line transposition

e) Bergeron transmission line model

Faults were simulated at time intervals of 24^0 of inception point of the fault in one period ($360^0/24^0$=15 fault inception points) and the maximum overvoltage at any of the measuring locations was recorded. Additional information on fault philosophy are described in section 3 .8 .

Figures 3 .16 , 3 .17 and 3 .18 indicate the maximum overvoltages recorded anywhere along the ac and dc lines for two different ac system strengths, seven different fault types and three different system configurations. The system strengths used in the simulation are 6800 and 1700 MVA, which corresponds to short circuit ratios (SCR) of 11.33 and 2.84 respectively. Each Figure (3 .16 , 3 .17 and 3 .18) compares the results between the stronger and the weaker system. The system configurations are the following:

a) ac line transposed (hybrid line);

b) no coupling between the ac and dc lines (ac and dc lines on different towers);

c) ac line untransposed (hybrid line).

Figures 3 .19 and 3 .20 show the same results of the Figures 3 .16 , 3 .17 and 3 .18 but in a different way. In this case each Figure compares the results between system configuration for each system strength.

From these Figures we can conclude:

a) the dc line overvoltages are more severe for the stronger (6800 MVA) system. Note also that the ac–dc hybrid line considered here can also experience overvoltages due to the new fault types (CF and CFG) which would not be experienced by a dc line in isolation. The latter would experience only the LGdc type of fault.

b) the ac line overvoltages are larger when the system is weaker for all faults involving only the ac conductors (LL, LLG, LLLG, LGac). However when the fault involves a dc conductor (CFG, CF, LGdc), the overvoltage is larger for the stronger system. One possible explanation for this is that the dc fault current is larger for the stronger system and thus there is a larger coupling into the unfaulted ac conductor.

c) the overvoltages are larger when the ac–dc system is electromagnetically coupled. This is more pronounced for ac line overvoltages when the faults involving only the dc conductors.

d) in general the overvoltages on the dc line and on the stronger system are larger when the ac conductors are untransposed.

e) with ac–dc contact faults and dc line faults the ac overvoltages are smaller for the weaker system.

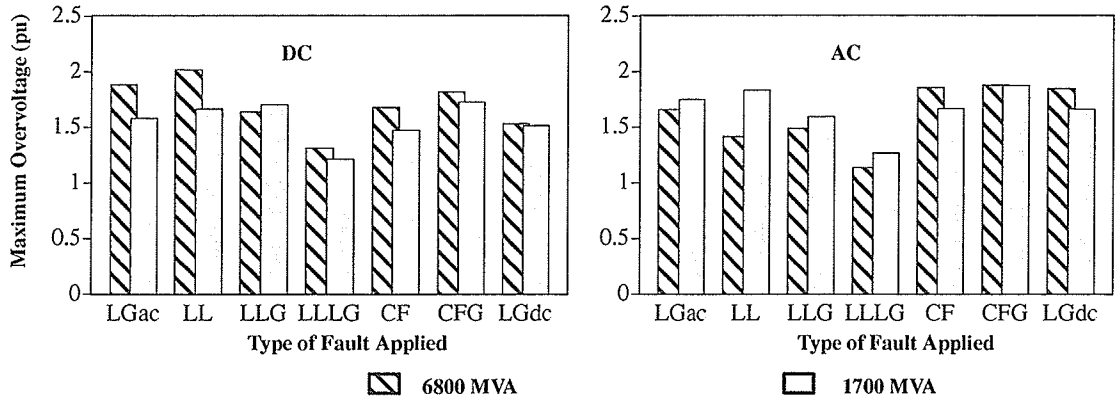

Figure 3 .16 : Maximum dc and ac line overvoltage for different types of faults.

(ac line transposed)

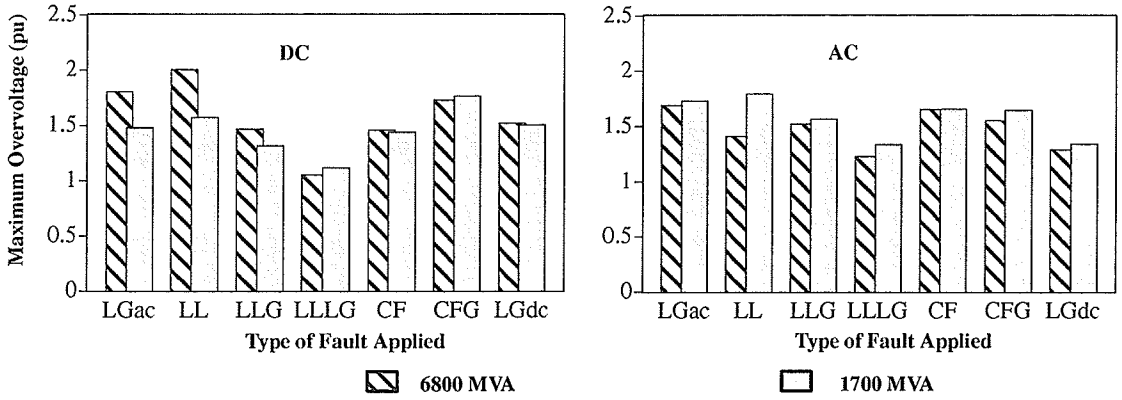

Figure 3 .17 : Maximum dc and ac line overvoltage for different types of faults.

(no coupling between ac and dc lines)

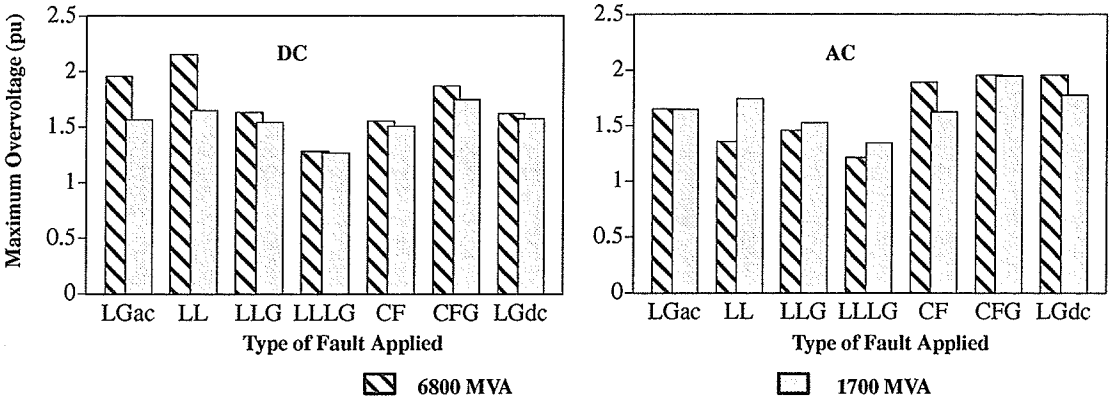

Figure 3 .18 : Maximum dc and ac line overvoltage for different types of faults.

(ac line not transposed)

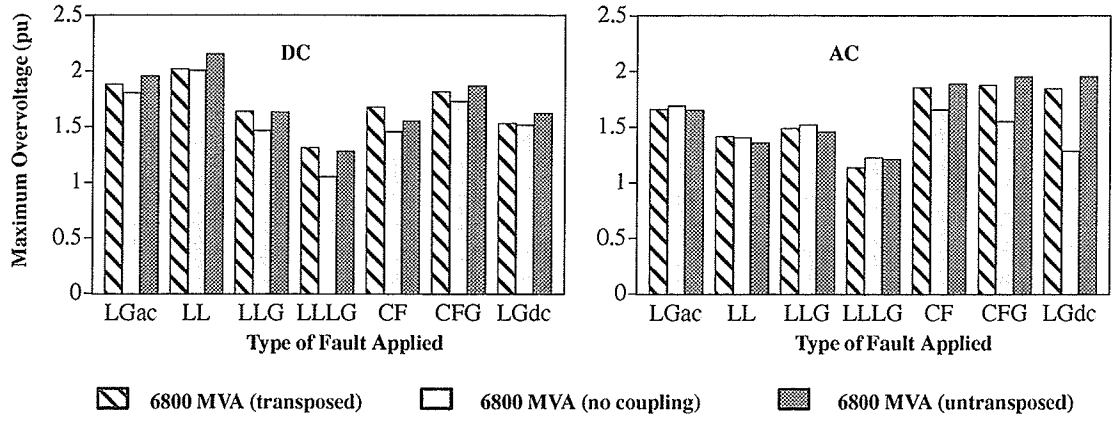

Figure 3 .19 : Maximum dc and ac line overvoltage for different types of faults and system configuration.

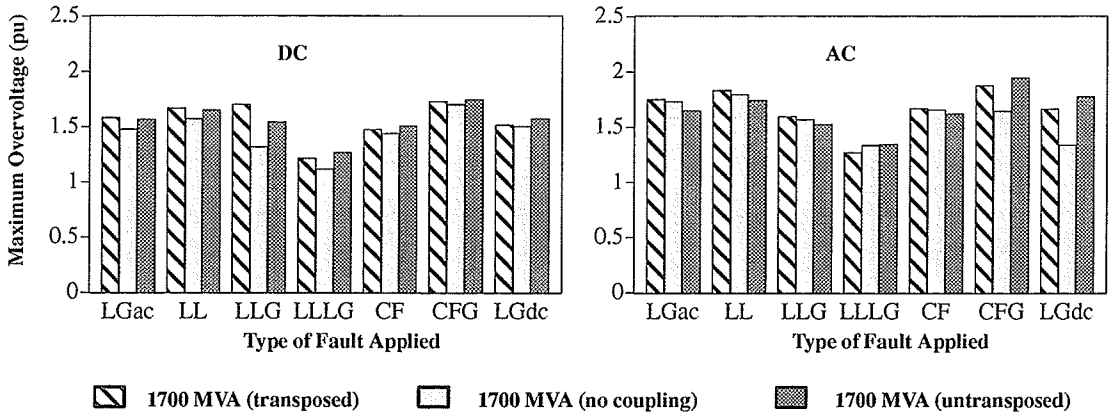

Figure 3 .20 : Maximum dc and ac line overvoltage for different types of faults and system configurations.

Figures 3 .21 , 3 .22 , 3 .23 and 3 .24 indicate the maximum ac and dc line overvoltages calculated anywhere along the ac and dc lines, as a function of the location where the fault was applied. These overvoltages were calculated for two different ac system strengths, seven different fault types and three different system configurations.

The main conclusions derived are shown in tables 3 .3 and 3 .4 .

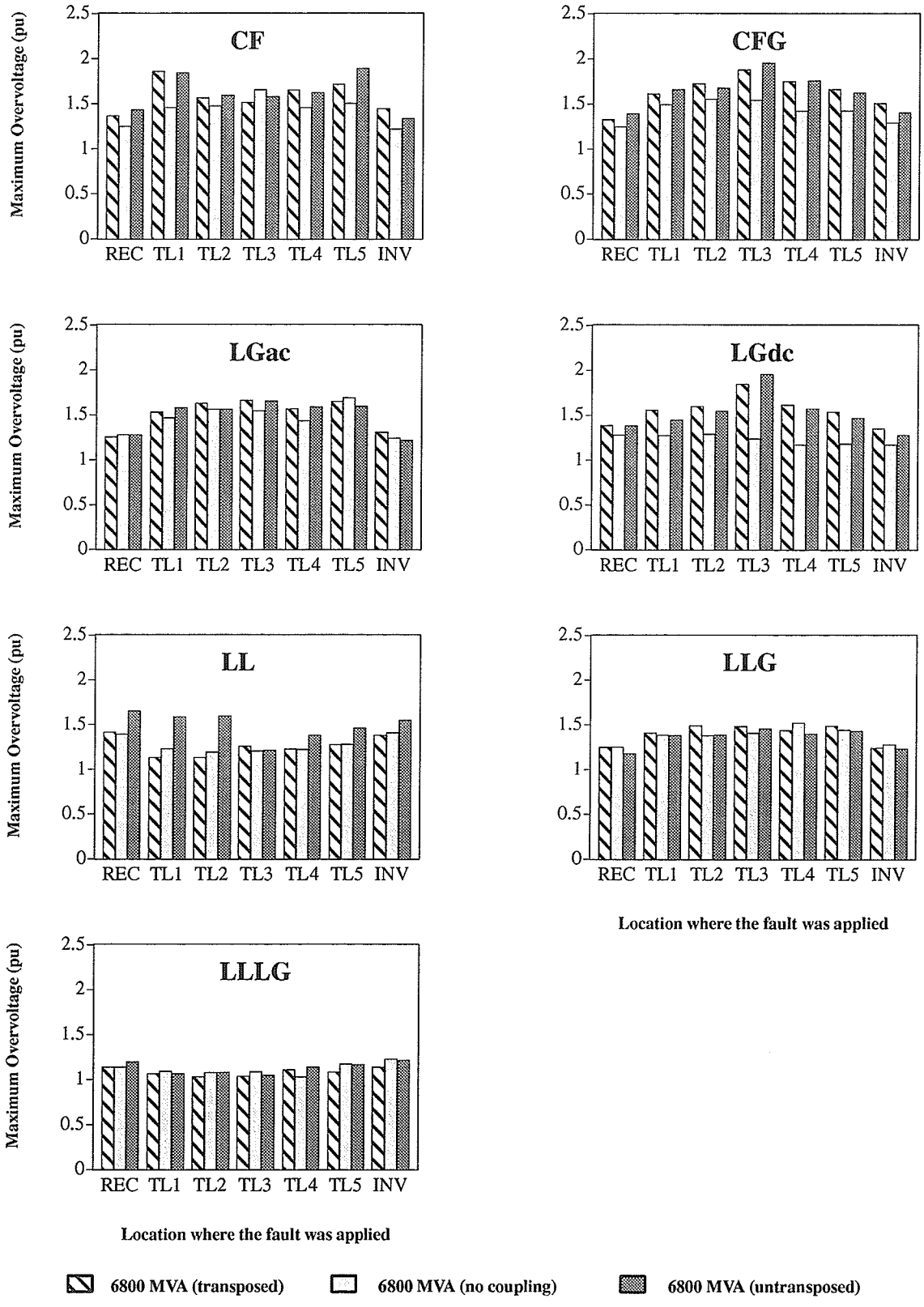

Figure 3 .21 : Maximum ac line overvolatge at points along the line as a function of location where the fault was applied (SCR=11.33).

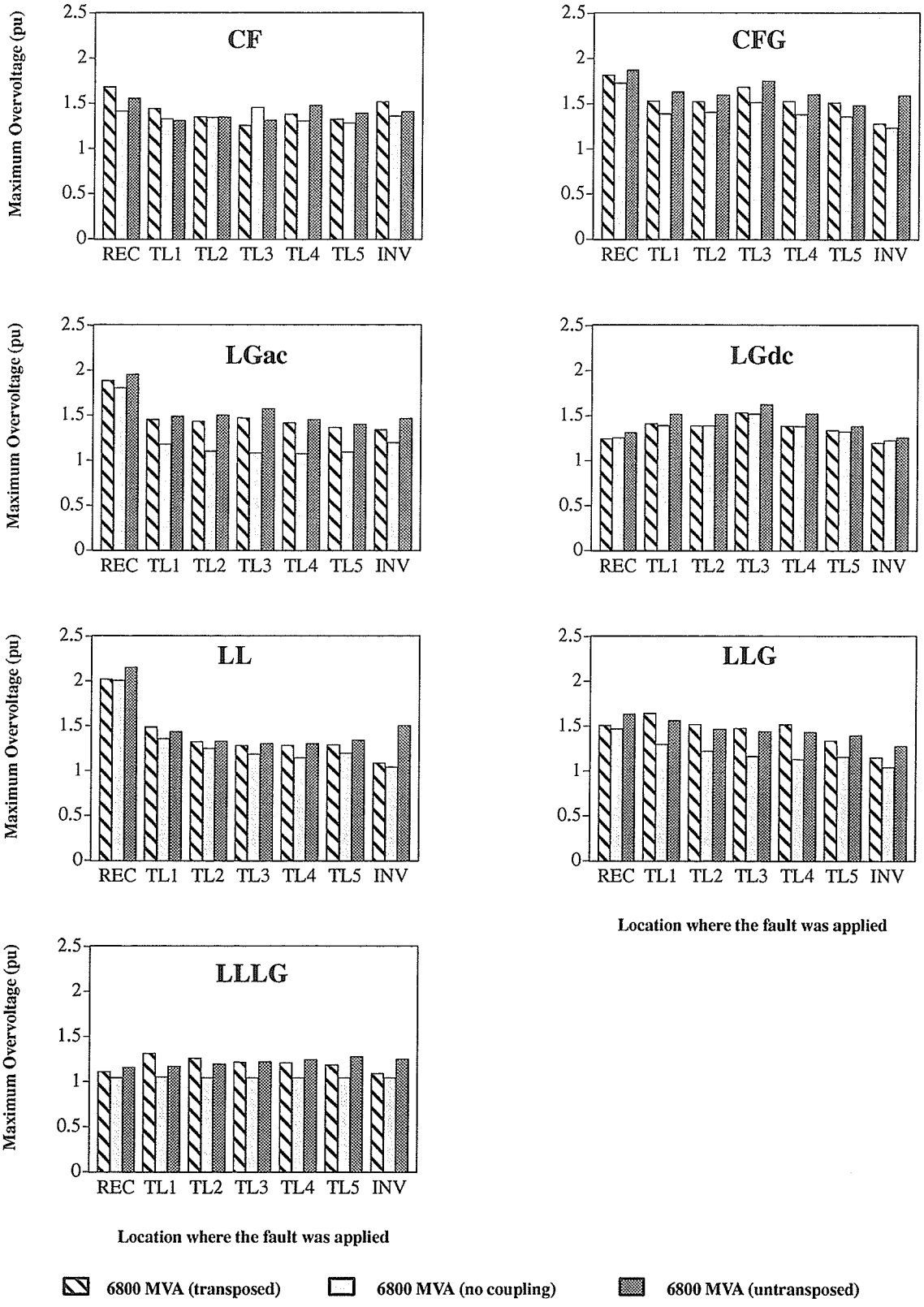

Figure 3 .22 : Maximum dc line overvoltage at points along the line as a function of location where the fault was applied (SCR=11.33).

Table 3 .3 : Comparison between ac and dc line results, SCR=11.33

fault type	ac line (Figure 3 .21)	dc line (Figure 3 .22)
CF	1–overvoltages are higher when the faults are applied in the middle of the line; 2–overvoltages for the transposed and untransposed cases are approximately the same; 3–overvoltages are lower for the uncoupled case.	1–overvoltages are higher when the faults are applied in the extremities of the line 2–overvoltages for the transposed and untransposed cases are approximately the same; 3–overvoltages are lower for the uncoupled case.
CFG	1–overvoltages for the transposed and untransposed cases are approximately the same; 2–overvoltages are lower for the uncoupled case. 3–overvoltages are higher when the faults are applied in the middle of the line;	1–overvoltages for the transposed and untransposed cases are approximately the same; 2–overvoltages are lower for the uncoupled case.
LGac	1–overvoltages are higher when the faults are applied in the middle of the line; 2–overvoltages for the transposed case are higher than for untransposed.	1–overvoltages are higher when the faults are applied at the REC; 2–overvoltages are lower for the uncoupled case.
LGdc	1–overvoltage are higher when the faults are applied in the middle of the line; 2–overvoltages for the transposed case are higher than for untransposed; 3–overvoltages are lower for the uncoupled case.	1–overvoltages are higher in the middle of the line; 2–overvoltages for the untransposed case are higher than the case transposed; 3–overvoltages are lower for the uncoupled case.
LL	1–overvoltages for the transposed case are much higher than the case untransposed (in the Rec);	1–overvoltages are higher when the faults are applied in the extremities of the line; 2–overvoltages for the untransposed case are higher than the case transposed; 3–overvoltages are lower for the uncoupled case.
LLG	1–overvoltages are higher when the faults are applied in the middle of the line.	1–overvoltages are lower for the uncoupled case.
LLLG	1–overvoltages are lower compared to the other fault types	1–overvoltages are lower for the uncoupled case.

Table 3 .4 : Comparison between ac and dc line results, SCR=2.84

fault type	ac line	dc line
CF	1–overvoltages are higher when the faults are applied in the middle of the line.	1–overvoltages are lower for the uncoupled case.
CFG	1–overvoltages for the untransposed case are larger than the case transposed; 2–overvoltages are lower for the no coupled case.	1–overvoltages are higher when the faults are applied in the middle of the line; 2–overvoltages are lower for the uncoupled case.
LGac	1–overvoltages are higher in the middle of the line and at REC; 2–overvoltages for the transposed case are larger than the case untransposed.	1–overvoltages for the transposed case are larger than the case untransposed; 2–overvoltages are lower for the uncoupled case.
LGdc	1–overvoltages are lower for the no coupled case.	1–overvoltages for the transposed case are larger than the case untransposed; 2–overvoltages are lower for the uncoupled case.
LL	1–overvoltages are higher when the faults are applied at REC.	1–overvoltages are higher when the faults are applied at REC; 2–overvoltages for the untransposed case are larger than the case transposed; 3–overvoltages are lower for the uncoupled case.
LLG	1–overvoltages are higher when the faults are applied in the middle of the line.	1–overvoltages are higher when the faults are applied at TL1 and TL2; 2–overvoltages are lower for the uncoupled case.
LLLG	1–overvoltages are lower compared to the other fault types.	1–overvoltages for the transposed case are larger than the case untransposed; 2–overvoltages are lower for the uncoupled case.

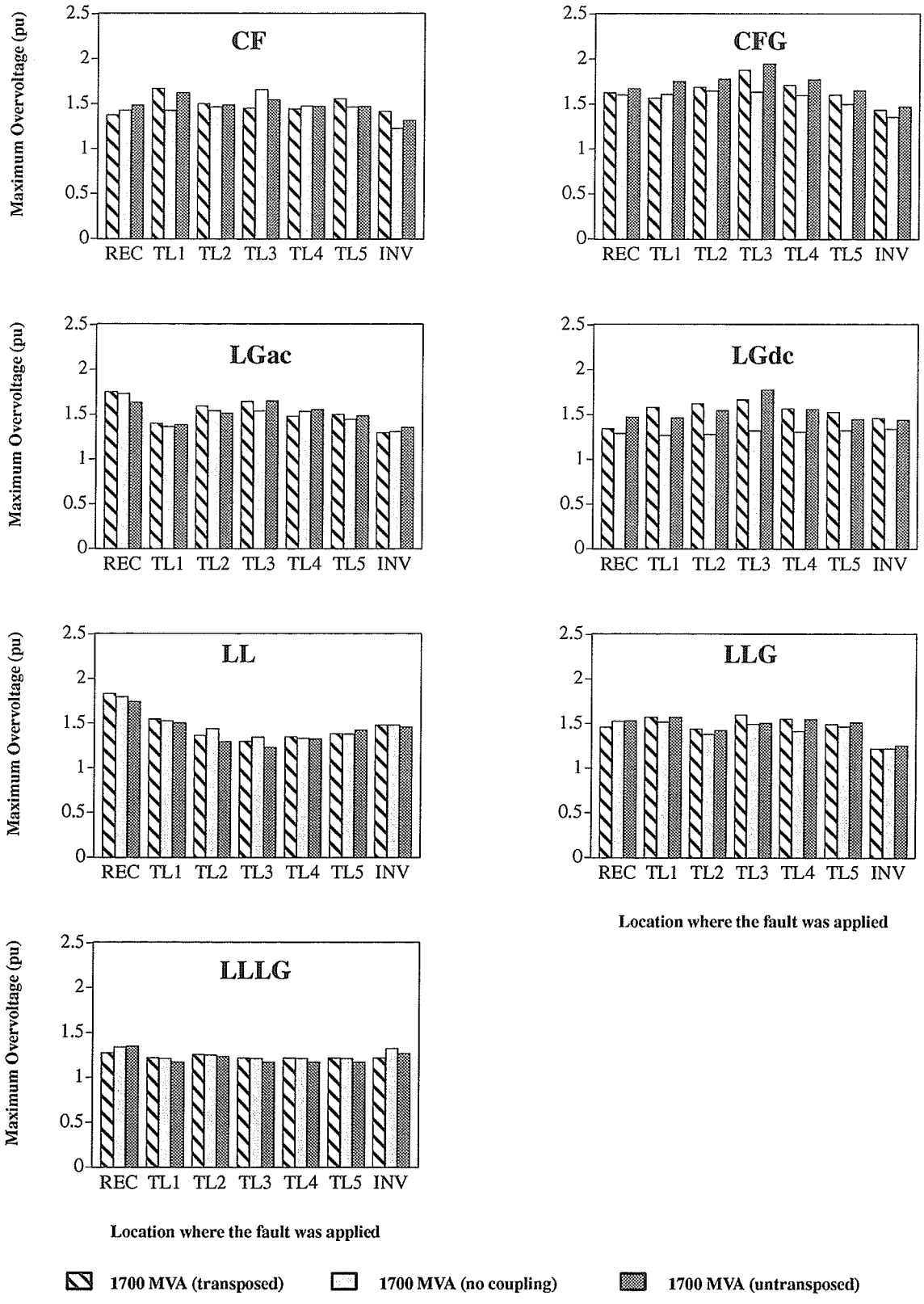

Figure 3 .23 : Maximum ac line overvoltage at points along the line as a function of location where the fault was applied (SCR=2.84).

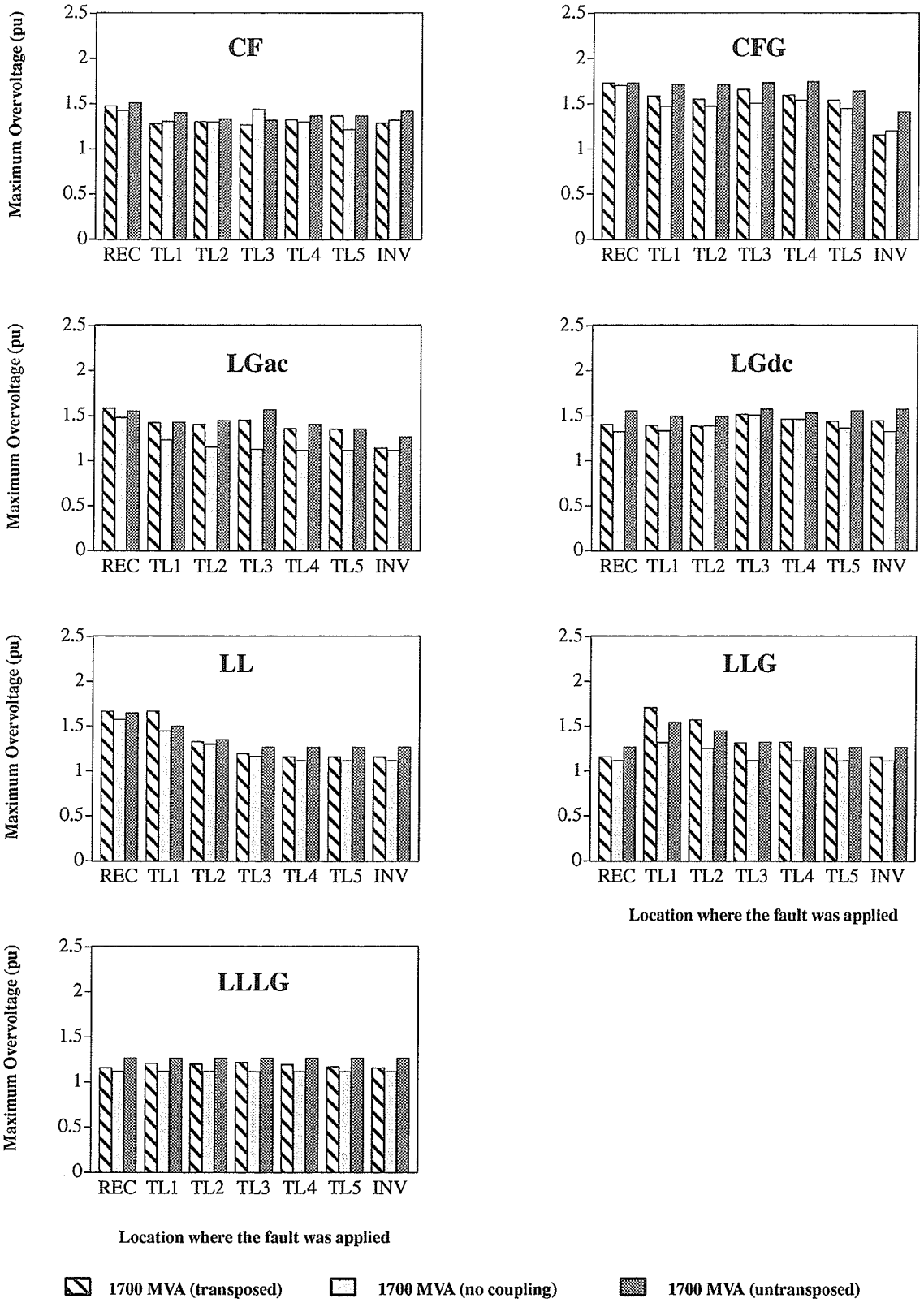

Figure 3 .24 : Maximum dc line overvoltage at points along the line as a function of location where the fault was applied (SCR=2.84).

3 .2 .1 AC AND DC OVERVOLTAGES WAVEFORM

3 .2 .1 .1 FAULT APPLIED AT THE RECTIFIER SIDE

Figures 3 .25 , 3 .26 and 3 .27 show typical waveforms of four fault types for which maximum overvoltages were given in Figures 3 .21 , 3 .22 , 3 .23 and 3 .24 . The curves include the following:

a) voltage across the 60 Hz blocking filter at the rectifier;

b) the rectifier end positive and negative pole dc current;

c) the rectifier end positive pole and negative pole dc voltages;

d) the three ac phase voltages measured at the rectifier.

e) ac line current

When the fault is applied at the rectifier side and the negative–sequence voltage has high magnitude, the overvoltage on the dc line will be mainly due to the 2nd harmonic component generated from this sequence component. Table 3 .5 shows the maximum percentage magnitude of the negative–sequence voltage (related to the positive–sequence voltage) for each type of fault when the fault is applied at the rectifier side.

Table 3 .5 : Negative–sequence voltage in the rectifier for different fault types

Fault type	Maximum negative–sequence voltage (faults applied at REC)	
	(%)	(kV)
LGac	40	56
LL	54	76
LLG	35	50
LLLG	16	22
CF	6	8
CFG	38	54
LGdc	2	3

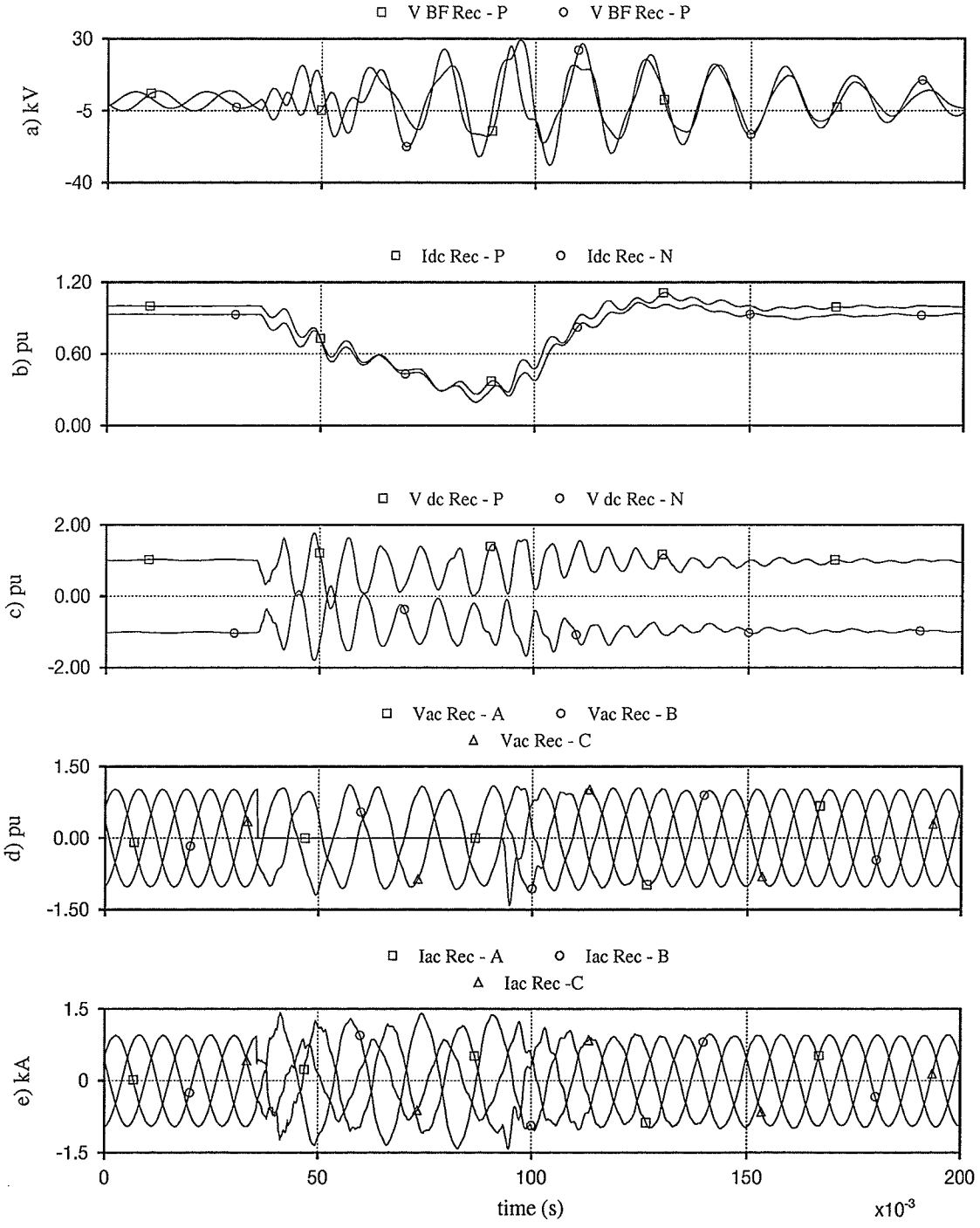

Figure 3 .25 : Voltage and current waveforms for ac–dc contact fault (CF).
(fault applied at REC)

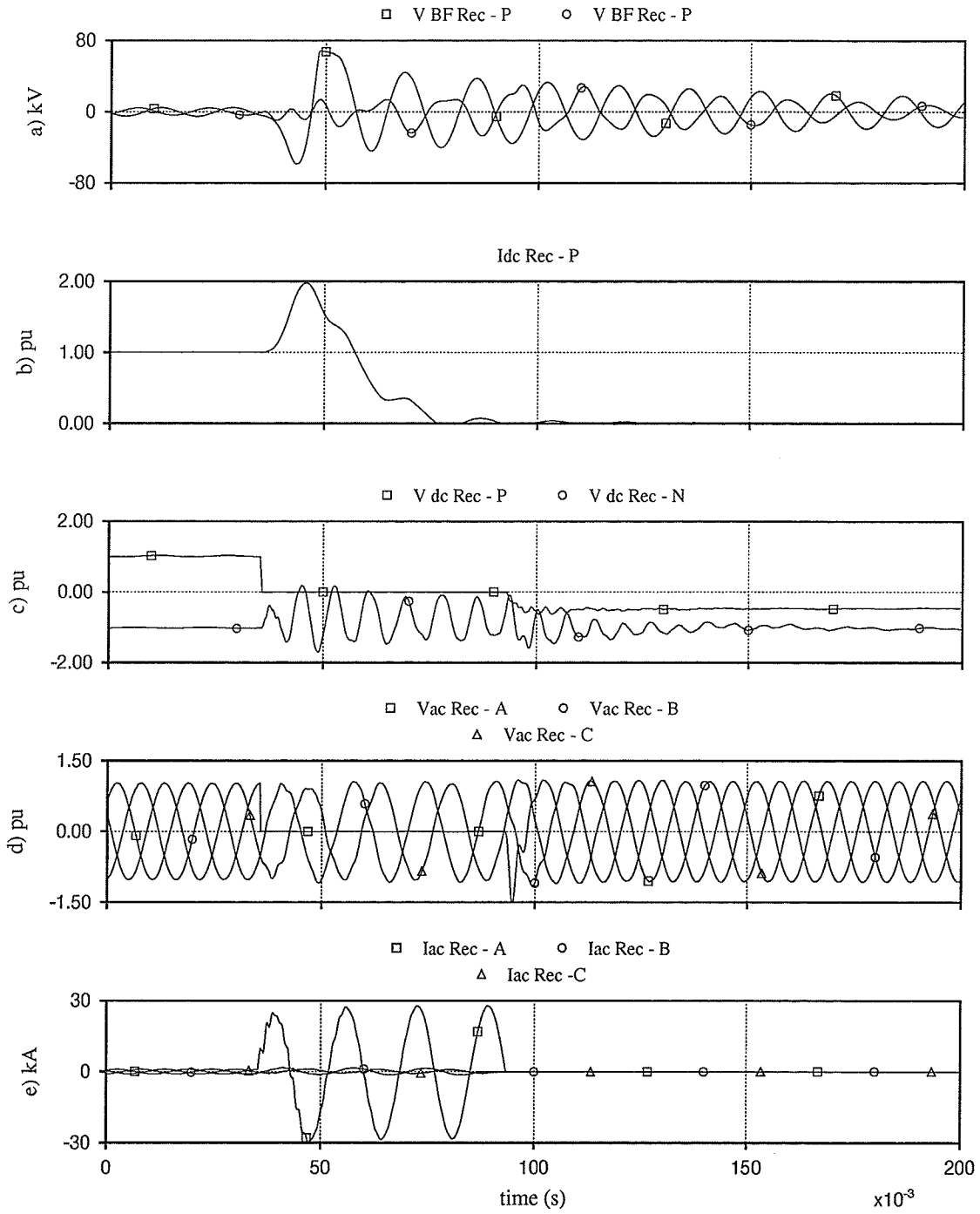

Figure 3 .26 : Voltage and current waveforms for ac–dc contact fault to ground (CFG).
(fault applied at REC)

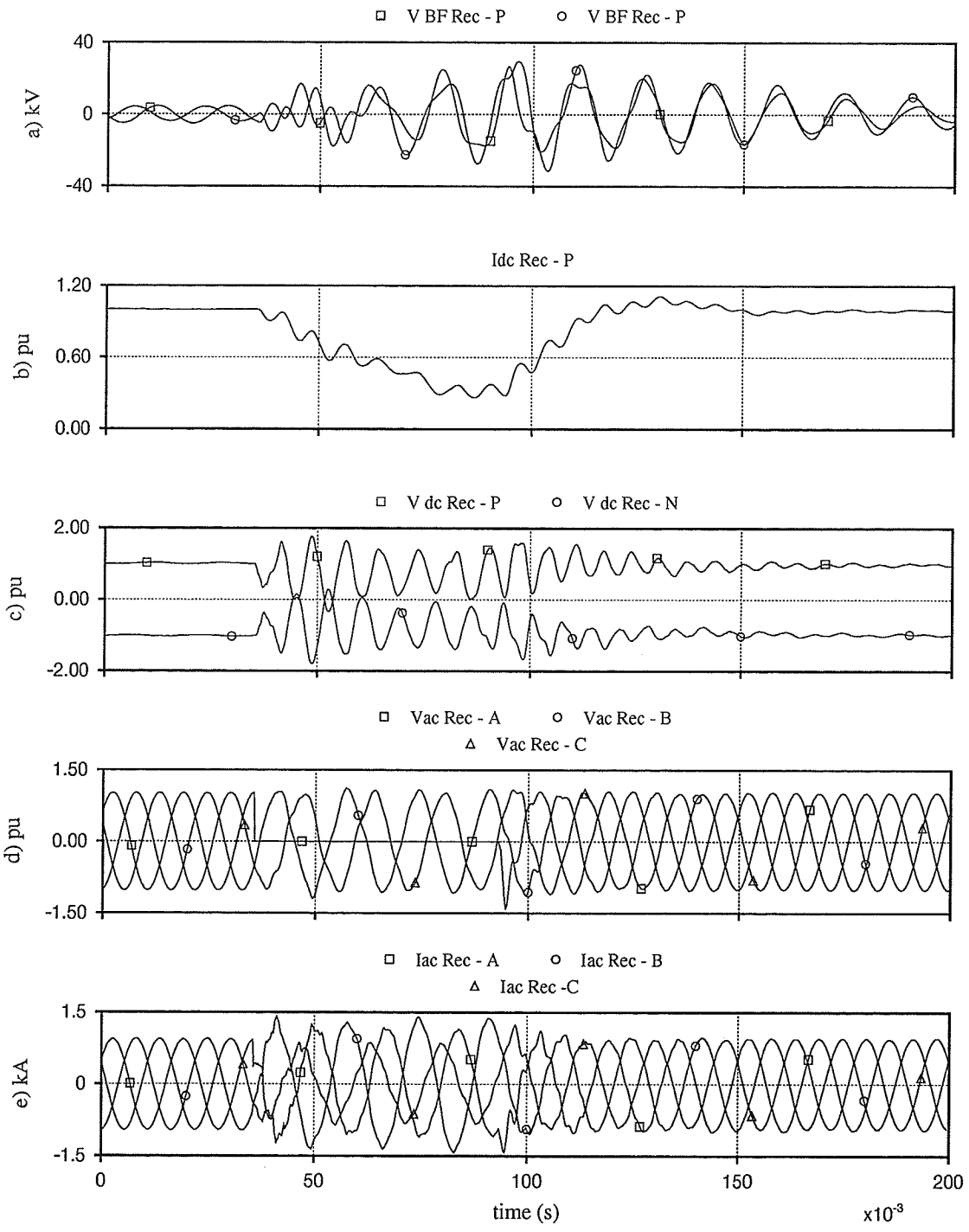

Figure 3 .27 : Voltage and current waveforms for ac single line to ground fault (LGac).
(fault applied at REC)

3 .2 .1 .2 FAULT APPLIED IN THE MIDDLE OF THE LINE

Figures 3 .28 , 3 .29 and 3 .30 show typical waveforms of three fault types for which maximum overvoltages were given in Figures 3 .21 , 3 .22 , 3 .23 and 3 .24 . The curves include the following:

a) voltage across the 60 Hz blocking filter at the rectifier;

b) the rectifier end positive and negative pole dc current;

c) the rectifier end positive pole and negative pole dc voltages;

d) the three ac phase voltages measured at the rectifier.

e) ac line current

When the fault is applied in the middle of the line the overvoltages are mainly due to two main factors. One is related to the effect of the transient set up by the traveling wave along the line. The other factor is due to the 60 Hz coupling effect between the ac and the dc line.

The negative–sequence voltage generated on the rectifier due to the unbalanced condition is negligible compared to the transient effects described above. Therefore the 2nd harmonic overvoltage presents slight effect on the dc line overvoltage when the fault is applied in the middle of the line. Table 3 .6 shows the maximum percentage magnitude of the negative–sequence voltage (related to the positive–sequence voltage) for each type of fault when the fault is applied in the middle of the line.

Figures 3 .31 , 3 .32 and 3 .33 show the waveforms for the ac single line to ground fault applied in the middle of the line (195 km from the rectifier), at different instant along the sinewave, on the negative crest, zero crossing and positive crest voltage, respectively.

When the ac single line fault is applied on the negative and the positive crest voltage of the phase under fault (phase "b") the maximum dc line overvoltage is caused by the the high frequency electromagnetic transient coupling effect generated from the ac line under fault.

Table 3 .6 : Maximum negative–sequence voltage in the rectifier for different fault types

Fault type	Maximum negative–sequence voltage (fault applied at TL3)	
	(%)	(kV)
LGac	2	3
LL	6	8
LLG	5	7
LLLG	2	3
CF	2	3
CFG	4	5
LGdc	1	2

When the ac single line fault is applied on the zero crossing voltage the maximum dc line overvoltage is caused by the 60 Hz electromagnetic coupling effect from the ac line under fault.

Figures 3 .34 , 3 .35 and 3 .36 show the waveforms of the ac–dc contact fault to ground applied in the middle of the line. In the case of contact faults between one ac conductor and the positive pole dc conductor to ground in the middle of the line, the maximum overvoltage occurs when the fault is applied at the positive crest voltage on the ac line. This results from the addition of the electromagnetic transient generated during the fault from the ac conductor to the transient generated from the positive dc conductor. When the fault is applied on the negative crest voltage the transient generated from the ac conductor is subtracted from the transient generated from the positive pole dc conductor and the dc line overvoltage will be only due the 60 Hz electromagnetic coupling effect.

Figures 3 .37 , 3 .38 and 3 .39 show the waveforms for the ac–dc contact fault. In this type of fault the overvoltages are mainly due to the coupling effect between the lines.

Figures 3 .40 , 3 .41 and 3 .42 show the waveforms for the dc line to ground fault. In this type of fault the ac and dc overvoltages are higher when the fault is applied in the middle of the line.

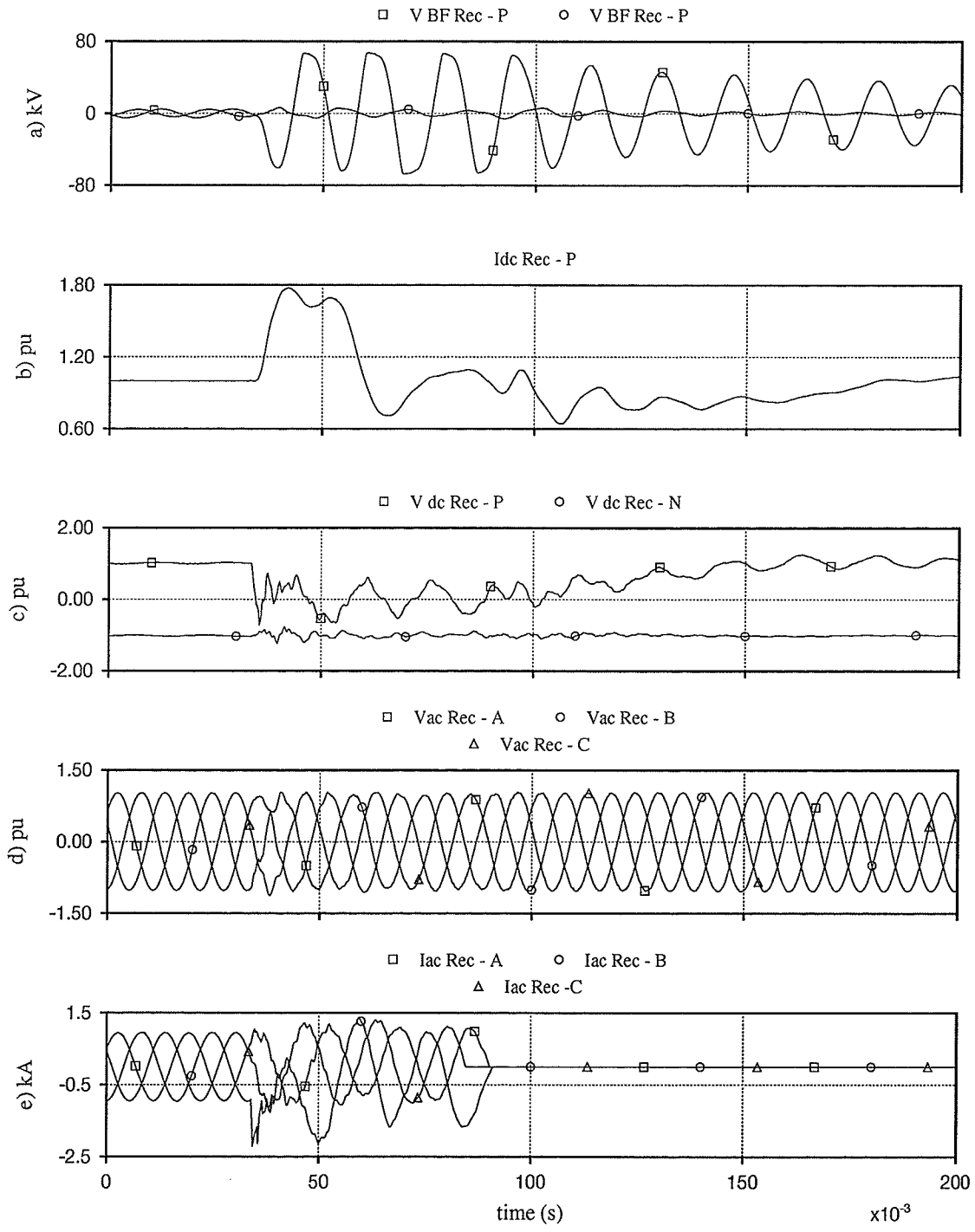

Figure 3 .28 : Voltage and current waveforms for ac–dc conductor contact fault (CF).
(fault applied at TL3)

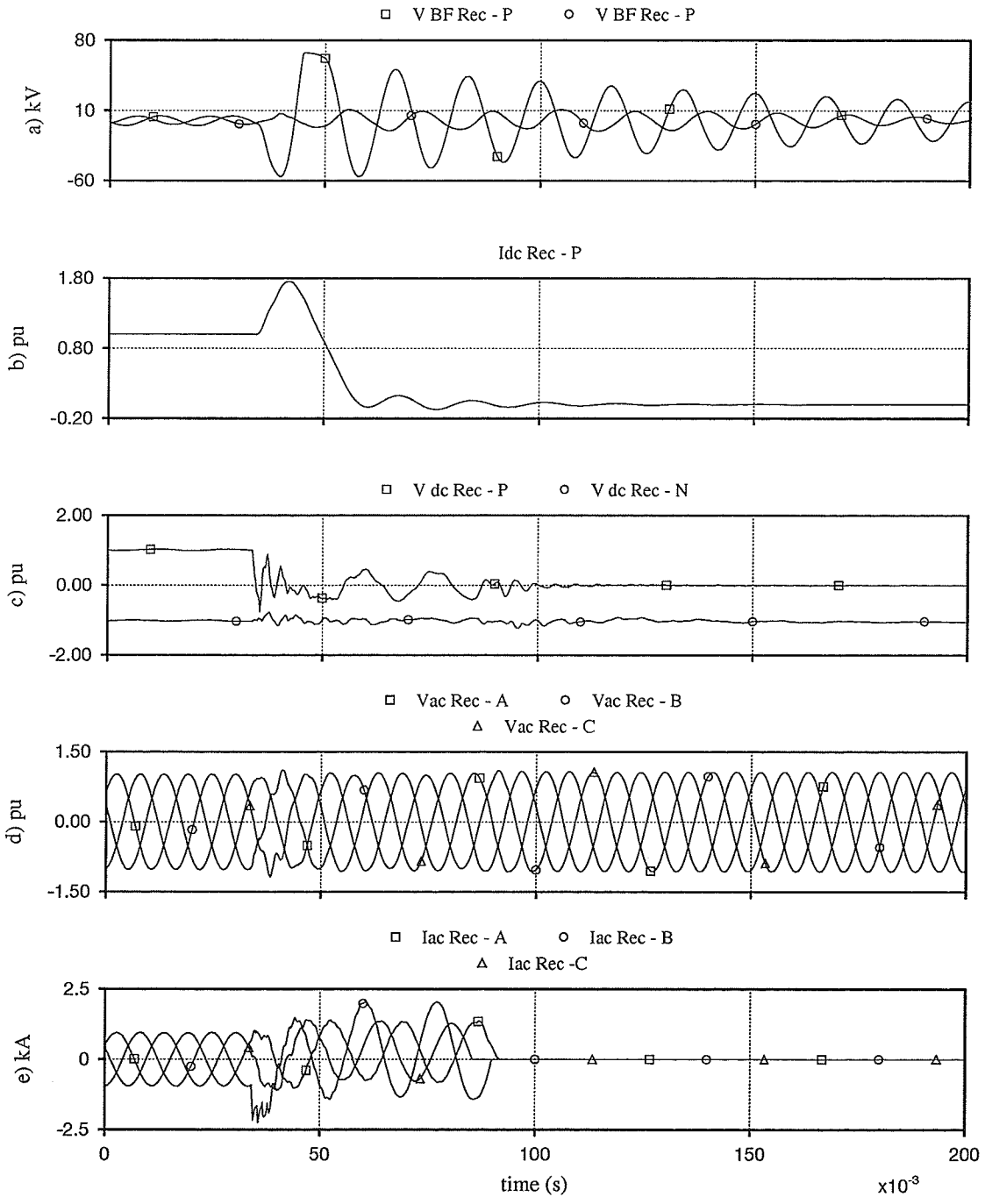

Figure 3 .29 : Voltage and current waveforms for ac–dc conductor contact fault to ground (CFG). (fault applied at TL3)

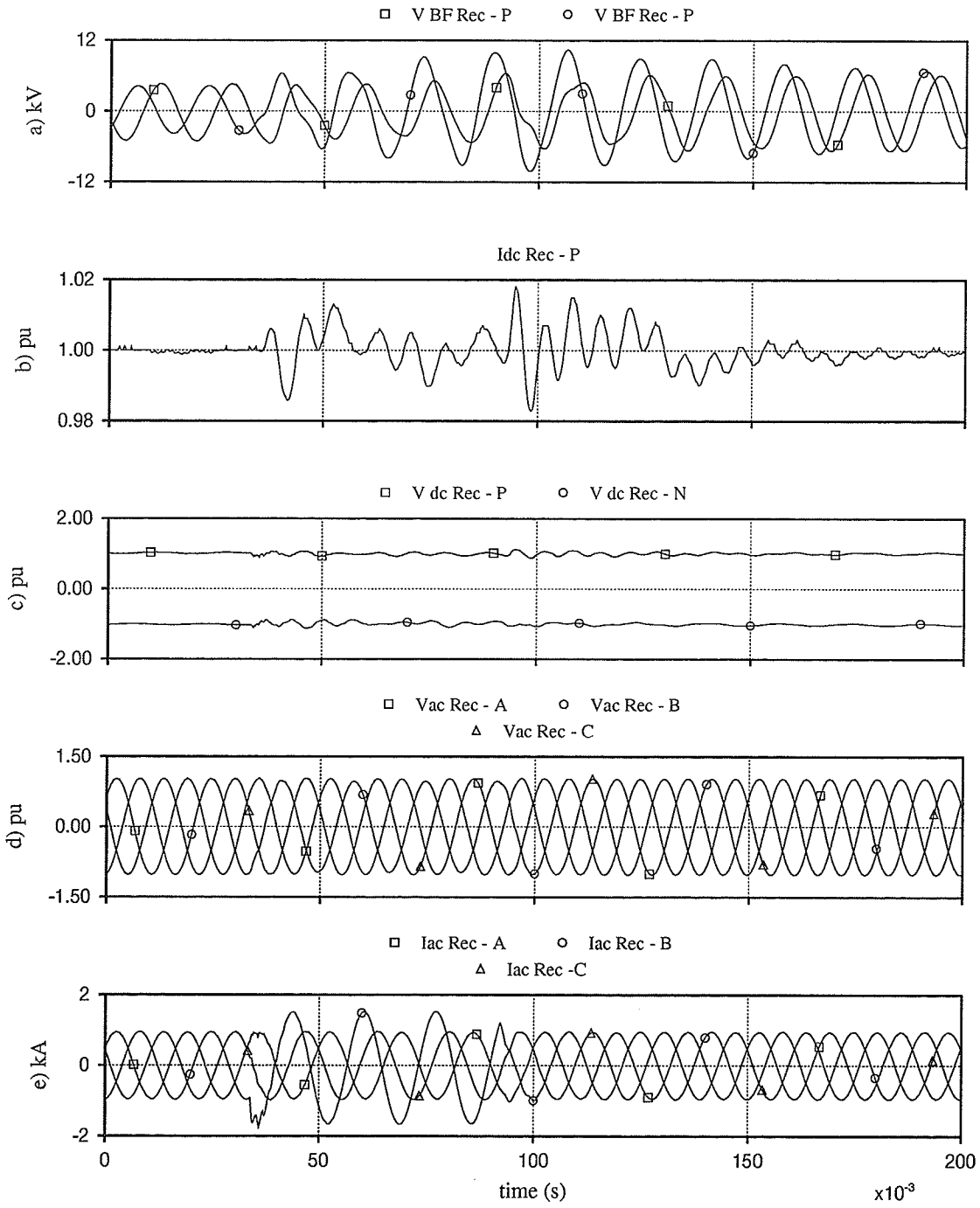

Figure 3 .30 : Voltage and current waveforms for ac single line to ground fault (LGac).
(fault applied at TL3)

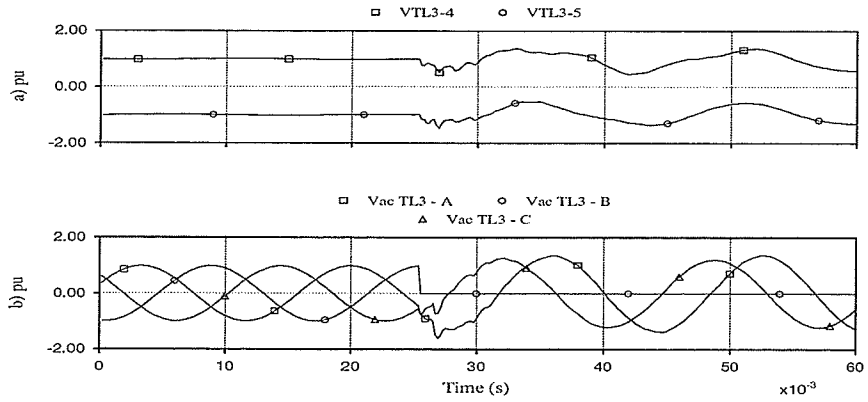

Figure 3 .31 : Voltage waveforms for ac single line to ground fault.
(fault applied at TL3 at crest of positive voltage phase "b")

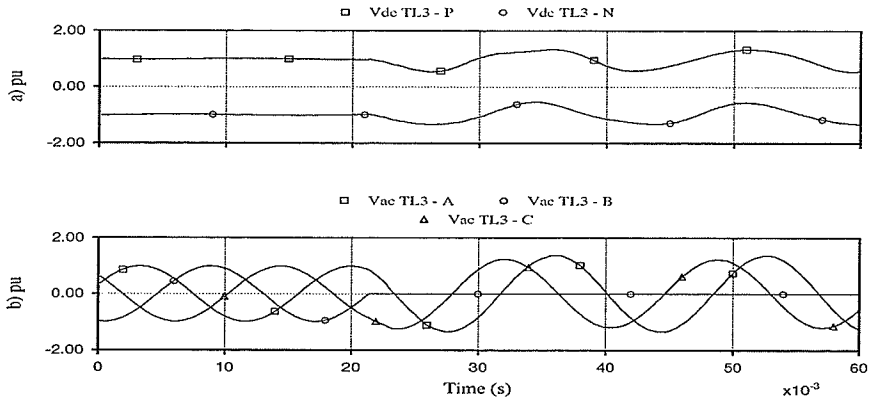

Figure 3 .32 : Voltage waveforms for ac single line to ground fault.
(fault applied at TL3 at zero crossing voltage phase "b")

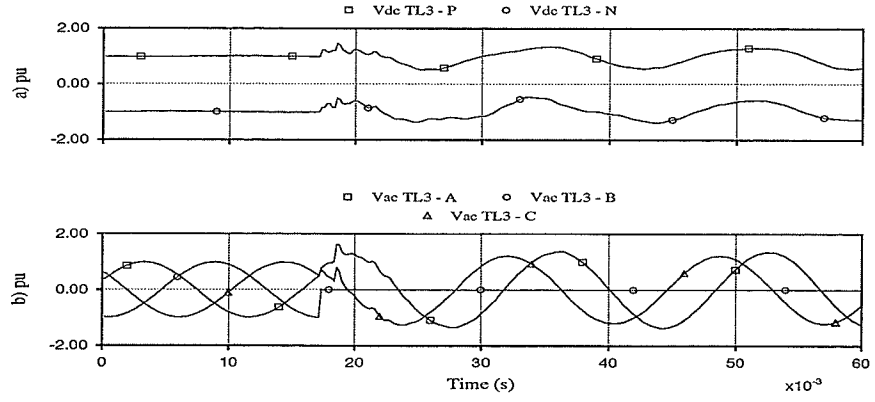

Figure 3 .33 : Voltage waveforms for ac single line to ground fault.
(fault applied at TL3 at crest of negative voltage phase "b")

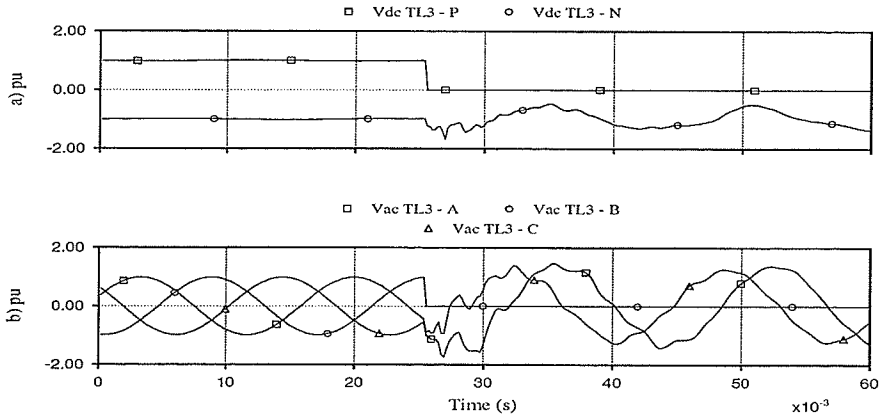

Figure 3 .34 : Voltage waveforms for ac–dc contact fault to ground.
(fault applied at TL3 at crest of positive voltage phase "b")

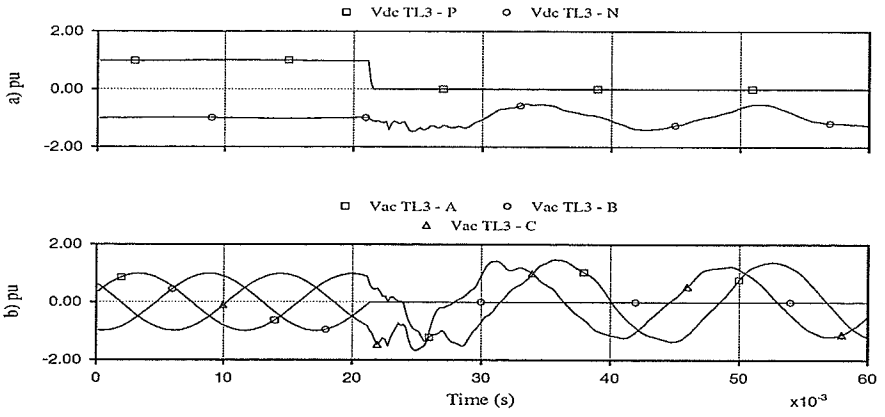

Figure 3 .35 : Voltage waveforms for ac–dc contact fault to ground.
(fault applied at TL3 at zero crossing voltage phase "b")

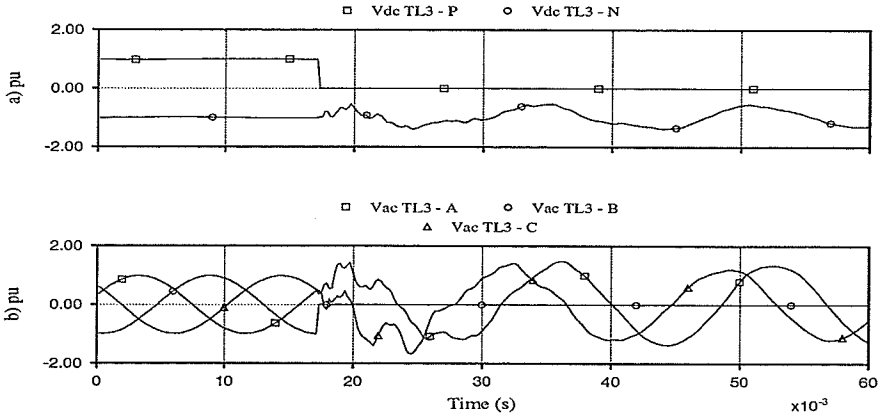

Figure 3 .36 : Voltage waveforms for ac–dc contact fault to ground.
(fault applied at TL3 at crest of negative voltage phase "b")

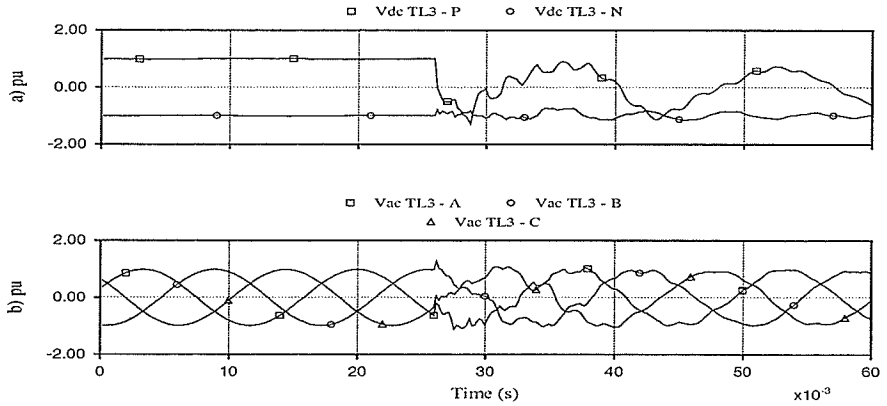

Figure 3 .37 : Voltage waveforms for ac–dc contact fault.
(fault applied at TL3 at crest of positive voltage phase "b")

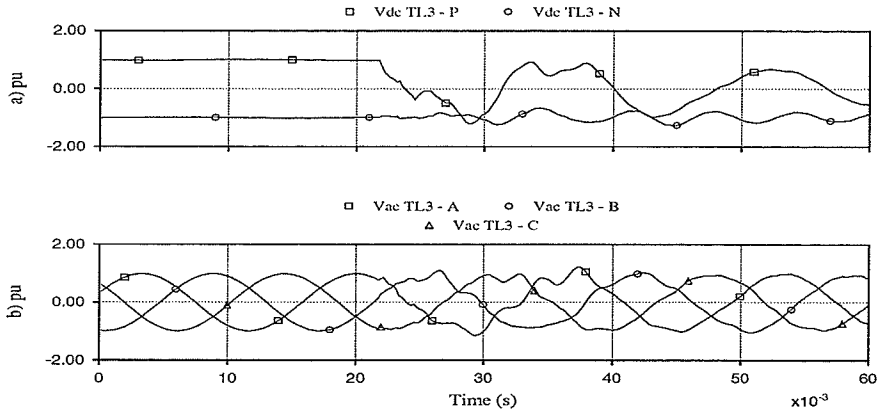

Figure 3 .38 : Voltage waveforms for ac–dc contact fault.
(fault applied at TL3 at zero crossing voltage phase "b")

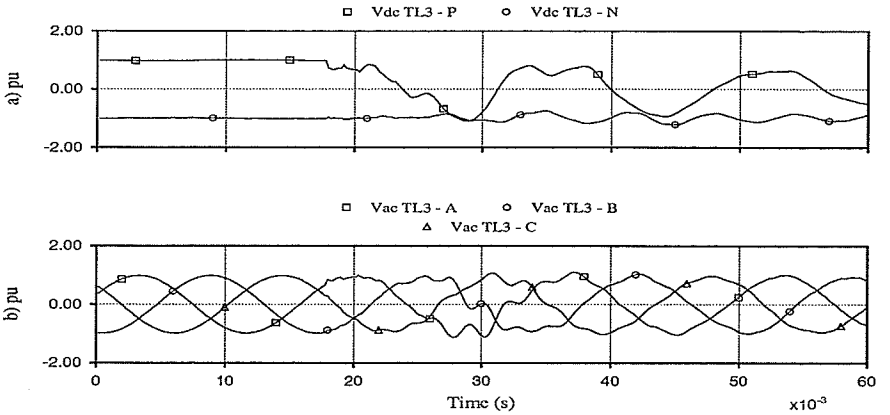

Figure 3 .39 : Voltage waveforms for ac–dc contact fault.
(fault applied at TL3 at crest of negative voltage phase "b")

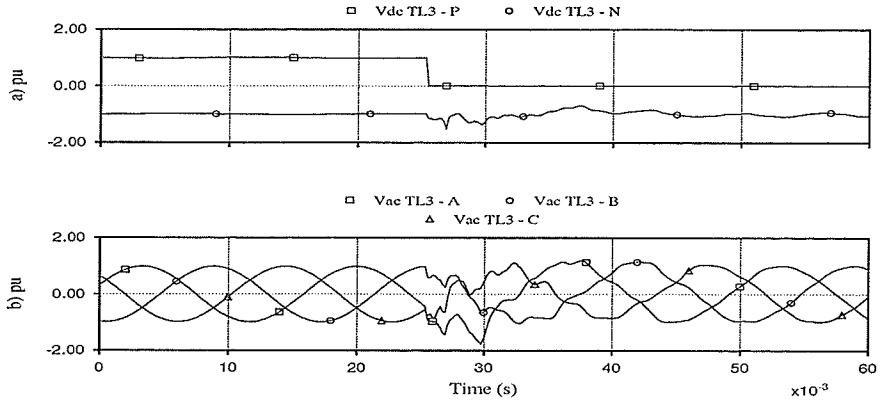

Figure 3 .40 : Voltage waveforms for dc line to ground fault.
(fault applied at TL3 at instant of the crest of positive voltage phase "b")

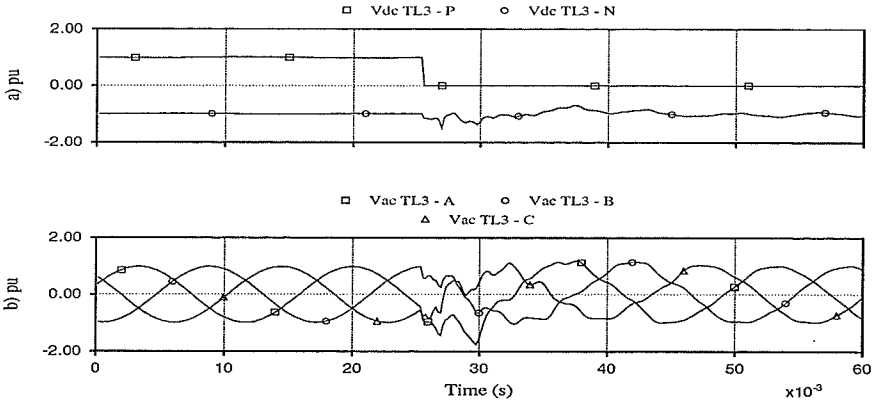

Figure 3 .41 : Voltage waveforms for dc line to ground fault.
(fault applied at TL3 at instant of the zero crossing voltage phase "b")

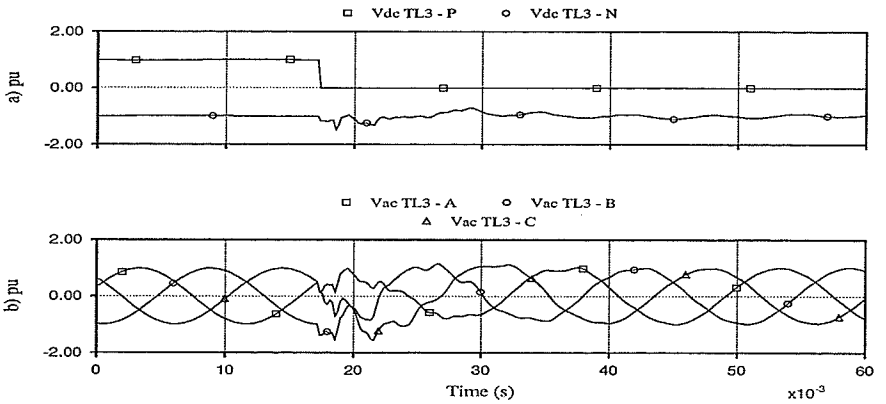

Figure 3 .42 : Voltage waveforms for dc line to ground fault.
(fault applied at TL3 at instant of the crest of negative voltage phase "b")

3 .3 OVERVOLTAGES ON THE BLOCKING FILTERS

As described earlier the blocking filters at the neutral point of the HVDC converters prevent the flow of 60 Hz currents induced by the ac line into the dc circuit. This avoids saturation of the converter transformers. However faults such as ac–dc contact faults or line to ground faults on the converter ac system can set up a 60 Hz oscillation in this tuned filter. Although the dc current has only a small 60 Hz component, the dc voltage can have a significant 60 Hz component.

Figure 3 .43 shows the dc current and voltages for an ac–dc contact fault. The fault is cleared by opening the ac circuit breakers on the three phase line at either end. In this case the blocking filter arrester was not modeled and the overvoltage on the blocking filter was approximately 270 kV. It is important to limit the overvoltage across the blocking filter because it increases the insulation level requirement for the converter valves.

Figure 3 .44 shows the same fault with a 39 kV rated metal oxide gapless arrester protecting the blocking filter. The residual voltage of the arrester is 78 kV crest (10 kA, 8/20 μs). In order to rapidly damp out the filter oscillation, a resistor was placed across the capacitor to reduce the quality factor of the blocking filter to 50. The peak overvoltage was then limited to 68 kV crest .

Figure 3 .45 shows the dc overvoltage and arrester energy in the rectifier side for ac–dc contact fault for three different configurations in the blocking filter. In the first case the ac–dc contact fault was applied with the blocking filter without arrester and the resistor R1 as shown in Figure 3 .46 a). In the second case the same fault was applied with 39 kV arrester protecting the blocking filter. The energy absorbed by the arrester was 2630 kJ. For this energy absorption twelve parallel columns are required (based on an energy capability of 7 kJ / kV(of rated voltage) per arrester column. No attempt was made to determine the fault case which would be the limit for the energy rating of the blocking filter arresters. In the last case the ac–dc contact fault was applied with the blocking filter with a 39 kV arrester and the resistor R1=1885 ohms as shown in Figure 3 .46 b). In this case the energy absorbed by the arrester was 2470 kJ. The resistor R1 reduced the energy absorbed by the arrester by 6.1%.

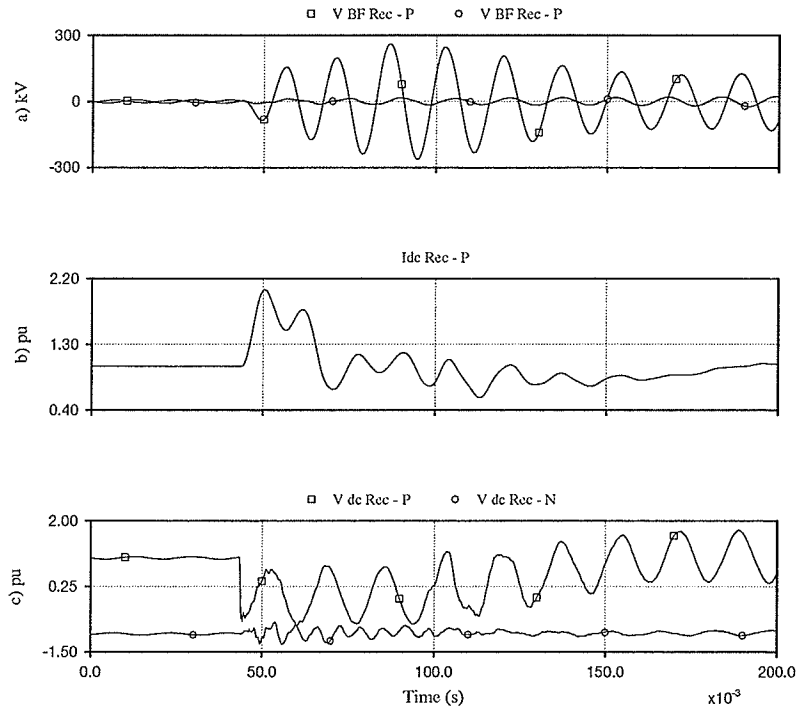

Figure 3 .43 : Voltage and current waveforms for ac–dc contact fault (without blocking filter arrester).

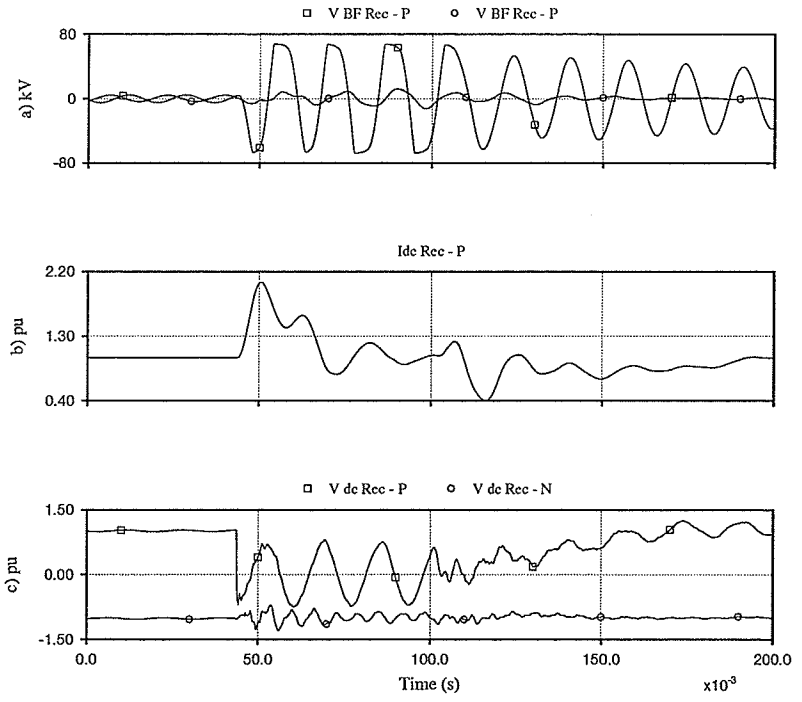

Figure 3 .44 : Voltage and current waveforms for ac–dc contact fault (with blocking filter arrester).

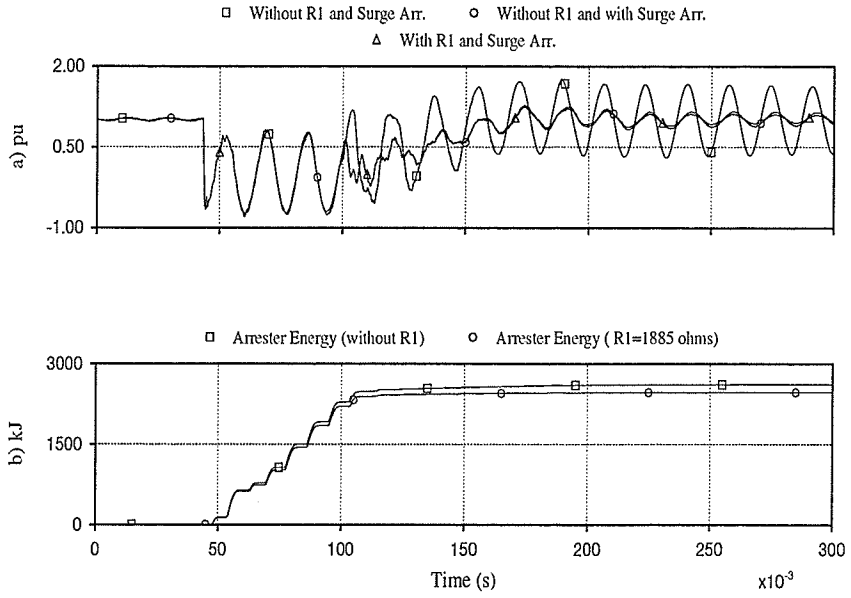

Figure 3 .45 : Waveforms for ac–dc contact fault for different blocking filter configurations.

a) Rectifier dc voltage

b) Blocking filter arrester energy

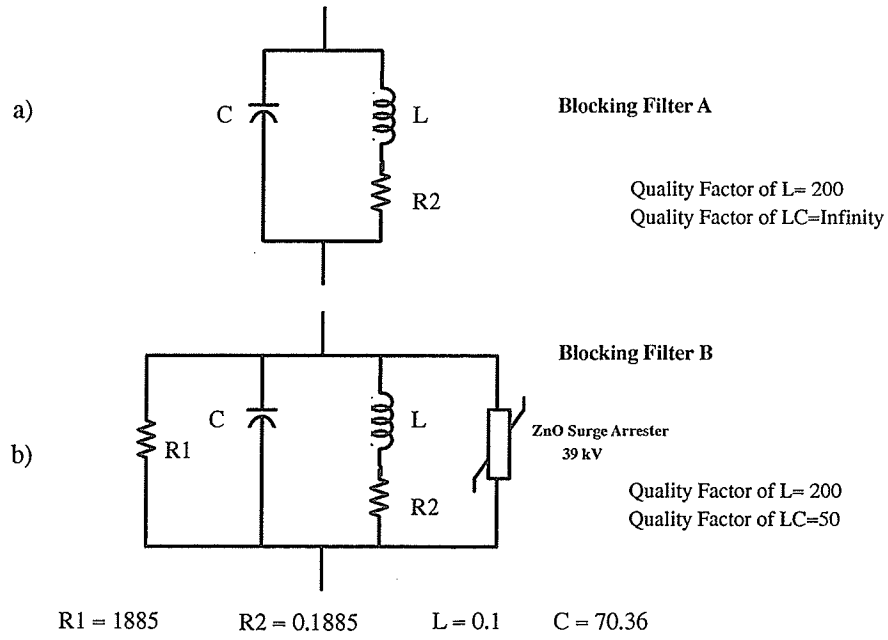

All resistances in **Ω**, *inductances in H* and *capacitances in μF*

Figure 3 .46 : Blocking filter design

3 .4 TRANSMISSION LINE MODEL COMPARISON

BERGERON MODEL

The bergeron model is based on a distributed L–C parameter travelling wave line model with lumped resistance. This model produces a constant surge impedance and is essentially a single frequency model. The Bergeron method can be used for any general fundamental frequency impedance studies such as relay testing or matching load–flow results.

THE FREQUENCY–DEPENDENT LINE MODEL

The frequency–dependent line model is basically a distributed R–L–C travelling wave model which incorporates the frequency dependence of all parameters. Because the Bergeron model is adequate for studies which essentially only require the correct fundamental frequency impedance, the frequency–dependent line model should be used for all studies which require frequencies other than the fundamental to be represented accurately. The frequency–dependent line model is based on the theory developed by J. Marti [19]. The results for the ac and dc overvoltages with the frequency dependent transmission line model and the Bergeron model were compared. The comparison was performed only for the strongest system (SCR=11.33) with the case of hybrid ac–dc line (ac line transposed) and for the case where there was no electromagnetic coupling between the ac and dc lines. Figure 3 .47 shows the results for the hybrid ac–dc line case. Figure 3 .48 shows the results for the case without electromagnetic coupling between the ac–dc lines.

The simulation show that the Bergeron model results in overvoltages that exceed the ones calculated more accurately from the from the frequency dependent transmission line model. Hence if one is interested in a worst case design, one could still use the Bergeron model.

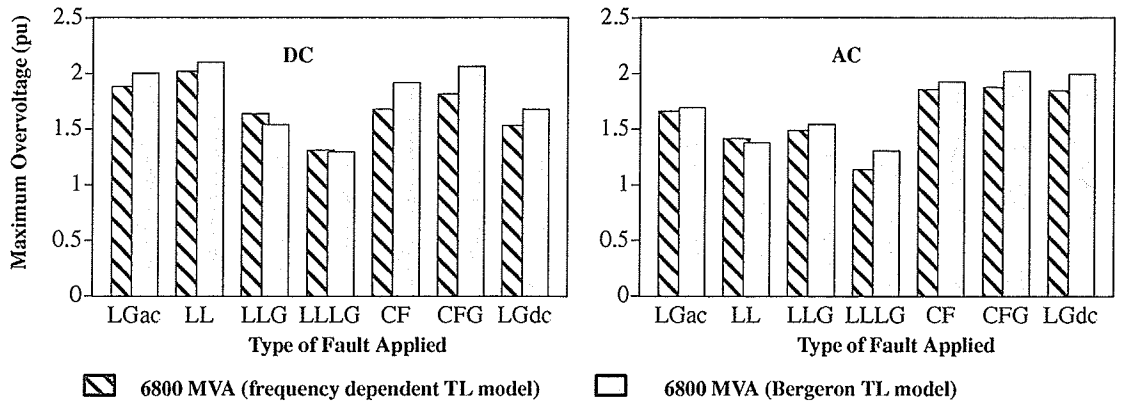

Figure 3 .47 : Maximum dc and ac and dc line overvoltage for different types of faults.
(ac line transposed).

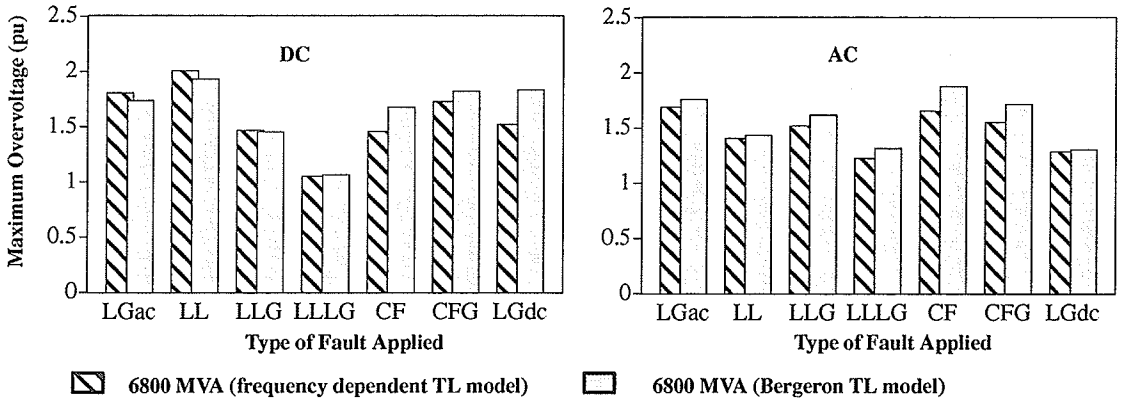

Figure 3 .48 : Maximum dc and ac line overvoltage for different types of faults.
(no coupling between ac and dc lines).

3 .5 EFFECT OF BLOCKING FILTER ON AN AC UNTRANSPOSED LINE

The overvoltages were compared for two different configurations in the hybrid ac–dc system, SCR=11.33. In one configuration the ac conductors were untransposed and with blocking filter (BF) present and in the other configuration the ac conductors were transposed in the absence of blocking filter. Figure 3 .49 shows the results of this overvoltage study. The results indicate that for most of the faults the dc line overvoltages are slightly higher for the case when the ac conductors are transposed

and without blocking filter, except for dc line to ground and line to line fault where the higher dc line overvoltage occurs for the other configuration. The ac line overvoltage results show that for most of the faults the higher overvoltage occurs for the case when the ac conductors are untransposed.

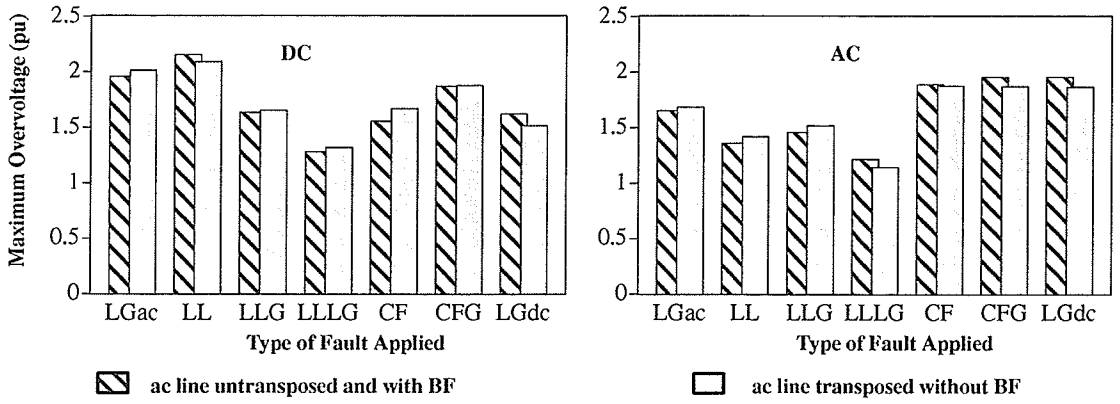

Figure 3 .49 : Maximum dc and ac line overvoltage for different types of faults.

3 .6 EFFECT OF GROUND RESISTIVITY ON OVERVOLTAGE

A study of the effect of the ground resistivity on the ac and dc overvoltage was carried out. The hybrid ac–dc system with SCR=11.33 and the ac line transposed was used as the base case. Figure 3 .50 shows the overvoltages obtained for ground resistivities (ρ) equal to 10 , 100 and 1000 ohms–m.

The sensitivity studies showed that the magnitude of calculated dc line overvoltage increases with ground resistivity with the overvoltage being increased up to 7.8 % for 1000 ohms–m resistivity and being reduced up to 9.1% with a ground resistivity of 10 ohms–m. The magnitude of calculated ac line overvoltage is higher for higher ground resistivity for all faults involving only the ac conductors (LGac, LL, LLG, and LLLG) with the overvoltage being increased up to 37 %. However when the fault involves a dc conductor (CF, CFG and LGdc) the ac line overvoltages are higher for lower the ground resistivity.

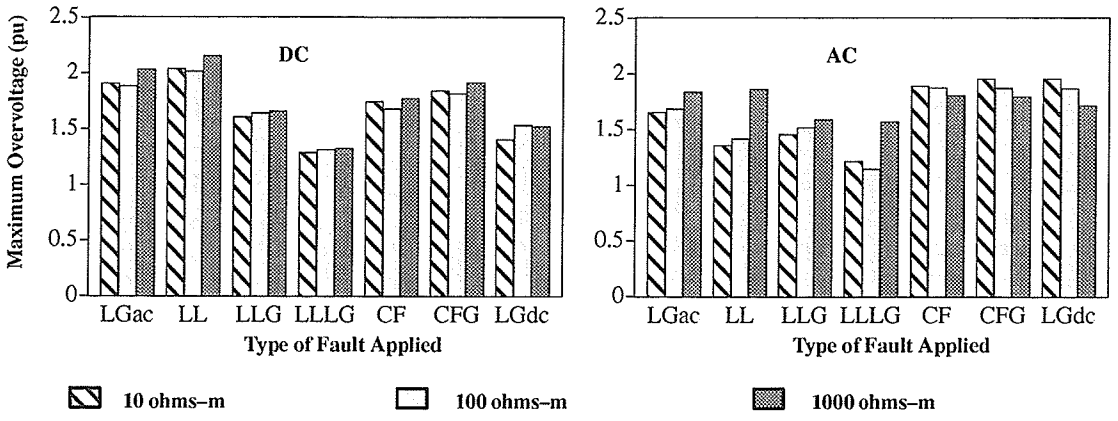

Figure 3 .50 : Maximum dc and ac line overvoltage for different types of faults.
(ac line transposed)

3 .7 AC LINE TRANSPOSED VERSUS DC LINE TRANSPOSED

The overvoltages were compared for two different configurations in the hybrid ac–dc system, SCR=11.33. In one configuration the ac conductors were transposed and in the other configuration the dc conductors are transposed (with ac line line untransposed). Figure 3 .51 shows the results of this overvoltage study. It is seen that for most of the faults the dc line overvoltages are higher for the case when the dc conductors are transposed for all faults involving the dc conductors and lower for faults involving only ac conductors. Except for dc line to ground and line to line fault where the higher dc line overvoltage occurs for the other configuration. The ac line overvoltage results show that for most of the faults the higher overvoltage occurs for the case where the ac conductors are untransposed.

The results for the ac line overvoltages indicate that the magnitude of calculated ac overvoltages are approximately the same for both cases except for three phase to ground fault (LLLG) and contact fault (CF) were the overvoltages are larger for the case with the dc line transposed.

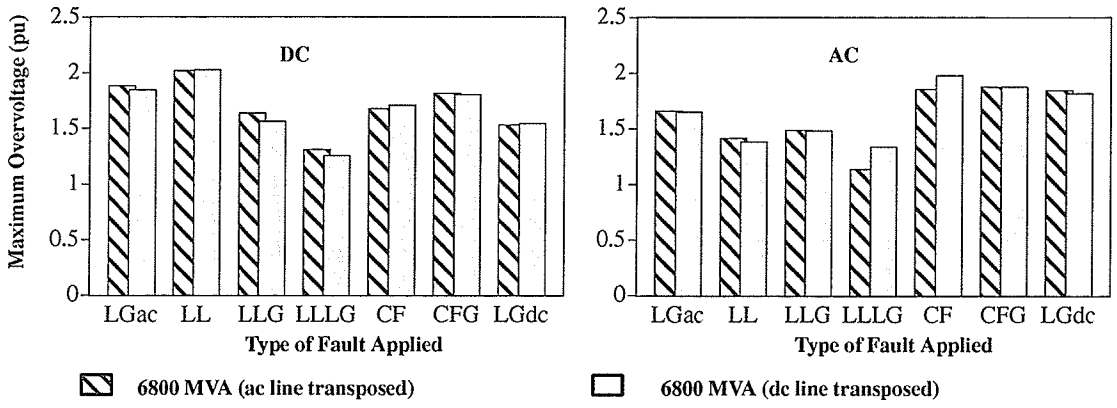

Figure 3 .51 : Maximum dc and ac and dc line overvoltage for different types of faults.
(ac line transposed)

3 .8 FAULT PHILOSOPHY

The duration of all types of faults was set to 50 milliseconds and the fault was cleared at current zero. Except for ac–dc conductor contact fault (CF) and ac–dc conductor contact fault to ground (CFG) the faults were cleared by opening circuit breakers at both ends on the ac line.

In the overvoltage studies faults were simulated at time intervals of 24^0 of inception point of the fault in one period ($360^0/24^0$=15 fault inception points) and the maximum overvoltage at any of the measuring locations was recorded.

The faults were applied at either the sending or receiving ends or at any one of the five equally spaced locations in between (TL1, ..., TL5). Each segment represents 65 km of line. The overvoltages were recorded at any locations along the ac–dc lines. Appendix A shows the PSCAD/EMTDC draft diagram of the faults logic applied in the overvoltage studies.

3 .8 .1 DC LINE FAULT

Short circuits on the dc line are cleared by firing control of the valves. The main characteristic of a dc line short–circuit is that once started, due to any permanent or temporary fault, it will not be extinguished by itself until the current is brought down to zero and the arc deionizes.

As the fault occurs, the dc line voltage collapses, the rectifier current tends to rise and the inverter current tends to fall. The only means of clearing a dc line fault is to force the firing angle of the rectifier beyond 90^0, say $\alpha=135^0$, as soon as the fault is detected. This operation to force the firing angle to 135^0 is called **forced retard**. This firing angle is kept at that value until arc extinction and deionization are likely to be completed.

The protection philosophy in our study was to apply the forced retard (set $\alpha=135^0$) 5 ms after fault inception and maintain it for 200 ms to de–energize the dc line and clear the fault; following which the firing angle is ramped down to 0^0 in 100 ms. Figure 3 .52 shows how the control action of the forced retard was designed. A maximum select block is used so that the forced retard alpha order is override to the normal firing control during the recovery from the dc line fault after which the normal firing control order mode resume its operation.

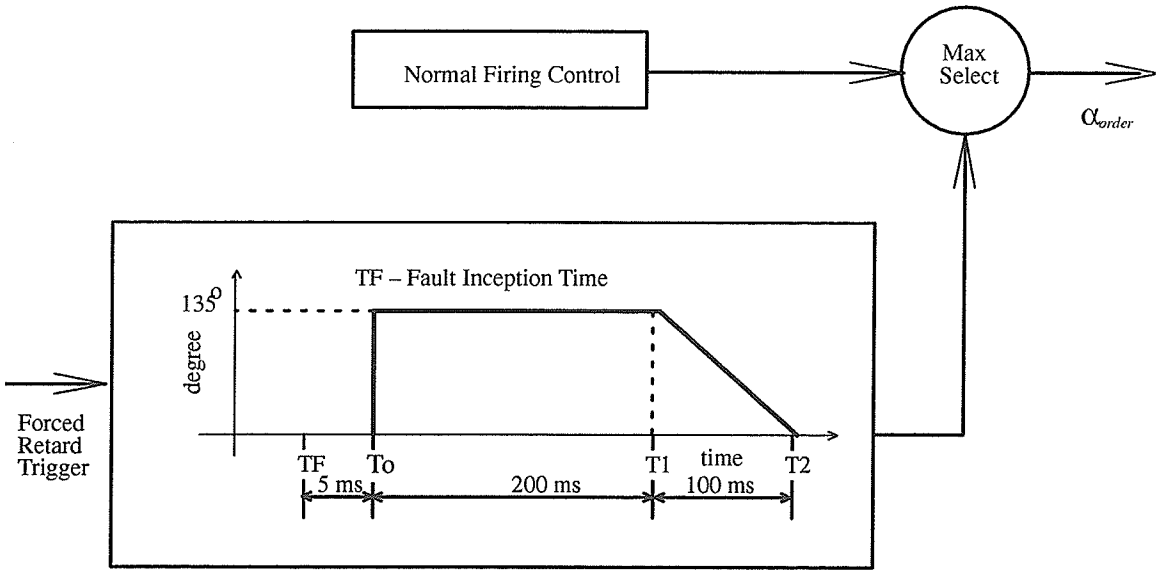

Figure 3 .52 : Forced retard strategy applied in the rectifier.

3 .8 .2 AC–DC CONDUCTOR CONTACT FAULT

The ac–dc conductor contact faults (CF) were applied between the positive pole and its closest ac conductor. The circuit breakers, at both ends of the ac line, were set to trip 50 ms after the fault was applied.

3 .9 AC–DC CONDUCTOR CONTACT FAULT TO GROUND

When the ac–dc conductor contact fault is also simultaneously connected to ground the dc controller senses this as a dc line to ground fault and forces the dc current to zero, removing the cause of the dc overvoltages. The circuit breakers, at both ends of the ac line were set to trip 50 ms after the fault was applied.

In the beginning of the study it was identified that the opening of the three phases circuit breakers, at both ends of the ac line, resulted in excessive overvoltages on the unfaulted ac conductors. Figure 3 .53 shows an example of ac–dc conductor contact fault to ground (CFG) between phase "*c*" and the closest dc conductor (positive pole) at intersection TL5. The fault was applied at negative crest of phase "*c*" voltage. In this example the tripping time of the breakers (top) was selected to be equal to 41.33 seconds, which correspond to the highest overvoltage on the ac line.

It was concluded that the magnitude of these ac line overvoltages are related to the phase sequence of the opening of the circuit breakers. In order to reduce these overvoltages multiple simulations were run in the hybrid system to find out the most appropriate phase trip sequence of circuit breakers, on both side of the ac transmission line.

PSCAD/EMTDC has a "multiple run feature" which is able to run the same simulation a multiple number of times, optimizing a selected parameter by varying an associated value on each run iteration. The ac line overvoltage was the optimized parameter and the tripping time of the breakers (top) was selected as the associate value to be changed in multiple run. A multiple run of 134 cases was simulated, from top=36.67 to top=53.33 ms (within one cycle), with interval of 1.24e–4 seconds ((1/60)/134) and the maximum ac line overvoltage was recorded.

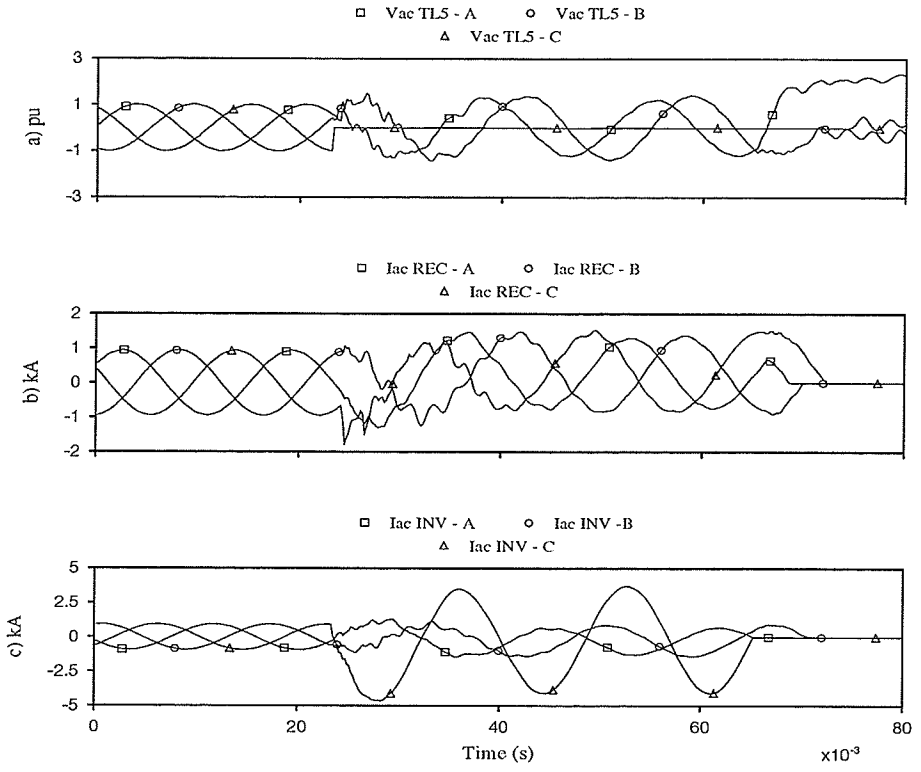

Figure 3 .53 : Voltage and current waveforms for ac–dc contact fault to ground.

(three phases circuit breakers were ordered to trip)

After carried out many cases of this type of fault, at different locations along the hybrid line and with different tripping time, it was concluded that the best way to clear this type of fault, with lower overvoltage stress, is through the opening of only the ac conductor under fault, at both ends.

The main reason for these overvoltages is because in three phase breakers operation it can happens that the unfaulted ac conductor once open in one end will be charged by the the coupling effect from the other ac–dc conductors.

Figure 3 .54 shows the plot (from multiple run) of the magnitude of the maximum ac line overvoltage versus the tripping time for the ac–dc conductor contact fault to ground applied at intersection TL5. This Figure shows two example cases. In the first one the breakers at the rectifier and inverter ends are ordered to trip the three phases. In the second only the phase under fault is

ordered to trip at both ends. As you can see the ac line overvoltages are much higher for the first case. The maximum ac line overvoltages for the second case are slightly the same for all selected tripping time.

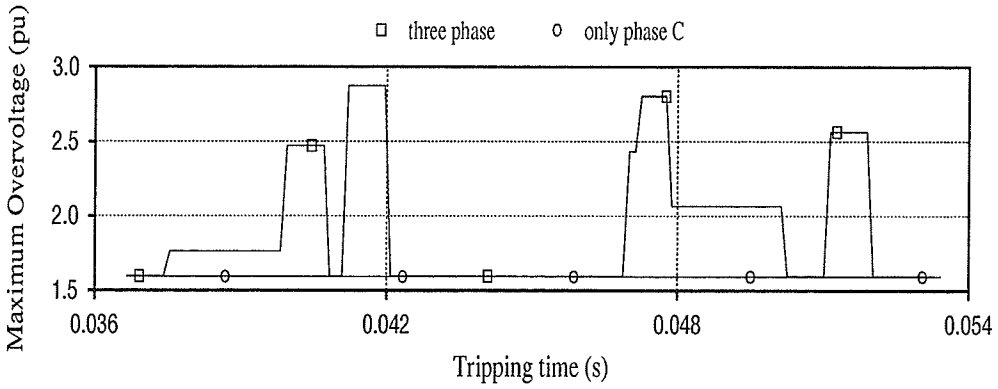

Figure 3 .54 : Maximum ac line overvoltage x tripping time of the circuit breakers.

The same type of fault shown in Figure 3 .53 is now applied in the same position (TL5), with the same trip time (top=41.33 ms), which correspond the worst case (highest overvoltage). In this case only the breaker on phase "*c*" (the closest ac conductor to the positive pole at location TL5) was ordered to trip at both ends. Figure 3 .55 shows that the ac line overvoltage was substantially lower compared to the case when the three phase breakers were ordered to trip.

3 .10 SUMMARY

The following observations resulted from this chapter:

– faults involving the ac conductor to ground closer to the rectifier converter introduce negative sequence voltage on the bus which converts to a second harmonic overvoltage on the dc side.

– dc line overvoltages at other line locations (TL1, TL2, ... etc.) are mainly fundamental frequency overvoltages due to the coupling effect between the ac and dc lines.

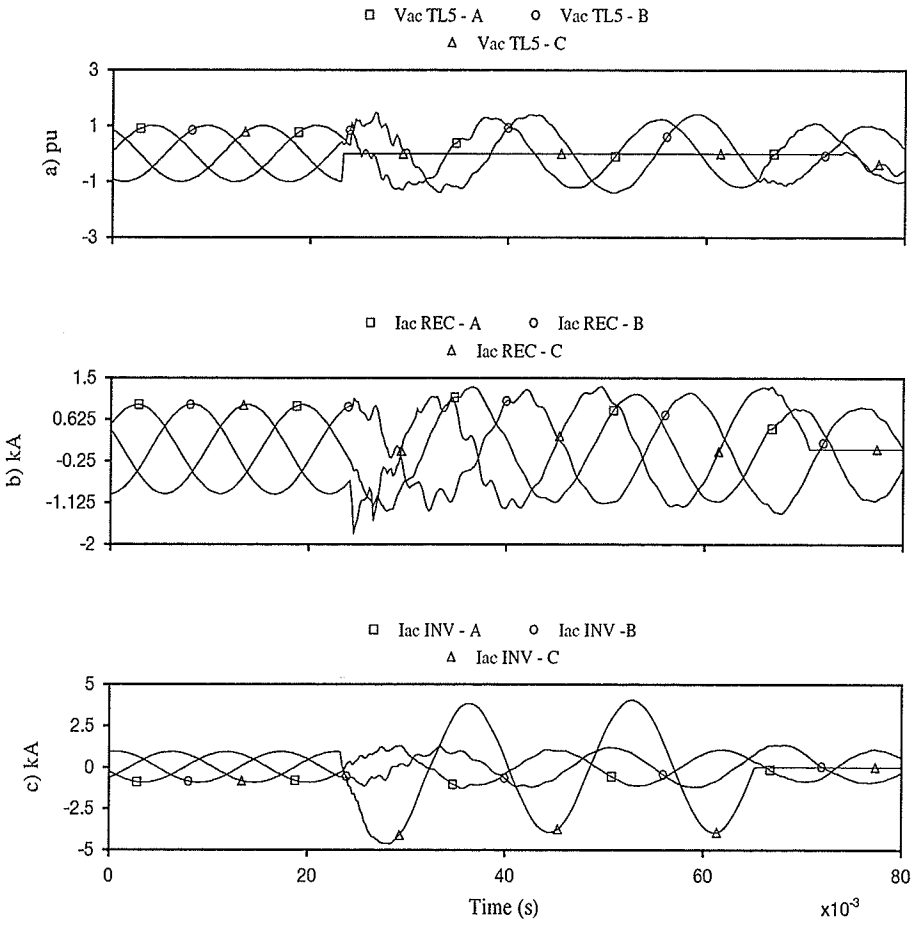

Figure 3 .55 : Voltage and current waveforms for ac–dc contact fault to ground.

(only phase "c" breakers were ordered to trip)

– the dc line overvoltages are more severe for the stronger (6800 MVA) system.

– overvoltages on the ac line increased with a decrease in system strength for faults involving the ac conductors.

– with ac–dc contact faults and dc line faults the ac overvoltages are smaller for the weaker system.

– the overvoltages are larger when the ac–dc system are electromagnetically coupled. This is more pronounced for ac line overvoltages when the faults involve only the dc conductors.

–in general the overvoltages on the ac and dc lines are larger when the ac and dc lines are coupled.

– the overvoltages are higher for the Bergeron transmission line model compared to the frequency dependent transmission line model.

– overvoltages for the dc line in a hybrid ac–dc environment are higher than for a a dc line alone

– transposition of the ac conductors reduces the overvoltages.

– the blocking filter in the dc neutral has a tendency to oscillate, which can cause overvoltages on the dc line. These oscillations can be damped by a resistor–arrester combination across the filter.

– resonances may exist in the ac or dc system which can cause harmonic overvoltages.

Chapter 4

Firing Angle Modulation for Eliminating DC Line 60 Hz Currents

4.1 INTRODUCTION

It is a well known property of the dc conversion process that a current component of frequency f on the dc side appears on the ac side as a component of frequency $f_0 \pm f$, f_0 being the fundamental ac frequency, taken here to be 60 Hz [4], [20], [21]. If the dc transmission line lies adjacent to an ac transmission line, there is a possibility for a fundamental frequency (60 Hz) current component to be induced into the dc line, referred to as (I_{60}). This current would then appear in the secondary winding of the converter transformer as a dc component (I_{dc}) and also a 120 Hz component (I_{120}) superimposed on the fundamental 60 Hz component. This dc current component eventually flows as transformer magnetizing current and offsets the knee of the flux–current characteristic and if excessive, causes unsymmetrical saturation of the converter transformer. This can lead to an increase in audible noise and result in possible loss of life expectancy of the transformer [4], [22]. Other reported problems are inaccurate control and protection measurements because of saturation of current transformers on the ac side. Because of the very low magnetizing current requirement of HVDC transformers, even a few tens of amperes of dc current is considered by some as excessive.

There are several instances where a dc and ac line follow adjacent corridors and such induction effects could be detrimental. With the added difficulty of obtaining transmission line rights of way there is considerable interest in having hybrid ac–dc transmission systems in which ac and dc conductors are placed on the same tower structure. The coupling of the 60 Hz component would be even more severe in such cases.

Several alternatives have been proposed for mitigating the dc currents in the transformer windings. One proposed alternative is to use dc side blocking filters for the 60 Hz induced currents. This scheme sometimes results in increased dc side overvoltages. Another alternative is to transpose the ac lines. This option does not completely eliminate the induced harmonics especially when ac and dc conductors are on the same tower as in hybrid ac–dc lines. Another possible alternative is to use modulation of the converter's firing angle. This method appears to have the advantage of not requiring as extensive modifications to the power equipment as in the other choices. We explore this alternative in this chapter and chapter 5 . Some theoretical results are presented on an idealized system to understand the essential phenomena. Subsequent investigations are carried out on a realistic system using an electromagnetic transients simulation program (PSCAD/EMTDC) [7]. The results indicate that it is possible to eliminate the dc currents in the transformer using such a scheme. However, there are some undesirable side–effects such as the generation of non–characteristic harmonics [23].

4 .2 MEASUREMENT OF THE COUPLING BETWEEN THE AC AND DC LINE

The fundamental frequency current flowing on the dc side of the converter, I_{60}, will be seen as a second harmonic, I_{120}, and dc components, I_{dc}, in the converter transformer secondary winding, as shown in Figure 4 .1 . The dc component current is the main concern to the ac–dc hybrid system, as it can result in saturation of the converter transformer. Therefore we have to maintain the induced current on the dc line from the ac line, as low as possible in order to minimize adverse impact on the ac–dc hybrid system.

Positive sequence currents of various magnitudes were introduced in the ac line, and the effect on the dc system was observed, as shown in Figure 4 .2 . The current in the ac side varied from 0.0 to 1.4 kA crest. Plots of the induced current in the dc line are shown in Figure 4 .3 . Coupling effects with two different blocking filters and two different ac line configurations were investigated.

The fundamental frequency current flowing on the dc side of the converter, I_{60}, the second harmonic current, I_{120}, and dc current components, I_{dc}, in the converter transformer secondary winding were measured for the following configuration:

a) ac line untransposed and with blocking filter type A;

b) ac line untransposed and with blocking filter type B;

c) ac line untransposed and without blocking filter;

d) ac line transposed and without blocking filter.

The blocking filter type A is the one shown in Figure 3 .46 a), but without the resistor R2 (ideal blocking filter).

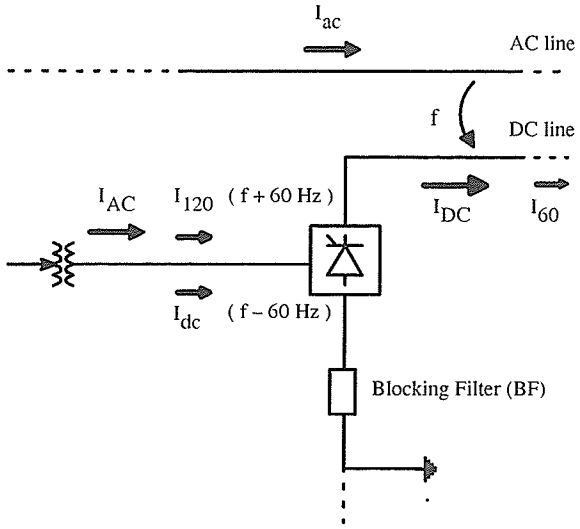

Figure 4 .1 : Conceptual circuit illustrating the coupling between the ac line and dc line and the effect in the secondary of the HVDC converter transformer.

Figure 4 .3 c) shows the plots of fundamental frequency current, I_{60}, induced in the dc line. The corresponding dc, I_{dc}, and the second harmonic, I_{120}, components introduced into the secondary of the converter transformer are shown in Figure 4 .3 a) and 4 .3 b), respectively.

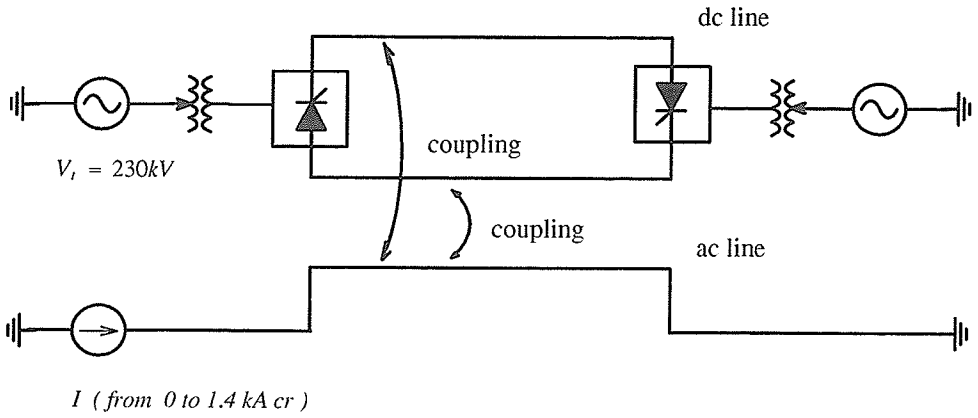

Figure 4 .2 : Conceptual circuit for driving current in coupled line.

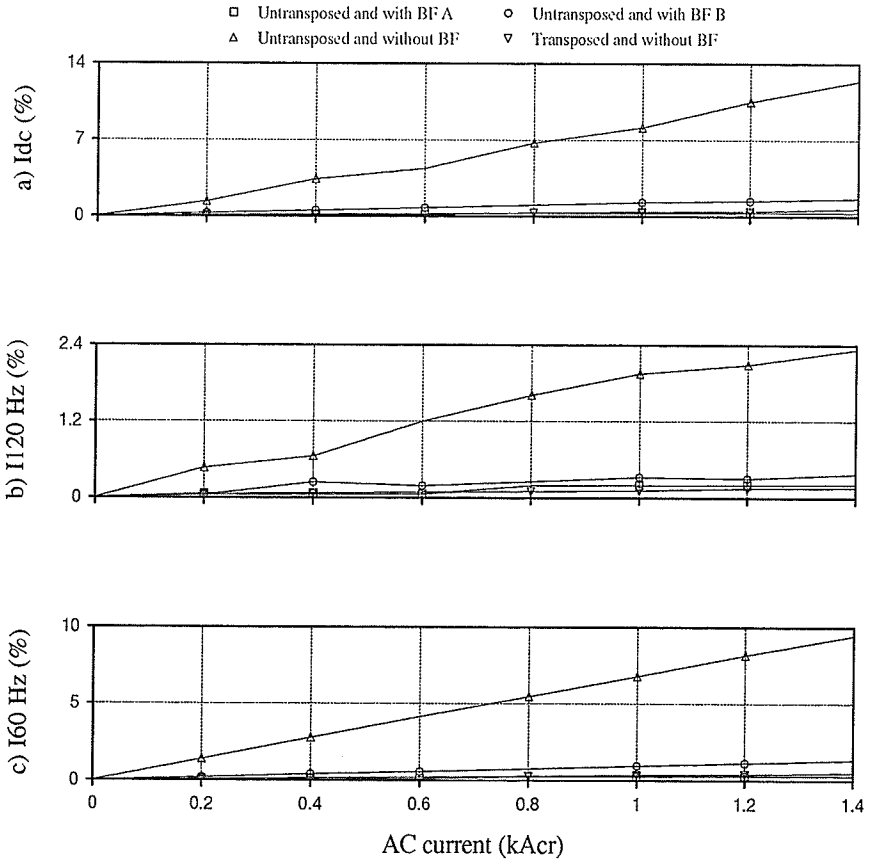

Figure 4 .3 : Percentage of current, a) dc component in the secondary o the transformer, b) 2nd harmonic component in the secondary of the transformer, c) Fundamental component in the dc line induced from the ac line.

The quantities I_{60}, I_{dc} and I_{120} in Figure 4 .3 are defined by Equation 4 .1 .

$$I_{60}\ (\%) = \frac{I_{60}}{I_{DC}} \qquad (4.1)$$

$$I_{dc}\ (\%) = \frac{I_{dc}}{I_{AC}}$$

$$I_{120}\ (\%) = \frac{I_{120}}{I_{AC}}$$

Figure 4.4 shows the same result of Figure 4.3 except that each plot shows the three components of current (I_{dc}, I_{120} and I_{60}) for each system configuration, such as with and without transposition and with different blocking filters.

In reference [4] is cited that the limit for the dc component in the dc line, I_{dc}, is often 0.1% of the rated dc current. This value is unrealistically small. Without considering the ac–dc coupling effect, the dc offset solely due to the firing angle unsymmetry can exceed this limit.

Assuming the firing angle unsymmetry of the converter is $\pm\ 0.1^0$, which is a very good value. The dc offset in the transformer winding is in the worst case as high as 0.11% of the dc current value, as shown in Figure 4.5.

$$I_{offset} = \frac{4\ .\ 0.1^0}{360^0}\ I_d = 0.11\%\ I_d$$

However,

$$I_d = \frac{\sqrt{3}}{\sqrt{2}}\ I_{ac_{rms}}\ ,\quad hence,\quad I_{offset} = 0.11\%\ \frac{\sqrt{3}}{\sqrt{2}}\ I_{ac_{rms}} = 0.13\ I_{ac_{rms}} \qquad (4.2)$$

According to the estimation above, the dc offset limit of 0.1% for the converter transformer is extremely small. In the practice the converter transformer must be designed for a higher dc offset.

4.3 RELATION BETWEEN THE 60 HZ COMPONENT IN THE DC LINE AND THE DC COMPONENT IN THE SECONDARY OF THE TRANSFORMER

Figure 4.6 shows the six–pulse bridge converter circuit with the notation adopted from reference [20]. The power source in Figure 4.6 is assumed to be balanced sinusoidal of constant voltage and

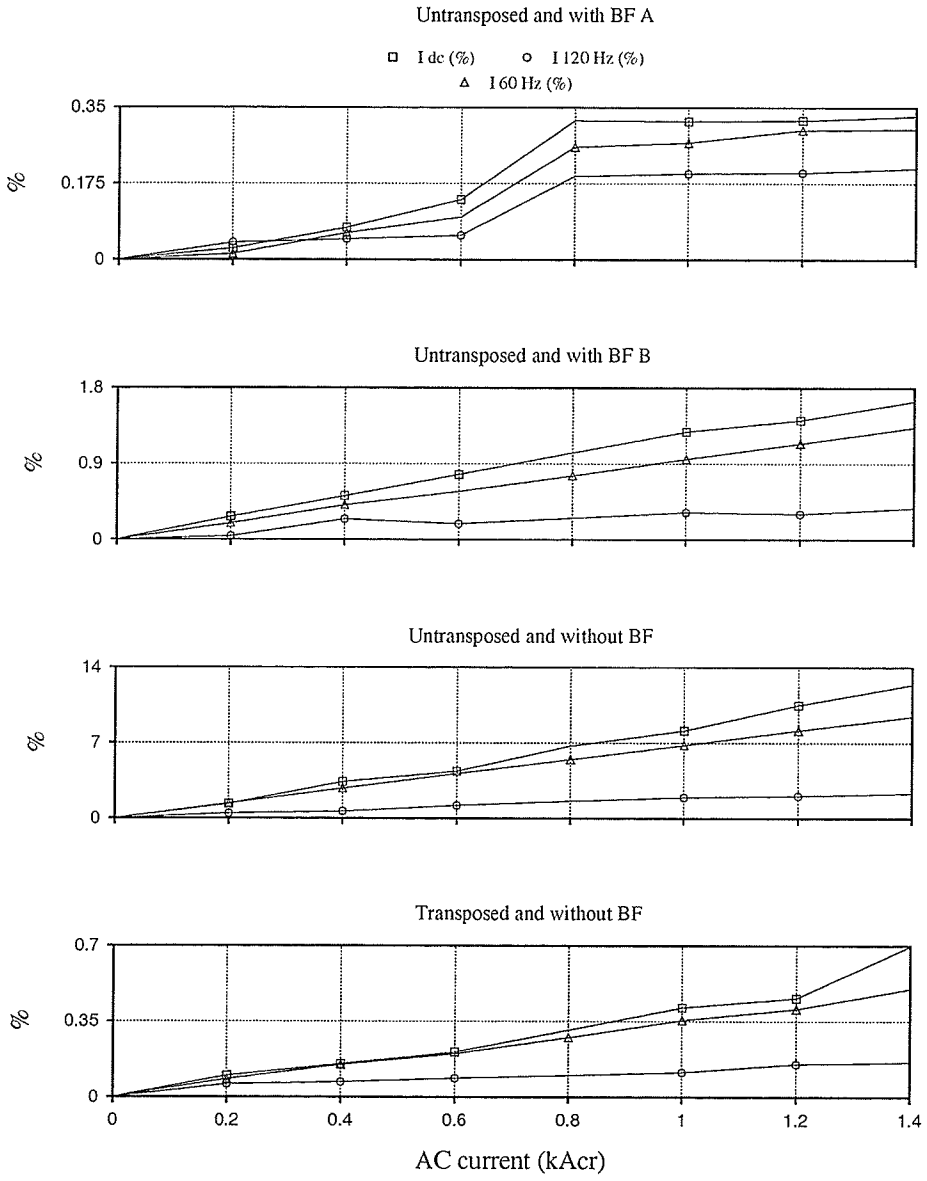

Figure 4 .4 : Percentage of dc, 2nd harmonic and 60 Hz current.

frequency in series with equal lossless inductances. The circuit in Figure 4 .6 contains a three–phase 60 Hz voltage source, a dc current source and a one–phase 60 Hz current source. In the analysis of this circuit, the effect of the three sources are superimposed. The 60 Hz current source represents the fundamental frequency current component induced from the ac line into the dc line.

In this section the study of coupling between the ac line and the dc line will be conducted with two different approaches. Fist of all the induced 60 Hz current in the dc line and the dc current reflected to

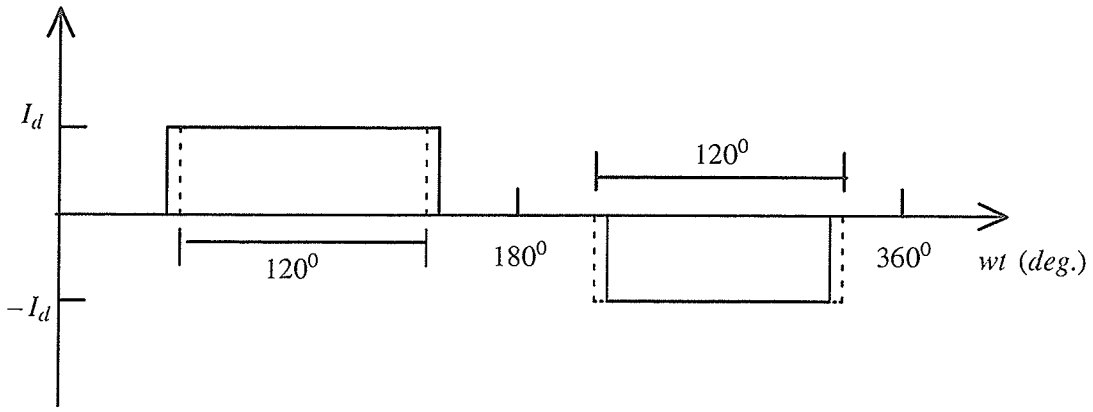

Figure 4 .5 : Dc offset current in the converter transformer winding.

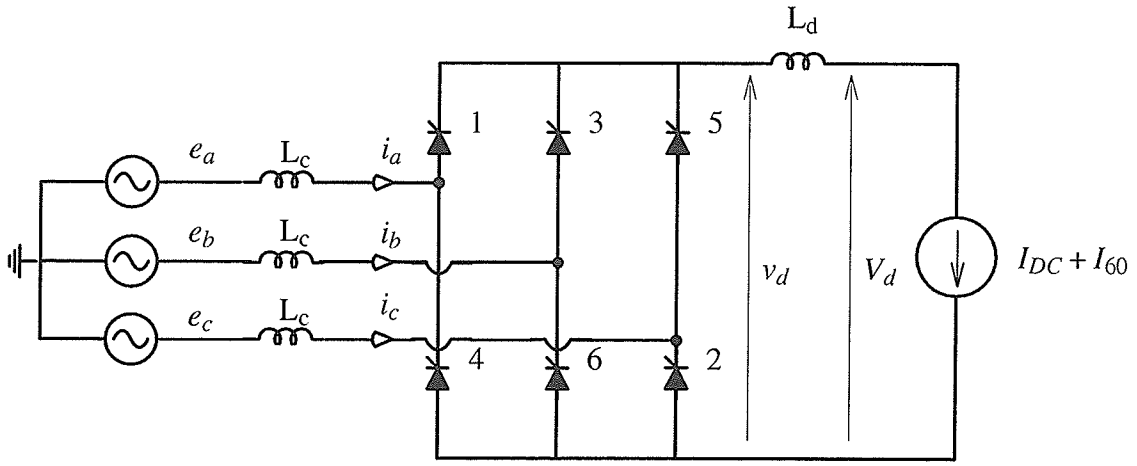

Figure 4 .6 : Configuration of a six–pulse bridge converter. The valves are numbered in their firing order.

the secondary of the transformer will be analyzed analytically and a relation between this two currents will be identified. Secondly the analytical calculation is then validated by using a simple simulated case with a six–pulse converter bridge.

4 .3 .1 ANALYTICAL APPROACH

The instantaneous line–to–neutral voltage of the source are taken as:

$$e_a = E_m \cos(\omega t + \frac{\pi}{3}) \qquad (4.3)$$

$$e_b = E_m \cos(\omega t - \frac{\pi}{3})$$

$$e_c = E_m \cos(\omega t - \pi)$$

corresponding to the horizontal projections of the rotating vectors shown in Figure 4.7.

The corresponding line–to–line voltages are:

$$e_{ac} = e_a - e_c = \sqrt{3} E_m \cos(\omega t + \frac{\pi}{6}) \qquad (4.4)$$

$$e_{bc} = e_b - e_c = \sqrt{3} E_m \cos(\omega t - \frac{\pi}{6})$$

$$e_{ba} = e_b - e_a = \sqrt{3} E_m \cos(\omega t - \frac{\pi}{2}) = \sqrt{3} E_m \sin(\omega t)$$

$$e_{ca} = e_c - e_a = \sqrt{3} E_m \cos(\omega t - 5\frac{\pi}{6})$$

$$e_{cb} = e_c - e_b = \sqrt{3} E_m \cos(\omega t + 5\frac{\pi}{6})$$

$$e_{ab} = e_a - e_b = \sqrt{3} E_m \cos(\omega t + \frac{\pi}{2}) = -\sqrt{3} E_m \sin(\omega t)$$

Instantaneous currents and voltages of the three–phase bridge are shown in Figure 4.8, where the voltage of the three phase source is equal to 230 kV (phase–to–phase rms) and the dc current is equal to 1.5 kA. The 60 Hz current source, which represent the coupling effect, is assumed to be 10% of the total dc current, 0.15 kA. This value of 60 Hz current source would correspond to a situation where in the hybrid system we have a circulation of approximately 1.4 kA crest flowing in the ac line as shown in Figure 4.3. We have chosen this value of amplitude for 60 Hz current to exacerbate the coupling effect between the ac and the system.

Equations of the instantaneous secondary current of the converter transformer, for each phase, are shown in Equations 4.5, 4.6 and 4.7 for each interval of firing angle and commutation. Ia, Ib and Ic are the three phase currents on the valve side of the converter transformer. The constant A is the crest value of the induced 60 Hz current in the dc line connected to this six–pulse bridge. λ is the angle of the induced fundamental frequency component measured from the crossing zero of line–line

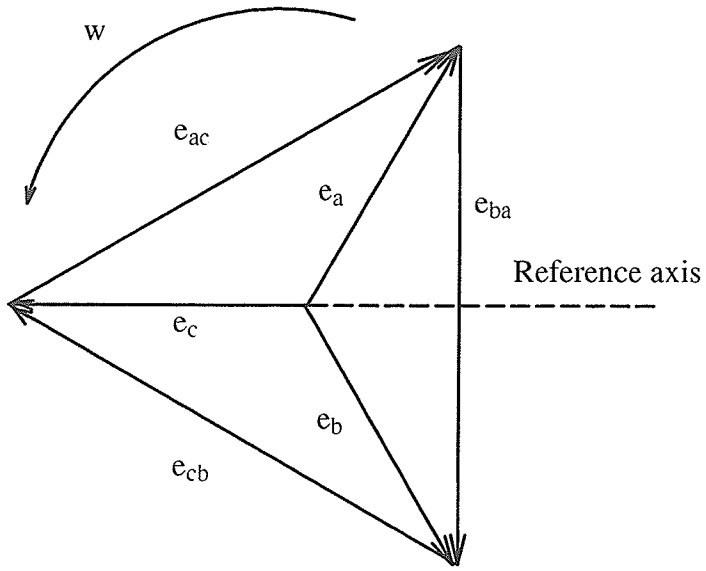

Figure 4.7 : Representation of the rotating vectors from the six–pulse bridge voltage source.

voltage e_{ba} on its positive gradient. Note that λ is completely arbitrary because the induced current can in theory have any phase angle.

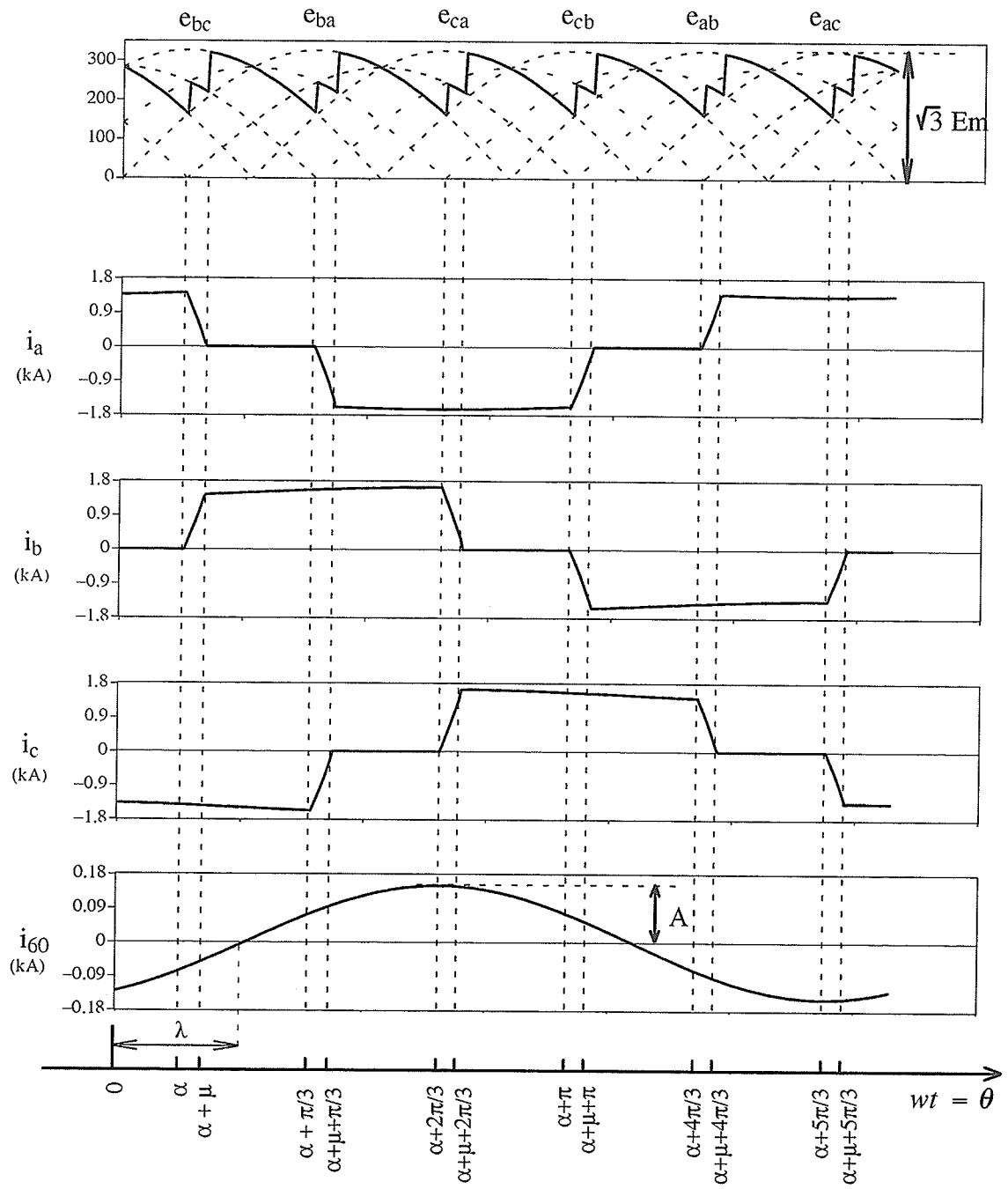

Figure 4 .8 : Instantaneous currents and voltages of six–pulse bridge converter with modulation of the firing angles. (With Overlap)

$$I_d = 1.5\ kAcr \qquad E_m = 230\frac{\sqrt{2}}{\sqrt{3}} = 187.8kVcr$$

$$A = 0.15\ kAcr \qquad \lambda = \frac{\pi}{3}$$

$$I_a = \begin{cases} I_d' , & 0 < \theta < \alpha \\ I_d' - I_{s2}\cos\alpha + I_{s2}\cos\theta , & \alpha < \theta < \alpha+\mu \\ 0 , & \alpha+\mu < \theta < \alpha+\frac{\pi}{3} \\ -I_{s2}\cos\alpha + I_{s2}\cos(\theta-\frac{\pi}{3}) , & \alpha+\frac{\pi}{3} < \theta < \alpha+\mu+\frac{\pi}{3} \\ -I_d' , & \alpha+\mu+\frac{\pi}{3} < \theta < \alpha+\pi \\ -I_d' + I_{s2}\cos\alpha + I_{s2}\cos\theta , & \alpha+\pi < \theta < \alpha+\mu+\pi \\ 0 , & \alpha+\mu+\pi < \theta < \alpha+4\frac{\pi}{3} \\ I_{s2}\cos\alpha + I_{s2}\cos(\theta-\frac{\pi}{3}) , & \alpha+4\frac{\pi}{3} < \theta < \alpha+\mu+4\frac{\pi}{3} \\ I_d' , & \alpha+\mu+4\frac{\pi}{3} < \theta < 2\pi \end{cases} \quad (4.5)$$

$$I_b = \begin{cases} 0 , & 0 < \theta < \alpha \\ I_{s2}\cos\alpha - I_{s2}\cos\theta , & \alpha < \theta < \alpha+\mu \\ I_d' , & \alpha+\mu < \theta < \alpha+2\frac{\pi}{3} \\ I_d' - I_{s2}\cos\alpha - I_{s2}\cos(\theta+\frac{\pi}{3}) , & \alpha+2\frac{\pi}{3} < \theta < \alpha+\mu+2\frac{\pi}{3} \\ 0 , & \alpha+\mu+2\frac{\pi}{3} < \theta < \alpha+\pi \\ -I_{s2}\cos\alpha - I_{s2}\cos\theta , & \alpha+\pi < \theta < \alpha+\mu+\pi \\ -I_d' , & \alpha+\mu+\pi < \theta < \alpha+5\frac{\pi}{3} \\ -I_d' + I_{s2}\cos\alpha - I_{s2}\cos(\theta+\frac{\pi}{3}) , & \alpha+5\frac{\pi}{3} < \theta < \alpha+\mu+5\frac{\pi}{3} \\ 0 , & \alpha+\mu+5\frac{\pi}{3} < \theta < 2\pi \end{cases} \quad (4.6)$$

$$
I_c = \begin{cases}
-I_d' , & 0 < \theta < \alpha + \frac{\pi}{3} \\
-I_d' + I_{s2}\cos\alpha - I_{s2}\cos\left(\theta - \frac{\pi}{3}\right) , & \alpha + \frac{\pi}{3} < \theta < \alpha + \mu + \frac{\pi}{3} \\
0 , & \alpha + \mu + \frac{\pi}{3} < \theta < \alpha + 2\frac{\pi}{3} \\
I_{s2}\cos\alpha + I_{s2}\cos\left(\theta + \frac{\pi}{3}\right) , & \alpha + 2\frac{\pi}{3} < \theta < \alpha + \mu + 2\frac{\pi}{3} \\
I_d' , & \alpha + \mu + 2\frac{\pi}{3} < \theta < \alpha + 4\frac{\pi}{3} \\
I_d' - I_{s2}\cos\alpha - I_{s2}\cos\left(\theta - \frac{\pi}{3}\right) , & \alpha + 4\frac{\pi}{3} < \theta < \alpha + \mu + 4\frac{\pi}{3} \\
0 , & \alpha + \mu + 4\frac{\pi}{3} < \theta < \alpha + 5\frac{\pi}{3} \\
-I_{s2}\cos\alpha + I_{s2}\cos\left(\theta + \frac{\pi}{3}\right) , & \alpha + 5\frac{\pi}{3} < \theta < \alpha + \mu + 5\frac{\pi}{3} \\
-I_d' , & \alpha + \mu + 5\frac{\pi}{3} < \theta < 2\pi
\end{cases} \qquad (4.7)
$$

where:

$I_d' = I_d + I_{60}$, where $I_{60} = A \sin(\theta + \lambda)$

I_d = Constant ripple–free direct current flowing in the dc line

A = crest value of the induced 60 Hz current in the dc line

λ = Phase difference between the ac line and the reference voltage Em

$I_{s2} = \frac{\sqrt{3}E_m}{2\omega L_c}$, from reference [20]

μ = overlap angle

E_m = crest value of line–to–neutral alternating voltage

In Figure 4.8 , I_d = 1.5 kA dc, A = 0.15 kA crest, $\lambda = \pi/3$ and E_m=187.8 kV_{crest} (230kV phase–phase $_{rms}$). E_m is the crest value of line–to–neutral alternating voltage (230 kV rms phase–phase).

The average (or direct current) of phase "*a, b and c*", I_{a0}, I_{b0} and I_{c0}, can be determined by integrating the instantaneous current over the period from 0 to 2π. For wt=θ, the current I_{a0}, I_{b0} and I_{c0} are equal to:

$$I_{a_0} = \frac{1}{2\pi} \int_0^{2\pi} I_a \, d\theta \qquad (4.8)$$

$$I_{b_0} = \frac{1}{2\pi} \int_0^{2\pi} I_b \, d\theta$$

$$I_{c_0} = \frac{1}{2\pi} \int_0^{2\pi} I_c \, d\theta$$

Substituting Equations 4.5 to 4.7 into equation 4.8 we obtain the following relation (see Appendix B.1).

$$I_{a_0}^2 + I_{b_0}^2 + I_{c_0}^2 = \frac{9}{2} \left[\frac{A}{\pi} \right]^2 \qquad (4.9)$$

A is the crest value of the fundamental frequency current in the dc line and I_{a0}, I_{b0} and I_{c0} are the dc component in the secondary of the converter transformer. In terms of rms value of the induced current(A_{rms}) the relation in the Equation 4.9 will be:

$$I_{a_0}^2 + I_{b_0}^2 + I_{c_0}^2 = 9 \left[\frac{A_{rms}}{\pi} \right]^2$$

$$\boxed{\frac{\sqrt{I_{a_0}^2 + I_{b_0}^2 + I_{c_0}^2}}{A_{rms}} = \frac{3}{\pi}} \qquad (4.10)$$

where:

$$A_{rms} = \frac{A}{\sqrt{2}}$$

4.3.2 SIMULATION APPROACH

The Equation 4.10 was confirmed by using a simplified six–pulse bridge converter as shown in Figure 4.6 and a detailed ac–dc hybrid system as shown in Figure 2.3. An electromagnetic transient simulation program PSCAD/EMTDC was used in this study. Appendix A shows the PSCAD/EMTDC draft diagram.

Figure 4.9 shows how the relation between the dc components, from phases *a*, *b* and *c* on the valve side of the converter transformer and the 60 Hz component in the dc line was measured in a detailed ac–dc hybrid system.

For initial comparison, we simulated the simpler circuit configuration in Figure 4.6 and compared the results with the theoretical relationship of Equation 4.10. The results are shown in Figure 4.10.

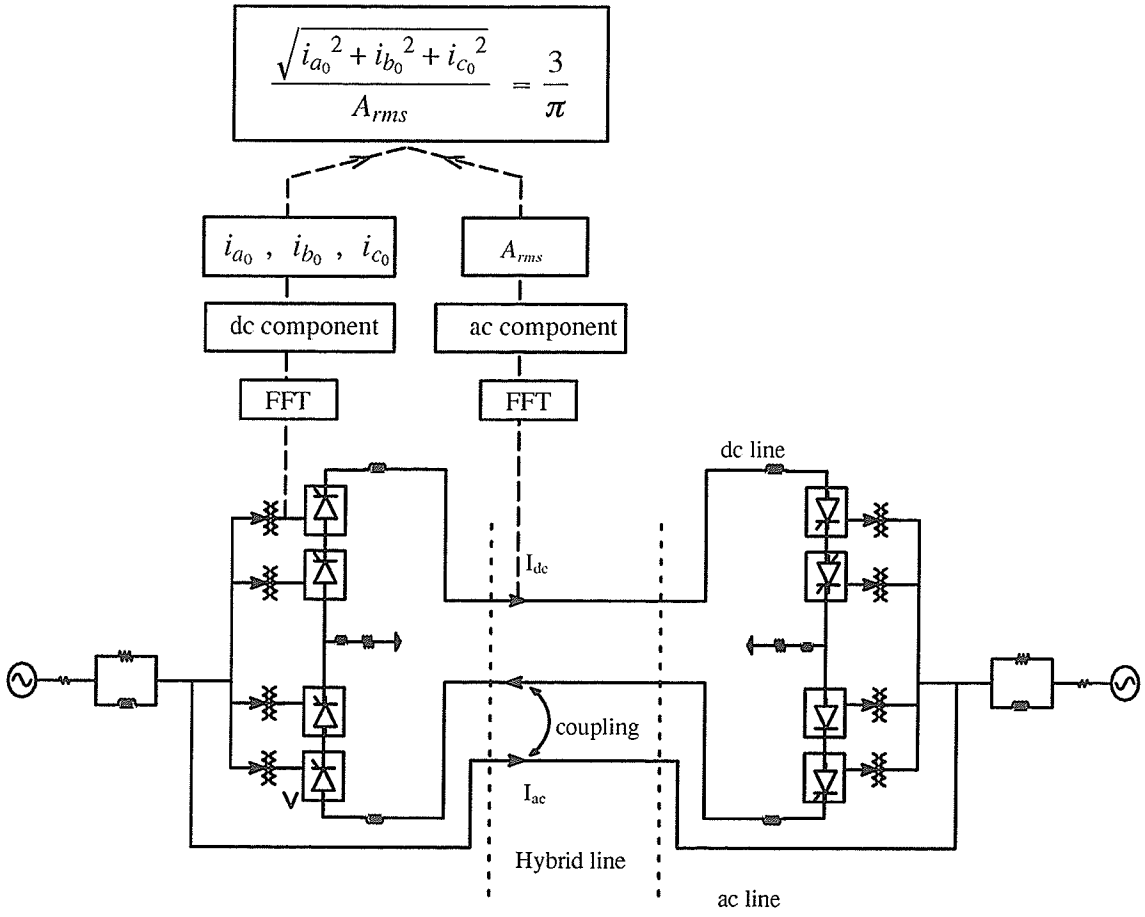

Figure 4 .9 : Simplified diagram of the hybrid system and the measurement of the relation of the dc component and the 60 Hz component.

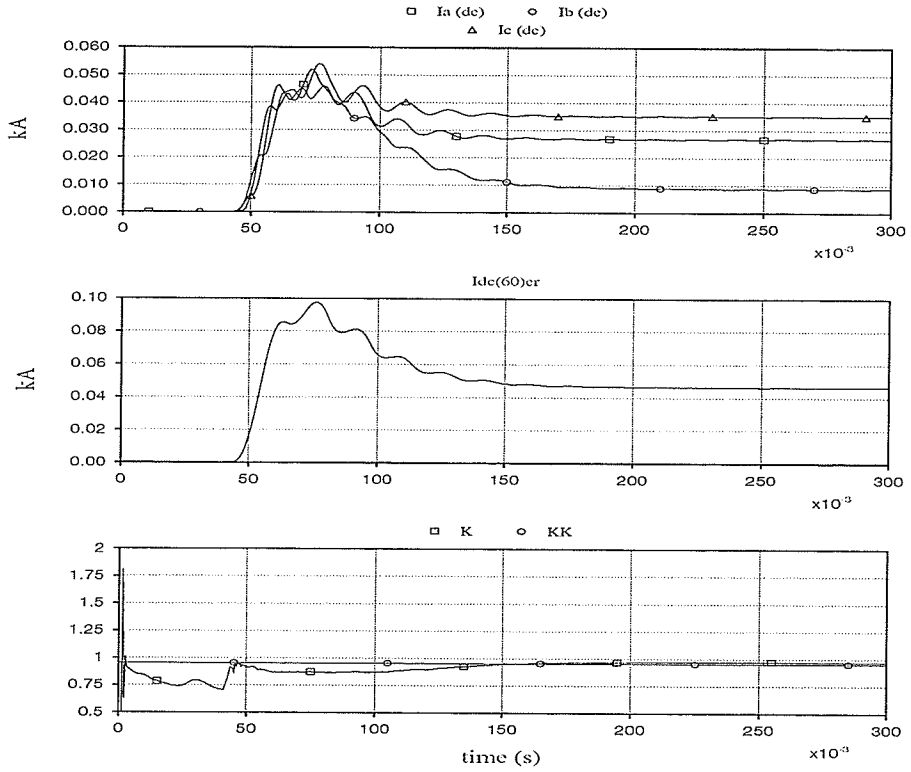

Figure 4 .10 : Relation between the ac components and dc component, according to Equation 4 .10 .

From Figure 4 .10 , the variable KK and K are defined as:

$$KK = \frac{\sqrt{i_{a_0}{}^2 + i_{b_0}{}^2 + i_{c_0}{}^2}}{A_{rms}}$$

$$K = \frac{3}{\pi} = 0.955$$

Note that the theoretical value (K) matches the value (KK) obtained from simulation in the steady state.

4 .4 FIRING ANGLE MODULATION TO ELIMINATE THE 60 HZ CURRENT

4 .4 .1 ANALYTICAL APPROACH

In this section we investigate a method for eliminating the 60 Hz component of current, I_{60}, in the dc line. As there is coupling between the ac line and the dc line, there will be a 60 Hz current flowing in the dc line. This section will describe how this 60 Hz current can be reduced or eliminated from the dc transmission line.

It will be shown that a 60 Hz voltage of controllable phase and magnitude can be generated by controlling the firing angle of each valve independently. This 60 Hz voltage can then be used to eliminate the original 60 Hz inducing source. This type of operation in the converter is called **firing angle modulation**. To generate the 60 Hz component current from the six–pulse bridge converter, the firing angle was selected by using the following Equation:

$$\alpha_i = \alpha_o + \alpha_m \sin\left[\frac{\pi}{3}(i-1) - \phi_\alpha\right] \qquad (4.11)$$

where:

α_i = firing angle for the valve i

α_o = base firing angle from valve group control

α_m = amplitude of the 60 Hz firing angle

ϕ_α = phase of the modulation signal

In the analysis for the elimination the 60 Hz current component, two different assumptions are taking into account, that will be presented in two different sections. In the section 4 .4 .1 .1 the six–pulse bridge converter will be represented without overlap and in the section 4 .4 .1 .2 the overlap will be included in the analysis.

4 .4 .1 .1 WITHOUT OVERLAP ANGLE

First of all let us analyze the case without the commutation reactance in which only two valves conduct simultaneously. In this case the transfer of current from one valve to another in the same row, which is called commutation, must occur instantly, that is without overlap.

The ac voltage and current sources in Figure 4 .6 , in both ac and dc sides, generate characteristic harmonics plus the 60 Hz component in the dc side and dc and second harmonic component in the ac side. The main goal is to eliminate the dc component current in the secondary of the converter transformer in order to eliminate the problem of saturation in the transformer. But in this section the objective is to show how we can eliminate the 60 Hz component current in the dc line by using firing angle modulation.

Waveforms of instantaneous voltage of ac source and direct voltage and modulation of the firing angle shown in Figure 4 .11 . The average direct voltage *Vd,* is determined by integrating the instantaneous voltage v_d in the dc side over a period from 0 to 2 π.

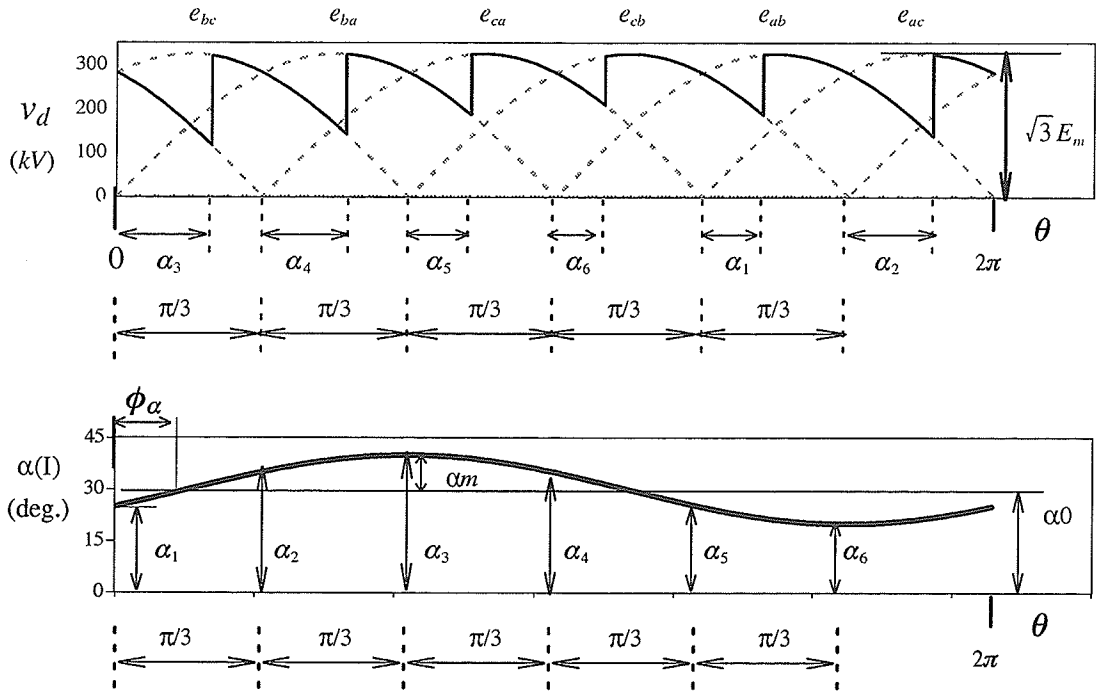

$$\alpha_i = \alpha_o + \alpha_m \sin\left[\frac{\pi}{3}(i-1) - \phi_\alpha\right]$$

Figure 4 .11 : Waves of instantaneous voltage of ac source and direct voltage and modulation of the firing angle, without overlap.

$$V_d = \frac{1}{2\pi}\left[\int_0^{\alpha_3} e_{ac}\, d\theta + \int_{\alpha_3}^{\frac{\pi}{3}+\alpha_4} e_{bc}\, d\theta + \int_{\frac{\pi}{3}+\alpha_4}^{2\frac{\pi}{3}+\alpha_5} e_{ba}\, d\theta + \int_{2\frac{\pi}{3}+\alpha_5}^{\pi+\alpha_6} e_{ca}\, d\theta \;..\right. \qquad (4.12)$$

$$\left. + \int_{\pi+\alpha_6}^{4\frac{\pi}{3}+\alpha_1} e_{cb}\, d\theta + \int_{4\frac{\pi}{3}+\alpha_1}^{5\frac{\pi}{3}+\alpha_2} e_{ab}\, d\theta + \int_{5\frac{\pi}{3}+\alpha_2}^{2\pi} e_{ac}\, d\theta\right]$$

V_d is the average value of the dc line voltage.

$$V_d = \frac{1}{2\pi}\left[\int_0^{\alpha_3} \sqrt{3}\,E_m \cos\,(\theta+\frac{\pi}{6})\, d\theta + \int_{\alpha_3}^{\frac{\pi}{3}+\alpha_4} \sqrt{3}\,E_m \cos\,(\theta-\frac{\pi}{6})\, d\theta \;..\right.$$

$$+ \int_{\frac{\pi}{3}+\alpha_4}^{2\frac{\pi}{3}+\alpha_5} \sqrt{3}\,E_m \sin\theta\, d\theta + \int_{2\frac{\pi}{3}+\alpha_5}^{\pi+\alpha_6} \sqrt{3}\,E_m \cos\,(\theta-5\frac{\pi}{6})\, d\theta \;..$$

$$+ \int_{\pi+\alpha_6}^{2\frac{\pi}{3}+\alpha_1} \sqrt{3}\,E_m \cos\,(\theta+5\frac{\pi}{6})\, d\theta - \int_{4\frac{\pi}{3}+\alpha_1}^{5\frac{\pi}{3}+\alpha_2} \sqrt{3}\,E_m \sin\,\theta\, d\theta \;..$$

$$\left. + \int_{5\frac{\pi}{3}+\alpha_2}^{2\pi} \sqrt{3}\,E_m \cos\,(\theta+\frac{\pi}{6})\, d\theta\right]$$

$$V_d = \frac{\sqrt{3}}{2\pi} E_m\, K_0 \qquad (4.13)$$

where:

$$K_0 = \sum_{i=1}^{i=6} \cos\alpha_i$$

The fundamental frequency voltage component, V_{d60}, generated in the dc side can be determined by using Fourier series, as described in detail in Appendix B.2.

From the theory of Fourier series we have:

$$v(wt) = \frac{a_o}{2} + \sum_{n=1}^{n=\infty} C_n \cos\,(\,n\,wt+\phi_n\,) \qquad (4.14)$$

$$c_{1_{V_d}} = \sqrt{(a_{1_{V_d}})^2 + (b_{1_{V_d}})^2} \qquad (4.15)$$

$c_{1_{V_d}}$ is the magnitude of the fundamental frequency voltage component in the dc side of the six–pulse bridge converter which was generated by the modulation of the firing angle.

$$\phi_{1_{V_d}} = -\operatorname{atan}\frac{a_{1_{V_d}}}{b_{1_{V_d}}} \qquad (4.16)$$

$\phi_{1_{V_d}}$ is the phase angle of the fundamental frequency voltage component.

Figure 4.12 shows the plot of c_{1vd} as a function of the amplitude α_m for different values of α_0. As we can see there is a linear relationship between c_{1vd} and α_m. It was found that the values of c_{1vd} do not change with variation of ϕ_α. The value of c_{1vd} in Figure 4.12 was calculated for E_m=1.0 pu and α_m and α_0 in degree.

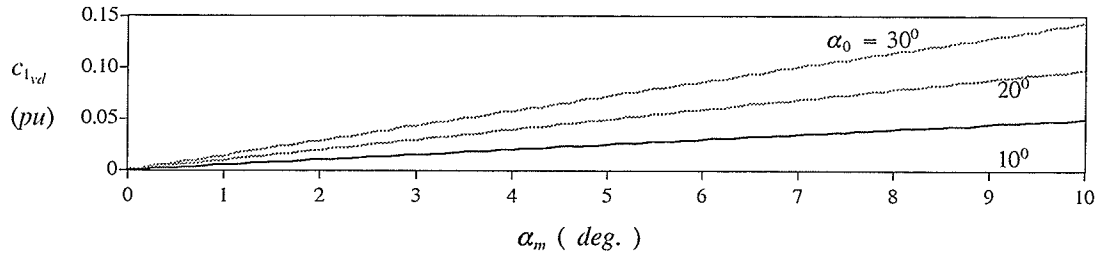

Figure 4.12 : Fundamental frequency voltage component as function of α_m and α_0 (E_m=1.0 pu).

We can fit a relationship as shown in Equation 4.17 to the results in Figure 4.12 .

$$c_{1_{vd}} \cong 5.0010^{-4}\, \alpha_0\, \alpha_m \,, \quad \text{for } \alpha_0 = 10\ deg. \qquad (4.17)$$
$$c_{1_{vd}} \cong 4.9510^{-4}\, \alpha_0\, \alpha_m \,, \quad \text{for } \alpha_0 = 20\ deg.$$
$$c_{1_{vd}} \cong 4.8010^{-4}\, \alpha_0\, \alpha_m \,, \quad \text{for } \alpha_0 = 30\ deg.$$

Where α_0 and α_m are given in Equation 4.11 .

Figure 4.13 shows the plot of ϕ_{1vd} as a function of the phase angle ϕ_α for different values of α_0. In this case there is a linear relationship between ϕ_{1vd} and ϕ_α. It was found that the values of ϕ_{1vd} do not

change with variation of α_m. The Equation 4.18 represents the parametric relation between ϕ_{1vd}, $\phi\alpha$ and α_0.

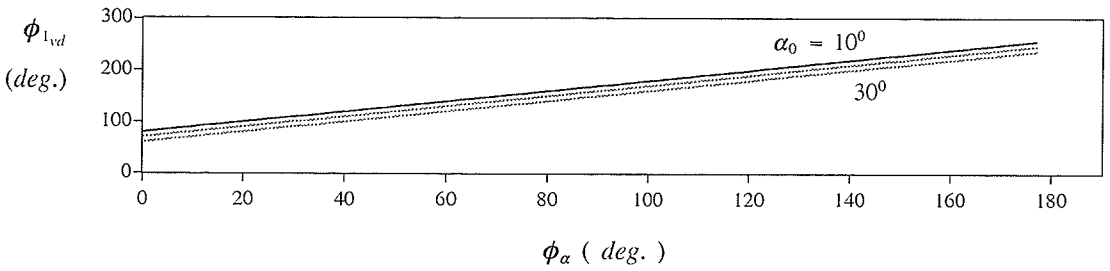

Figure 4.13 : Phase angle of the fundamental component voltage as function of $\phi\alpha$ and α_0 (E_m=1.0 pu).

$$\phi_{1_{V_d}} \cong \phi_\alpha + (90^0 - \alpha_0) \qquad (4.18)$$

With these results in Figure 4.12 and 4.13 we can generate the fundamental frequency voltage on the dc line which will produce a flow of 60 Hz current that will cancel out the fundamental frequency current induced in the dc line from the ac line. By knowing the value of α_0 and selecting an appropriate value for α_m and $\phi\alpha$.

Figure 4.14 shows the voltage V_d for firing angle α_0=60 and α_0=120 degrees, with α_m=0.0 and α_m=10.0 degrees. Figure 4.15 shows that the characteristic c_{1vd} x α_m for alpha=α_0 and alpha=(180–α_0) are the same (α_0=40, 60 and 80 degrees).

4.4.1.2 WITH OVERLAP ANGLE

Now we consider a more realistic case where the inductance of the converter transformer is represented. In this situation the current in the secondary of the transformer can only change at a finite rate, and therefore the transfer of current from one phase to another requires a finite time, called commutation time or overlap time, μ, where μ is the overlap angle. In normal operation the value of μ is less than 60°. Typical full–load values of μ are from 20 to 25° [20]. Figure 4.16 shows the instantaneous voltage of the six–pulse bridge v_d converter where the overlap is represented. The

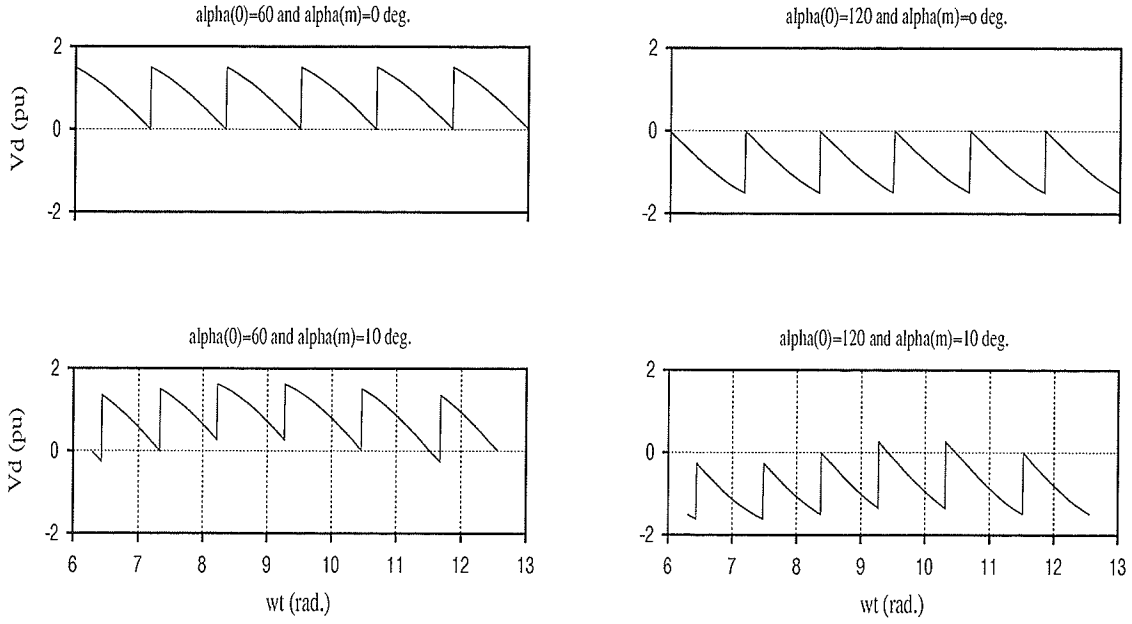

Figure 4 .14 : Dc voltage for firing angle α_0=60 and 120 deg. (μ=0 and α_m=0 and 10 deg.).

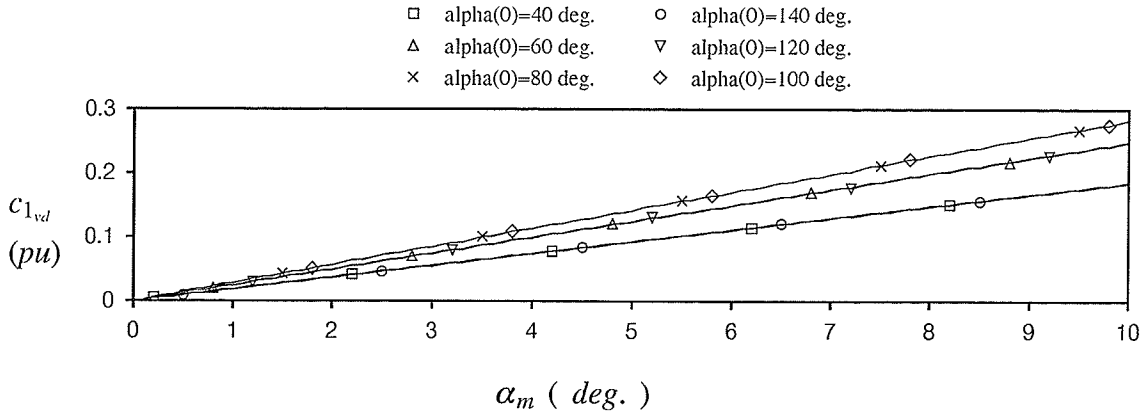

Figure 4 .15 : Fundamental frequency voltage component as function of α_m and α_0 (E_m=1.0 pu).

modulation of the firing angle was performed in order to eliminate the 60 Hz current induced from the ac line into the dc line for the ac–dc hybrid system. The average value of the voltage in the dc side of the six–pulse bridge converter, *Vd*, can be found by integrating v_d in Figure 4 .16 over the interval from 0 to 2π.

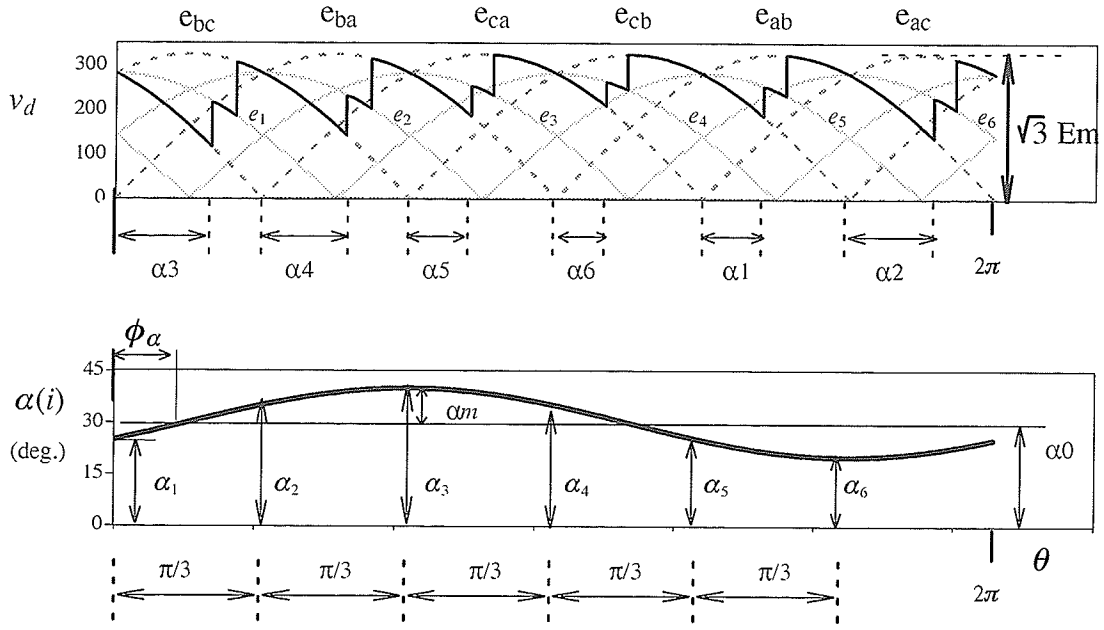

$$\alpha_i = \alpha_o + \alpha_m \sin\left[\frac{\pi}{3}(i-1) - \phi_\alpha\right]$$

Figure 4.16 : Waves of instantaneous voltage of ac source and direct voltage and modulation of the firing angle, with overlap.

$$V_d = \frac{1}{2\pi}\left[\int_0^{\alpha_3} e_{ac}\, d\theta + \int_{\alpha_3}^{\alpha_3+\mu} e_1\, d\theta + \int_{\alpha_3+\mu}^{\frac{\pi}{3}+\alpha_4} e_{bc}\, d\theta + \int_{\frac{\pi}{3}+\alpha_4}^{\frac{\pi}{3}+\alpha_4+\mu} e_2\, d\theta \;..\right. \qquad (4.19)$$

$$+ \int_{\frac{\pi}{3}+\alpha_4+\mu}^{2\frac{\pi}{3}+\alpha_5} e_{ba}\, d\theta + \int_{2\frac{\pi}{3}+\alpha_5}^{2\frac{\pi}{3}+\alpha_5+\mu} e_3\, d\theta + \int_{2\frac{\pi}{3}+\alpha_5+\mu}^{\pi+\alpha_6} e_{ca}\, d\theta + \int_{\pi+\alpha_6}^{\pi+\alpha_6+\mu} e_4\, d\theta \;..$$

$$+ \int_{\pi+\alpha_6+\mu}^{5\frac{\pi}{3}+\alpha_1} e_{cb}\, d\theta + \int_{4\frac{\pi}{3}+\alpha_1}^{4\frac{\pi}{3}+\alpha_1+\mu} e_5\, d\theta + \int_{4\frac{\pi}{3}+\alpha_1+\mu}^{5\frac{\pi}{3}+\alpha_2} e_{ab}\, d\theta + \int_{5\frac{\pi}{3}+\alpha_2}^{5\frac{\pi}{3}+\alpha_2+\mu} e_6\, d\theta \;..$$

$$\left. + \int_{5\frac{\pi}{3}+\alpha_2+\mu}^{2\pi} e_{ac}\, d\theta \right]$$

V_d is the average value of the dc line voltage.

Where e_i, i=1,6 are defined as:

$$e_1 = \frac{3}{2} E_m \cos(\theta) \qquad (4.20)$$

$$e_2 = \frac{3}{2} E_m \cos(\theta - \frac{\pi}{3})$$

$$e_3 = \frac{3}{2} E_m \cos(\theta - 2\frac{\pi}{3})$$

$$e_4 = -\frac{3}{2} E_m \cos(\theta)$$

$$e_5 = \frac{3}{2} E_m \cos(\theta + 2\frac{\pi}{3})$$

$$e_6 = \frac{3}{2} E_m \cos(\theta + \frac{\pi}{3})$$

$$V_d = \frac{\sqrt{3} E_m}{2\pi} \left[\int_0^{\alpha_3} \cos(\theta + \frac{\pi}{6})\, d\theta + \int_{\alpha_3}^{\alpha_3+\mu} \frac{\sqrt{3}}{2} \cos\theta \, d\theta + \int_{\alpha_3+\mu}^{\frac{\pi}{3}+\alpha_4} \cos(\theta - \frac{\pi}{6})\, d\theta \right. \quad .. (4.21)$$

$$+ \int_{\frac{\pi}{3}+\alpha_4}^{\frac{\pi}{3}+\alpha_4+\mu} \frac{\sqrt{3}}{2} \cos(\theta - \frac{\pi}{3})\, d\theta + \int_{\frac{\pi}{3}+\alpha_4+\mu}^{2\frac{\pi}{3}+\alpha_5} \sin\theta \, d\theta \quad ..$$

$$+ \int_{2\frac{\pi}{3}+\alpha_5}^{2\frac{\pi}{3}+\alpha_5+\mu} \frac{\sqrt{3}}{2} \cos(\theta - 2\frac{\pi}{3})\, d\theta + \int_{2\frac{\pi}{3}+\alpha_5+\mu}^{\pi+\alpha_6} \cos(\theta - 5\frac{\pi}{6})\, d\theta \quad ..$$

$$- \int_{\pi+\alpha_6}^{\pi+\alpha_6+\mu} \frac{\sqrt{3}}{2} \cos\theta \, d\theta + \int_{\pi+\alpha_6+\mu}^{4\frac{\pi}{3}+\alpha_1} \cos(\theta + 5\frac{\pi}{6})\, d\theta \quad ..$$

$$+ \int_{4\frac{\pi}{3}+\alpha_1}^{4\frac{\pi}{3}+\alpha_1+\mu} \frac{\sqrt{3}}{2} \cos(\theta + 2\frac{\pi}{3})\, d\theta + \int_{4\frac{\pi}{3}+\alpha_1+\mu}^{5\frac{\pi}{3}+\alpha_2} \cos(\theta + \frac{\pi}{2})\, d\theta \quad ..$$

$$+ \left. \int_{5\frac{\pi}{3}+\alpha_2}^{5\frac{\pi}{3}+\alpha_2+\mu} \frac{\sqrt{3}}{2} \cos(\theta + \frac{\pi}{3})\, d\theta + \int_{5\frac{\pi}{3}+\alpha_2+\mu}^{2\pi} \cos(\theta + \frac{\pi}{6})\, d\theta \right]$$

$$V_d = \frac{\sqrt{3} E_m}{4\pi} \left[K_1 (1 + \cos\mu) - K_2 \sin\mu \right] \qquad (4.22)$$

where:

$$K_1 = \sum_{i=1}^{i=6} \cos \alpha_i$$

$$K_2 = \sum_{i=1}^{i=6} \sin \alpha_i$$

The fundamental frequency voltage component, V_{d60}, generated in the dc side can be determined by using Fourier series, as described in detail in Appendix B.3.

$$c_{1V_d} = \sqrt{(a_{1V_d})^2 + (b_{1V_d})^2} \qquad (4.23)$$

c_{1V_d} is the magnitude of fundamental frequency voltage component in the dc side which was generated by the modulation of the firing angle of the six–pulse bridge converter.

$$\phi_{1V_d} = -\operatorname{atan} \frac{a_{1V_d}}{b_{1V_d}} \qquad (4.24)$$

ϕ_{1V_d} is the phase angle of the fundamental frequency voltage component.

From Equation 4.23 and 4.24, the magnitude and phase of the fundamental component generated from the six–pulse bridge can be plotted as shown in Figures 4.17 and 4.18.

Figure 4.17 shows the plot of c_{1vd} as a function of the amplitude α_m for different values of α_0 and μ. As we can see there is a linear relationship between c_{1vd} and α_m. It was found that the values of c_{1vd} do not change with variation of ϕ_α. The value of c_{1vd} in Figure 4.17 was calculated for E_m=1.0 pu and α_m and α_0 in degree.

Figure 4.18 shows the plot of ϕ_{1vd} as a function of the phase angle ϕ_α for different values of α_0. In this case there is a linear relationship between ϕ_{1vd} and ϕ_α (as in the case without commutation reactance). It was found that the values of ϕ_{1vd} do not change with variation of α_m. Equation 4.26 represents the parametric relation between ϕ_{1vd}, ϕ_α, α_0 and μ obtained empirically from the detailed calculation.

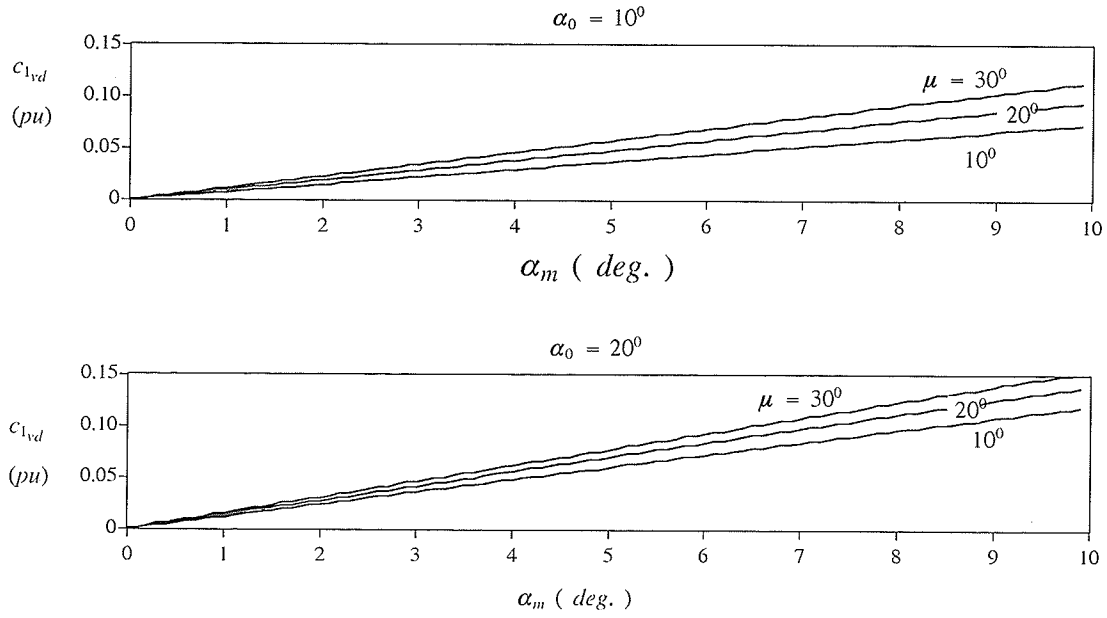

Figure 4 .17 : Fundamental frequency voltage component as function of α_m and α_0 (E_m=1.0 pu).

We can fit a relationship as shown in Equation 4 .25 to the results in Figure 4 .17 .

$$c_{1_{vd}} \cong 2.47\ 10^{-4}\ (\ 2\ \alpha_0 + \mu\ )\ \alpha_m\ ,\quad \text{for } \alpha_0 = 10\ deg.\ \text{and } \mu = 10\ deg. \qquad (4.25)$$

$$c_{1_{vd}} \cong 2.40\ 10^{-4}\ (\ 2\ \alpha_0 + \mu\ )\ \alpha_m\ ,\quad \text{for } \alpha_0 = 10\ deg.\ \text{and } \mu = 20\ deg.$$

$$c_{1_{vd}} \cong 2.40\ 10^{-4}\ (\ 2\ \alpha_0 + \mu\ )\ \alpha_m\ ,\quad \text{for } \alpha_0 = 20\ deg.\ \text{and } \mu = 10\ deg.$$

$$c_{1_{vd}} \cong 2.32\ 10^{-4}\ (\ 2\ \alpha_0 + \mu\ )\ \alpha_m\ ,\quad \text{for } \alpha_0 = 20\ deg.\ \text{and } \mu = 20\ deg.$$

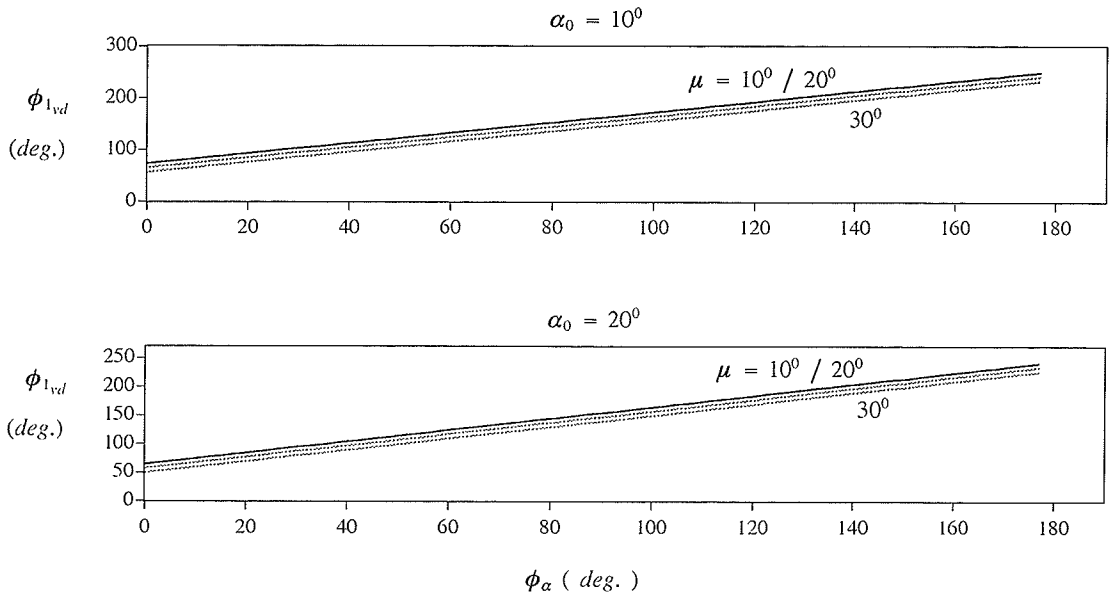

Figure 4.18 : Phase angle of the fundamental component voltage as function of $\phi\alpha$ and α_0 (E_m=1.0 pu).

$$\phi_{1_{V_d}} \cong \phi_\alpha + (96^0 - (\alpha_0 + \mu)) \qquad (4.26)$$

We can thus generate the fundamental frequency voltage on the dc line which will produce a flow of 60 Hz current that will cancel out the fundamental frequency current induced in the dc line from the ac line. By knowing the value of α_0 and μ and selecting an appropriate value for α_m and $\phi\alpha$.

Figure 4.19 shows the voltage V_d for firing angles α_0 =60 and α_0=120 degrees, with overlap angle μ=10 degrees and α_m=0 and 10 degrees. Figure 4.20 shows the characteristic c_{1vd} x α_m for alpha=α_0 and alpha=(180–α_0) (α_0=40, 60 and 80 degrees), which are not the same (for μ different of zero) as we have concluded in the case without overlap angle in the section 4.4.1.1.

4.4.2 ALTERNATIVE ANALYTICAL MODULATION APPROACH

A more approximate analytical approach is used to find out the fundamental frequency voltage of the dc side of the six–pulse bridge converter that will cancel out the coupling effect between the ac and dc lines. The dc converter will be considered without and with overlap angle. It will be seen that this

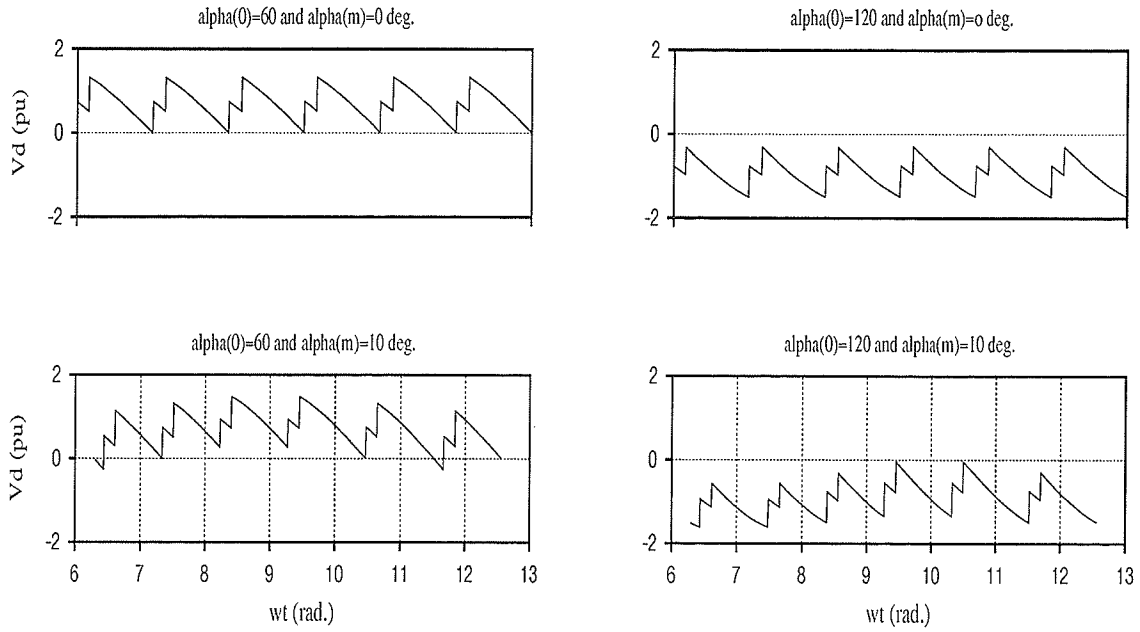

Figure 4 .19 : Dc voltage for firing angle α0=60 and 120 deg. (μ=10 deg. and αm=0 and 10 deg.).

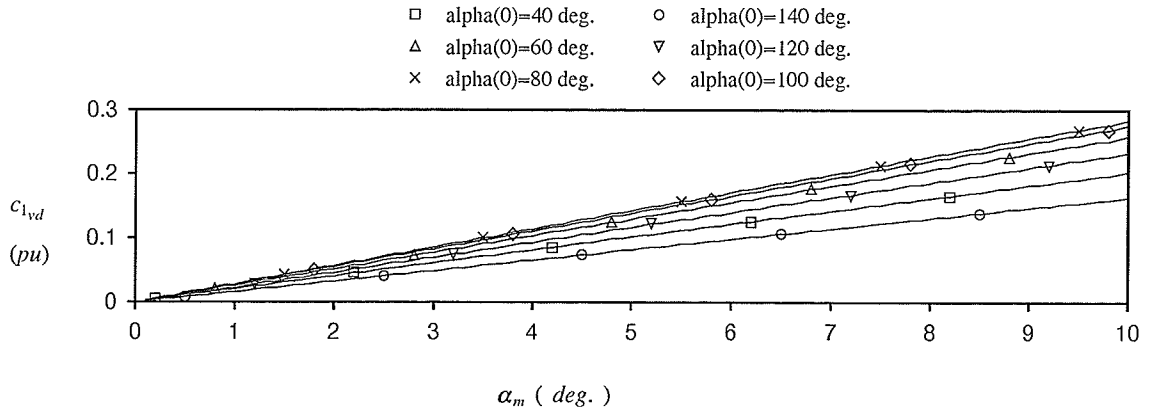

Figure 4 .20 : Fundamental frequency voltage component as function of α_m and α_0 (E_m=1.0 pu).

approximate (but simpler) approach yields results almost identical to the more complicated approach presented earlier.

4.4.2.1 WITHOUT OVERLAP ANGLE

The average direct voltage V_d for the six–pulse bridge converter circuit excluding the overlap angle is given by [20]:

$$V_d = V_{do}\cos(\alpha) \qquad (4.27)$$

$$V_{do} = 1.35\ E_{LL_{rms}} \qquad \left(1.35 = \frac{3\sqrt{2}}{\pi}\right)$$

$E_{LL_{rms}}$ is the line–to–line rms voltage of the six–pulse bridge convertor.

V_{do} is usually called the ideal no–load direct voltage.

To generate the 60 Hz component current from the six–pulse bridge converter, the firing angle was selected by using the following Equation:

$$\alpha = \alpha_o + \alpha_m \sin\ (\ wt + \phi_\alpha\ )$$

Note that this is identical to the discrete time instant of valve firing.

$$V_d = V_{do}\cos\ (\ \alpha_o + \alpha_m \sin\ (\ wt + \phi_\alpha\ )\ )$$

From the trigonometry identity we have:

$$\cos(x \pm y) = \cos\ (x)\cos\ (x) \mp \sin\ (x)\sin\ (y)$$

$$V_d = V_{do}\Big[\cos(\alpha_o)\cos(\alpha_m \sin(wt + \phi_\alpha)) - \sin(wt_o)\sin(\alpha_m \sin(wt + \phi_\alpha))\Big]$$

$$V_d = \underbrace{V_{do}\cos(\alpha)}_{\text{dc component}} - \underbrace{V_{do}\sin(\alpha_o)\alpha_m \sin(wt + \phi_\alpha)}_{\text{ac component}} = V_{d_{dc}} - V_{d_{60}}$$

$$V_{d_{60}} = V_{do}(\sin\alpha_o)\alpha_m \sin(wt + \phi_\alpha) \qquad (4.28)$$

$$V_{d_{60}cr} = V_{do}(\sin\alpha_o)\alpha_m \qquad (\text{crest value}) \qquad (\cong V_{do}\alpha_o\alpha_m \text{ for } \textit{small}\ \alpha_0) \qquad (4.29)$$

This agrees with the observed relationship in Equation 4.17 obtained from the more exact approach. The values of α_0 and α_m in Equation 4.17 are in degrees and the values in Equation 4.29 are in radians. We can rewrite Equation 4.29 as:

$$V_{d_{60}cr} \cong V_{do}\alpha_o\alpha_m = 1.35\ E_{LL_{rms}}\ \alpha_0\ \alpha_m = \frac{3\sqrt{2}\sqrt{3}}{\pi\sqrt{2}} E_m\ (\alpha_0 + \alpha_m)\frac{\pi}{180}$$

$$V_{d_{60}cr} \cong 5.04\ 10^{-4}\alpha_0\alpha_m \quad (\text{ for } E_m = 1.0\ pu\ ) \qquad (4.30)$$

Figure 4.21 shows the characteristic V_{d60cr} x α_0 obtained from the simple analytical calculation, using Equation 4.29, and from the analytical approach obtained in Equation 4.15.

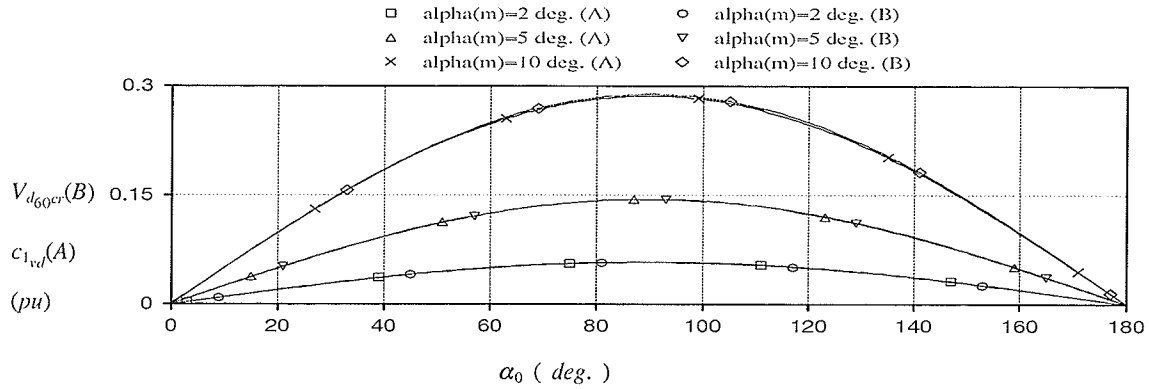

Figure 4.21 : Fundamental frequency voltage component as function of α_m and α_0 (μ=0 and E_m=1.0 pu).

4.4.2.2 WITH OVERLAP ANGLE

The average direct voltage V_d for the six–pulse bridge converter circuit considering the overlap angle is given by [20]:

$$V_d = V_{do}\cos(\alpha) - \frac{3}{\pi}X_c I_d \qquad (4.31)$$

$$I_d = \frac{E_{LL_{rms}}}{\sqrt{2}X_c}\left[\cos(\alpha) - \cos(\alpha+\mu)\right] \qquad (4.32)$$

$$I_{s2} = \frac{E_{LL_{rms}}}{\sqrt{2}X_c}$$

$$\alpha = \alpha_o + \alpha_m \sin\ (\ wt + \phi_\alpha\ )\ \ ,\theta = w\ t \qquad (4.33)$$

$$V_d = V_{do} \cos\left[\ \alpha_o + \alpha_m \sin\ (\ wt + \phi_\alpha\ )\ \right] - \frac{3}{\pi} X_c I_d$$

$$V_d = V_{do}\left[\cos(\alpha_o)\cos(\alpha_m \sin(wt+\phi_\alpha)) - \sin(\alpha_o)\sin(\alpha_m \sin(wt+\phi_\alpha))\right] - \frac{3}{\pi} X_c I_d$$

$$K_3 = \alpha_m \sin(wt+\phi_\alpha)$$

K_3 is a small number for small α_m , then :

$$\cos(K_3) \cong 1 \quad \text{and} \quad \sin(K_3) \cong K_3$$

$$V_d = V_{do}\left[\cos(\alpha_o) - \sin(\alpha_o)\ K_3\right] - \frac{3}{\pi} X_c I_d$$

$$I_d = I_{s2}\left[\cos(\alpha_o) - \cos(\alpha_o + \mu\ ) - \sin(\alpha_o)\ K_3 + \sin(\alpha_o + \mu\ )\ K_3\right]$$

$$V_d = V_{do}\left[\cos(\alpha_o) - \sin(\alpha_o)\ K_3\right] \ ..$$

$$- \frac{3}{\pi} X_c\ I_{s2}\ \left[\cos(\alpha_o) - \cos(\alpha_o + \mu) - \sin(\alpha_o) K_3 + \sin(\alpha_0 + \mu) K_3\ \right]$$

$$V_d = \underbrace{V_{do}\left[\cos(\alpha_o)\right] - \frac{3}{\pi} X_c\ I_{s2}\ \left[\cos(\alpha_o) - \cos(\alpha_o + \mu)\right]}_{\text{dc component}} \ ..$$

$$\underbrace{- V_{do} \sin(\alpha_o)\ K_3 - \frac{3}{\pi} X_c I_{s2}\ \left[-\sin(\alpha_o)\ K_3 + \sin(\alpha_o + \mu\ )\ K_3\right]}_{\text{ac component}} = V_{d_{dc}} + V_{d60}$$

$$V_{d_{60}} = -V_{do} \sin(\alpha_o)\ K_3 - \frac{3}{\pi} X_c I_{s2}\ K_3\ \left[-\sin(\alpha_o) + \sin(\alpha_o + \mu\ )\ \right]$$

$$V_{d_{60}} = \left[\ \frac{3}{\pi} X_c I_{s2} - V_{do}\right] \sin(\alpha_o)\ K_3 - \frac{3}{\pi} X_c I_{s2}\ K_3\ \sin(\alpha_o + \mu\ )$$

$$I_{s2} = \frac{E_{LL_{rms}}}{\sqrt{2}X_c} \quad \text{and} \quad V_{do} = 1.35\ E_{LL_{rms}} \qquad \left(1.35 = \frac{3\sqrt{2}}{\pi} \right)$$

$E_{LL_{rms}}$ is the line–to–line rms voltage of the six–pulse bridge convertor.

$$V_{d_{60}} = \frac{-3}{\sqrt{2}\pi} E_{LL_{rms}} \left[\sin(\alpha_o) + \sin(\alpha_o + \mu) \right] K_3$$

$$V_{d_{60}} = \frac{-3}{\sqrt{2}\pi} E_{LL_{rms}} \alpha_m \left[\sin(\alpha_o) + \sin(\alpha_o + \mu) \right] \sin(wt + \phi_\alpha)$$

$$V_{d_{60_{cr}}} = \frac{-3}{\sqrt{2}\pi} E_{LL_{rms}} \alpha_m \left[\sin(\alpha_o) + \sin(\alpha_o + \mu) \right] \qquad \text{(crest value)} \qquad (4.34)$$

$$V_{d_{60_{cr}}} = \frac{-3}{\sqrt{2}\pi} E_{LL_{rms}}\ K_4\ \alpha_m \qquad \text{(crest value)} \qquad (4.35)$$

where:

$$K_4 = \sin\alpha_o + \sin(\alpha_o + \mu)$$

$$V_{d_{60_{cr}}} \cong \frac{-3}{\sqrt{2}\pi} E_{LL_{rms}} (\ 2\alpha_0 + \mu\ )\alpha_m \quad (\textit{for small } \alpha_0 \textit{ and } \mu) \qquad (4.36)$$

This agrees with the observed relationship in Equation 4.25 obtained from the more exact approach. The values of α_0 and α_m in Equation 4.25 are in the degree and the values in Equation 4.36 are in radians. We can rewrite the Equation 4.36 as:

$$|V_{d_{60cr}}| \cong \frac{3}{\sqrt{2}\pi} E_{LL_{rms}} (\ 2\alpha_0 + \mu\ )\alpha_m = \frac{3}{\sqrt{2}\pi} \frac{\sqrt{3}}{\sqrt{2}} E_m (2\alpha_0 + \mu) \frac{\pi}{180} (\alpha_m) \frac{\pi}{180}$$

$$|V_{d_{60cr}}| = 2.52\ 10^{-4} (\ 2\alpha_0 + \mu\ )\alpha_m \quad (\text{ for } E_m = 1.0\ pu\ ) \qquad (4.37)$$

Figure 4.22 shows the characteristic V_{dc60cr} x α_0 obtained from the simple analytical calculation, Equation 4.34, and from the analytical approach obtained in Equation 4.23.

4.4.3 SIMULATION APPROACH

The results of the analytical approach obtained from sections 4.4.1 and 4.4.2 are verified in this section by using simulation approach on a simplified six–pulse bridge converter. Appendix A shows the PSCAD/EMTDC draft diagram used in this study.

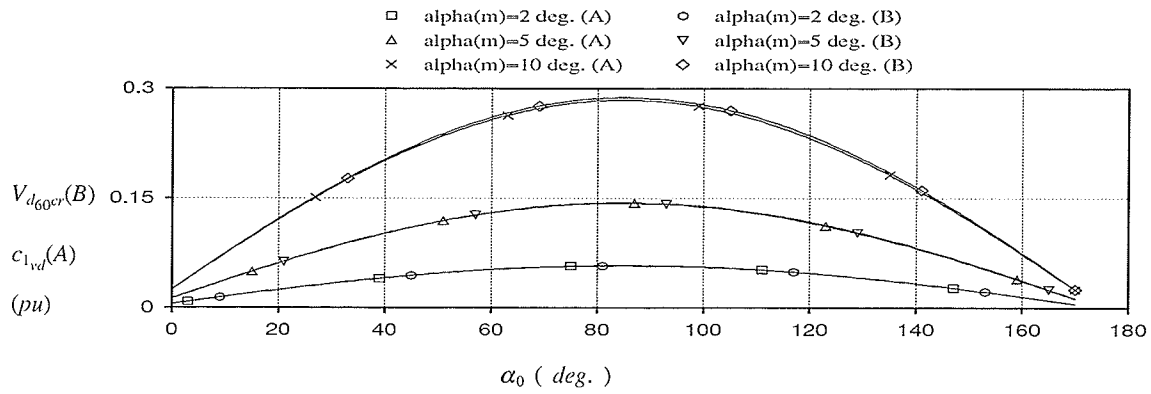

Figure 4 .22 : Fundamental frequency voltage component as function of α_m and α_0 (μ=10 deg. and E_m=1.0 pu).

In order to illustrate the elimination of the I_{60} component, we consider the simplified dc system of Figure 4 .23 . Here we introduce the fundamental frequency current, I_{60}, through the ac voltage source in series with the inverter. The inverter is represented by a dc source. This ac voltage source is introduced in order to simulate the coupling effect between the ac line and the dc line. The inverter is itself modelled for this simplified example as a voltage source *Vdi* behind a resistance R_{di} . R_{dc} represents the sum of line resistance and the source resistance R_{di}.

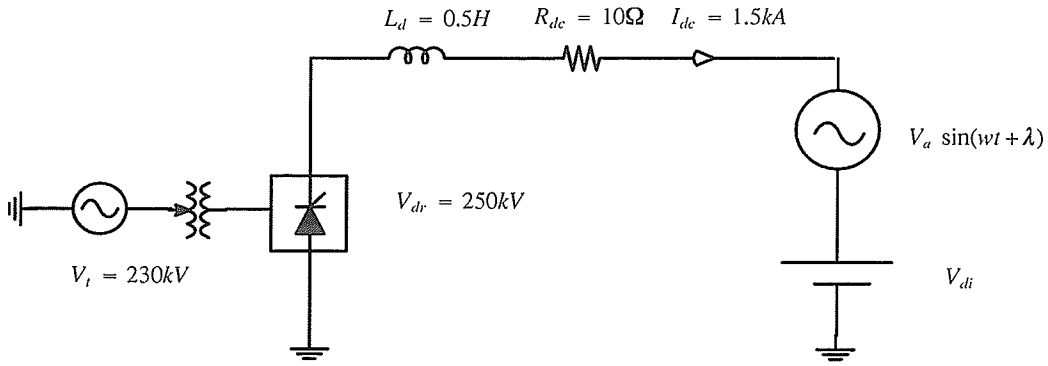

Figure 4 .23 : Simplified dc system.

We will show that it is possible to introduce a modulation in α_i in each valve of the six–pulse bridge converter as indicated by the Equation 4 .33 and in Figure 4 .24 . The 60 Hz voltage generated from

this modulation(V_{d60}) can have any desired magnitude and phase angle. Here α_0 is the average value of the firing angle order α and α_m the modulation magnitude. ϕ_α is the phase of the modulation signal measured from the crossing zero of line–line voltage e_{ba} on its positive gradient.

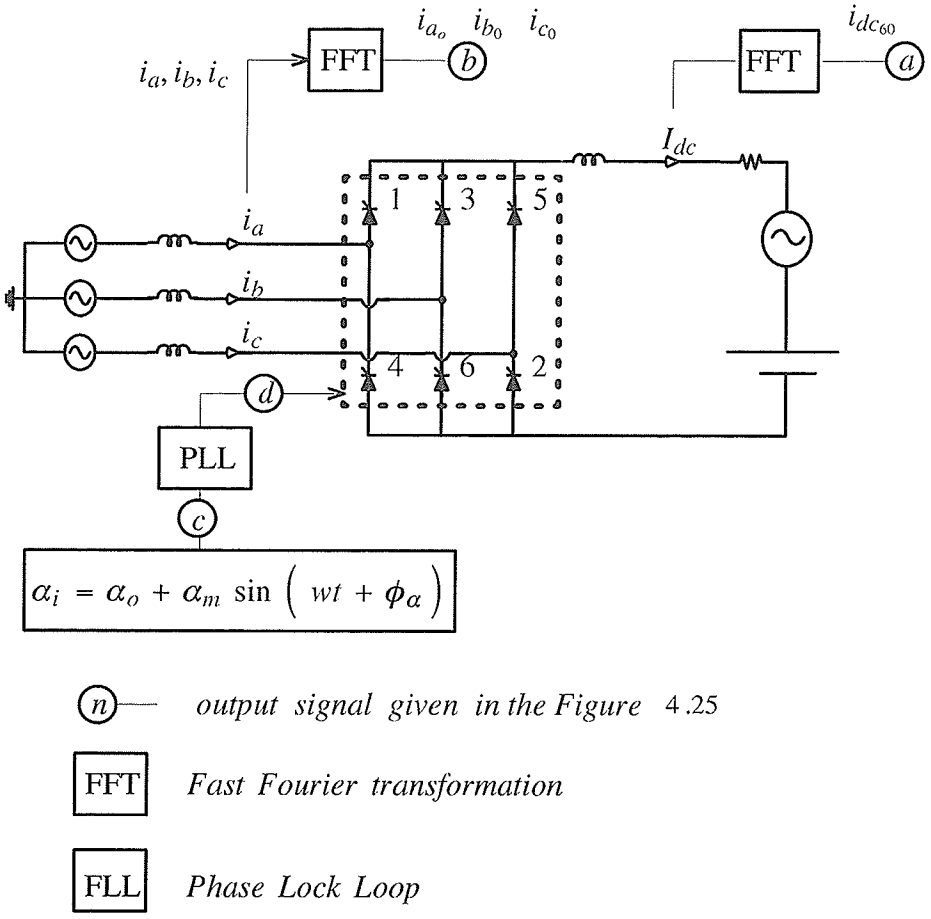

Figure 4 .24 : Configuration of a six–pulse bridge converter.

The fundamental frequency current, $I_{60,}$ can be eliminated by introducing the fundamental frequency voltage, $V_{d60,}$ through the modulation, that will cancel out the induced 60 Hz voltage. This is evident from the simulated waveforms in Figure 4 .25 . The amplitude Va , from Figure 4 .23 , of the inducing source was selected to be 13.8 kV so as to obtain a magnitude of 73A crest for I_{60} which is about 5% of the rated dc current of 1.5 kA. For the simulation results shown in Figure 4 .25 , the inducing 60 Hz voltage has been applied at time = 0.6 s or 0.2 s from the start of the time scale. The modulation has been applied at t=1.2 s. A modulation amplitude $\alpha_m = 5^0$ and a phase angle $\phi_\alpha = 180^0$

were required for this action. All dc and fundamental components shown in the graphs have been obtained with an on–line Discrete Fourier Transformation (FFT).

Figure 4.25 also shows the absolute values of the dc current components Ia_0, Ib_0, Ic_0 in the converter transformer. Note that these components do not disappear with the elimination of I_{60} as would be expected from Equation 4.10 with A=0. Indeed in this particular case, their magnitudes actually increase.

The above observation appears contrary to the $f_0 \pm f$ rule discussed in the Introduction of this chapter. However it must be noted that due to the modulation of the firing angle, the assumption of equidistant firing of the valves is no longer valid and so dc currents can exist on the ac side without the complementary 60 Hz components existing on the dc side. **Thus if our aim is to eliminate the transformer dc currents, we must not eliminate I_{60} by control action.**

Note also in Figure 4.26 that the 60 Hz oscillations in the dc current before the application of the modulation signal die out as required and only the normal 6th harmonic ripple remains.

Figure 4.27 shows a plot of the harmonics of the current in phase "*a*" in the secondary of the converter transformer for the case shown in Figure 4.25. The harmonics were measured by using the Discrete Fourier Transformation: a) before the application of the 60 Hz voltage source, from 0.5 to 0.6 s (interval A); b) during the application of the 60 Hz voltage source, from 1.0 to 1.2 s (interval B) and c) during the application of the modulation of the firing angles, from 1.5 to 1.6 s (interval C).

As expected there is a significant increase in the dc and 2nd harmonic component when the 60 Hz voltage source is applied. The dc component increased from 0.27% to 2.0% and the 2nd harmonic increased from 0.29% to 2.6%. The others harmonic components have not change significantly.

When the modulation of the firing angle was introduced the dc component remained almost the same in phase "*a*" and increased a little in the phases *b* and *c*. The subsequent even harmonics, 2nd, 4th, 6th, 8th, 10th and 12th increased from 2.6, 0.6, 0.72, 0.51, 0.38, 0.29% to 4.5, 4.72, 3.88, 3.48, 3.55, 2.86%, respectively.

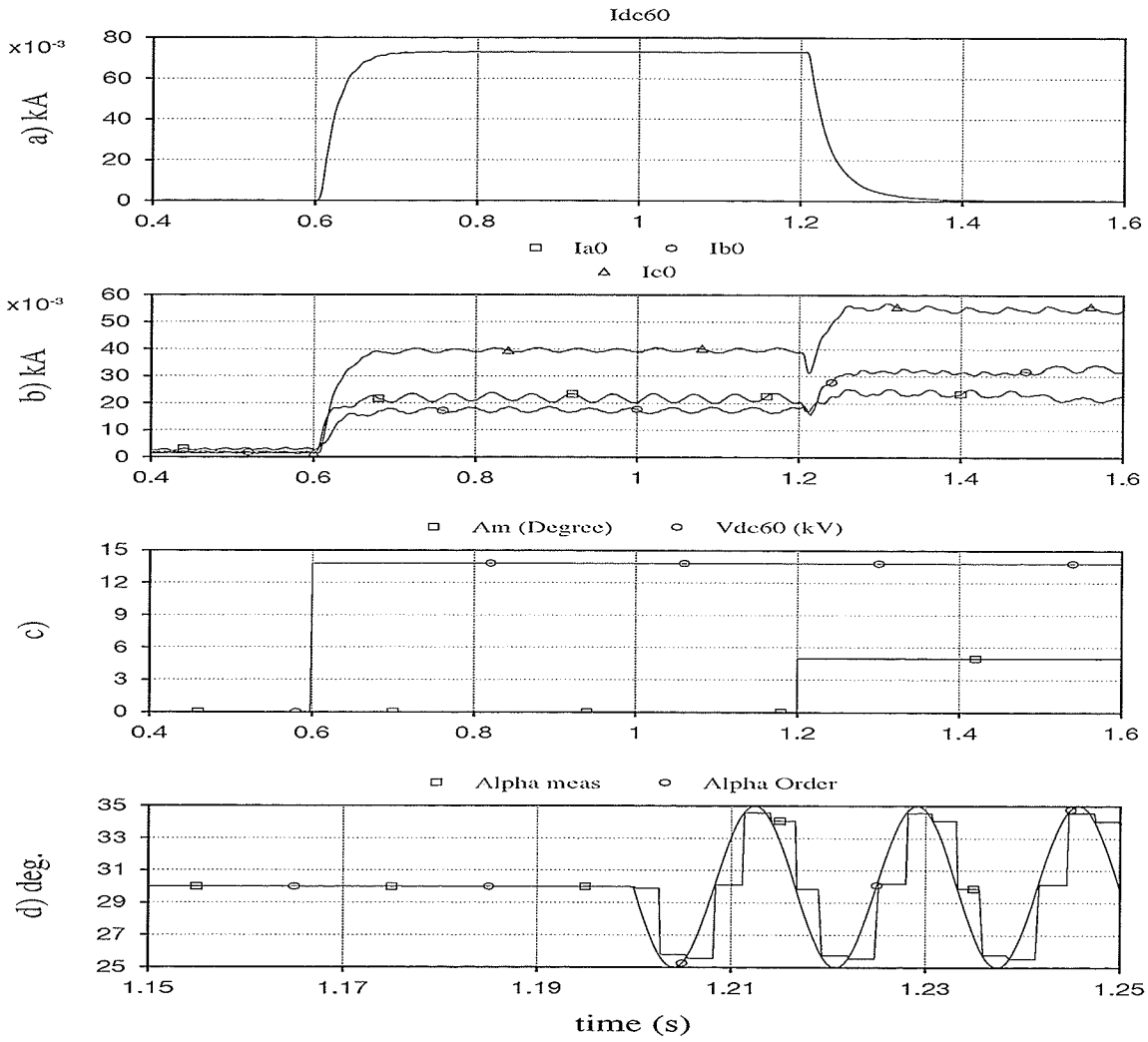

Figure 4 .25 : Simulation of the coupling effect in a six–pulse bridge converter, a) Induced 60 Hz current in the dc line, b) Magnitude of the dc current in the three phases of the secondary of the converter transformer, c) α_m modulation and crest value of the 60 Hz voltage source; d) α measured and α_i modulated and e) Current in the secondary of the converter transformer.

This method of using the technique of firing angle modulation shows that merely eliminating the fundamental frequency component on the dc side does not remove the dc component in the converter transformer windings.

In fact if the modulation described above does make Id free of a 60 Hz component, the dc value of the phase *"a"* current (I_{a0}) is as shown in Equation 4 .38 (derived without including overlap). This is because the lengths of the positive and negative conducting intervals for phase *"a"* are no longer

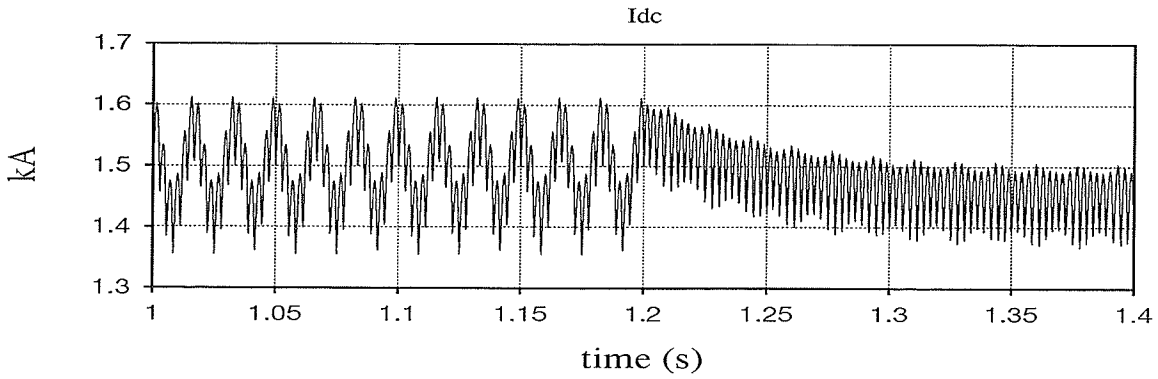

Figure 4 .26 : Dc current.

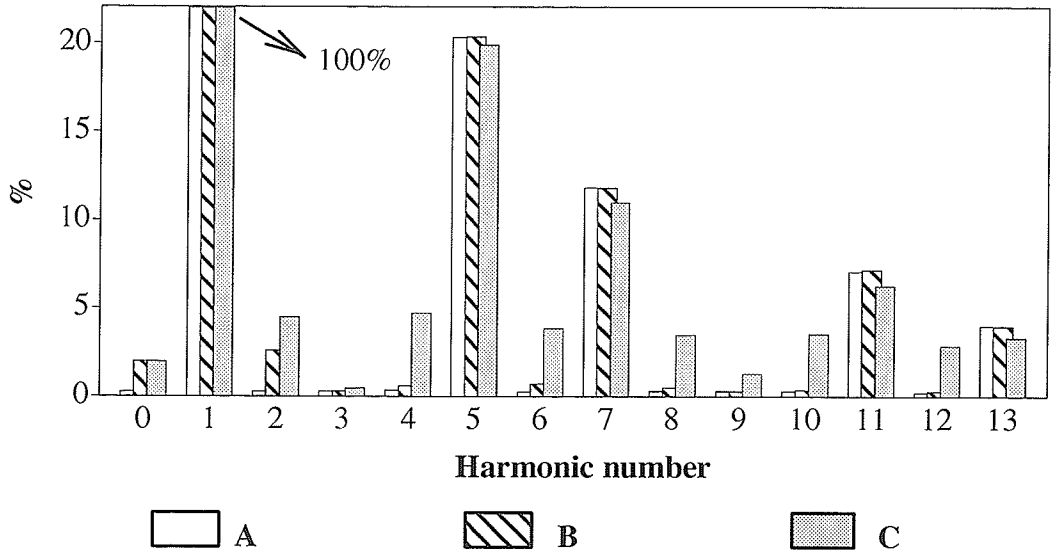

Figure 4 .27 : Harmonic Spectrum of the secondary current transformer I_a.
A – without 60 Hz voltage source and without modulation (from 0.5 to 0.6 sec.)
B – with 60 Hz voltage source and without modulation (from 1.1 to 1.2 sec.)
C – with 60 Hz voltage source and with modulation (from 1.5 to 1.6 sec.)

constant. Because the firing angles are now not all the same (Equation 4 .33), I_{a0} cannot be exactly zero.

$$I_{a0} \cong I_d\ (\alpha_3 - \alpha_1 + \alpha_6 - \alpha_4) \qquad (4.38)$$

We must therefore seek a method of directly eliminating the dc components in the three transformer phases. This method is presented in the next chapter.

4 .5 SUMMARY

The following observations resulted from this chapter:

– the fundamental frequency current induced from the ac line into the dc line is larger when the ac line in an hybrid system is not transposed and without blocking filter. Hence the dc and 2nd harmonic component current in the secondary of the converter transformer will be larger.

– a relation between the fundamental frequency component current in the dc line and the dc component current on the ac side was determined analytically and confirmed by a simulation case in a simple six–pulse bridge.

– the elimination of I_{60} by control action does not eliminate converter transformer dc components.

– non–characteristic harmonics are introduced as a result of the control action and can have significant amplitudes.

Chapter 5

Firing Angle Modulation for Eliminating Converter Transformer DC Currents

This chapter explores the possibility of eliminating the dc components in the converter transformer windings. The feasibility of such a solution using a theoretical approach on a simplified system and later extend the analysis to more detailed systems is investigated by means of simulation.

5 .1 THEORETICAL CONSIDERATIONS

The cyclical switching action of dc converters characteristically demodulates dc side current ripple into converter transformer current components at other frequencies. The predominant ac–side components are at frequencies equal to the sum and difference of the dc–side ripple frequency and fundamental. Thus, a fundamental frequency current flowing on the dc–side of the converter, referred to as I_{60}, will be seen as having second harmonic and dc components in the converter transformer secondary winding. Figure 5 .1 illustrates the wave shapes which will exist when there is a fundamental component current flowing in the dc line. This Figure shows the dc current with superimposed I_{60}, and also the current in phases *a*, *b* and *c* in the secondary of the converter transformer. The currents are represented with numerical values. Such as: dc current, I_d=1.5 kA, amplitude of the 60 Hz component, A=0.15 kA, the phase angle, $\lambda=-60^0$, and base firing angle $\alpha_0=30^0$. An expression for I_a, I_b and I_c as a function of angle $\theta=wt$ are given in the Equations 5 .2 , 5 .3 and 5 .4 . We can conclude that the dc component in phase "*a*, *b* and *c*" , I_{a0}, I_{b0} and I_{c0}, can be calculated as in Equation 5 .5 .

Here we have used the symbol I_d' for the dc current to indicate that it has I_{60} superimposed on it. The analytical expressions for Equation 5 .5 after substitution from Equations 5 .2 , 5 .3 and 5 .4 are presented in Equations 5 .6 , 5 .7 and 5 .8 .

In order to eliminate the dc component in the secondary of the converter transformer we require that I_{a0}, I_{b0} and I_{c0} are simultaneously zero. A numerical procedure using the Newton–Raphson method is then used to find $d\alpha_1$ through $d\alpha_6$ that satisfy the requirement: $I_{a0}=0$, $I_{b0}=0$ and $I_{c0}=0$.

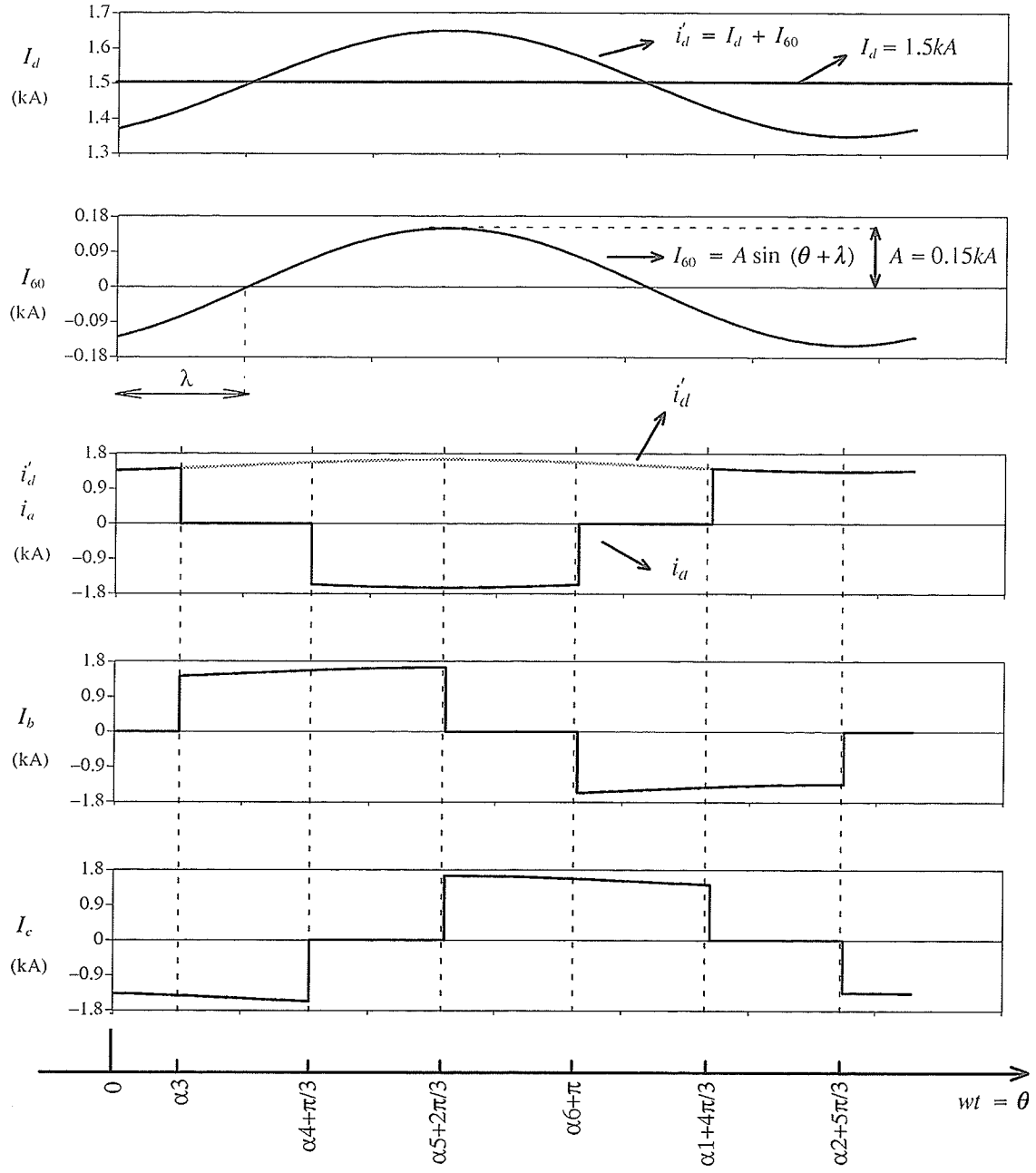

Figure 5 .1 : Instantaneous currents of six–pulse bridge converter with modulation of the firing angles.
(without overlap angle)

The increment of the firing angle in the valve **i** is called $d\alpha_i$. This increment is added to the base firing angle α_0. Hence the firing angle at valve **i** is given by:

$$\alpha_i = \alpha_0 + d\alpha_i \qquad (5.1)$$

$$I_a = \begin{cases} I_d + A\sin(\theta+\lambda) & \alpha_0 + d\alpha_3 < \theta < \alpha_0 + d\alpha_1 - 2\frac{\pi}{3} \\ -I_d - A\sin(\theta+\lambda) & \alpha_0 + d\alpha_6 + \pi < \theta < \alpha_0 + d\alpha_4 + \frac{\pi}{3} \end{cases} \qquad (5.2)$$

$$I_b = \begin{cases} I_d + A\sin(\theta+\lambda) & \alpha_0 + d\alpha_5 + 2\frac{\pi}{3} < \theta < \alpha_0 + d\alpha_3 \\ -I_d - A\sin(\theta+\lambda) & \alpha_0 + d\alpha_2 + 5\frac{\pi}{3} < \theta < \alpha_0 + d\alpha_6 + \pi \end{cases} \qquad (5.3)$$

$$I_c = \begin{cases} I_d + A\sin(\theta+\lambda) & \alpha_0 + d\alpha_1 + 4\frac{\pi}{3} < \theta < \alpha_0 + d\alpha_5 + 2\frac{\pi}{3} \\ -I_d - A\sin(\theta+\lambda) & \alpha_0 + d\alpha_4 + \frac{\pi}{3} < \theta < \alpha_0 + d\alpha_2 - \frac{\pi}{3} \end{cases} \qquad (5.4)$$

$$I_{a_0} = \int_0^{2\pi} I_a\,(\theta)\; d\theta \qquad (5.5)$$

$$I_{a_0} = \frac{1}{2\pi}\left[\int_{\alpha_0+d\alpha_1-2\frac{\pi}{3}}^{\alpha_0+d\alpha_3} I_d + A\sin(\theta+\lambda))\; d\theta + \int_{\alpha_0+d\alpha_4+\frac{\pi}{3}}^{\alpha_0+d\alpha_6+\pi} -I_d - A\sin(\theta+\lambda))\; d\theta\right]$$

$$I_{b_0} = \frac{1}{2\pi}\left[\int_{\alpha_0+d\alpha_5+2\frac{\pi}{3}}^{\alpha_0+d\alpha_3} I_d + A\sin(\theta+\lambda))\; d\theta + \int_{\alpha_0+d\alpha_6+\pi}^{\alpha_0+d\alpha_2+5\frac{\pi}{3}} -I_d - A\sin(\theta+\lambda))\; d\theta\right]$$

$$I_{c_0} = \frac{1}{2\pi}\left[\int_{\alpha_0+d\alpha_5+2\frac{\pi}{3}}^{\alpha_0+d\alpha_1+4\frac{\pi}{3}} I_d + A\sin(\theta+\lambda))\; d\theta + \int_{\alpha_0+d\alpha_2-\frac{\pi}{3}}^{\alpha_0+d\alpha_4+\frac{\pi}{3}} -I_d - A\sin(\theta+\lambda))\; d\theta\right]$$

$$I_{a_0} = \frac{1}{2\pi}\Bigg[-I_d\, d\alpha_1 - I\, d\alpha_3 + I_d\, d\alpha_4 - I_d\, d\alpha_6 \;\ldots$$
$$- A\left[\cos(\lambda + \alpha_o + d\alpha_1 + \frac{\pi}{3}) + \cos(\lambda + \alpha_o + d\alpha_3) \;\ldots\right.$$
$$\left. + \cos(\lambda + \alpha_o + d\alpha_4 + \frac{\pi}{3}) + \cos(\lambda + \alpha_6 + d\alpha_6)\right]\Bigg] \qquad (5.6)$$

$$I_{b_0} = \frac{1}{2\pi}\Bigg[-I_d\, d\alpha_2 - I\, d\alpha_3 + I_d\, d\alpha_5 - I_d\, d\alpha_6 \;\ldots \qquad (5.7)$$
$$- A\Big[\sin(\lambda + \alpha_o + d\alpha_5 + \frac{\pi}{6}) + \cos(\lambda + \alpha_0 + d\alpha_3) \;\ldots$$
$$+ \sin(\lambda + \alpha_o + d\alpha_2 + \frac{\pi}{6}) + \cos(\lambda + \alpha_0 + d\alpha_6)\Big]\Bigg]$$

$$I_{c_0} = \frac{1}{2\pi}\Bigg[I_d\, d\alpha_1 + I\, d\alpha_2 - I_d\, d\alpha_4 - I_d\, d\alpha_5 \;\ldots \qquad (5.8)$$
$$- A\Big[\cos(\lambda + \alpha_o + d\alpha_1 + \frac{\pi}{3}) - \sin(\lambda + \alpha_0 + d\alpha_5 - \frac{\pi}{6}) \;\ldots$$
$$+ \cos(\lambda + \alpha_o + d\alpha_4 + \frac{\pi}{3}) - \sin(\lambda + \alpha_0 + d\alpha_2 + \frac{\pi}{6})\Big]\Bigg]$$

In this system of three equations, $I_{a0}=0$, $I_{b0}=0$ and $I_{c0}=0$, there are 6 variables, $d\alpha_1, d\alpha_2, d\alpha_3, d\alpha_4, d\alpha_5, d\alpha_6$. Where I_d, A, λ and α_o are known parameters. We have to find some relationship between these variables in order to transform these 6 variables into 3 variables.

Let us assume that the dc current in the phase "*a*" is positive. If, for instance, $I_{a0} > 0$, and we want to make the current in phase "*a*" equal zero, $I_{a0}=0$. The magnitude of the current I_{a0} can be reduced by decreasing the area A_1 and increasing the area A_2 in Figure 5.2. The area A_1 can be decreased by reducing the width of the positive conduction period and increasing the width of the negative conduction period for I_a. This may be achieved by increasing the values of $d\alpha_1$ and $d\alpha_6$, and decrease $d\alpha_3$ and $d\alpha_4$, as shown in Figure 5.2. The arrows pointing to the right side means that the value of α_i should be increased and the arrows pointed to the left side means that α_i should be decreased. The same process can be repeated in the other phases.

We need 3 degrees of freedom to simultaneously reduce I_{a0}, I_{b0} and I_{c0} to zero. We select these 3 quantities as $d\alpha_a$, $d\alpha_b$ and $d\alpha_c$ respectively.

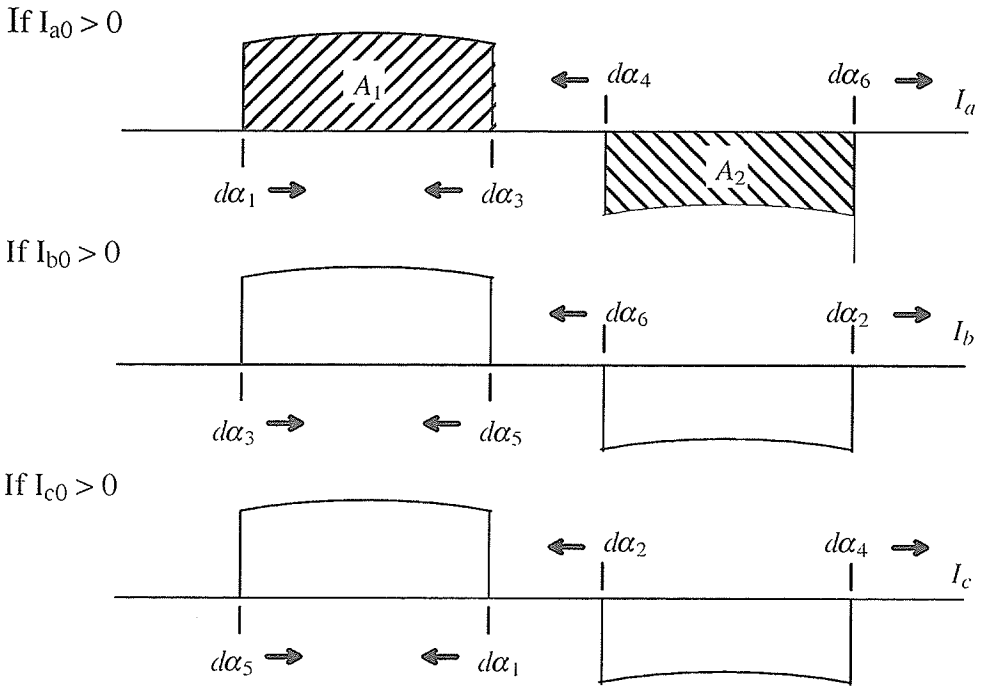

Figure 5 .2 : Modulation of the firing angle.

Considering that the variation of the width in phase "a, b and c" necessary to reduce I_{a0}, I_{b0} and I_{c0} to zero are $d\alpha_a$, $d\alpha_b$ and $d\alpha_c$, respectively. Then we can write the variables $d\alpha_1$, $d\alpha_2$, $d\alpha_3$ $d\alpha_4$, $d\alpha_5$ and $d\alpha_6$ as a function of $d\alpha_a$, $d\alpha_b$ and $d\alpha_c$, as shown in the Equation 5 .9 .

$$d\alpha_1 = d\alpha_a - d\alpha_c \qquad d\alpha_4 = d\alpha_c - d\alpha_a$$
$$d\alpha_2 = d\alpha_b - d\alpha_c \qquad d\alpha_5 = d\alpha_c - d\alpha_b$$
$$d\alpha_3 = d\alpha_b - d\alpha_a \qquad d\alpha_6 = d\alpha_a - d\alpha_b \qquad (5.9)$$

Now we have three equations (I_{a0}=0, I_{b0}=0 and I_{c0}=0) and three variables ($d\alpha_a$, $d\alpha_b$ and $d\alpha_c$) which makes possible to solve the system of Equations 5 .10 . Denoting these variables $d\alpha_a$, $d\alpha_b$ and $d\alpha_c$ by x_1, x_2 and x_3, respectively, we have

$$I_{a_0} = f(x_1, x_2, x_3) = 0$$
$$I_{b_0} = f(x_1, x_2, x_3) = 0$$
$$I_{c_0} = f(x_1, x_2, x_3) = 0 \qquad (5.10)$$

We may rewrite the equations 5 .6 , 5 .7 and 5 .8 as a function of x_1, x_2 and x_3.

$$I_{a_0} = \frac{1}{2\pi}\Bigg[\Big[\; I_d\,(-4x_1+2x_2+2x_3)\Big] - A\Big[\cos(\lambda+\alpha_o+(x_1-x_3)+\frac{\pi}{3}) + \cos(\lambda+\alpha_o+(x_2-x_1)) \;..\; + \cos(\lambda+\alpha_o+(x_3-x_1)+\frac{\pi}{3}) + \cos(\lambda+\alpha_0+(x_1-x_2))\Big]\Bigg] \qquad (5.11)$$

$$I_{b_0} = \frac{1}{2\pi}\Bigg[\Big[\; I_d\,(2x_1-4x_2+2x_3)\Big] + A\Big[\sin(\lambda+\alpha_o+(x_3-x_2)+\frac{\pi}{6}) + \cos(\lambda+\alpha_o+(x_2-x_1)) \;..\; + \sin(\phi+\alpha_o+(x_2-x_3)+\frac{\pi}{6}) + \cos(\phi+\alpha_0+(x_1-x_2))\Big]\Bigg] \qquad (5.12)$$

$$I_{c_0} = \frac{1}{2\pi}\Bigg[\Big[\; I_d\,(2x_1+2x_2-4x_3)\Big] + A\Big[\sin(\lambda+\alpha_o+(x_1-x_3)+\frac{\pi}{3}) - \sin(\lambda+\alpha_o+(x_3-x_2)+\frac{\pi}{6}) \;..\; + \cos(\lambda+\alpha_o+(x_3-x_1)+\frac{\pi}{3}) - \sin(\lambda+\alpha_0+(x_2-x_3)+\frac{\pi}{6})\Big]\Bigg] \qquad (5.13)$$

5 .1 .1 NEWTON–RAPHSON METHOD [26]

In order to solve a set of N nonlinear equations in the N unknowns *x1, x2, ..., xn,* we may use the Newton Raphson method [27].

A typical problem gives N functional relations to be zeroed, involving variables x_i, i=1,2 ... N

$$f_i(x_1, x_2, \;..\;, x_n) = 0 \qquad i = 1, 2, \;..\;, N.$$

If we let X denote the entire vector of values x_i then, in the neighborhood of X, each of the functions f_i can be expanded in Taylor series.

$$f_i(X+\delta X) = f_i(X) + \sum_{j=1}^{N} \frac{\partial f_i}{\partial x_j} \partial x_j + O(\delta X^2) \qquad (5.14)$$

By neglecting terms of δX^2 and higher, we obtain a set of linear equations for the corrections δX that move each function closer to zero simultaneously, namely

$$\sum_{j=1}^{N} \alpha_{ij}\, \delta x_j = \beta_i$$

$$\alpha_{ij}\, \delta x_j \equiv \frac{\partial f_i}{\partial x_j} \qquad \beta_i \equiv -f_i \qquad (5.15)$$

The matrix equation can be solved by LU decomposition as described in [27]. The correction are then added to the solution vector,

$$x_i^{new} = x_i^{old} + \partial x_i \qquad i = 1, \ldots, N \qquad (5.16)$$

and the process is iterated to convergence.

We have to determine the values of *x1*, *x2* and *x3* in the system of equations given in 5 .10 . To solve this system of equations by using Newton–Raphson method we need to write the expression of the partial derivative of the functions I_{a0}, I_{b0} and I_{c0}.

The partial derivatives of I_{a0} is

$$\frac{dI_{a_0}}{dx_1} = \frac{1}{2\pi}\left[-4I_d + A\left[\sin(\lambda+\alpha_o+(x_1-x_3)+\frac{\pi}{3}) - \sin(\lambda+\alpha_o+(x_2-x_1)) \ldots \right.\right.$$
$$\left.\left. - \sin(\lambda+\alpha_o+(x_3-x_1)+\frac{\pi}{3}) + \sin(\lambda+\alpha_o+(x_1-x_2)) \right]\right]$$

$$\frac{dI_{a_0}}{dx_2} = \frac{1}{2\pi}\left[2I_d + A\left[\sin(\lambda+\alpha_o+(x_2-x_1)) - \sin(\lambda+\alpha_o+(x_1-x_2)) \right]\right]$$

$$\frac{dI_{a_0}}{dx_3} = \frac{1}{2\pi}\left[2I_d + A\left[-\sin(\lambda+\alpha_o+(x_1-x_3)+\frac{\pi}{3}) + \sin(\lambda+\alpha_o+(x_3-x_1)+\frac{\pi}{3}) \right]\right] \qquad (5.17)$$

The partial derivatives of I_{b0} is

$$\frac{dI_{b_0}}{dx_1} = \frac{1}{2\pi}\left[2I_d + A\left[\sin(\lambda + \alpha_o + (x_2 - x_1)) - \sin(\lambda + \alpha_o + (x_1 - x_2))\right]\right]$$

$$\frac{dI_{b_0}}{dx_2} = \frac{1}{2\pi}\left[-4I_d + A\left[-cos(\lambda + \alpha_o + (x_3 - x_2) + \frac{\pi}{6}) + \sin(\lambda + \alpha_o + (x_2 - x_1)) \ldots + \cos(\lambda + \alpha_o + (x_2 - x_3) + \frac{\pi}{6}) - \sin(\lambda + \alpha_o + (x_1 - x_2))\right]\right]$$

$$\frac{dI_{b_0}}{dx_3} = \frac{1}{2\pi}\left[2I_d + A\left[\cos(\lambda + \alpha_o + (x_3 - x_2) + \frac{\pi}{6}) - \cos(\lambda + \alpha_o + (x_2 - x_3) + \frac{\pi}{6})\right]\right] \quad (5.18)$$

The partial derivatives of I_{c0} is

$$\frac{dI_{c_0}}{dx_1} = \frac{1}{2\pi}\left[2I_d + A\left[-\sin(\lambda + \alpha_o + (x_1 - x_3) + \frac{\pi}{3}) + \sin(\lambda + \alpha_o + (x_3 - x_1) + \frac{\pi}{3})\right]\right]$$

$$\frac{dI_{c_0}}{dx_2} = \frac{1}{2\pi}\left[2I_d + A\left[\cos(\lambda + \alpha_o + (x_3 - x_2) + \frac{\pi}{6}) - \cos(\lambda + \alpha_o + (x_2 - x_3) + \frac{\pi}{6})\right]\right]$$

$$\frac{dI_{c_0}}{dx_3} = \frac{1}{2\pi}\left[-4I_d + A\left[\sin(\lambda + \alpha_o + (x_1 - x_3) + \frac{\pi}{3}) - \cos(\lambda + \alpha_o + (x_3 - x_2) + \frac{\pi}{6}) \ldots - \sin(\phi + \alpha_o + (x_3 - x_1) + \frac{\pi}{3}) + \cos(\phi + \alpha_o + (x_2 - x_3) + \frac{\pi}{6})\right]\right]$$

Appendix C shows a Fortran program called FIRINANG that was developed in order to find the values of x_1, x_2 and x_3 from the system of equation given in the Equation 5.10. An example case is performed in the next section.

5 .2 ELIMINATION OF CONVERTER TRANSFORMER DC CURRENTS

5 .2 .1 NUMERICAL CALCULATION APPROACH

In order to illustrate the elimination of the dc current, we consider the example case shown in Figure 5 .1 . The dc current is I_d=1.5 kA, the amplitude of the 60 Hz current induced from the ac line into the dc line is A=0.15 kA, the base firing angle is α_0=30^0 and the phase λ=–60^0. In this case the number of variables N are equal of the number of phases in the ac system, N=3.

a) input data for the program FIRINANG are:

$I_d = 1.5kA$ dc current in the dc line

$A = 0.15kA$ crest value of the 60 Hz component

$\alpha_0 = 30^0$ base firing angle

$\lambda = -60^0$ phase angle

$N = 3$ number of phases

b) output data for the program FIRINANG are (firing angle modulation):

$\alpha_1 = 25.1,\quad \alpha_2 = 30.0,\quad \alpha_3 = 34.9,\quad \alpha_4 = 34.9,\quad \alpha_5 = 30.0,\quad \alpha_6 = 25.1$

In order to confirm the calculation of the firing angle modulation, the values of the dc currents I_{a0}, I_{b0} and I_{c0} resulting from such firing were calculated using numerical integration of the transformer currents I_a, I_b and I_c. The results are shown in Table 5 .1 . The same calculation of the currents was performed without using the modulation of the firing angle, which means the firing angle α_i was equal to 30^0 for i=1,2, ...6. The comparison is shown in table 5 .1 .

Table 5 .1 : Comparison of the dc component I_{a0}, I_{b0}, I_{c0} with modulation and without modulation

Id = 1.5 kA, A = 0.15 kA, $\lambda = -60^0$		
	current with firing angle modulation	current without firing angle modulation
	(A)	(A)
firing angle ==>	α_1=25.1 α_2=30.0 α_3=34.9 α_4=25.1 α_5=30.0 α_6=25.1	α_i = 30.0, i=1, 2, ... 6
$\|I_{a0}\|$	0.9E–05	82.9
$\|I_{b0}\|$	0.5E–05	41.3
$\|I_{c0}\|$	0.5E–05	41.6

As we can see the values of the dc component of the currents I_a, I_b and I_c was reduced to practically zero when the modulation of the firing angle was applied. The initial guess values of the x_i was 2^0, for i=1, 2 and 3. Only three iterations were necessaries in the Newton–Raphson subroutine in order to reach the given tolerance of 1.0E–5.

5 .2 .2 SIMULATION APPROACH ON A SIMPLE SYSTEM

This process of modulation of the firing angle by using the Newton–Raphson method was applied to the simplified system as shown in Figure 5 .3 , which was simulated on the electromagnetic transient simulation program PSCAD/EMTDC. Appendix A shows the PSCAD/EMTDC draft diagram used in this study.

The current source represents the induced current from the ac line into the dc line, I_d superimposed with I_{60}. The current source would ensure that the I_{60} component was always present. The angles calculated for $\alpha_1, \alpha_2, \ldots \alpha_6$, for a base order of $\alpha_0 = 30^0$, were respectively as described in the previous section: 25.1, 30.0, 34.9, 34.9, 30.0 and 25.1.

In order to verify these calculated values of $\alpha_1, \alpha_2, \ldots \alpha_6$ by using the simulation approach, the usual dc controls were bypassed and separate firing angles from this non–equidistant set were applied to each of the six valves.

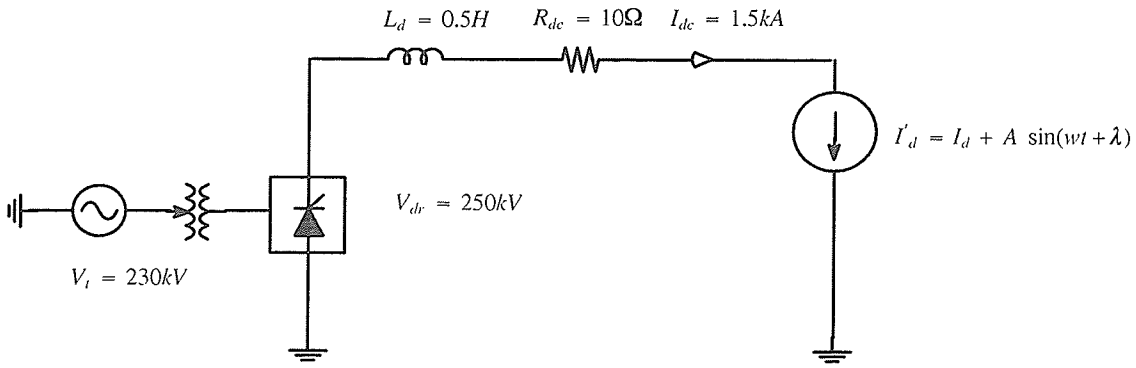

Figure 5 .3 : Simplified dc system.

Figures 5 .4 and 5 .5 show the simulation results for three different time interval situations, labeled A , B and C. In the first interval (A), from 0.0 to 0.1 seconds, the dc six–pulse bridge converter was operating without the 60Hz current source applied and the firing angle was constant and equal to 30^0. In the second interval (B), from 0.1 to 0.3 seconds, the 60 Hz current source was applied and the firing angle was still constant and equal to 30^0. And finally in the the last interval (C), from 0.3 to 0.6 seconds, the firing angles α_i were applied at each valve in the six–pulse bridge and with the 60 Hz current source still been applied in order to represent the coupling.

As we can see from Figures 5 .4 and 5 .5 in the interval B, where only the 60 Hz current source was applied, the dc component of the current in phases a, b and c increased from approximately zero to 84 , 43 and 41 amperes, respectively. In the interval C, where the firing angle modulation was applied (α_1=25.1, α_2=30.0, α_3=34.9, α_4=34.9, α_5=30.0, α_6=25.1), the dc components of the converter transformer disappeared completely, which confirms the theoretical calculation used in the previous section (Newton–Raphson method).

Figure 5 .6 shows a plot of the harmonics of the current in phase *"a"* in the secondary of the converter transformer for the three time intervals, A, B and C. The harmonics were calculated by using the Discrete Fourier Transformation, before the application of the 60 Hz current source, from

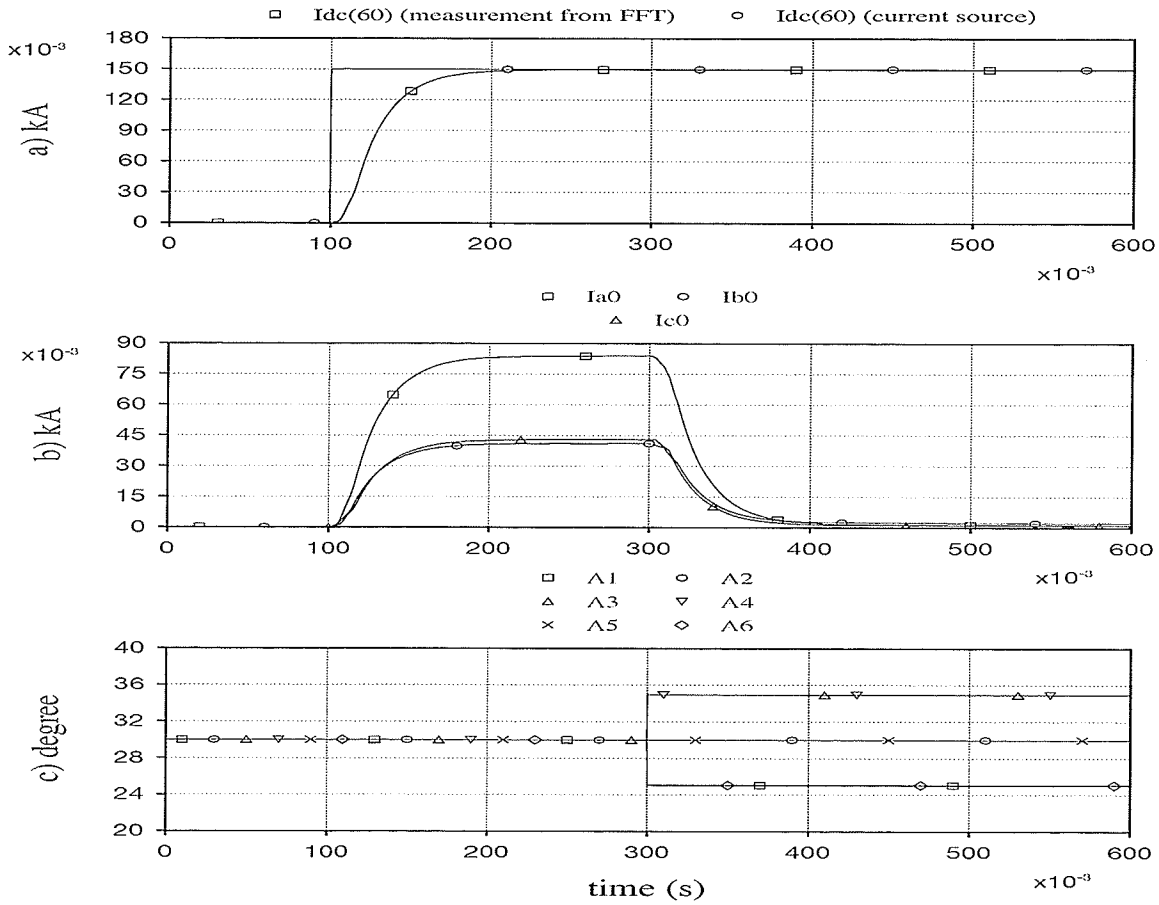

Figure 5 .4 : Dc current elimination in phase currents of a simplified six–pulse bridge converter system a) 60 Hz current source and 60 Hz current measurement in the dc line (crest), b) Magnitude of the dc current in the three phases of the secondary of the converter transformer, c) Firing angle a_m modulation from Newton–Raphson.

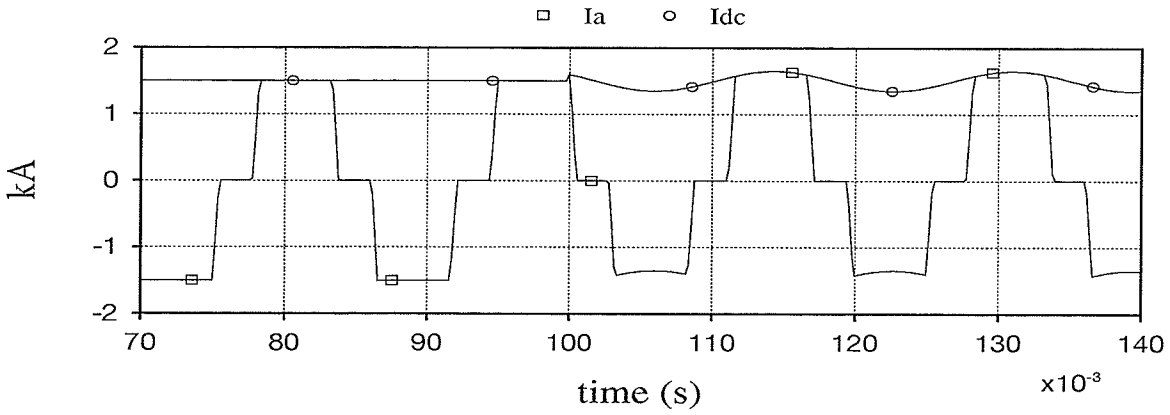

Figure 5 .5 : Dc current (Idc) and phase current (Ia).

0.0 to 0.1 seconds, during the application of the 60 Hz current source, from 0.1 to 0.3 seconds, and during the application of the modulation of the firing angles, from 0.3 and 0.6 seconds.

As expected there is a significant increase in the dc and 2nd harmonic component when the 60 Hz current source was applied. The dc component increased from 0.0% to 7.1% and the 2nd harmonic increased from 0.0% to 5.0%. The others harmonics have not changed significantly.

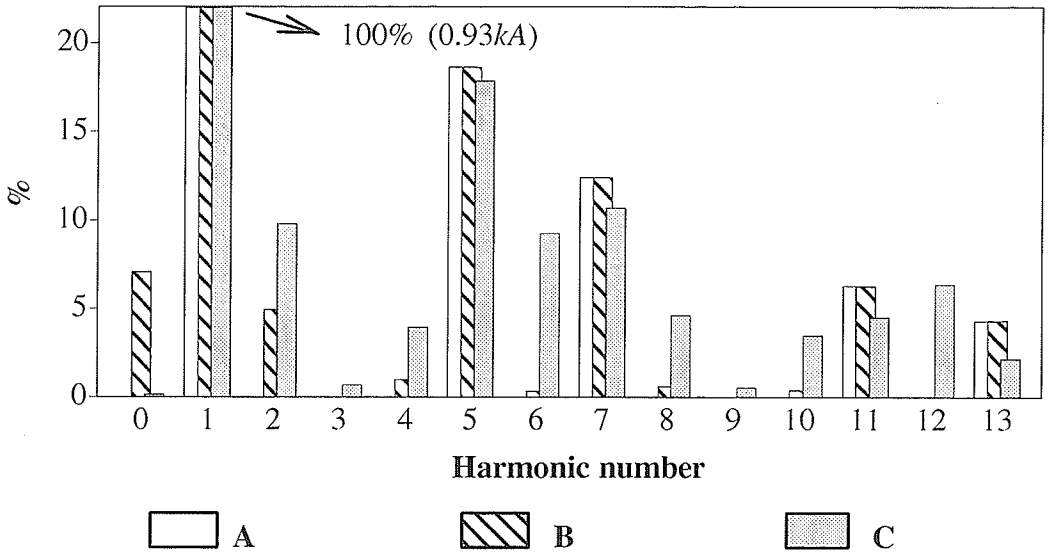

Figure 5 .6 : Harmonic Spectrum of the current I_a in the secondary of the transformer.
A – without 60 Hz current source and without modulation (from 0.0 to 0.1 s)
B – with 60 Hz current source and without modulation (from 0.1 to 0.3 s)
C – with 60 Hz current source and with modulation (from 0.3 to 0.6 s)

When the modulation of the firing angle took action, in the time interval C, the dc components were reduced to approximately zero in all the three phases in the converter transformer. The subsequent even harmonics, 2nd, 4th, 6th, 8th, 10th and 12th increased from 5.0, 1.0, 0.2, 0.6, 0.4, 0.0 to 9.2, 3.24, 7.8, 3.8, 2.8, 4.5%, respectively. The ac side characteristic harmonics, 5th, 7th, 11th and 13th, were reduced from 18.6, 12.4, 6.2 and 4.4 to 17.5, 10.6, 4.3 and 2.3.

5 .3 DESIGNING OF A CONTROL SYSTEM

The analysis in the sections 5 .1 and 5 .2 show that there is a solution for the simultaneous elimination of all dc components on the ac side. However it does not suggest any means for designing such a control system. One observation that can be made is shown in Figure 5 .7 where the calculated firing angle values are plotted against the time (angle) at which the firing occurs. Notice that they appear to lie on a sine wave. Thus one possible method is to use a modulation signal similar to that shown in the Chapter 4 .

Equations 5 .19 shows how the sine wave fitted with the α_i values obtained in Newton–Raphson method in the previous section. Where α_m=5.78^0, α_0=30^0 and ϕ=271^0.

$$\alpha(wt) = \alpha_o + \alpha_m \sin (wt + \phi) \qquad (5.19)$$

$$\alpha(\theta_i) = \left[25.06, 30.00, 34.94, 34.94, 30.00, 25.06 \right], \qquad i = 1, 2, \ldots 6$$

$$\theta_i = k60^0 + \alpha(i) , \qquad k = 0, 1 \ldots 5$$

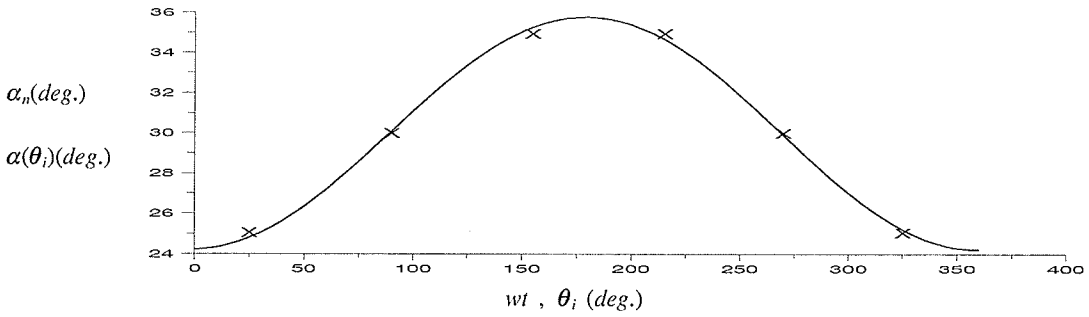

Figure 5 .7 : Theoretically calculated α_i values fitted with a sine wave.

However obtaining the amplitude and phase for the modulating signal in an on–line control system is more complicated in comparison to the method presented below and is hence not discussed further in this thesis.

Control logic for the firing angle modulation was developed for both dc and second harmonic currents with application in an static var compensators [28], [29].

The fundamental concept in designing the control system that eliminates the dc component in the secondary of the converter transformer is based on the discussion in section 5 .1 and shown in Figure 5 .2 .

Consider the phase current waveform for I_a as in Figure 5 .1 . If there is a net positive dc component, its magnitude can be reduced by reducing the width of the positive conduction period for I_a and increasing the width of the negative conduction period. This may be achieved by increasing the values of α_1 and α_6 while decreasing the values of α_3 and α_4. The same process can then be repeated in the other phases. The control system of Figure 5 .8 then comes to mind.

In this control concept, the proportional–integral (PI) controller for each phase keeps increasing or decreasing the relevant firing angles in order to reduce the dc component to zero. Note that the same firing angle affects different phases in different ways, i.e., α_1 must be increased in order to make I_{a0} more negative and decreased to make I_{c0} more negative. If the gains are properly chosen, the controller is able to achieve a steady state and eliminate all three dc components. The positive and negative contributions are then added to the firing angle order α_0 at the output summing junctions. The firing angle order α_0 is the pre–modulation firing angle order from the main controls. The angles are then passed on to a phase–locked loop based firing control system which issues firing pulses to the valves.

5 .4 TEST ON A SIMPLE SYSTEM

Figure 5 .9 shows the simulation results for such a controller operating on the simplified system shown in Figure 5 .3 . The 60 Hz current source, which represent the coupling effect, is applied at 0.1 seconds. The controller is enabled at 0.3 seconds. Note that the dc components quickly vanish after the controller is enabled. The original firing angles for each valve are all equal initially, but take on different values after the controller is enabled.

These values can be made exactly equal to the theoretical values calculated from the Newton–Raphson procedure discussed in the previous sub–section 5 .1 .1 , by choosing an appropriate value for the phase angle λ in the current source. The angles obtained from the simulation,

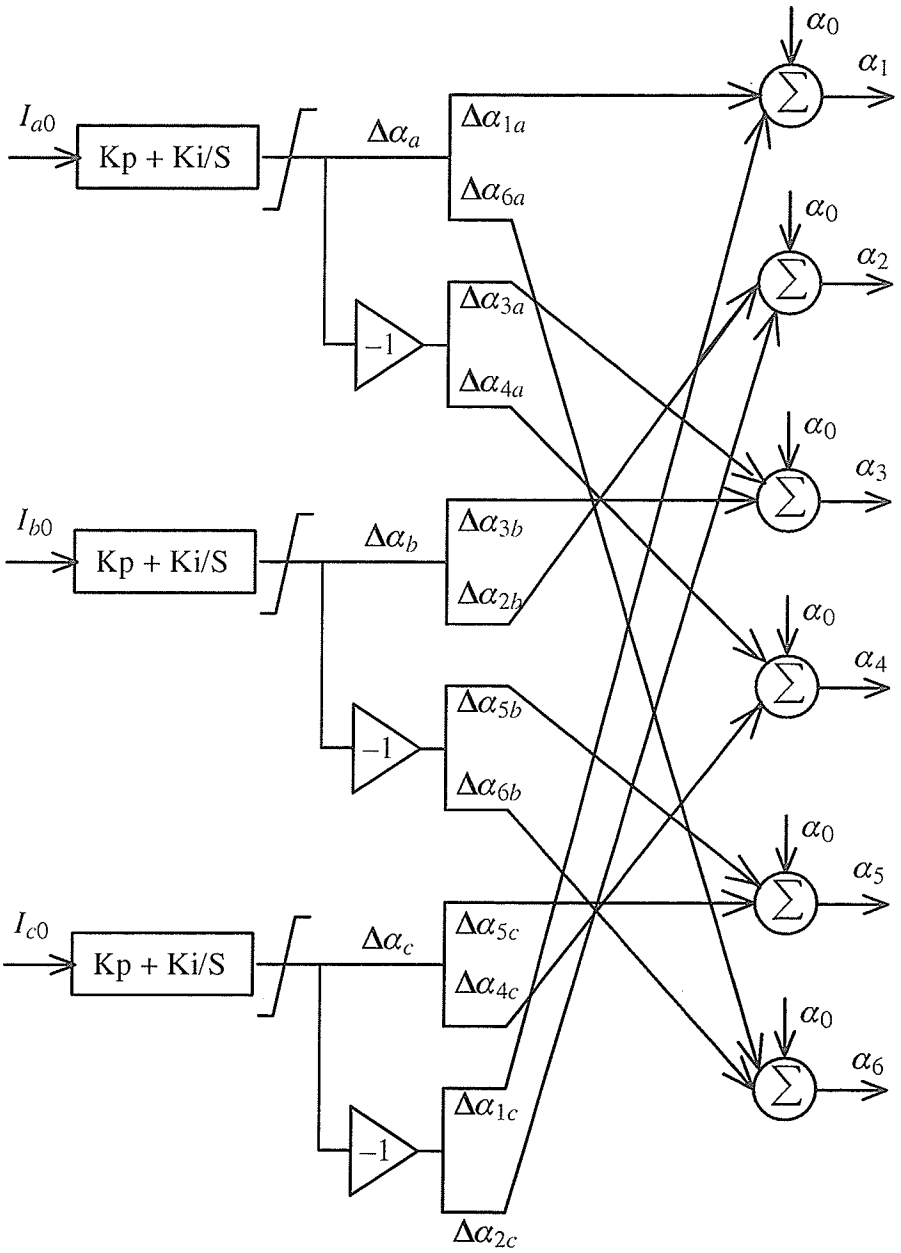

Figure 5 .8 : Proposed control system.

for a base order of $\alpha_0=30^0$ were respectively as follows: [25.8^0, 31.1^0, 35.3^0, 34.2^0, 28.9^0 and 24.7^0]. These are close, but differ slightly from the calculated angle in equation 5 .19 . This is because more than one solution exists for the angles αi and the controller has converged to a slightly different one.

Note that as a current source was used on the dc side for the I_{60} component, it is not eliminated by this control action. It was noticed in this simulated case that the dc voltage did not change when the modulation in the firing angles was applied.

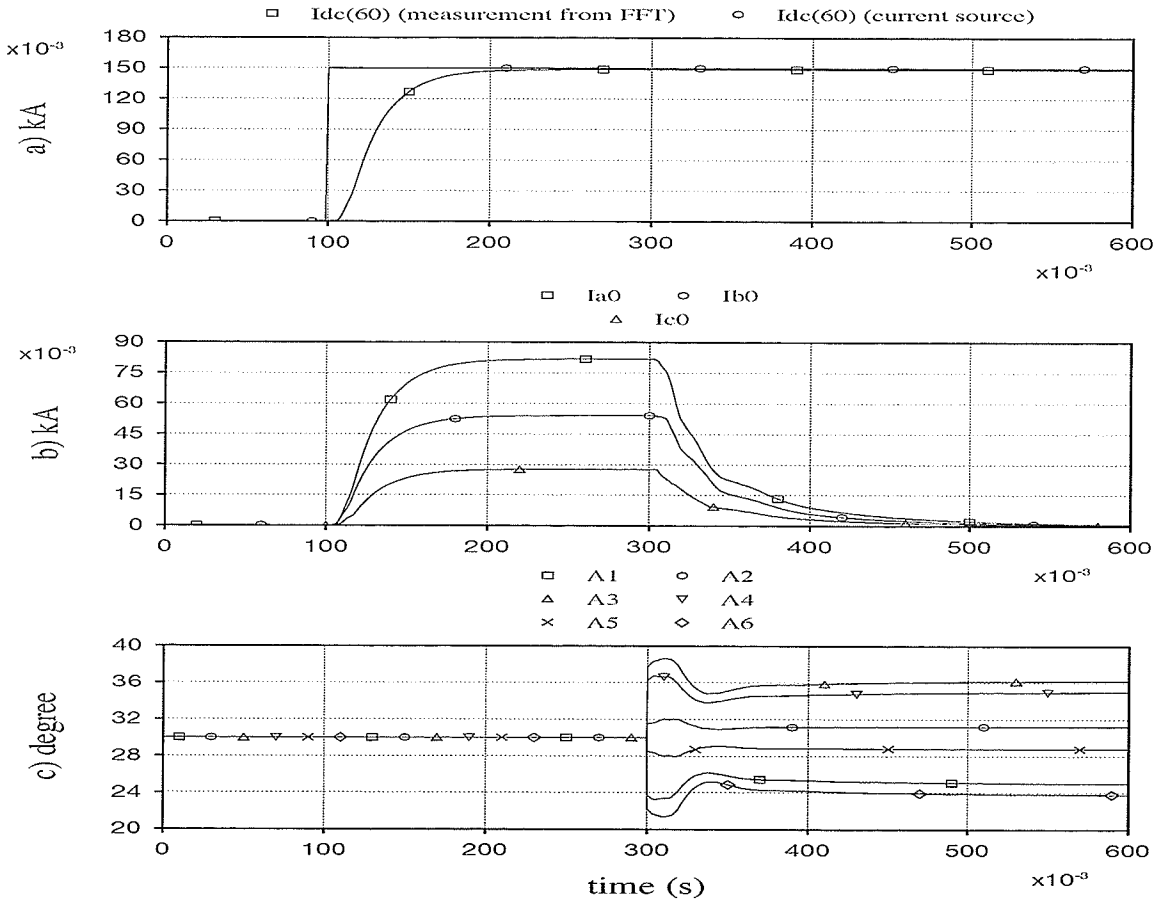

Figure 5 .9 : Dc current elimination in phase currents of a simplified six–pulse bridge converter system a) 60 Hz current source and 60 Hz current measurement in the dc line (crest), b) Magnitude of the dc current in the three phases of the secondary of the converter transformer, c) Firing angle α_i modulation from control action.

Figure 5 .10 shows a plot of the harmonics of the current in phase "*a*" in the secondary of the converter transformer for the case shown in Figures 5 .9 . As in Figure 5 .6 the harmonics were measured using the Discrete Fourier Transformation, before the application of the 60 Hz current source, from 0.0 to 0.1 seconds, during the application of the 60 Hz current source, from 0.1 to 0.3 seconds, and during the application of the modulation of the firing angles, from 0.3 and 0.6 seconds.

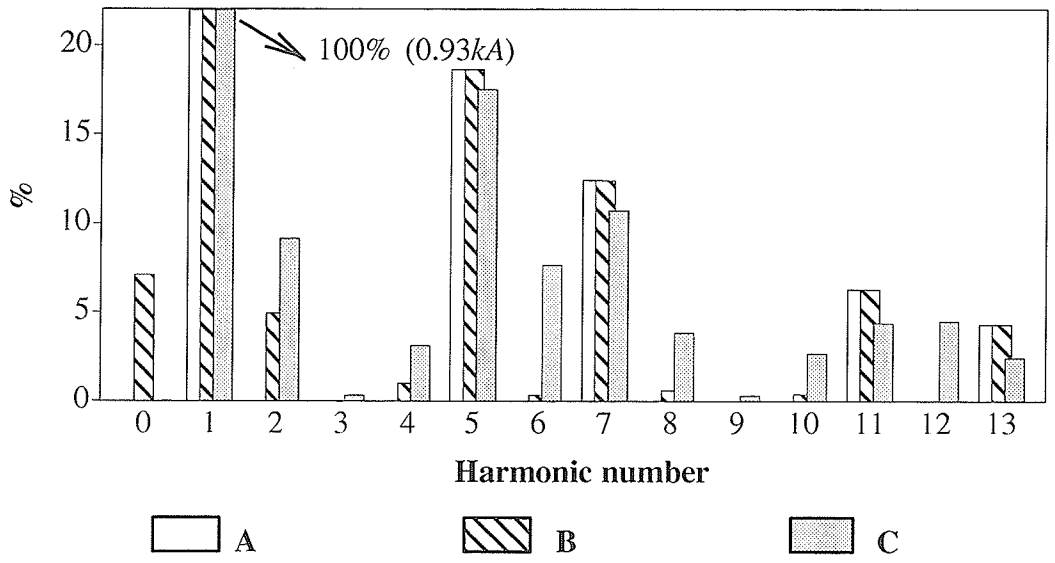

Figure 5 .10 : Harmonic spectrum of the secondary current transformer I_a.
A – without 60 Hz current source and without modulation (from 0.0 to 0.1 s)
B – with 60 Hz current source and without modulation (from 0.1 to 0.3 s)
C – with 60 Hz current source and with modulation (from 0.3 to 0.6 s)

The results for the harmonics analyses from Figure 5 .10 are similar to the one shown in Figure 5 .6 as was expected, by the reason the firing angle modulation in both cases are close.

5 .5 TEST ON A LARGE HYBRID AC–DC SYSTEM

5 .5 .1 AC LINE UNTRANSPOSED AND WITHOUT BLOCKING FILTER SCR = 11.33 , Q = 33% (200 MVAR)

The control concept was now applied to the rectifiers of the positive pole of the bipolar dc transmission system described in Chapter 2 , with SCR=11.33 (short circuit ratio) and Q=33% (percentage of reactive power related to the total power transmitted) (Q=0.33x600MW=200 Mvar). As can be seen from Figure 5 .11 which shows the firing angles and the dc components together with I_{60}, the controller significantly reduces the dc components. We have simulated the untransposed case to exacerbate I_{60} which would of course be much reduced if we had transposed the ac conductors. Note that in this particular case, the magnitude of I_{60} is slightly decreased but not reduced to zero with

the elimination of transformer dc currents. In fact depending on the phase of the ac line currents, I_{60} can either increase or decrease as a result of the control action. Appendix A shows the PSCAD/EMTDC draft diagram used in this study.

Figure 5 .12 and 5 .13 show the plot of the harmonics in the transformer secondary current, in phase "*a*", in both sides, rectifier and inverter, for the case discussed above. There is is a significant reduction in the dc component in both rectifier and inverter sides. In the rectifier there is an increase in the even non–characteristic harmonics, which is more significant in the second harmonic (from 3.1% to 7.1%). In the inverter there was not a significant change in the harmonics, except for the dc component.

One of the concerns of applying this control method was that because the magnitude of I_{60} can actually rise, it is possible that elimination of dc currents at one end may cause an increase in their values in the transformers at the other end. It was also felt that if control was applied at both ends, the two controllers might fight each other. Nevertheless when the simulations were repeated with controllers active at both ends the controllers were still able to eliminate the dc components. The firing angles, the dc components and the 60 Hz component in the dc line at either end (positive pole) for this situation are shown in Figure 5 .14 . The control effort at the rectifier is considerable with a maximum deviation of about 7^0 from the nominal value. The effort at the inverter is much less with a deviation of about 4^0 in this particular case. Note that the extinction angle controller of the inverter would modify the value of α_0 to maintain the ordered minimum extinction angle so the modulation does not result in commutation failures.

Figure 5 .15 show the plot of the harmonics in the transformer secondary current, in phase "*a*", in both sides, rectifier and inverter, for the case discussed above. There is a significant reduction in the dc component in both rectifier and inverter sides. In the rectifier there is a increase in the even–non–characteristic harmonics, which is more significant in the second harmonic (from 4.5% to 7.0%). In the inverter there was not a significant change in the harmonics, except for the dc component.

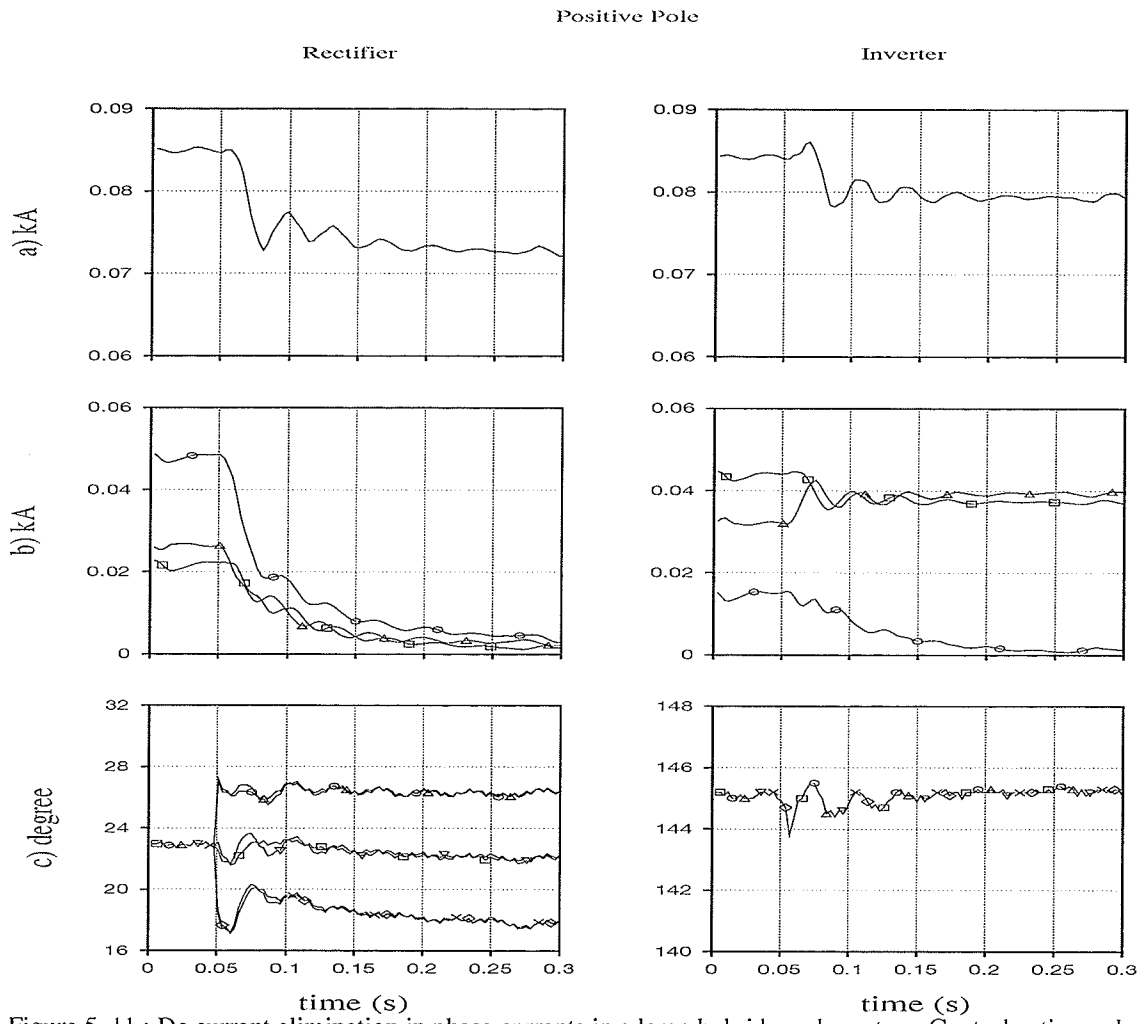

Figure 5 .11 : Dc current elimination in phase currents in a large hybrid ac–dc system. Control action only in the rectifier side and positive pole. Ac line untransposed and without blocking filter
a) 60 Hz current measurement in the dc line (crest), b)Magnitude of the dc component in the converter transformer (3 phases), c) Firing angle α_j modulation.

Further simulations were carried out with control applied to all eight converters on both poles. The controls worked successfully by eliminating the dc components in each transformer, as shown in Figure 5 .16 .

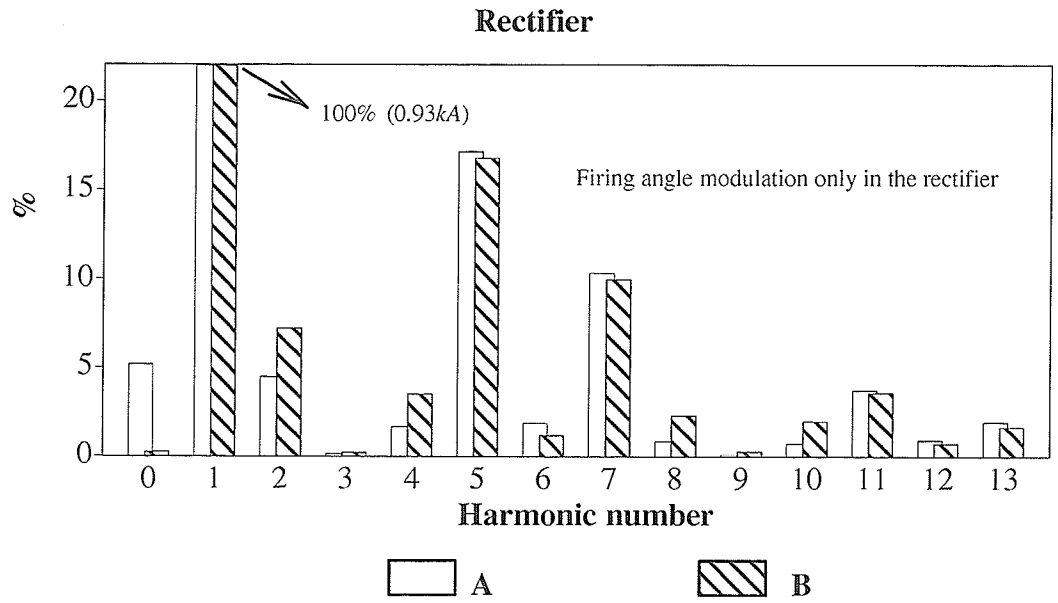

Figure 5 .12 : Harmonic spectrum of the secondary current transformer I_a (**Rec., Pos. Pole**).

A – without modulation

B – with modulation only in the rectifier positive pole

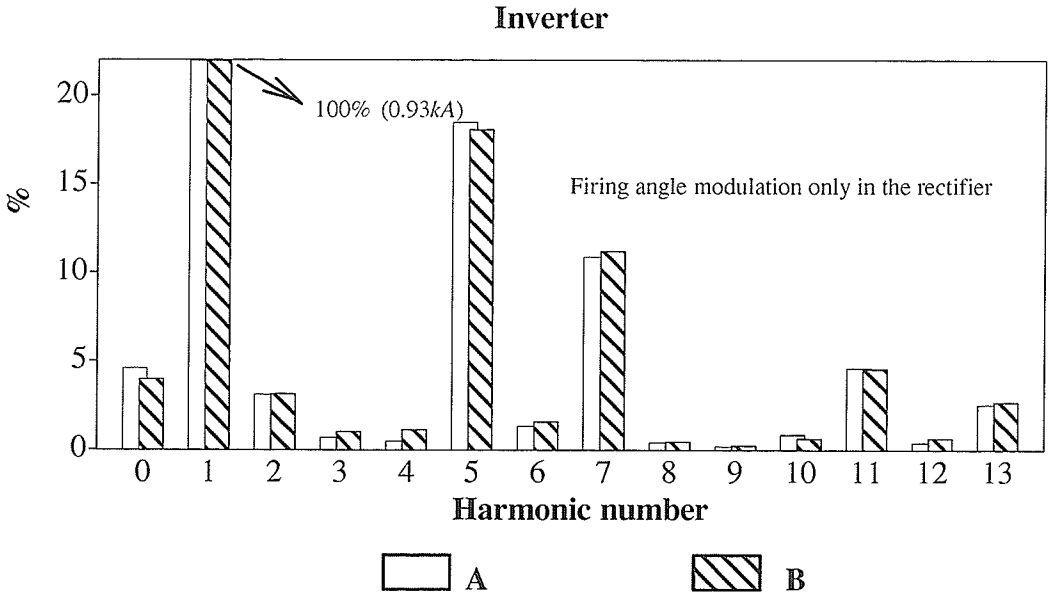

Figure 5 .13 : Harmonic spectrum of the secondary current transformer I_a (**Inv., Pos. Pole**).

A – without modulation

B – with modulation only in the rectifier positive pole

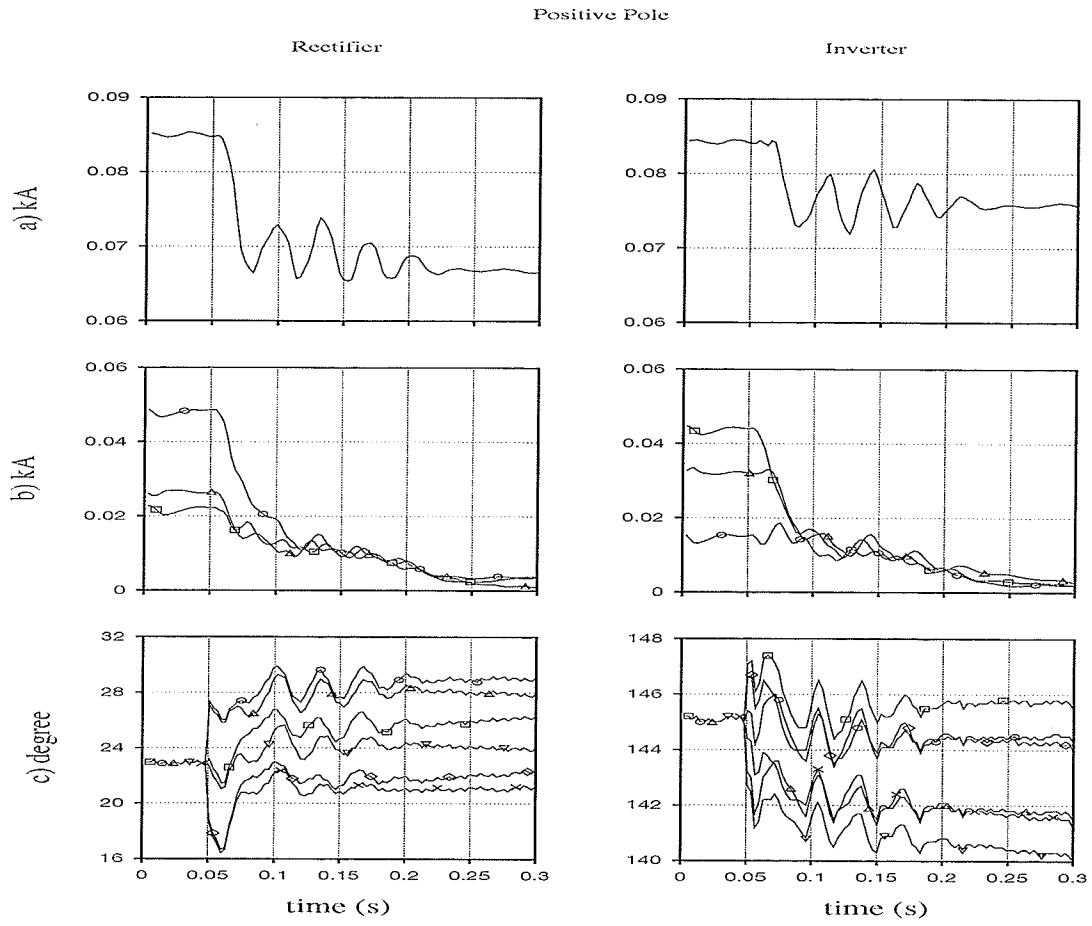

Figure 5 .14 : Dc current elimination in phase currents in a large hybrid ac–dc system. Control action on both sides and only positive pole. Ac line untransposed and without blocking filter, SCR=11.33, Q=33% a) 60 Hz current measurement in the dc line (crest), b)Magnitude of the dc component in the converter transformer (3 phases), c) Firing angle α_i modulation.

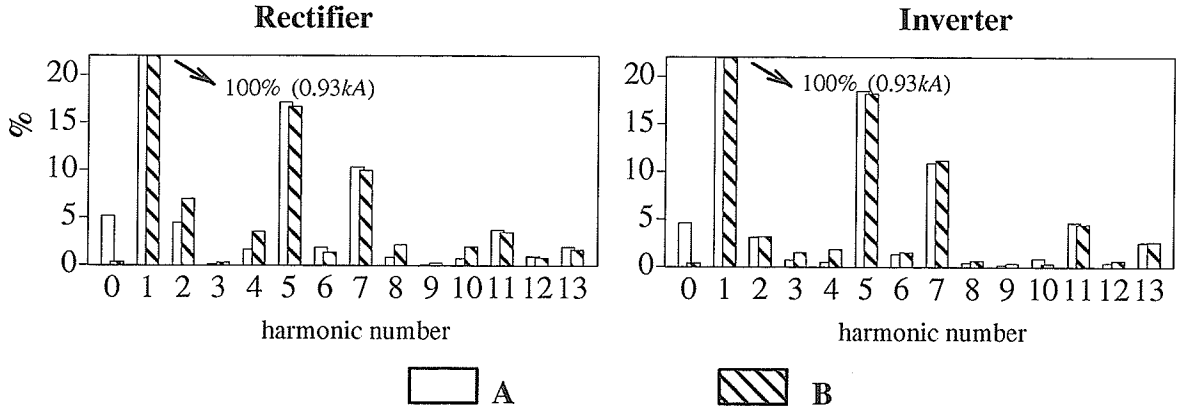

Figure 5 .15 : Harmonic spectrum of the secondary current transformer I_a **(Rec. and Inv. / Pos. Pole)**

A – without modulation

B – with modulation in the rectifier and inverter (only positive pole)

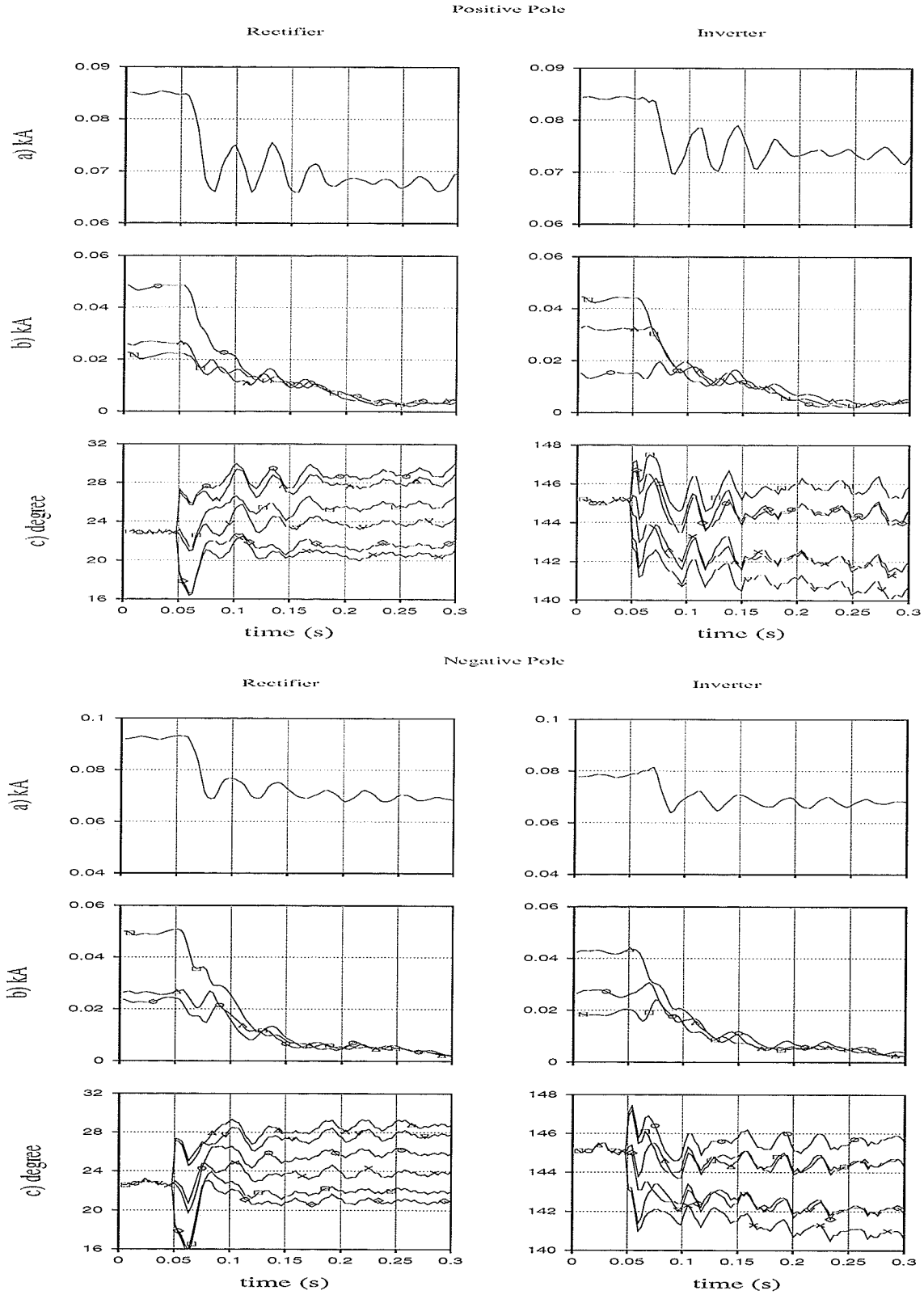

Figure 5 .16 : Dc current elimination in phase currents in a large hybrid ac–dc system. Control action on both sides and poles. Ac line untransposed and without blocking filter, SCR=11.33, Q=33%
a) 60 Hz current measurement in the dc line (crest), b)Magnitude of the dc component in the converter transformer (3 phases), c) Firing angle α_i modulation.

5 .5 .2 AC LINE TRANSPOSED AND WITHOUT BLOCKING FILTER SCR = 11.33 AND Q = 33% (200 MVAR)

The control concept was now applied to all eight converters on both poles with the ac line transposed, with the same SCR (short circuit ratio) and Q (percentage of reactive power). The ac line transposition was performed at three equally spaced locations of 130 km along the line. As can be seen from Figure 5 .17 which shows the magnitude of the 60 Hz current measurement in the dc line (crest), the magnitude of the dc current component in the three phases of the secondary of the converter transformer and the firing angle α_m modulation. The controller significantly reduces the dc component. The control effort at the rectifier is much less compared with the case in the section 5 .5 .1 where the ac line was untransposed. The maximum deviation of α_i at the rectifier is 1.15^0 from the base firing angle value of 21.6^0. The effort at the inverter is less with a deviation of 0.9^0 in this case. These values of deviation are approximately the same for both poles.

5 .5 .3 AC LINE UNTRANSPOSED AND WITHOUT BLOCKING FILTER SCR = 2.42 AND Q=60% (360 MVAR)

The performance of the modulation action was investigated in a weaker system in order to verify if harmonic instability occurs. As described earlier the coupling between the ac line and the dc line will produce a 60 Hz current component in the dc line. This 60 Hz current will be referred to the secondary of the converter transformer as a dc and 2nd harmonic current component. In an HVDC system usually a weaker source presents a high impedance close to the 2nd harmonic frequency. As in the modulation we are only eliminating the dc current component in the secondary of the converter transformer and the 2nd harmonic, on the other hand, has been increased because of this modulation action. One concern of this modulation is that this 2nd harmonic could generate harmonic instability in a system with high impedance at this frequency. Therefore a weaker system with SCR=2.42 and with reactive power, in the filters and the shunt capacitors, of 60% of the total power transmitted (360Mvar) in the dc system was studied. Before applying the modulation in this large hybrid weak system a total system impedance versus frequency was performed.

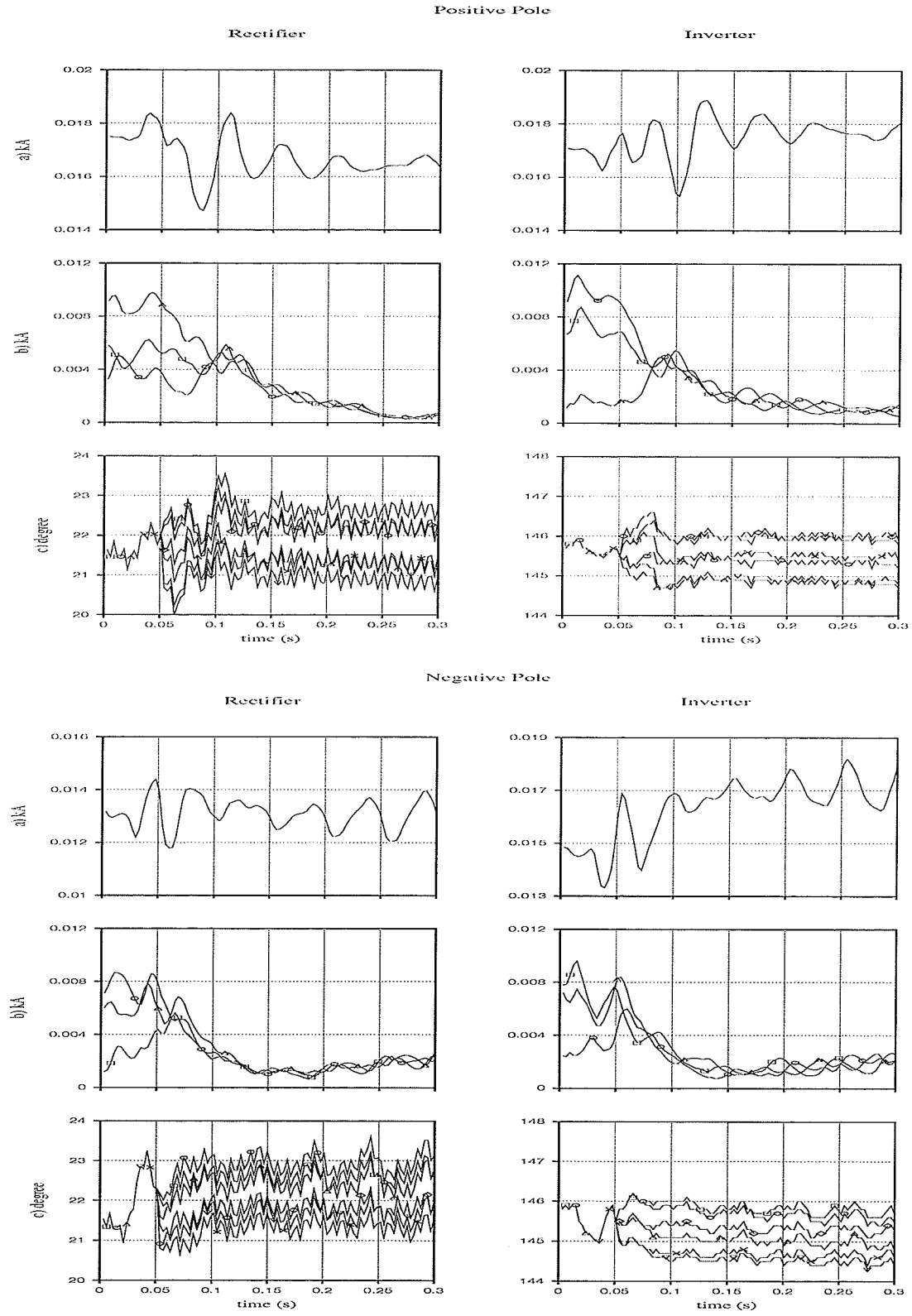

Figure 5 .17 : Dc current elimination in phase currents in a large hybrid ac–dc system. Control action on both sides and poles. Ac line transposed and without blocking filter, SCR=11.33 and Q=33%.
a) 60 Hz current measurement in the dc line (crest), b)Magnitude of the dc component in the converter transformer (3 phases), c) Firing angle α_i modulation.

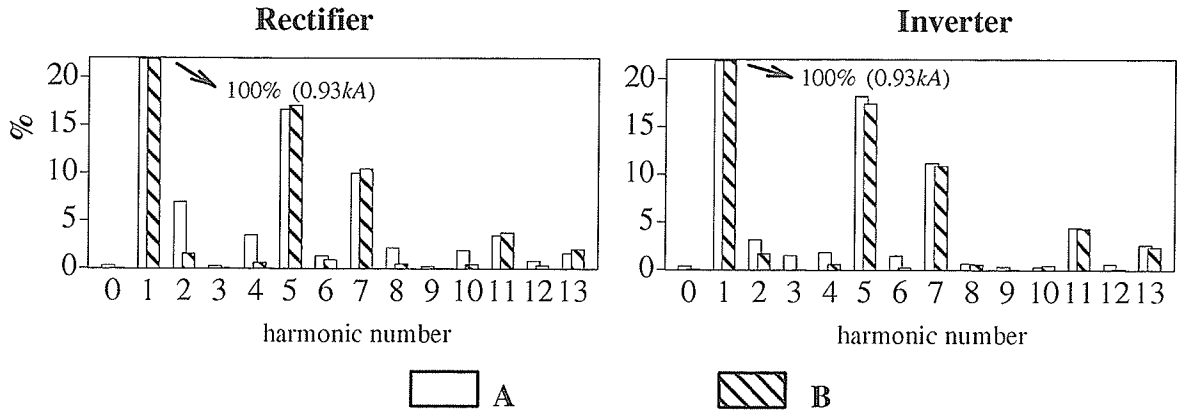

Figure 5 .18 : Harmonic spectrum of the secondary current transformer I_a (Rec. and Inv., pos. pole). SCR=11.33, Q=33%

A – with modulation (ac line untransposed)

B – with modulation (ac line transposed)

5 .5 .3 .1 FREQUENCY SCANNING OF THE HYBRID SYSTEM

The weaker ac source system with SCR=2.42 and filters configuration with total reactive power of Q=60% (percentage of reactive power) (360 Mvar) of the dc transmitted power are shown in Figure 5 .19 . The total system impedance variation versus frequency plots for the ac system in isolation, as viewed from the terminal buses are shown in Figure 5 .20 . It shows the presence of a high parallel resonance at 120 Hz at the sending and receiving ends. A possibility of harmonic instability is thus expected for this system condition.

The system impedance responses calculated in Figure 5 .20 have not taken into account the connection of the dc and ac lines. Therefore, the dc system has no effect on the ac system. However, in the actual system the impedance seen from the rectifier or the inverter might affect by the dc system especially if the ac system is weak.

Using simulation it is possible to identify the presence of a potential instability in the combined ac–dc system more accurately compared to the previous methods. With the hybrid system operating in the steady state, a small current with a wide range of frequencies is injected into the ac bus as shown in

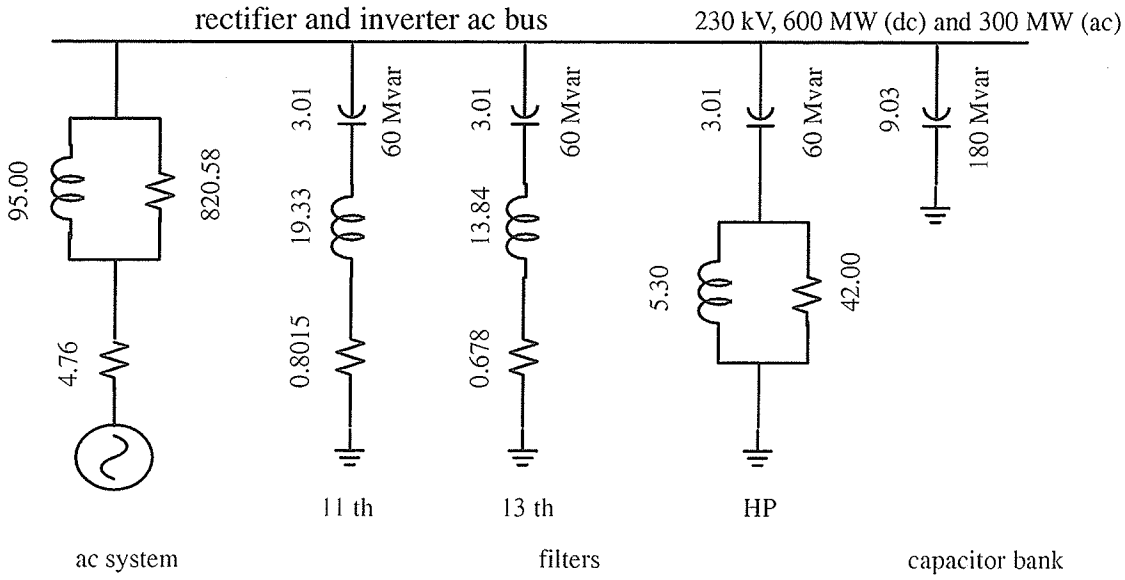

Figure 5 .19 : Rectifier and Inverter ac system configuration.

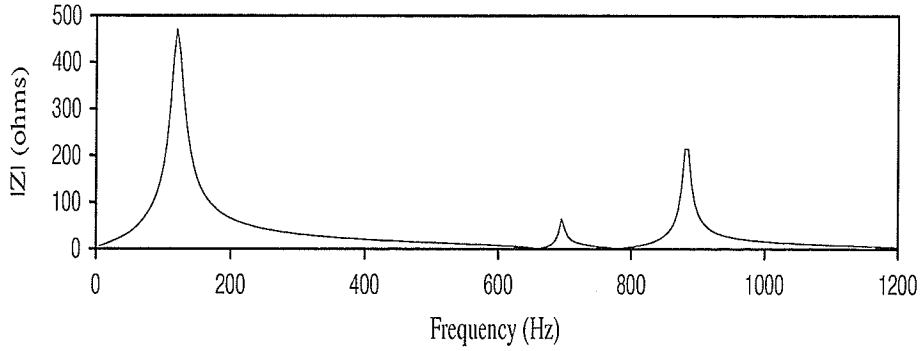

Figure 5 .20 : Total ac system impedance versus frequency (Rec. and Inv. SCR=2.42, Q=60%).

Figure 5 .21 . The system impedance can be calculated by measuring the ac bus harmonic voltage *Vh* in response to the injected harmonic current I_h.

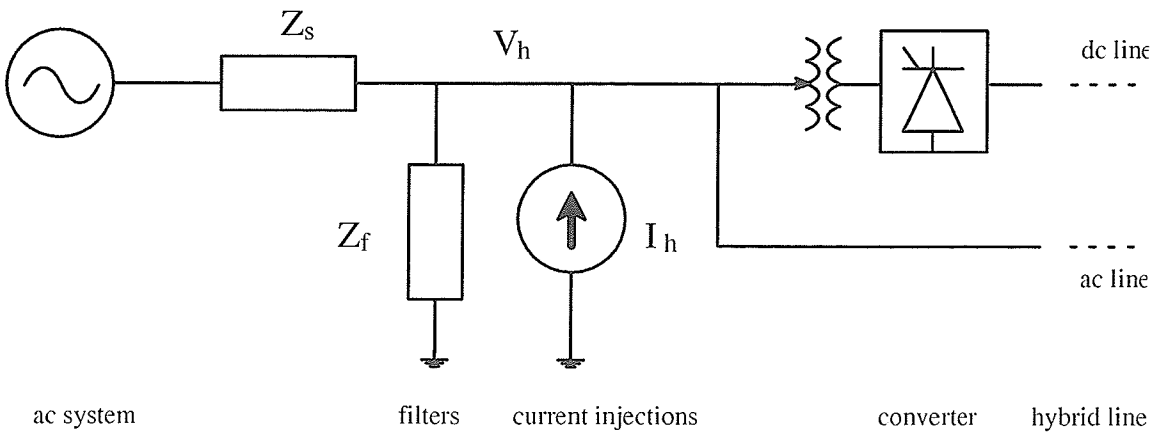

Figure 5 .21 : Frequency scanning method for system impedance of the hybrid ac–dc system.

The actual system impedance response of the hybrid system with SCR=2.42 and Q=60% (percentage of reactive power) was obtained by the frequency scanning method described above. In the steady state, a series of small harmonic currents (i.e. 5, 10, ... 1200 Hz at the magnitude of 2 A (less than 0.1% of the fundamental current in ac source) are injected into the rectifier ac bus in the manner described above.

The frequency spectrum of the ac bus voltage contains harmonic components from 5 Hz to 1200 Hz in response to the injected harmonic currents. Note that the distortion in the ac bus voltage is very small and guarantees the assumption of small disturbance that does not significantly change the operation of the system.

The rectifier ac impedance can be easily obtained by calculating the ratio of the ac bus voltage to the injected harmonic current of 2 A at each frequency. The measured rectifier ac impedance versus frequency characteristics obtained by the frequency scanning method is shown in Figure 5 .22 . The results are plotted together with the calculated frequency responses using the simplified formulation presented earlier in Figure 5 .20 for comparison.

Comparing the spectra from the simplified calculation and measurement from 0 Hz to 1200 Hz in Figure 5 .22 , there are some major differences between the simplified analysis method and

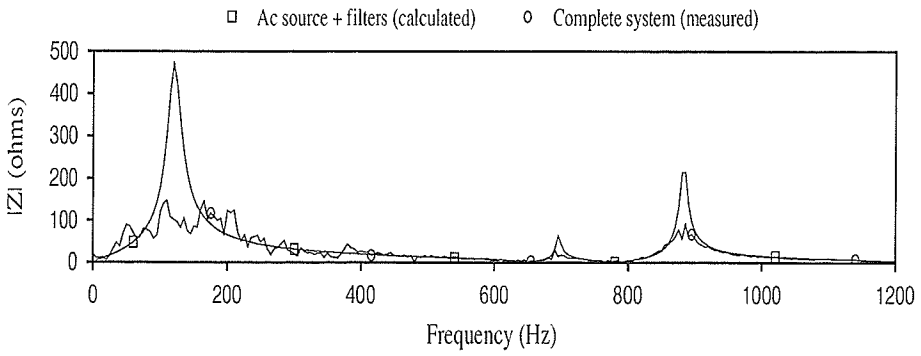

Figure 5 .22 : The total ac system impedance x frequency (Rec. and Inv. SCR=2.42, Q=60%).

frequency scanning method. In the simplified analysis, the dc system is assumed to be a current source with infinite impedance. As in the frequency scanning method, the high (not infinite) equivalent impedance of the dc system is reflected in the simulation result. The dc system provides some damping to the harmonics which results in the considerably lower impedance magnitude measured by the frequency scanning method.

The control concept was now applied to the rectifiers and inverter in both poles of the dc transmission system with SCR=2.42. As can be seen from Figure 5 .23 which shows the firing angles and the dc components together with I_{60}, the controller significantly reduces the dc components. We have simulated the untransposed case to exacerbate I_{60} which would of course be much reduced if we had transposed the ac conductors.

Figure 5 .24 shows the plot of the harmonics in the transformer secondary current, in phase "*a*", on both sides, rectifier and inverter, for the case discussed above. There is is a significant reduction in the dc component in both rectifier and inverter sides.

As we can see the 2nd harmonic in both sides remained almost the same. These results confirm that the modulation of the firing angles presents even good results when the control action is applied in a weaker system with high impedance at 120 Hz.

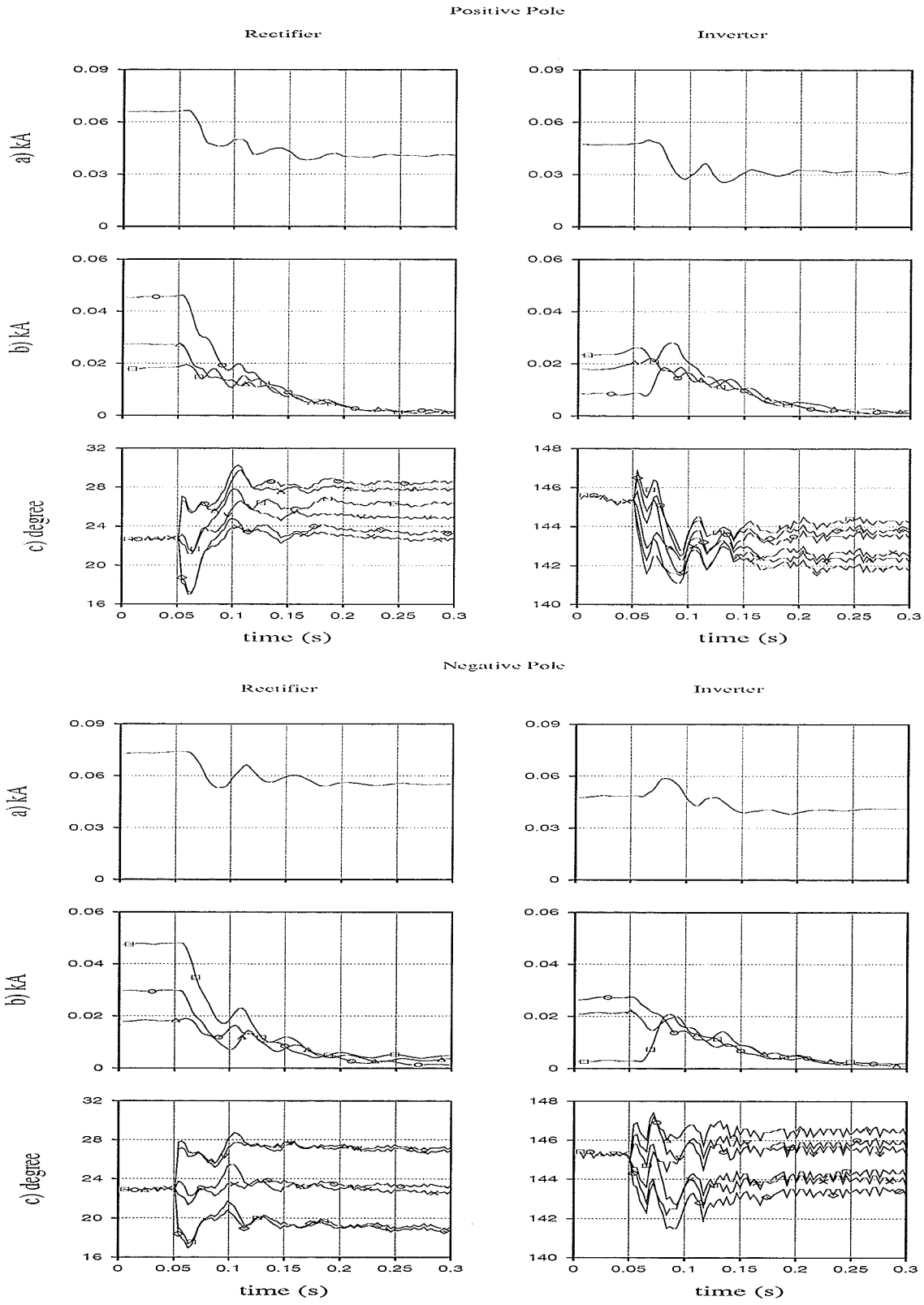

Figure 5 .23 : Dc current elimination in phase currents in a large hybrid ac–dc system. Control action on both sides and poles. Ac line untransposed and without blocking filter, SCR=2.42 and Q=60%
a) 60 Hz current measurement in the dc line (crest), b)Magnitude of the dc component in the converter transformer (3 phases), c) Firing angle α_i modulation.

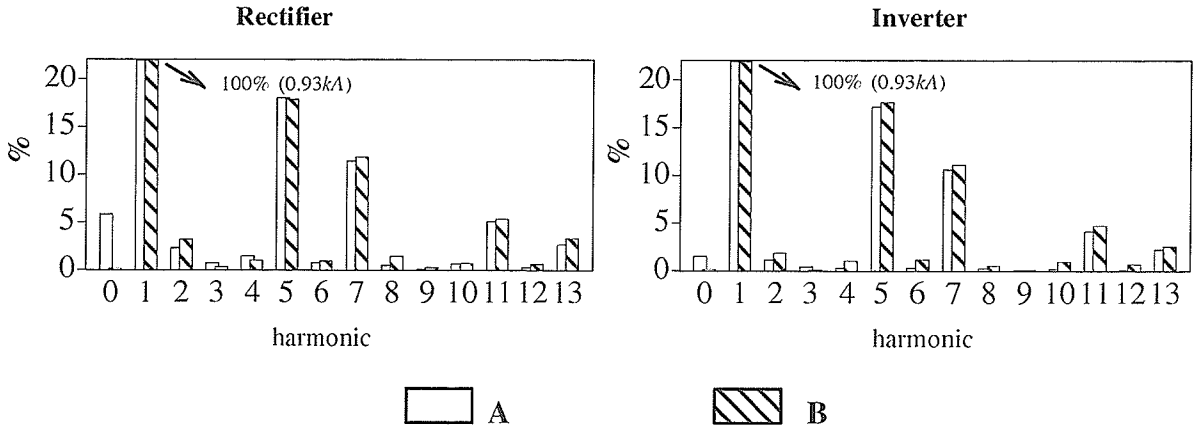

Figure 5 .24 : Harmonic spectrum of the secondary current transformer I_a (Rec. and Inv, both poles).

A – without modulation

B – with modulation in all poles

5 .6 DRAWBACKS

The major drawback of the control method to eliminate the dc components is that it can lead to the generation of non–characteristic harmonics.

As we can see from plots of the harmonics in the transformer secondary current for the cases discussed in this section, there is an increase in the second and other harmonics. The second harmonic has a level of about 3 to 5% and the 4th and 8th about 1 to 3% of the fundamental. It should be noted that we have presented an extreme case of induction for the simulation cases without transposition, with about 60A of dc current in the transformer windings. In most situations when the lines are transposed or a larger distance apart, the modulation effort required is much lower and so are the generated non–characteristic harmonics. In many situations a certain level of these harmonics may be acceptable, however, in other situations such as when resonances exist at these frequencies, this method is not acceptable. In such situations I_{60} blocking filters may be used instead.

The increased steady state firing angles and extinction angles required tend to reduce the power transmission and increase the reactive power requirements of the system.

Another drawback of the scheme for eliminating the transformer dc components is that applying control to one terminal does not eliminate I_{60}. This necessitates the application of the control action at all the terminals.

It appears that the method is most suitable when used in conjunction with line transposition, in which case a much smaller level of modulation is required. This is because transposition significantly reduces I_{60} (Figure 4.3).

5.7 SIMULATION ASPECTS

Note that in the above examples, the angle deviations ranged from 1°–8°. A 50 ms time–step was used which corresponds to a little over 1o at 60 Hz. Thus in order to get accurate results one must interpolate the thyristor turn–on and turn–off times between time–steps. The electromagnetic transients program that is used must support this feature. Interpolation also eliminates the 1o firing angle jitter in the simulation and thus does not introduce any spurious non–characteristic harmonics. Wherever possible, an independent check on the simulation results was carried out, such as comparison with Equation 4.9 .

5.8 SUMMARY

The following observations resulted from this chapter:

– it is possible to eliminate the dc components in the converter transformer secondary winding by using Newton–Raphson method. It was confirmed the Newton–Raphson solution in an simple six–pulse bridge by using a simulation approach;

– the proposed method of directly eliminating the dc components works successfully in the stronger system (SCR=11.33) as well as in the weaker system (SCR=2.42);

– the control can be simultaneously applied at all terminals of a dc system without controller conflicts;

– non–characteristic harmonics are introduced as a result of the control action and can have significant amplitudes;

–the method of firing angle modulation is probably most likely to be used when original I_{60} levels are relatively low, for example in conjunction with ac line transposition.

Chapter 6

Conclusions

With transmission right–of–way at a premium, there are increased incentives to construct HVDC lines in close proximity to ac lines. Construction of ac and dc circuits on common structures may even be considered as an option for maximizing right–of–way utilization.

DC transmission provides an attractive solution to the problem of restricted right–of–way. It is anticipated this topic will become more important in the future, as electric power demand increases while construction of new overhead transmission lines becomes more difficult to achieve.

There are a number of technical question which would need to be addressed for ac and dc circuits on a common tower. Some of these concerns addressed in this thesis include:

–study of overvoltage profiles along the line and at the stations for various types of faults.

–steady state induction of fundamental frequency current in the dc circuit and the use of blocking filters to minimize this effect.

–protection of the ac and dc lines during contact faults.

6.1 OVERVOLTAGE STUDY

The following observations resulted from the overvoltage study:

– faults involving the ac conductor to ground closer to the rectifier converter introduce negative sequence voltage on the bus which converts to a second harmonic overvoltage on the dc side.

– dc line overvoltages at other line locations (TL1, TL2, ... etc.) are mainly fundamental frequency overvoltages due to the coupling effect between the ac and dc lines.

– the dc line overvoltages are more severe for the stronger (6800 MVA) system.

– overvoltages on the ac line increased with a decrease in system strength for faults involving the ac conductors.

– with ac–dc contact faults and dc line faults the ac overvoltages are smaller for the weaker system.

– the overvoltages are larger when the ac–dc system are electromagnetically coupled. This is more pronounced for ac line overvoltages when the faults involve only the dc conductors.

–in general the overvoltages on the ac and dc lines are larger when the ac and dc lines are coupled.

– the overvoltages are higher for the Bergeron transmission line model compared to the frequency dependent transmission line model.

– overvoltages for the dc line in a hybrid ac–dc environment are higher than for a a dc line alone

– transposition of the ac conductors reduces the overvoltages.

– the blocking filter in the dc neutral has a tendency to oscillate, which can cause overvoltages on the dc line. These oscillations can be damped by a resistor–arrester combination across the filter.

– resonances may exist in the ac or dc system which can cause harmonic overvoltages.

6 .2 FIRING ANGLE MODULATION

The following observations resulted from the firing angle modulation study:

– the elimination of I_{60} by control action does not eliminate converter transformer dc components.

– the proposed method of directly eliminating the dc components works successfully in the stronger system (SCR=11.33) as well as in the weaker system (SCR=2.42).

– the control can be simultaneously applied at all terminals of a dc system without controller conflicts.

– non–characteristic harmonics are introduced as a result of the control action and can have significant amplitudes.

–the method of firing angle modulation is probably most likely to be used when original I_{60} levels are relatively low, for example in conjunction with ac line transposition.

6 .3 SUGGESTIONS FOR FUTURE STUDIES

Increasing the power transmission capability on existing transmission line rights of way is an area of increasing interest in North America. A number of methods of increasing transmission capability are described in the literature. One way is to add a dc circuit to an transmission line. The major areas of investigation this alternative include theoretical electrical aspects as well as structural aspects of the transmission line towers.

The author suggest the following aspects to be study for the future:

1–Survey of Tower Types

A survey should be carried out to determine the configuration and structure in common use by utilities for transmission voltages ranging from 110 up to 500 kV that appear to be good candidates for conversion to hybrid transmission lines.

2– Converter transformer core saturation

Saturation of the converter transformer due to 60 Hz current in the dc line should be investigated to obtain an understanding of its cause and sensitivity to various parameters.

3– Lightning Performance

The number of lightning flashovers of the dc circuits will be high when shield wires are modified in order to include the dc conductor in the same tower. The number of lightning outages on the 230 kV Gulfport transmission line should be investigated.

4– Ac–dc conductor contact fault

Contact faults between conductors of the ac and dc circuits on the hybrid transmission line result in ac voltages and currents on the dc circuit and vice verse. Ac current in the dc circuit could saturate power transformers causing tripping of these transformers. DC currents could also be present when ac circuit breakers are required to operate. These factors should be investigated.

5– Electrical Field effects

A program should be developed to calculate the electrical field effects from a hybrid transmission line. An electrical field test in an high voltage laboratory should be carried out in order to measure the main parameters of the hybrid ac–dc line (electric field, RI, AN, etc.).

References

[1] Terada, D., "Transformer for Superposed Ac–Dc Power Transmission", Electrical Engineering in Japan, Vol. 91, No. 1, 1971.

[2] Woodford, D.A. and Young, A.H. "Using DC to Increase Capacity of AC Transmission Circuits", IEEE Canadian Review, March 1989 pp. 15–18.

[3] Woodford, D.A., "Secondary Arc Effect in ac/dc Hybrid Transmission", CEA report ST–312, February 1991.

[4] Larsen, E.V., Walling, R.A. and Bridenbaugh, "Parallel ac/dc Transmission Lines Steady State Induction Issues", IEEE Transactions on Power Delivery, Vol. 4, No.1, January 1989, pp. 667–673.

[5] Ramesh, K., Adhikari, T., Kapoor, S.C. Gupta, D.P., "Parallel Operation of ac and dc Lines Running on the Same Tower", Paper 14–06, 1988 CIGRE Session, 28 August – 3rd September. 1988.

[6] Nakra H.L., Bui L.S., Iyoda L., "System Consideration in Converting One Circuit of a Double Circuit ac Line to dc", IEEE Transaction on Power Apparatus and System, Vol. PAS–103, No.10, October 1984, pp. 3096–3103.

[7] Woodford, D.A.."Validation of Digital Simulation of DC Links", IEEE Transmissions on Power Apparatus and System, Vol. PAS–102, No. 6, June 1983, pp. 1616–1623.

[8] A.H.Young, "Conceptual Outilines of AC–DC Hybrid Towers", Project E4.59.2 from the Manitoba HVDC Research Centre, June 17, 1988

[9] Chartier, V.L., Sarkinen, S.H., Stearns, R.D., Burns A.L., "Investigation of Corona and Field Effects of ac–dc Hybrid Transmission Lines", IEEE, Vol. PAS–100, No. 1 January 1981, pp. 72–80.

[10] Maruvada S.P., Drogi, S.,"Field and Ion Interactions of Hybrid ac–dc Transmission Lines", IEEE Transaction on Power Apparatus and System, Vol. 3, No. 3, July 1988.

[11] Maruvada S.P., Trinh N.G.,"A Basis for Setting Limits to Radio Interference from High Voltage Transmission Lines",IEEE Vol. PAS–04, No. 5, September/October 1975, pp. 1714–1724.

[12] "Radio Noise Design Guide for High Voltage transmission Lines", IEEE, Vol. Pas–90, No. 2, march/April 1971, pp. 833–842.

[13] "Transmission Line Reference Book, 345 and Above", Published by EPRI, Second Edition, 1982.

[14] Perry, D.E.,"An Analysis of Transmission Line Audible Noise Levels based Upon Field and Three–Phase Test Line Measurements", IEEE, Vol. PAS–91, No.3, May/June 1972, pp. 857–865.

[15] "A comparison of Methods for Calculating Audible Noise of High Voltage Transmission Lines", IEEE, Vol. PAS–101, No. 10, October, 1982, pp. 4090–4099.

[16] M.Szechtman et. al., "CIGRE Benchmark Model for DC Controls", Electra, Vol. 135, April 1991, pp. 54–73

[17] R. Verdolin, A.M. Gole, E. Kuffel, N. Diseko, B. Bisewski, "Induced Overvoltages on an Ac–Dc Hybrid Transmission System", CEA Conference March 1993, paper 100.

[18] R. Verdolin, A.M. Gole, E. Kuffel, N. Diseko, B. Bisewski, "Induced Overvoltages on an Ac–Dc Hybrid Transmission System", IEEE Transmission and Distribution Committee, Summer Meeting, San Francisco, CA, July 24–28, 1994, 94 SM 482–0 PWRD.

[19] J.R. Marti, "Accurate Modelling of Frequency–Dependent Transmission Lines in Electromagnetic Transient Simulations", IEEE Transmissions on Power Apparatus and Systems, Vol. PAS–101, No. 1 January 1982, pp. 147–155.

[20] Kimbark, E.W., "Direct Current Transmission", Volume I, 1971, John Wiley & Sons

[21] Arrilaga, J., "High Voltage Direct Current Transmission", 1988, IEE Power Engineer Series, 6.

[22] "'HVDC Converter Transformer Electromagnetics", Electric Report on EPRI Project RP1424–3, Electric Power Research Institute, Palo Alto, California, 1982.

[23] A.M. Gole, R. Verdolin, E. Kuffel, "Firing Angle Modulation for Eliminating Transformer DC Currents in Coupled AC–DC Systems", 1995 IEEE Winter Power Meeting.

[24] Deri, A., Tevan, G., Semlyen A., Castanheira A.," The Complex Ground Return Plane A Simplified Model for Homogeneous and Multi–Layer Earth Return", IEEE Transaction on Power Apparatus and System, Vol. PAS–100, No.8, August 1981, pp. 3686–3693.

[25] Chopra N., Gole A.M., Chang J., Haywood, R.H., "Zero Sequence Current in AC Lines Caused by Transients in Adjacent DC Lines", IEEE Transaction on Power Delivery, Vol. 3, No. 4, October 1988, pp. 1873–1879.

[26] R. H. Pennington, "Introductory Computer Methods and Numerical Analysis", Collier–Macmillan Limited, London, Second Edition, 1970

[27] W. H. Press, B. P. Flannery, S. A. Teukosky, W. T. Vettering, "Numerical Recipes The Art of Scientific Computing", 1986.

[28] G.B. Mazur, R.W. Menzies, "Damping of Harmonic Resonances in Static Compensators by Modulation of the TCR Firing Angle", Proc. IEEE/CSEE Conference on High Voltage Transmission System in China, Beijing, October 1897, pp. 597–603.

[29] G.B. Mazur, R.W. Menzies, "Firing Angle Modulation of a Thyristor Controller Reactor for the Control of Power System Harmonics", Second International Conference on Harmonics in Power System, October 1986, Winnipeg.

Appendix A

PSCAD/EMTDC DRAFT FILES FROM THE SIMULATION STUDIES

OVERVOLTAGES STUDIES

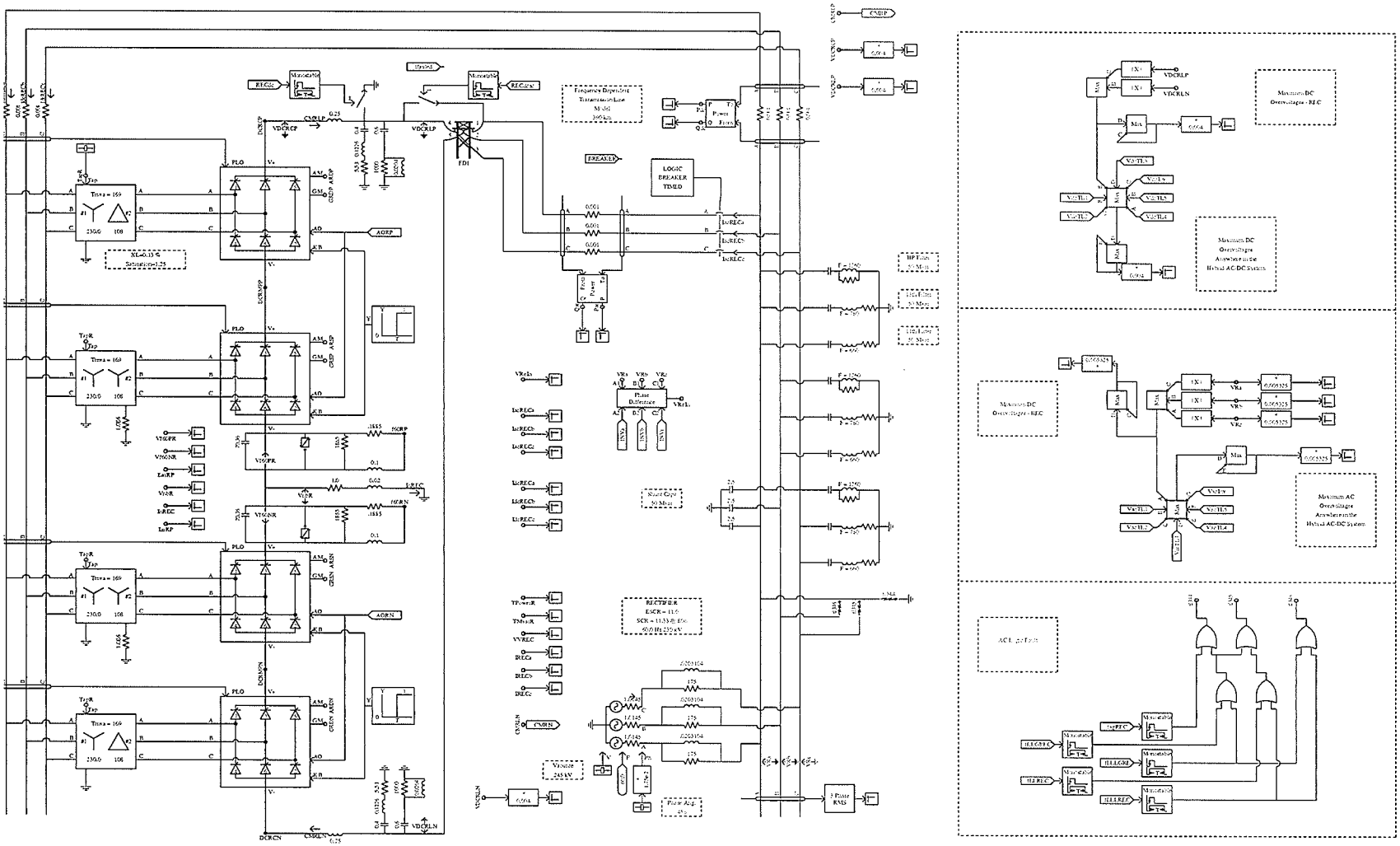

Figure A.1: Hybrid ac–dc system – rectifier side –REC

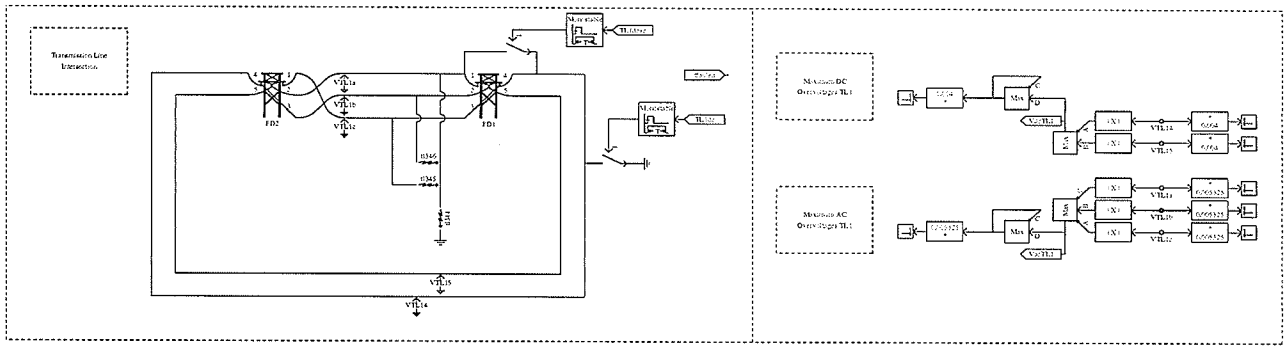

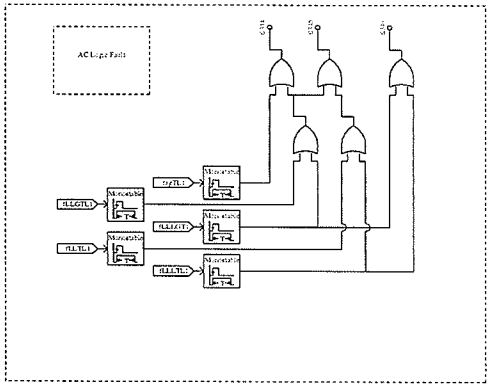

Figure A.2: Transmission line location – TL1

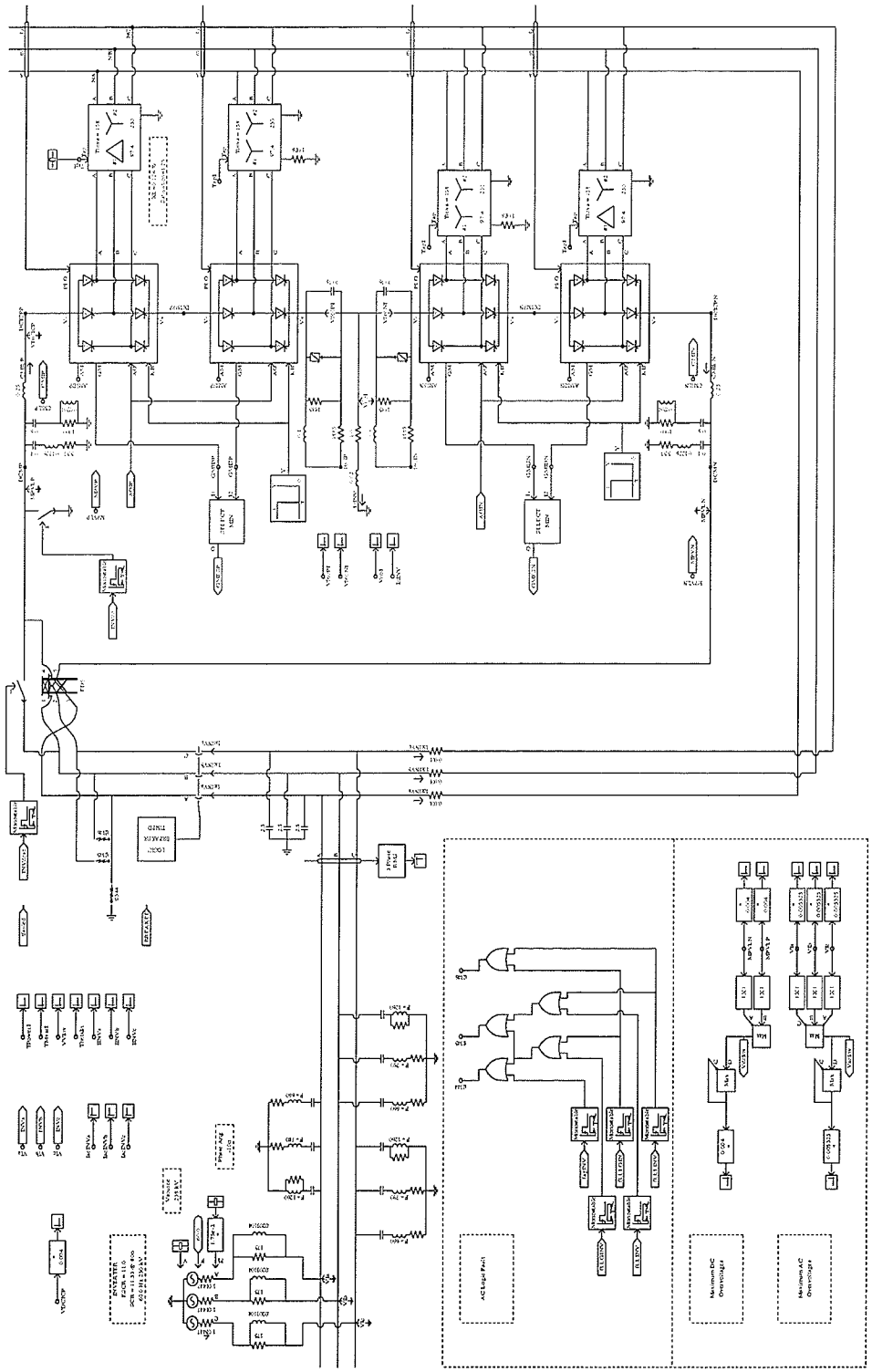

Figure A.3: Hybrid ac–dc system inverter side – INV

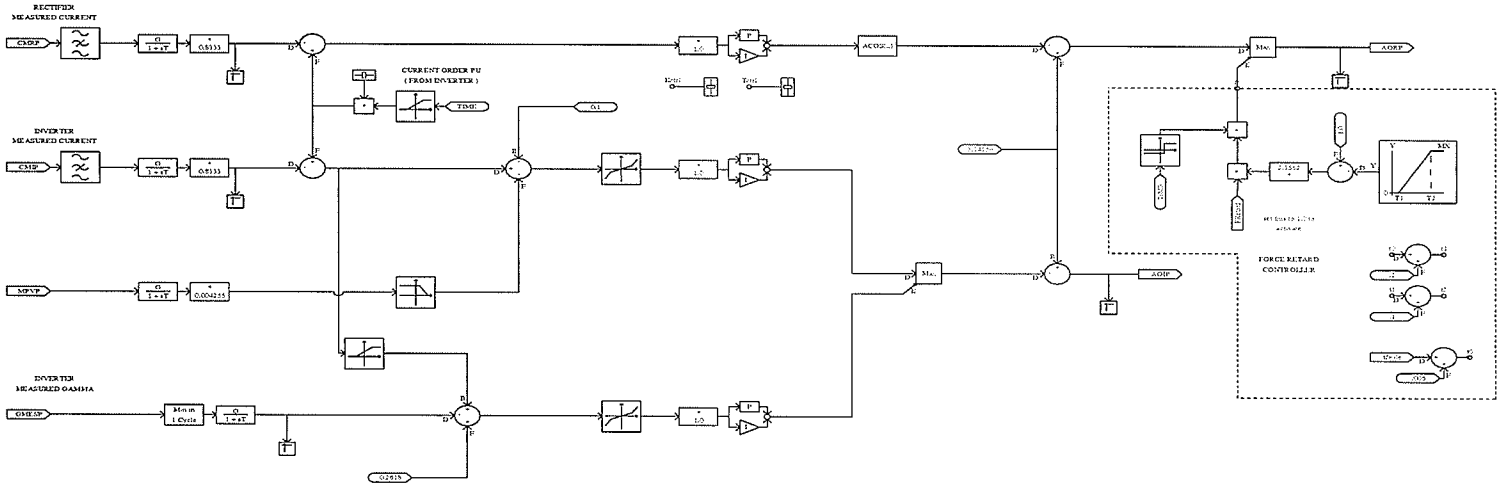

Figure A.4: Hybrid ac–dc system – rectifier and inverter controls positive pole

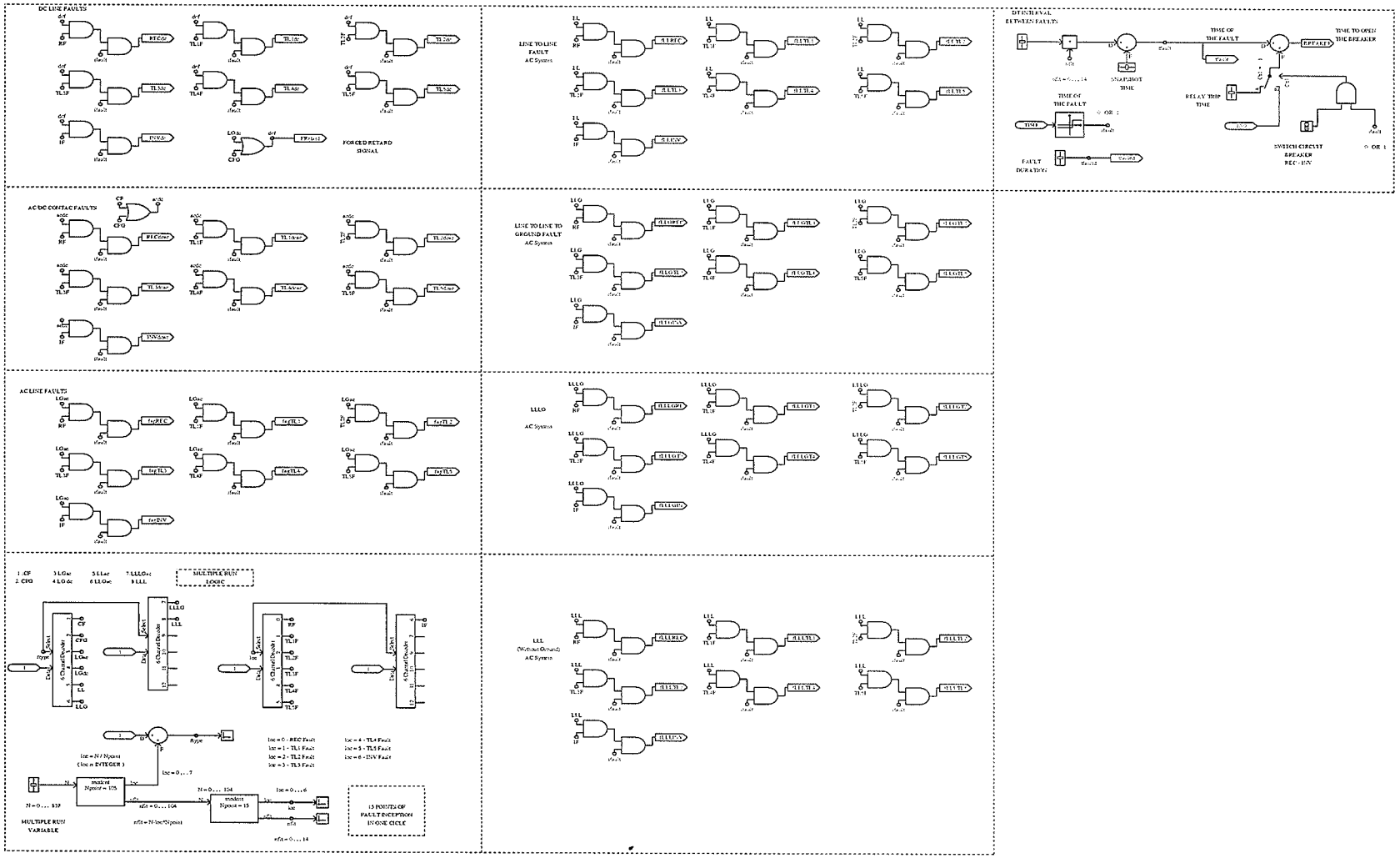

Figure A.5: Ac and dc faults logic controls

PSCAD/EMTDC DRAFT FILES FROM THE SIMULATION STUDIES

FIRING ANGLE MODULATION ON A SIMPLIFIED DC SYSTEM

(from sections 4 .3 .2 , 4 .4 .3 and 5 .2 .2)

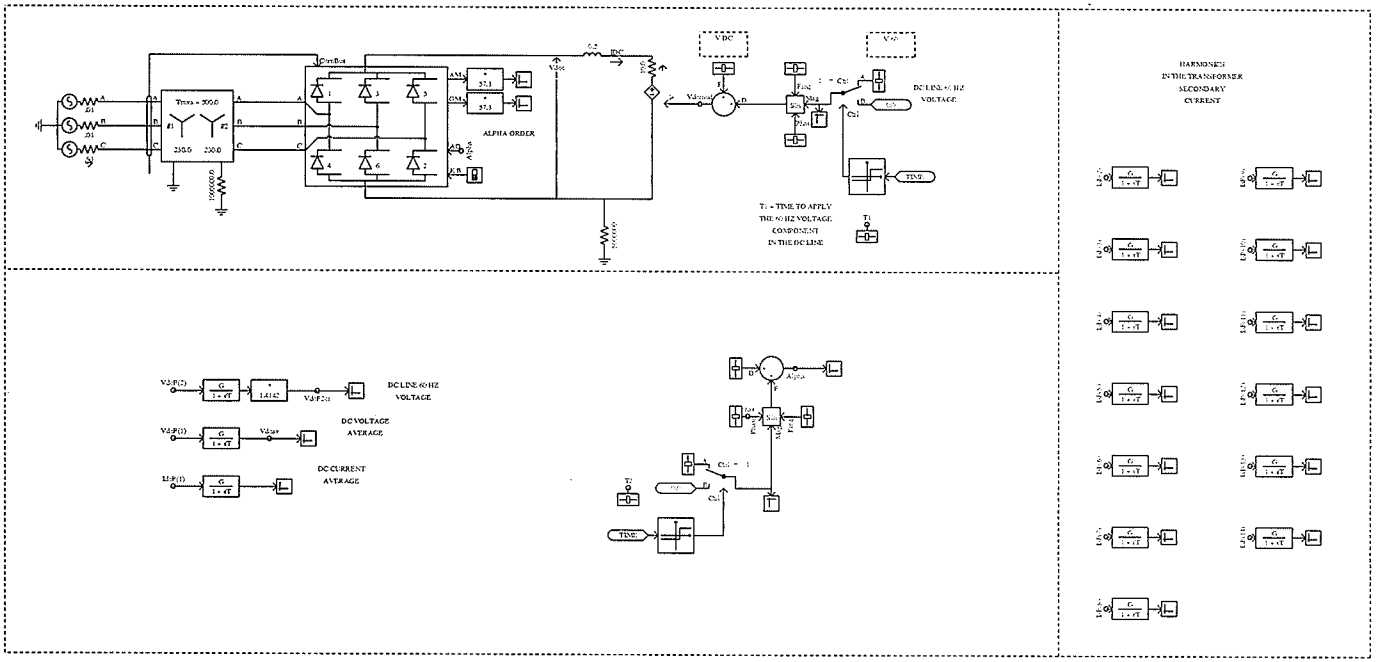

Figure A.6: Firing angle modulation on a simplified dc system. (Elimination of dc line 60 Hz current).

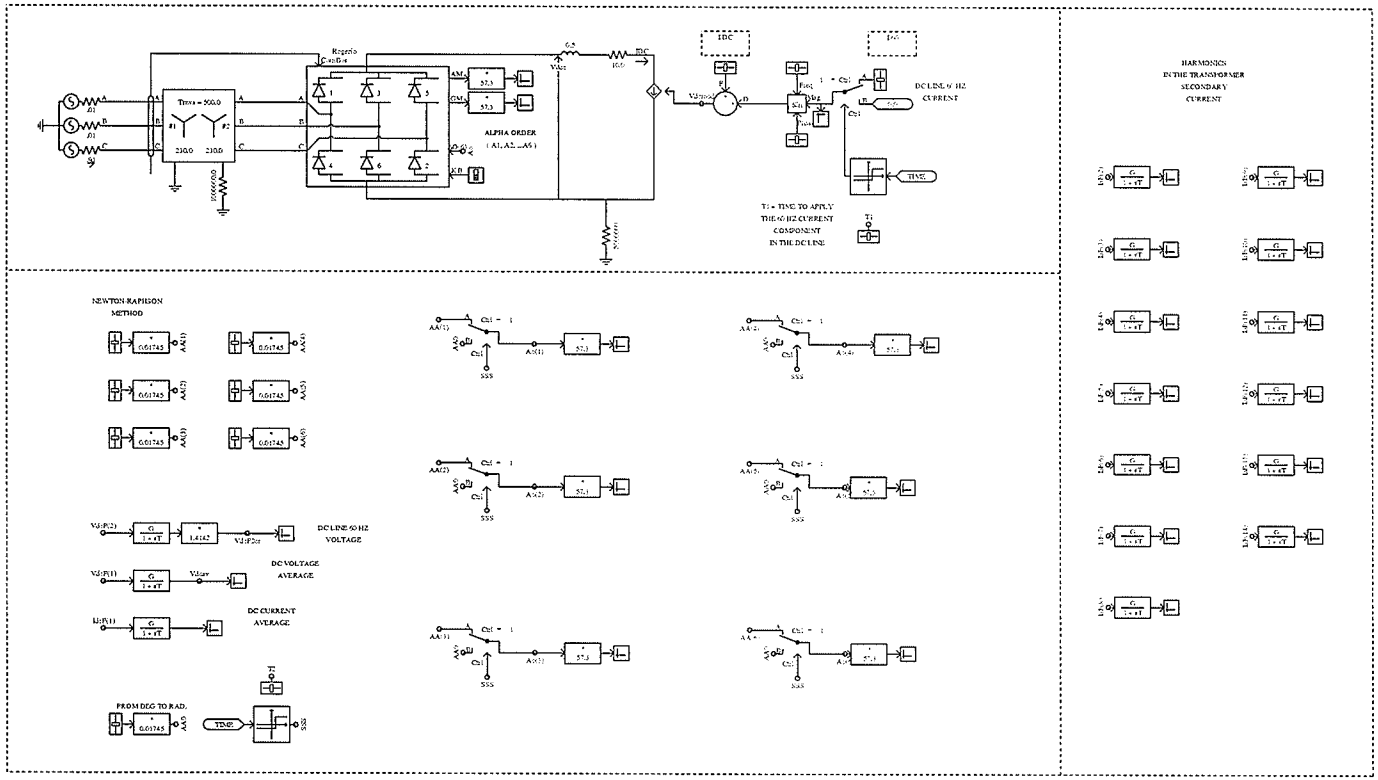

Figure A.7: Firing angle modulation on a simplified dc system. (Newton–Raphson method).

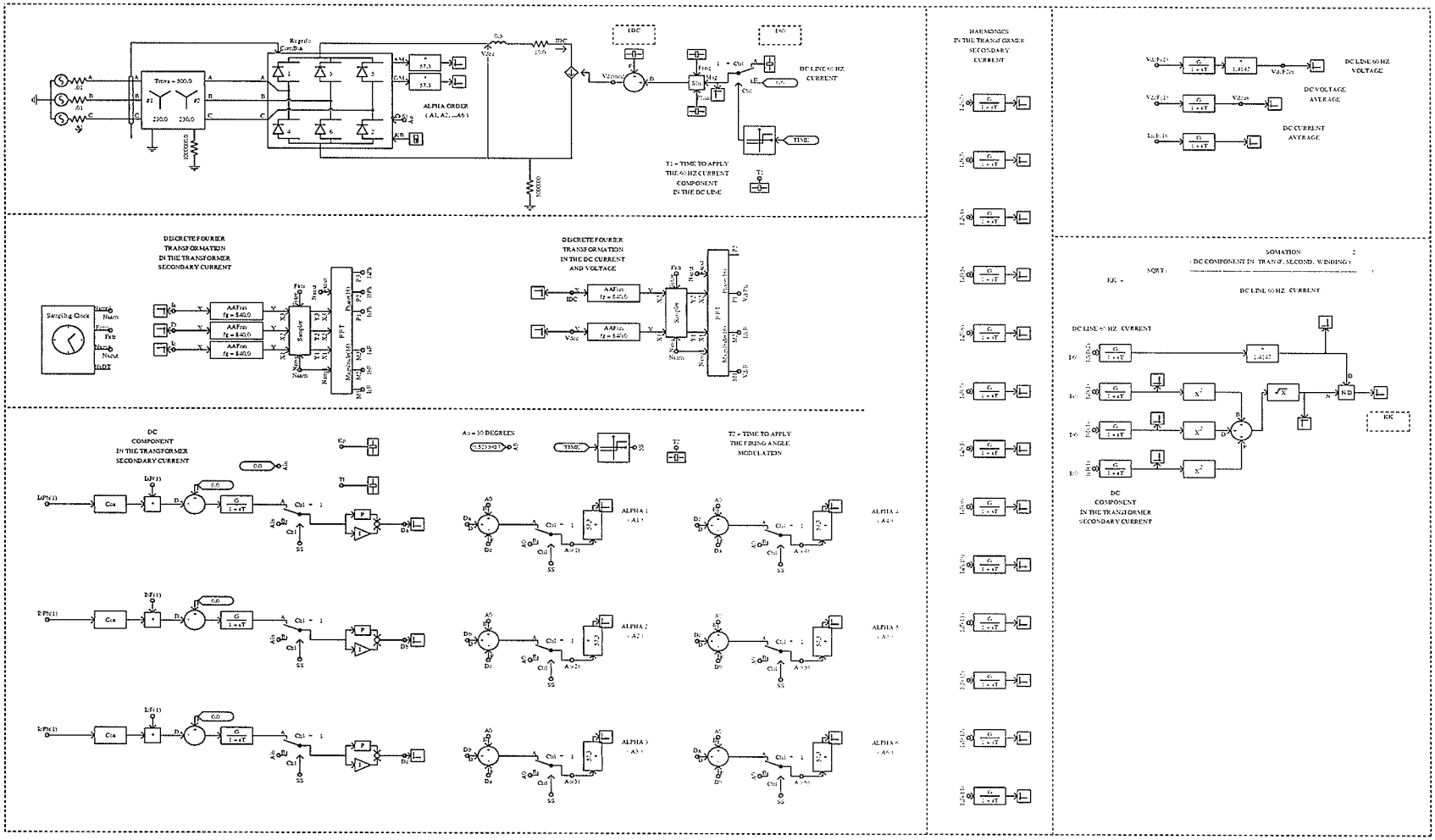

Figure A.8: Firing angle modulation on a simplified dc system. (Elimination of transformer dc current).

PSCAD/EMTDC DRAFT FILES

FIRING ANGLE MODULATION

ON A LARGE DC SYSTEM

(from section 5 .5)

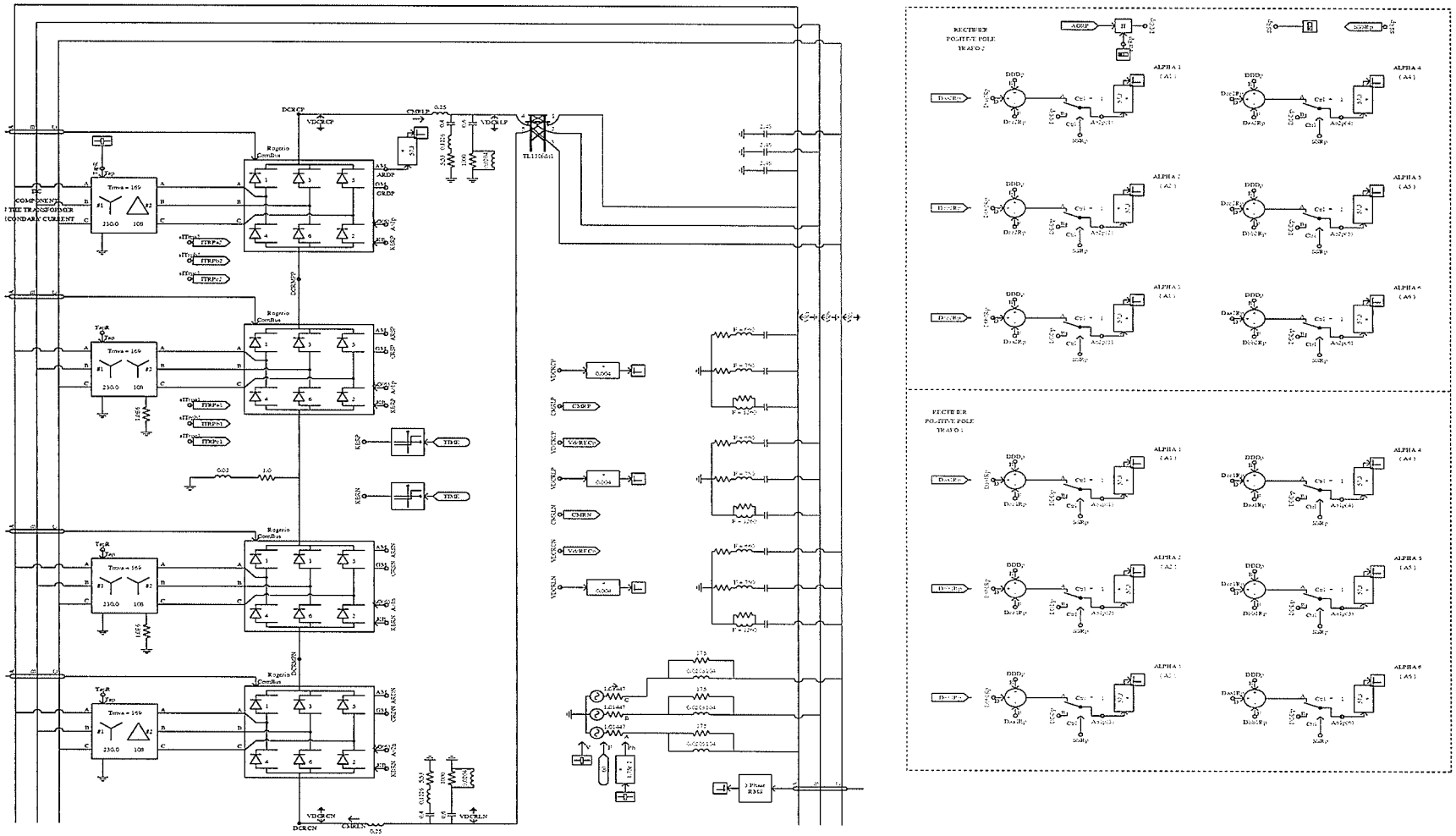

Figure A.9: Firing angle modulation with control action in the rectifier positive pole.

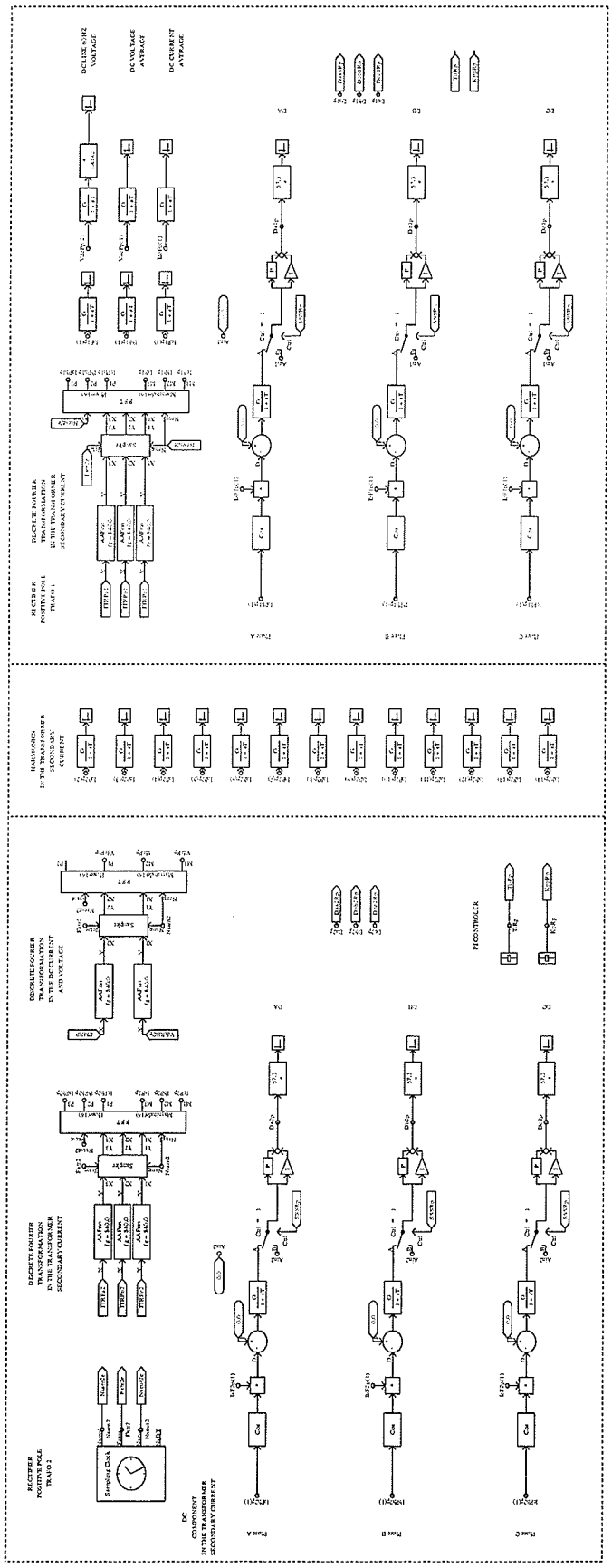

Figure A.10: Firing angle modulation with control action in the rectifier positive pole.

APPENDIX B

B.1 RELATION BETWEEN THE 60 HZ COMPONENT IN THE DC LINE AND THE DC COMPONENT IN THE SECONDARY OF THE TRANSFORMER.

$$I_{a_0} = \frac{1}{2\pi}\left[\int_0^{\alpha} I_d' \, d\theta \;+\; \int_{\alpha}^{\alpha+\mu} (I_d' - I_{s2}\cos\alpha + I_{s2}\cos\theta)\, d\theta \;\;..\right. \tag{B.1}$$

$$+ \int_{\alpha+\frac{\pi}{3}}^{\alpha+\mu+\frac{\pi}{3}} (-I_{s2}\cos\alpha + I_{s2}\cos\,(\theta - \frac{\pi}{3})\, d\theta \;+\; \int_{\alpha+\mu+\frac{\pi}{3}}^{\alpha+\pi} -I_d' \, d\theta \;\;..$$

$$+ \int_{\alpha+\pi}^{\alpha+\mu+\pi} (-I_d' + I_{s2}\cos\alpha + I_{s2}\cos\theta)\, d\theta \;\;..$$

$$\left. + \int_{\alpha+4\frac{\pi}{3}}^{\alpha+\mu+4\frac{\pi}{3}} (I_{s2}\cos\alpha + I_{s2}\cos(\theta - \frac{\pi}{3})\, d\theta \;+\; \int_{\alpha+\mu+4\frac{\pi}{3}}^{2\pi} I_d' \, d\theta \right]$$

$$I_{b_0} = \frac{1}{2\pi}\left[\int_{\alpha}^{\alpha+\mu} (I_{s2}\cos\alpha - I_{s2}\cos\theta)\, d\theta \;+\; \int_{\alpha+\mu}^{\alpha+2\frac{\pi}{3}} I_d' \, d\theta \;\;..\right. \tag{B.2}$$

$$+ \int_{\alpha+2\frac{\pi}{3}}^{\alpha+\mu+2\frac{\pi}{3}} (I_d' - I_{s2}\cos\alpha - I_{s2}\cos\,(\theta + \frac{\pi}{3})\, d\theta \;\;..$$

$$+ \int_{\alpha+\pi}^{\alpha+\mu+\pi} (-I_{s2}\cos\alpha - I_{s2}\cos\,(\theta)\, d\theta \;+\; \int_{\alpha+\mu+\pi}^{\alpha+5\frac{\pi}{3}} -I_d' \, d\theta \;\;..$$

$$\left. + \int_{\alpha+5\frac{\pi}{3}}^{\alpha+\mu+5\frac{\pi}{3}} (-I_d' + I_{s2}\cos\alpha - I_{s2}\cos\,(\theta + \frac{\pi}{3})\, d\theta \right]$$

$$I_{c_0} = \frac{1}{2\pi}\left[\int_0^{\alpha+\frac{\pi}{3}} -I_d'\, d\theta + \int_{\alpha+\frac{\pi}{3}}^{\alpha+\mu+\frac{\pi}{3}} (-I_d' + I_{s2}\cos\alpha - I_{s2}\cos\,(\theta-\frac{\pi}{3})\, d\theta \quad \ldots (B.3)\right.$$

$$+ \int_{\alpha+2\frac{\pi}{3}}^{\alpha+\mu+2\frac{\pi}{3}} (I_{s2}\cos\alpha + I_{s2}\cos\,(\theta+\frac{\pi}{3})\, d\theta \quad + \int_{\alpha+\mu+2\frac{\pi}{3}}^{\alpha+4\frac{\pi}{3}} I_d'\, d\theta \quad \ldots$$

$$+ \int_{\alpha+4\frac{\pi}{3}}^{\alpha+\mu+4\frac{\pi}{3}} (I_d' - I_{s2}\cos\alpha - I_{s2}\cos\,(\theta-\frac{\pi}{3})\, d\theta \quad \ldots$$

$$\left. + \int_{\alpha+5\frac{\pi}{3}}^{\alpha+\mu+5\frac{\pi}{3}} (-I_{s2}\cos\alpha + I_{s2}\cos\,(\theta+\frac{\pi}{3})\, d\theta \quad + \int_{\alpha+\mu+5\frac{\pi}{3}}^{2\pi} -I_d'\, d\theta \right]$$

and the solution for the Equations B.1, B.2 and B.3 become:

$$I_{a_0} = \frac{A}{\pi}\left[\cos\,(\,\alpha+\mu+\lambda+\pi\,) + \cos\,(\,\alpha+\mu+\lambda-2\frac{\pi}{3}\,)\right]$$

$$I_{b_0} = \frac{A}{\pi}\left[\cos\,(\,\alpha+\mu+\lambda\,) + \cos\,(\,\alpha+\mu+\lambda+5\frac{\pi}{3}\,)\right]$$

$$I_{c_0} = \frac{A}{\pi}\left[\cos\,(\,\alpha+\mu+\lambda+2\frac{\pi}{3}\,) + \cos\,(\,\alpha+\mu+\lambda+\frac{\pi}{3}\,)\right]$$

making $\alpha + \mu + \lambda = \sigma$

$$I_{a_0} = \frac{A}{\pi}\left[\cos\,(\,\sigma+\pi\,) + \cos\,(\,\sigma-2\frac{\pi}{3}\,)\right] \qquad (B.4)$$

$$I_{b_0} = \frac{A}{\pi}\left[\cos\,(\,\sigma\,) + \cos\,(\,\sigma+5\frac{\pi}{3}\,)\right] \qquad (B.5)$$

$$I_{c_0} = \frac{A}{\pi}\left[\cos\,(\,\sigma+2\frac{\pi}{3}\,) + \cos\,(\,\sigma+\frac{\pi}{3}\,)\right] \qquad (B.6)$$

using the trigonometric relation:

$\cos(x) - \cos(y) = -2 \sin\{(x+y)/2\} \sin\{(x-y)/2\}$

the Equations B.4, B.5 and B.6 become:

$$I_{a_0} = -\frac{2A}{\pi}\left[\sin\left(\sigma-\frac{\pi}{3}\right) + \sin\left(-\frac{\pi}{3}\right)\right] = \frac{\sqrt{3}A}{\pi}\sin\left(\sigma-\frac{\pi}{3}\right)$$

$$I_{b_0} = -\frac{2A}{\pi}\left[\sin\left(\sigma+\frac{\pi}{3}\right) + \sin\left(-\frac{\pi}{3}\right)\right] = \frac{\sqrt{3}A}{\pi}\sin\left(\sigma+\frac{\pi}{3}\right)$$

$$I_{c_0} = \frac{2A}{\pi}\left[\cos\left(\sigma+\frac{\pi}{2}\right) + \cos\left(\frac{\pi}{6}\right)\right] = \frac{\sqrt{3}A}{\pi}\sin\left(\sigma+\pi\right)$$

In order to find the relation between the dc component in the secondary of the converter transformer, I_{a0}, I_{b0} and I_{c0}, for the three phases, and the fundamental component current, I_{60}, in the dc line we have:

$$I_{a_0}^2 + I_{b_0}^2 + I_{c_0}^2 = \frac{3A^2}{\pi^2}\left[\sin\left(\sigma-\frac{\pi}{3}\right)^2 + \sin\left(\sigma+\frac{\pi}{3}\right)^2 + \sin\left(\sigma+\pi\right)^2\right]$$

$$= \frac{3A^2}{\pi^2}\left[\frac{1-\cos\left(2\left(\sigma-\frac{\pi}{3}\right)\right)}{2} + \frac{1-\cos\left(2\left(\sigma-\frac{\pi}{3}\right)\right)}{2} + \frac{1-\cos\left(2\left(\sigma+\pi\right)\right)}{2}\right]$$

$$= \frac{3A^2}{\pi^2}\left[\frac{3}{2} - \frac{1}{2}\left[\cos\left(2\left(\sigma-\frac{\pi}{3}\right)\right) + \cos\left(2\left(\sigma+\frac{\pi}{3}\right)\right) + \cos\left(2\left(\sigma+\pi\right)\right)\right]\right]$$

$$= \frac{3A^2}{\pi^2}\left[\frac{3}{2} - \frac{1}{2}\underbrace{\left[\cos\left(2\sigma-2\frac{\pi}{3}\right) + \cos\left(2\sigma+2\frac{\pi}{3}\right) + \cos\left(2\sigma\right)\right]}_{=0}\right]$$

$$I_{a_0}^2 + I_{b_0}^2 + I_{c_0}^2 = \frac{9}{2}\left[\frac{A}{\pi}\right]^2 \qquad \text{(B.7)}$$

B.2 FIRING ANGLE MODULATION TO ELIMINATE THE 60 HZ CURRENT

B.2.1 WITHOUT OVERLAP ANGLE

The average value of the dc line voltage, V_d , is given by:

$$V_d = \frac{1}{2\pi}\left[\int_0^{\alpha_3} e_{ac}\, d\theta + \int_{\alpha_3}^{\frac{\pi}{3}+\alpha_4} e_{bc}\, d\theta + \int_{\frac{\pi}{3}+\alpha_4}^{\frac{2\pi}{3}+\alpha_5} e_{ba}\, d\theta + \int_{\frac{2\pi}{3}+\alpha_5}^{\pi+\alpha_6} e_{ca}\, d\theta \;\ldots \qquad \text{(B.8)}$$

$$+ \int_{\pi+\alpha_6}^{\frac{4\pi}{3}+\alpha_1} e_{cb}\, d\theta + \int_{\frac{4\pi}{3}+\alpha_1}^{\frac{5\pi}{3}+\alpha_2} e_{ab}\, d\theta + \int_{\frac{5\pi}{3}+\alpha_2}^{2\pi} e_{ac}\, d\theta\Bigg]$$

From the theory of Fourier series we have:

$$v(wt) = \frac{a_o}{2} + \sum_{n=1}^{n=\infty} C_n \cos\,(\, n\, wt + \phi_n\,) \qquad \text{(B.9)}$$

where:

$$w = \frac{2\pi}{T} = 2\pi f$$

$$\frac{a_o}{2} = \text{average value}$$

$$C_n = \sqrt{(a_n^2 + b_n^2)}$$

$$a_n = \frac{2}{T}\int_c^{c+T} v\,(wt)\cos\,(\,2\frac{n\pi}{T}t\,)\; d(wt) \qquad \text{(B.10)}$$

$$b_n = \frac{2}{T} \int_c^{c+T} v\ (wt) \sin\ (\ 2\frac{n\pi}{T} t\ )\ d(wt) \tag{B.11}$$

$$\phi_n = -\arctan\ (\ \frac{b_n}{a_n}\ ) \tag{B.12}$$

The modulation of the firing pulse of six–pulse bridge converter will generate 60 Hz voltage component in the dc side of the converter. The fundamental frequency component of the voltage V_d on the dc line, c_{1vd}, can be determined from Fourier series. For wt=θ, we have:

$$\begin{aligned} a_{1_{V_d}} = \frac{2}{2\pi}\Bigg[& \int_0^{\alpha_3} e_{ac}\cos\theta\ d\theta + \int_{\alpha_3}^{\frac{\pi}{3}+\alpha_4} e_{bc}\cos\theta\ d\theta + \int_{\frac{\pi}{3}+\alpha_4}^{2\frac{\pi}{3}+\alpha_5} e_{ba}\cos\theta\ d\theta \ \ldots \\ & + \int_{2\frac{\pi}{3}+\alpha_5}^{\pi+\alpha_6} e_{ca}\cos\theta\ d\theta + \int_{\pi+\alpha_6}^{4\frac{\pi}{3}+\alpha_1} e_{cb}\cos\theta\ d\theta + \int_{4\frac{\pi}{3}+\alpha_1}^{5\frac{\pi}{3}+\alpha_2} e_{ab}\cos\theta\ d\theta \ \ldots \\ & + \int_{5\frac{\pi}{3}+\alpha_2}^{2\pi} e_{ac}\cos\ \theta\ d\theta \Bigg] \end{aligned}$$

$$\begin{aligned} a_{1_{V_d}} = \frac{\sqrt{3}E_m}{\pi}\Bigg[& \int_0^{\alpha_3} \cos(\theta+\frac{\pi}{6})\cos\theta\ d\theta + \int_{\alpha_3}^{\frac{\pi}{3}+\alpha_4} \cos(\theta-\frac{\pi}{6})\cos\theta\ d\theta \ \ldots \\ & + \int_{\frac{\pi}{3}+\alpha_4}^{2\frac{\pi}{3}+\alpha_5} \sin\theta\cos\theta\ d\theta + \int_{2\frac{\pi}{3}+\alpha_5}^{\pi+\alpha_6} \cos(\theta-5\frac{\pi}{6})\cos\theta\ d\theta \ \ldots \\ & + \int_{\pi+\alpha_6}^{4\frac{\pi}{3}+\alpha_1} \cos(\theta+5\frac{\pi}{6})\cos\theta\ d\theta + \int_{4\frac{\pi}{3}+\alpha_1}^{5\frac{\pi}{3}+\alpha_2} \cos(\theta+\frac{\pi}{2})\cos\theta\ d\theta \ \ldots \\ & + \int_{5\frac{\pi}{3}+\alpha_2}^{2\pi} \cos(\theta+\frac{\pi}{6})\cos\ \theta\ d\theta \Bigg] \end{aligned}$$

$$b_{1_{V_d}} = \frac{2}{2\pi}\left[\int_0^{\alpha_3} e_{ac}\sin\theta\ d\theta + \int_{\alpha_3}^{\frac{\pi}{3}+\alpha_4} e_{bc}\sin\theta\ d\theta + \int_{\frac{\pi}{3}+\alpha_4}^{2\frac{\pi}{3}+\alpha_5} e_{ba}\sin\theta\ d\theta \ \ldots\right.$$
$$+ \int_{2\frac{\pi}{3}+\alpha_5}^{\pi+\alpha_6} e_{ca}\sin\theta\ d\theta + \int_{\pi+\alpha_6}^{4\frac{\pi}{3}+\alpha_1} e_{cb}\sin\theta\ d\theta + \int_{4\frac{\pi}{3}+\alpha_1}^{5\frac{\pi}{3}+\alpha_2} e_{ab}\sin\theta\ d\theta \ \ldots$$
$$\left. + \int_{5\frac{\pi}{3}+\alpha_2}^{2\pi} e_{ac}\sin\theta\ d\theta \right]$$

$$b_{1_{V_d}} = \frac{\sqrt{3}E_m}{\pi}\left[\int_0^{\alpha_3} \cos(\theta+\frac{\pi}{6})\sin\theta\ d\theta + \int_{\alpha_3}^{\frac{\pi}{3}+\alpha_4} \cos(\theta-\frac{\pi}{6})\sin\theta\ d\theta \ \ldots\right.$$
$$+ \int_{\frac{\pi}{3}+\alpha_4}^{2\frac{\pi}{3}+\alpha_5} \sin\theta\sin\theta\ d\theta + \int_{2\frac{\pi}{3}+\alpha_5}^{\pi+\alpha_6} \cos(\theta-5\frac{\pi}{6})\sin\theta\ d\theta \ \ldots$$
$$+ \int_{\pi+\alpha_6}^{4\frac{\pi}{3}+\alpha_1} \cos(\theta+5\frac{\pi}{6})\sin\theta\ d\theta + \int_{4\frac{\pi}{3}+\alpha_1}^{5\frac{\pi}{3}+\alpha_2} \cos(\theta+\frac{\pi}{2})\sin\theta\ d\theta \ \ldots$$
$$\left. + \int_{5\frac{\pi}{3}+\alpha_2}^{2\pi} \cos(\theta+\frac{\pi}{6})\sin\theta\ d\theta \right]$$

$$a_{1_{V_d}} = -\frac{\sqrt{3}E_m}{4\pi}\left[\sqrt{3}\cos\alpha_4\ \sin\alpha_4 + \sqrt{3}\cos\alpha_5\ \sin\alpha_5 \ \ldots\right. \qquad \text{(B.13)}$$
$$-\sqrt{3}\cos\alpha_1\ \sin\alpha_1 - \sqrt{3}\cos\alpha_2\ \sin\alpha_2 \ \ldots$$
$$-2\cos\alpha_3{}^2 - \cos\alpha_4{}^2 + \cos\alpha_5{}^2 + 2\cos\alpha_6{}^2 + \cos\alpha_1{}^2 - \cos\alpha_2{}^2 \ \ldots$$
$$\left. -\sqrt{3}\alpha_4 - \sqrt{3}\alpha_5 + \sqrt{3}\alpha_1 + \sqrt{3}\alpha_2 \right]$$

$$b_{1_{V_d}} = -\frac{\sqrt{3}E_m}{4\pi}\left[-2\sin\alpha_3\ \cos\alpha_3 - \sin\alpha_4\ \cos\alpha_4 + \cos\alpha_5\ \sin\alpha_5 \ \ldots\right. \qquad \text{(B.14)}$$
$$+ 2\sin\alpha_6\ \cos\alpha_6 + \sin\alpha_1\ \cos\alpha_1 - \cos\alpha_2\ \sin\alpha_2 \ \ldots$$
$$-\sqrt{3}(\cos\alpha_4)^2 - \sqrt{3}(\cos\alpha_5)^2 + \sqrt{3}(\cos\alpha_1)^2 + \sqrt{3}(\cos\alpha_2)^2 \ \ldots$$
$$\left. + 2\alpha_3 + \alpha_4 - \alpha_5 - 2\alpha_6 - \alpha_1 + \alpha_2 \right]$$

$$c_{1_{V_d}} = \sqrt{(\ a_{1_{V_d}}\ )^2 + (\ b_{1_{V_d}}\ )^2} \qquad \text{(B.15)}$$

$c_{1_{V_d}}$ is the crest value of the fundamental frequency voltage component in the dc side of the six–pulse bridge converter which was generated by the modulation of the firing pulse.

$$\phi_{1_{V_d}} = -\operatorname{atan}\frac{a_{1_{V_d}}}{b_{1_{V_d}}} \tag{B.16}$$

$\phi_{1_{V_d}}$ is the phase angle of the fundamental frequency voltage component.

B.2.1 WITH OVERLAP ANGLE

The average value of the dc line voltage, V_d , is given by:

$$V_d = \frac{\sqrt{3}E_m}{2\pi}\left[\int_0^{\alpha_3}\cos(\theta+\frac{\pi}{6})\,d\theta + \int_{\alpha_3}^{\alpha_3+\mu}\frac{\sqrt{3}}{2}\cos\theta\,d\theta + \int_{\alpha_3+\mu}^{\frac{\pi}{3}+\alpha_4}\cos(\theta-\frac{\pi}{6})\,d\theta \quad .. \text{(B.17)}\right.$$

$$+ \int_{\frac{\pi}{3}+\alpha_4}^{\frac{\pi}{3}+\alpha_4+\mu}\frac{\sqrt{3}}{2}\cos(\theta-\frac{\pi}{3})\,d\theta + \int_{\frac{\pi}{3}+\alpha_4+\mu}^{2\frac{\pi}{3}+\alpha_5}\sin\theta\,d\theta \quad ..$$

$$+ \int_{2\frac{\pi}{3}+\alpha_5}^{2\frac{\pi}{3}+\alpha_5+\mu}\frac{\sqrt{3}}{2}\cos(\theta-2\frac{\pi}{3})\,d\theta + \int_{2\frac{\pi}{3}+\alpha_5+\mu}^{\pi+\alpha_6}\cos(\theta-5\frac{\pi}{6})\,d\theta \quad ..$$

$$- \int_{\pi+\alpha_6}^{\pi+\alpha_6+\mu}\frac{\sqrt{3}}{2}\cos\theta\,d\theta + \int_{\pi+\alpha_6+\mu}^{4\frac{\pi}{3}+\alpha_1}\cos(\theta+5\frac{\pi}{6})\,d\theta \quad ..$$

$$+ \int_{4\frac{\pi}{3}+\alpha_1}^{4\frac{\pi}{3}+\alpha_1+\mu}\frac{\sqrt{3}}{2}\cos(\theta+2\frac{\pi}{3})\,d\theta + \int_{4\frac{\pi}{3}+\alpha_1+\mu}^{5\frac{\pi}{3}+\alpha_2}\cos(\theta+\frac{\pi}{2})\,d\theta \quad ..$$

$$\left.+ \int_{5\frac{\pi}{3}+\alpha_2}^{5\frac{\pi}{3}+\alpha_2+\mu}\frac{\sqrt{3}}{2}\cos(\theta+\frac{\pi}{3})\,d\theta + \int_{5\frac{\pi}{3}+\alpha_2+\mu}^{2\pi}\cos(\theta+\frac{\pi}{6})\,d\theta\right]$$

$$a_{1_{V_d}} = \frac{\sqrt{3}E_m}{2\pi}\left[\int_0^{\alpha_3}\cos(\theta+\frac{\pi}{6})\cos\theta\ d\theta + \int_{\alpha_3}^{\alpha_3+\mu}\frac{\sqrt{3}}{2}(\cos\theta)^2\ d\theta\ \ldots\right.$$

$$+\int_{\alpha_3+\mu}^{\frac{\pi}{3}+\alpha_4}\cos(\theta-\frac{\pi}{6})\cos\theta\ d\theta\ \ldots$$

$$+\int_{\frac{\pi}{3}+\alpha_4}^{\frac{\pi}{3}+\alpha_4+\mu}\frac{\sqrt{3}}{2}\cos(\theta-\frac{\pi}{3})\cos\theta\ d\theta + \int_{\frac{\pi}{3}+\alpha_4+\mu}^{2\frac{\pi}{3}+\alpha_5}\sin\theta\cos\theta\ d\theta\ \ldots$$

$$+\int_{2\frac{\pi}{3}+\alpha_5}^{2\frac{\pi}{3}+\alpha_5+\mu}\frac{\sqrt{3}}{2}\cos(\theta-2\frac{\pi}{3})\cos\theta\ d\theta + \int_{2\frac{\pi}{3}+\alpha_5+\mu}^{\pi+\alpha_6}\cos(\theta-5\frac{\pi}{6})\cos\theta\ d\theta\ \ldots$$

$$-\int_{\pi+\alpha_6}^{\pi+\alpha_6+\mu}\frac{\sqrt{3}}{2}(\cos\theta)^2\ d\theta + \int_{\pi+\alpha_6+\mu}^{4\frac{\pi}{3}+\alpha_1}\cos(\theta+5\frac{\pi}{6})\cos\theta\ d\theta\ \ldots$$

$$+\int_{4\frac{\pi}{3}+\alpha_1}^{4\frac{\pi}{3}+\alpha_1+\mu}\frac{\sqrt{3}}{2}\cos(\theta+2\frac{\pi}{3})\cos\theta\ d\theta + \int_{4\frac{\pi}{3}+\alpha_1+\mu}^{5\frac{\pi}{3}+\alpha_2}\cos(\theta+\frac{\pi}{2})\cos\theta\ d\theta\ \ldots$$

$$\left.+\int_{5\frac{\pi}{3}+\alpha_2}^{5\frac{\pi}{3}+\alpha_2+\mu}\frac{\sqrt{3}}{2}\cos(\theta+\frac{\pi}{3})\cos\theta\ d\theta + \int_{5\frac{\pi}{3}+\alpha_2+\mu}^{2\pi}\cos(\theta+\frac{\pi}{6})\cos\theta\ d\theta\right]$$

$$b_{1_{V_d}} = \frac{\sqrt{3}E_m}{2\pi}\left[\int_0^{\alpha_3}\cos(\theta+\frac{\pi}{6})\sin\theta\ d\theta + \int_{\alpha_3}^{\alpha_3+\mu}\frac{\sqrt{3}}{2}\cos\theta\sin\theta\ d\theta\ \ldots\right.$$

$$+\int_{\alpha_3+\mu}^{\frac{\pi}{3}+\alpha_4}\cos(\theta-\frac{\pi}{6})\sin\theta\ d\theta\ \ldots$$

$$+\int_{\frac{\pi}{3}+\alpha_4}^{\frac{\pi}{3}+\alpha_4+\mu}\frac{\sqrt{3}}{2}\cos(\theta-\frac{\pi}{3})\sin\theta\ d\theta + \int_{\frac{\pi}{3}+\alpha_4+\mu}^{2\frac{\pi}{3}+\alpha_5}(\sin\theta)^2\ d\theta\ \ldots$$

$$+\int_{2\frac{\pi}{3}+\alpha_5}^{2\frac{\pi}{3}+\alpha_5+\mu}\frac{\sqrt{3}}{2}\cos(\theta-2\frac{\pi}{3})\sin\theta\ d\theta + \int_{2\frac{\pi}{3}+\alpha_5+\mu}^{\pi+\alpha_6}\cos(\theta-5\frac{\pi}{6})\sin\theta\ d\theta\ \ldots$$

$$-\int_{\pi+\alpha_6}^{\pi+\alpha_6+\mu}\frac{\sqrt{3}}{2}\cos\theta\sin\theta\ d\theta + \int_{\pi+\alpha_6+\mu}^{4\frac{\pi}{3}+\alpha_1}\cos(\theta+5\frac{\pi}{6})\sin\theta\ d\theta\ \ldots$$

$$+\int_{4\frac{\pi}{3}+\alpha_1}^{4\frac{\pi}{3}+\alpha_1+\mu}\frac{\sqrt{3}}{2}\cos(\theta+2\frac{\pi}{3})\sin\theta\ d\theta + \int_{4\frac{\pi}{3}+\alpha_1+\mu}^{5\frac{\pi}{3}+\alpha_2}\cos(\theta+\frac{\pi}{2})\sin\theta\ d\theta\ \ldots$$

$$\left.+\int_{5\frac{\pi}{3}+\alpha_2}^{5\frac{\pi}{3}+\alpha_2+\mu}\frac{\sqrt{3}}{2}\cos(\theta+\frac{\pi}{3})\sin\theta\ d\theta + \int_{5\frac{\pi}{3}+\alpha_2+\mu}^{2\pi}\cos(\theta+\frac{\pi}{6})\sin\theta\ d\theta\right]$$

$$a_{1_{V_d}} = -\frac{\sqrt{3}E_m}{4\pi}\Bigg[(\cos\mu)^2\Big[\sqrt{3}\Big[\sin\alpha_4\cos\alpha_4+\sin\alpha_5\cos\alpha_5-\sin\alpha_1\cos\alpha_1 \;..\; \text{(B.18)}$$

$$-\sin\alpha_2\cos\alpha_2\Big]+\Big[-2(\cos\alpha_3)^2-(\cos\alpha_4)^2+(\cos\alpha_5)^2+2(\cos\alpha_6)^2\;..$$

$$+(\cos\alpha_1)^2-(\cos(\alpha_2)^2\Big]\Big]\;..$$

$$+\cos\mu\;\sin\mu\;\Big[\Big[\cos\alpha_4\sin\alpha_4-\cos\alpha_5\sin\alpha_5-\cos\alpha_1\sin\alpha_1+\cos\alpha_2\sin\alpha_2\;..$$

$$+2\cos\alpha_3\sin\alpha_3-2\sin\alpha_6\cos\alpha_6\Big]+\sqrt{3}\Big[(\cos\alpha_4)^2+(\cos\alpha_5)^2-(\cos\alpha_1)^2\;..$$

$$-(\cos\alpha_2)^2\Big]\Big]+\sqrt{3}\Big[-\alpha_4-\alpha_5+\alpha_1+\alpha_2\Big]\Bigg]$$

$$b_{1_{V_d}} = -\frac{\sqrt{3}E_m}{4\pi}\Bigg[(\cos\mu\;)^2\Big[-2\sin\alpha_3\cos\alpha_3-\sin\alpha_4\cos\alpha_4+\sin\alpha_5\cos\alpha_5\;..\; \text{(B.19)}$$

$$+2\sin\alpha_6\cos\alpha_6+\sin\alpha_1\cos\alpha_1-\sin\alpha_2\cos\alpha_2+\sqrt{3}\Big[-(\cos\alpha_4)^2-(\cos\alpha_5)^2\;..$$

$$+(\cos\alpha_1)^2+(\cos\alpha_2)^2\Big]\Big]\;..$$

$$+\cos\mu\;\sin\mu\;\Big[-2(\cos\alpha_3)^2-(\cos\alpha_4)^2+(\cos\alpha_5)^2+2(\cos\alpha_6)^2+(\cos\alpha_1)^2\;..$$

$$-(\cos\alpha_2)^2+\sqrt{3}\Big[\sin\alpha_4\cos\alpha_4+\sin\alpha_5\cos\alpha_5-\sin\alpha_1\cos\alpha_1-\sin\alpha_2\cos\alpha_2\Big]\Big]\;..$$

$$+\Big[2\alpha_3+\alpha_4-\alpha_5-2\alpha_6-\alpha_1+\alpha_2\Big]\Bigg]$$

$$c_{1_{V_d}} = \sqrt{(\,a_{1_{V_d}}\,)^2+(\,b_{1_{V_d}}\,)^2} \qquad \text{(B.20)}$$

APPENDIX C

This program is used to solve the analytical Equations for the firing angles α_1, α_2, ... α_6 to reduce or eliminate the dc current components in the secondary of the converter transformer. The solution is carried out by using the expression for the dc components, Ia_0, Ib_0 and Ic_0 and the partial derivatives of Ia_0, Ib_0 and Ic_0. The system of equation below (Equation 5 .10) is solved by using Newton–Raphson method, with x_1, x_2 and x_3 being the unknown variables.

$$I_{a_0} = f(x_1, x_2, x_3) = 0$$
$$I_{b_0} = f(x_1, x_2, x_3) = 0$$
$$I_{c_0} = f(x_1, x_2, x_3) = 0$$

Where the variables x_1, x_2 and x_3 represent the variables $d\alpha_a$, $d\alpha_b$ and $d\alpha_c$, respectively. Then we can write the variables $d\alpha_1$, $d\alpha_2$, $d\alpha_3$ $d\alpha_4$, $d\alpha_5$ and $d\alpha_6$ as a function of $d\alpha_a$, $d\alpha_b$ and $d\alpha_c$, as shown in the equation below (Equation 5 .9).

$$d\alpha_1 = d\alpha_a - d\alpha_c \qquad d\alpha_4 = d\alpha_c - d\alpha_a$$
$$d\alpha_2 = d\alpha_b - d\alpha_c \qquad d\alpha_5 = d\alpha_c - d\alpha_b$$
$$d\alpha_3 = d\alpha_b - d\alpha_a \qquad d\alpha_6 = d\alpha_a - d\alpha_b$$

The routine MNEWT in the program FIRINANG performs NTRIAL iterations starting from an initial guess at the solution vector X of length N variables. Iteration stops if either the sum of magnitudes of the functions f_i is less than some tolerance TOLF, or the sum of the absolute values of the corrections to dx_i is less than some tolerance TOLX. MNEWT calls the subroutine USRFUN which must return the matrix of partial derivatives α, and the negative of the function values β, as defined in Equation 5 .15 .

```
C       THIS PROGRAM CALCULATE THE ROOT OF THE FUNCTION F(X)
C       WHERE PARTICULARLY F REPRESENTS THE DC COMPONENTS IN
C       THE SECONDARY OF THE CONVERTER TRANSFORMER (IA0, IB0 AND
```

```
C       IC0) AND X REPRESENTS THE FIRING ANGLE MODULATION
C       ================================================
C                     BY ROGERIO VERDOLIN
C                          19 JUNE 1994
C       ================================================
        REAL X(3)
        COMMON ALPHA0,PHI,A,XID,DGRA,RADG
        COMMON PI,PI2,PI2I,PID3,PID6
        OPEN (UNIT=1,FILE='OUT.D')
        OPEN (UNIT=2,FILE='ALPHA.D')
C       COMMON ALPHA0,PHI,A,XID
C       ************************************************
C       CALCULATION OF CONSTANTS USED IN THE PROGRAM
C
        PI=ATAN(1.)*4.
        PI2=2*PI
        PI2I=1./PI2
        PID3=PI/3.
        PID6=PI/6.
        DGRA=PI/180.
        RADG=180./PI
C
C       ************************************************
C       INPUT DATA
C
C       ALPHA0          – BASE ALPHA ORDER
C       A               – AMPLITUDE OF 60 HZ COMPONENT
C       XIDDC           – CURRENT
C       PHIDG           – PHASE ANGLE IN DEGREE
C       NTRIAL          – MAXIMUM NUMBER OF ITERATIONS
C       N               – NUMBER OF OUTPUT VARIABLES
C       TOLF            – TOLERANCE FOR THE FUNCTION F(X)
C       TOLX            – TOLERANCE FOR X
C
        ALPHA0=30.*DGRA
        A=0.15
        XID=1.5
        PHIDG=–60.0
        PHI=PHIDG*DGRA
        NTRIAL=20
        TOLX=0.00001
        TOLF=0.00001
C
        N=3
        NP=3
C
C       END OF INPUT DATA
C       ************************************************
C       ************************************************
C       X(I)=INITIAL GUESS
C
```

```
      DO 12 I=1,N
12    X(I)=2.*DGRA
C     ****************************************************
      CALL MNEWT(NTRIAL,X,N,NP,TOLX,TOLF)
C     ****************************************************
C     OUTPUT DATA: X(1), X(2) AND X(3)
C
      DA1=(X(1)–X(3))*RADG
      DA2=(X(2)–X(3))*RADG
      DA3=(X(2)–X(1))*RADG
      DA4=(X(3)–X(1))*RADG
      DA5=(X(3)–X(2))*RADG
      DA6=(X(1)–X(2))*RADG
C
      A1=(ALPHA0+(X(1)–X(3)))*RADG
      A2=(ALPHA0+(X(2)–X(3)))*RADG
      A3=(ALPHA0+(X(2)–X(1)))*RADG
      A4=(ALPHA0+(X(3)–X(1)))*RADG
      A5=(ALPHA0+(X(3)–X(2)))*RADG
      A6=(ALPHA0+(X(1)–X(2)))*RADG
C
C     ****************************************************
C     WRITING OUTPUT DATA TO THE FILE ALPHA.D
      WRITE (2,222) ALPHA0*RADG,A,XID,PHIDG
      WRITE (1,222) DA1,DA2,DA3,DA4,DA5,DA6
      WRITE (2,222) A1,A2,A3,A4,A5,A6
C     ****************************************************
222   FORMAT (8(E10.4,1X))
1000  STOP
      END
C     ****************************************************
      SUBROUTINE MNEWT(NTRIAL,X,N,NP,TOLX,TOLF)
      INTEGER N,NTRIAL,NP
      INTEGER I,K,INDX(3)
      REAL TOLF,TOLX,X(3)
      REAL D,ERRF,FJAC(3,3),FVEC(3),P(3)
      N=3
      PI=ATAN(1.)*4
      PI2=2*PI
      DGRA=PI/180.
      RADG=180./PI
      DO 14 K=1,NTRIAL
C     WRITE (2,*) 'ITERACAO NUMBER='
C     WRITE (2,*) K
C     *********************************
      CALL USRFUN(X,N,NP,FVEC,FJAC)
C     *********************************
      ERRF=0.
      DO 11 I=1,N
11    ERRF=ERRF+ABS(FVEC(I))
      IF(ERRF.LE.TOLF) RETURN
```

```
      DO 12 I=1,N
12    P(I)=-FVEC(I)
C     **********************************
      CALL LUDCMP(FJAC,N,NP,INDX,D)
      CALL LUBKSB(FJAC,N,NP,INDX,P)
C     **********************************
      ERRX=0.
      DO 13 I=1,N
      ERRX=ERRX+ABS(P(I))
13    X(I)=X(I)+P(I)
      IF (ERRX.LE.TOLX) RETURN
14    CONTINUE
      RETURN
      END
C     ******************************************************
      SUBROUTINE USRFUN(X,N,NP,FVEC,FJAC)
      REAL X(N),FVEC(NP),FJAC(NP,NP)
      COMMON ALPHA0,PHI,A,XID,DGRA,RADG
      COMMON PI,PI2,PI2I,PID3,PID6
      PHIA0=PHI+ALPHA0
C     DA1=DAA-DAC, DA2=DAB-DAC, DA3=DAB-DAA
C     DA4=DAC-DAA, DA5=DAC-DAB, DA6=DAA-DAB
C
      DA1=X(1)-X(3)
      DA2=X(2)-X(3)
      DA3=X(2)-X(1)
      DA4=X(3)-X(1)
      DA5=X(3)-X(2)
      DA6=X(1)-X(2)
C
C     ******************************************************
C     DETERMINATION OF FUNCTION VALUES OF X IN FVEC
C     ******************************************************
C
      WRITE (1,*) 'DA1,....,DA6'
      WRITE (1,222) DA1,DA2,DA3,DA4,DA5,DA6
222   FORMAT (8(E10.3,1X))
      XK11=XID*(DA3-DA1+DA4-DA6)
      XK12=COS(PHIA0+DA1+PID3)+COS(PHIA0+DA3)
      XK13=COS(PHIA0+DA4+PID3)+COS(PHIA0+DA6)
      A0=PI2I*(XK11-A*(XK12+XK13))
      FVEC(1)=A0
C
      XK21=XID*(-DA2-DA3+DA5+DA6)
      XK22=SIN(PHIA0+DA2+PID6)+COS(PHIA0+DA3)
      XK23=SIN(PHIA0+DA5+PID6)+COS(PHIA0+DA6)
      B0=PI2I*(XK21+A*(XK22+XK23))
      FVEC(2)=B0
C
      XK31=XID*(DA1+DA2-DA4-DA5)
      XK32=COS(PHIA0+DA1+PID3)-SIN(PHIA0+DA2+PID6)
```

```
      XK33=COS(PHIA0+DA4+PID3)–SIN(PHIA0+DA5+PID6)
      C0=PI2I*(XK31+A*(XK32+XK33))
      FVEC(3)=C0
      WRITE (1,*) 'FVEC'
      WRITE (1,222) (FVEC(I),I=1,N)
C
C     ****************************************************************
C     DETERMINATION OF JACOBIAN MATRIX VALUES OF X IN FJAC
C     ****************************************************************
C
      FJAC(1,1)=PI2I*(–4*XID+
     *  A*(SIN(PHIA0+DA1+PID3)–SIN(PHIA0+DA3)
     *  –SIN(PHIA0+DA4+PID3)+SIN(PHIA0+DA6)))
      FJAC(1,2)=PI2I*(2*XID+A*(SIN(PHIA0+DA3)–SIN(PHIA0+DA6)))
      FJAC(1,3)=PI2I*(2*XID+
     *  A*(–SIN(PHIA0+DA1+PID3)+SIN(PHIA0+DA4+PID3)))
C
      FJAC(2,1)=PI2I*(2*XID+A*(SIN(PHIA0+DA3)–SIN(PHIA0+DA6)))
      FJAC(2,2)=PI2I*(–4*XID+
     *  A*(–COS(PHIA0+DA5+PID6)–SIN(PHIA0+DA3)
     *  + COS(PHIA0+DA2+PID6)+SIN(PHIA0+DA6)))
      FJAC(2,3)=PI2I*(2*XID+
     *  A*( COS(PHIA0+DA5+PID6)–COS(PHIA0+DA2+PID6)))
C
      FJAC(3,1)=PI2I*(2*XID+
     *  A*(–SIN(PHIA0+DA1+PID3)+SIN(PHIA0+DA4+PID3)))
      FJAC(3,2)=PI2I*(2*XID+
     *  A*( COS(PHIA0+DA5+PID6)–COS(PHIA0+DA2+PID6)))
      FJAC(3,3)=PI2I*(–4*XID+
     *  A*( SIN(PHIA0+DA1+PID3)–COS(PHIA0+DA5+PID6)
     *  –SIN(PHIA0+DA4+PID3)+COS(PHIA0+DA2+PID6)))
      RETURN
      END
C     ****************************************************
      SUBROUTINE LUDCMP(A,N,NP,INDX,D)
      INTEGER N,NP,INDX(N),NMAX
      REAL D,A(NP,NP),TINY
      PARAMETER (NMAX=500,TINY=1.0E–20)
      INTEGER I,IMAX,J,K
      REAL AAMAX,DUM,SUM,VV(NMAX)
      D=1.
      DO 12 I=1,N
      AAMAX=0.
      DO 11 J=1,N
      IF (ABS(A(I,J)).GT.AAMAX) AAMAX=ABS(A(I,J))
11    CONTINUE
      IF (AAMAX.EQ.0.) PAUSE 'SINGULAR MATRIXIN LUDCMP'
      VV(I)=1./AAMAX
12    CONTINUE
      DO 19 J=1,N
      DO 14 I=1,J–1
```

```
      SUM=A(I,J)
      DO 13 K=1,I-1
13    SUM=SUM-A(I,K)*A(K,J)
14    A(I,J)=SUM
      AAMAX=0.
      DO 16 I=1,N
      SUM=A(I,J)
      DO 15 K=1,J-1
15    SUM=SUM-A(I,K)*A(K,J)
      A(I,J)=SUM
      DUM=VV(I)*ABS(SUM)
      IF (DUM.GE.AAMAX) THEN
         IMAX=I
         AAMAX=DUM
      ENDIF
16    CONTINUE
      IF (J.NE.IMAX) THEN
      DO 17 K=1,N
      DUM=A(IMAX,K)
      A(IMAX,K)=A(J,K)
17       A(J,K)=DUM
         D=-D
      VV(IMAX)=VV(J)
      ENDIF
      INDX(J)=IMAX
      IF (A(J,J).EQ.0.) A(J,J)=TINY
      IF (J.NE.N) THEN
      DUM=1./A(J,J)
      DO 18 I=J+1,N
18    A(I,J)=A(I,J)*DUM
      ENDIF
19    CONTINUE
      RETURN
      END
C     **************************************************
      SUBROUTINE LUBKSB(A,N,NP,INDX,B)
      INTEGER N,NP,INDX(N)
      REAL A(NP,NP), B(N)
      INTEGER I,II,J,LL
      REAL SUM
      II=0
      DO 12 I=1,N
      LL=INDX(I)
      SUM=B(LL)
      B(LL)=B(I)
      IF (II.NE.0) THEN
         DO 11 J=II,I-1
11       SUM=SUM-A(I,J)*B(J)
      ELSE IF (SUM.NE.0) THEN
      II=I
      ENDIF
```

```
12      B(I)=SUM
        DO 14 I=N,1,-1
        SUM=B(I)
        DO 13 J=I+1,N
13      SUM=SUM-A(I,J)*B(J)
14      B(I)=SUM/A(I,I)
        RETURN
        END
C       ******************************************************
```